**UNIVERSITÀ
DEGLI STUDI
DI TRIESTE**

UNIVERSITÀ DEGLI STUDI DI TRIESTE

XXXIV CICLO DEL DOTTORATO DI RICERCA IN

Scienze della Terra, Fluidodinamica e Matematica. Interazioni e Metodiche

Seismic investigation and salt tectonics of the Mediterranean salt giant in the central Algerian basin

Settore scientifico-disciplinare: **GEO/11 GEOFISICA APPLICATA**

DOTTORANDO / A

Simon BLONDEL

COORDINATORE

PROF. Stefano MASET

SUPERVISORE DI TESI

PROF. Angelo CAMERLENGHI

CO-SUPERVISORE DI TESI

Anna DEL BEN

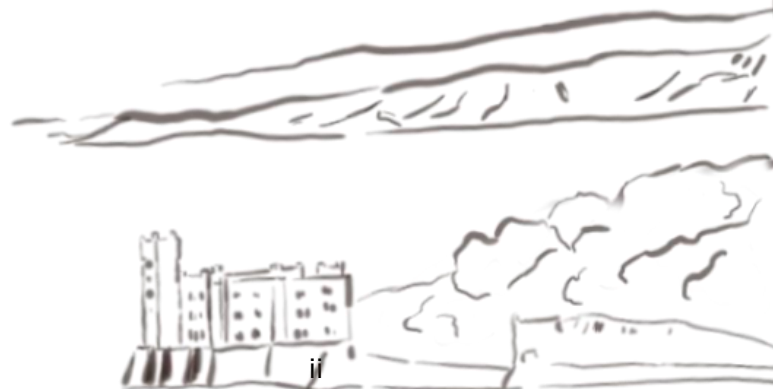**ANNO ACCADEMICO 2021/2022**

Seismic Imaging and Salt Tectonics of the Mediterranean Salt Giant in the Central Algerian Basin

Simon BLONDEL

[Subject]

Department of Mathematics and Geosciences

June 2022

Acknowledgements

I would like to thank the people who accepted to read and review this thesis. Hopefully I have managed to synthesize succinctly and clearly the main outcomes. I hope that it will be a pleasant reading.

My first acknowledgments go to my supervisors Angelo Camerlenghi and Anna Del Ben. I imagine that you were not anticipating I had such a dynamic and rebellious streak. But I think that we became very good colleagues who share many common opinions about the world. I thank Angelo for staying patient and available, for his support when I got into trouble with the hierarchy, for letting me freely devise new approaches, and for allowing me to participate to all the SALTGIANT courses. I dearly thank Anna for being so available, helpful, and kind. You always kept your door open, and you always dedicated me time for discussing my research, my ideas, but also my personal matters.

I want to praise the whole SALTGIANT network, particularly the ESRs. They made me feel like I was contributing to a great work. Having this unique chance to meet people from so many different backgrounds, with such different personalities, all passionate about their own field, will remain a unique part of my life. I feel like without the COVID-19 restrictions we could have achieved something incredible. I also thank my mate Jonathan Ford, who helped me a lot in understanding the practical aspect of processing. He contributed a lot to this work, notably by letting me use his house during the COVID confinement.

I want to emphasize all the admiration I have for the people who created the MEDSALT COST action and the SALTGIANT ETN. It is, I believe, the way we should do research. Through these networking events, I have met Sian Evans and Massimo Bellucci. Without them and their expertise, I am not sure I would have been able to trust my results and publish so quickly. Working together was not only fruitful, but it was also a lot of fun, even remotely, thanks to their integrity, their truthfulness, and their tolerance to my sour sense of humour.

Abstract

The Mediterranean Salt Giant (MSG) is a thick layer of Messinian evaporites (up to 4 km) that is thought to be deposited during an extreme paleo-environmental event known as the Messinian Salinity Crisis (MSC). After decades of research, there is not yet a consensual model explaining the emplacement and the evolution of the MSG. This is due to the deficiency of samples of the deep offshore MSG, particularly in the Western Mediterranean. Past scientific drilling operations were limited to the topmost MSG records because of the risks of intersecting zones of hazardous fluids and overpressure linked to evaporites. The European project SALTGIANT, in which the work of this thesis fits into, is dedicated to understanding the formation of the MSG and its implications for the microbial life, the drilling hazards and the geo-economics of the Mediterranean region and the history of oceanography. In that framework, this thesis aims to improve our seismic images of the offshore MSG and to use the new results to update our understanding of the Messinian salt tectonics. This work is focused on the Algerian basin, in the south-western Mediterranean Sea, where the salt was deposited in an already contractional tectonic setting. The objectives are: (i) to develop a robust and cost-effective strategy to reprocess legacy seismic data and assess the benefit of the reprocessed data and (ii) to use the new data to gain insights on the fluid flow and the salt tectonics of the MSG. I compile, reprocess, and interpret legacy academic seismic data acquired in the central Algerian basin. The re-processing is designed to improve as much as possible the salt and pre-salt structures, in an attempt to tackle the challenges imposed by the 2D narrow-azimuth and short-offset legacy data. It relies on an integrated approach combining geophysics and geological interpretation to iteratively build the velocity model. The new results allow a more reliable interpretation of salt structures and the seismic facies variations. They shed a new light on the tectono-sedimentary evolution of the central Algerian basin, highlighting the presence of seismic fluid indicators evidencing an active fluid circulation in the basin and its margins. Interpretation of the new seismic sections is done following the most recent nomenclature of the MSC seismic markers. New isochores and thickness maps are produced and compared with the spatial distribution of the salt structures. I interpret contractional salt tectonic structures, such as buckle folds, squeezed diapirs and related salt sheets as evidence of regional thick-skinned shortening episodes. I suggest that the extensional stage of the salt system (where the deformation is driven by gravity loading) was short-lived, and that many salt structures were driven by contractional tectonic loading during the Plio-Quaternary. I demonstrate that the initial shortening-related salt deformation in the late Messinian was focussed along the Algerian margin and later shifted outward toward the Balearic margin in the Plio-

Quaternary. The shifting of the deformation front is interpreted to be a result of the thickening and strengthening of the overburden. The second peak of deformation may have reactivated faults along the Emile-Baudot escarpment with thick-skinned deformation. I also observe a variation in the intensity of salt deformation along the margin from SW to NE, which I associate to variable tectonic loading applied along the Algerian margin or the pre-shortening distribution of salt. Fluid indicators are imaged within the Plio-Quaternary of the Algerian basin. They could be thermogenic or biogenic gas sourced from the Messinian Upper Unit, or from the pre-salt, migrating through a hydro-fractured salt. The new results also evidence numerous volcanic structures within the Formentera basin. The distribution of this volcanic edifice could affect fluid circulation, resulting in small-wavelength surface HF anomalies observed locally.

Table of Contents

List of abbreviations

BU1 Bedded Unit 1

BU2 Bedded Unit 2

BU3 Bedded Unit 3

DSDP Deep Sea Drilling Project

FBI Foraminifer Barren Interval

IODP International Ocean Discovery Program

LU Lower Messinian Unit

MSC Messinian Salinity Crisis

MSG Mediterranean Salt Giant

MU Mobile Messinian Unit

ODP Ocean Drilling Program

UU Upper Messinian Unit

UU1 Lower Upper Messinian Unit

UU2 Upper Upper Messinian Unit

PREAMBLE

This work is part of the SALTGIANT European Training Network, a European project funded by the European Union's Horizon 2020 research and innovation programme under the Marie Skłodowska-Curie grant agreement n° 765256.

It is part of Work Package 3 - Drilling hazards, that aims to develop a mechanistic and quantitative understanding of early salt deformation and sub-salt overpressure development that can be used by the oil industry to mitigate the risks associated with drilling in salt-capped hydrocarbon provinces.

The aim of this thesis was to identify and classify salt structures in different geological environments of the Mediterranean basin making use of the available offshore multi-channel seismic reflection data including regional vintage public data, academic data, and industry data. This initially included nine months of secondments in different institutions (the National Oceanography Center in Southampton (UK), the Ente Nazionale Idrocarburi in Milano (IT) and the Center for Marine Environmental Sciences in Bremen (DE)).

Due to the restrictive policy applied against the Coronavirus (COVID-19) Pandemic, most secondments could not be conducted, and industry data could not be used. They were also issues in obtaining additional public or academic data to identify the salt structures in different environments of the Mediterranean Sea. This led to a narrowing of the study area to the only Algerian basin and its Balearic margin. Only four months of secondment were conducted at the CNRS- Université de Montpellier 2 and Sorbonne Université - Institut des Sciences de la Terre de Paris – ISTeP, to further study the Algerian margin and its Balearic margin.

Chapter 1

Introduction

1.1 The Mediterranean region and the Mediterranean Salt Giant

The Mediterranean Sea is a symbol of European civilisation. Its strategic position - between Europe, Asia, and Africa - its climate and its heritage have always attracted people and investments. This unique environment represents less than 1% in surface area of the world oceans, but hosts between 4 and 18% of the world's marine biodiversity, of which more than a quarter are endemic (Würtz, 2010). But the risks weighing on this environment are numerous: demographic pressure, urbanism, mass tourism, land- and shipping-sourced pollution, overfishing, exploitation of subsurface resources etc. Climate change has exacerbated some of these risks in the Mediterranean basin, as the Mediterranean region has warmed more than the global world average (1.6°C in the Mediterranean, 1.1°C on average; UNEP/MAP and Plan Bleu, 2020). The regional warming has resulted in losses and damages to people, ecosystems, food systems, infrastructure, energy and water availability, public health, and the economy, which in turns increase tensions and conflicts between activities and states (Cramer *et al.*, 2018, 2020; Ali *et al.*, 2022). It is not yet clear how the Mediterranean will respond to global warming on the long-term. The hazard is particularly high because this is a semi-enclosed sea, connected to other seas and oceans only by the strait of Gibraltar, the strait of the Dardanelles and the Suez channel. Consequently, the water renewal period is high, in the order of hundred years in the eastern Mediterranean deep-water (Schlitzer *et al.*, 1991; Roether and Well, 2001). This means that the smallest contamination can affect the environment for a long time, highlighting the need to protect this environment.

In that context, the mining of the sub-surface's resources offshore adds one more stress to the fragile ecosystem of the Mediterranean Sea. The MSG plays an important role offshore for hydrocarbon accumulations because salt structures are effective traps and seals for petroleum systems (Farmer *et al.*, 1996). Recent hydrocarbon discoveries in the Eastern Mediterranean in the 2010s have particularly increased the investment of the oil and gas industry which now sees the Eastern Mediterranean as a major gas province to secure future energy supplies, changing the geo-economic and geo-political balance of the region (Bornstein, 2018).

The major risks associated to the exploration and the development of these resources are encountered during the drilling of the subsurface. Any drilling operation involve hazards for the environment, with the risk of accident or pollution through seepage of hydrocarbons into the sea. In an environment as vulnerable and confined as the Mediterranean Sea, this risk is not to be taken lightly. The risks linked to a blowout were brought to the fore of public consciousness in 2010, after the dramatic Deepwater Horizon blowout in 2010, that cause the death of eleven people and the spilling of ~ 4 million barrels of oil leaked into the Gulf of Mexico (Pinkston and Flemings, 2019). Since then,

measures to prevent the risk associated with drilling have been re-enforced. New safety guidelines and the rise of public awareness has complicated the permitting for the exploration of the offshore sub-surface, both for industrial and scientific purposes. The International Ocean Discovery program (IODP), who is today the main public program able to perform offshore scientific drilling worldwide, requires applicants to minimize the risks of an accident that could cause loss of life or property, damage to the environment, or handicap their activity (Graber, 2006). It is of paramount importance that we keep exploring the richness of the Mediterranean in a sustainable way. This means that if we want to propose new scientific surveying in the Mediterranean, we must not solely convince stakeholders of the pertinence of the research we carry out. We must also demonstrate a thorough knowledge of sub-surface conditions as well as the political and social contexts of the investigated waters, proving our commitment to considering the hazards and concerns linked to offshore investigations.

The origin of this thesis lies in lowering these risks within the scope of the 857-MDP2 IODP proposal: "Uncovering a Salt Giant: Umbrella proposal of the multi-phase drilling project (MDP)" (Camerlenghi *et al.*, 2014). This proposal aims at uncovering the Mediterranean Salt Giant (MSG). It encompasses several IODP drilling proposals: Probing deep Earth and surface connections (857A-Pre); Deep-Sea Records of the MSC (DREAM; 857B-Pre and 857C-Full); Deformation and fluid flow in the MSC salt giant; Probing the Salt Giant for its Deep Biosphere secrets. The aim of this proposal is to solve a long-lived scientific controversy: The origins and the nature of the Mediterranean Salt Giant (MSG).

1.1.1 The Mediterranean Salt Giant (MSG)

The MSG is a wide thick evaporite layer (up to 4 km; Haq *et al.*, 2020) that was deposited during a paleo-event known as the Messinian Salinity Crisis (MSC), during the Late Miocene (Selli, 1960; Hsü *et al.*, 1977; Krijgsman *et al.*, 1999; Ryan, 2009; Roveri, Flecker, *et al.*, 2014; Camerlenghi and Aloisi, 2019). It includes a high fraction of evaporites, salt rocks that was originally precipitated from a saturated surface or near surface brine driven by solar evaporation (Warren, 2016). It encompasses a wide range of lithology including carbonates, gypsum, anhydrite, halite, potassic salts etc. The term MSG was introduced after the Mediterranean cruise Deep Sea Drilling Project - Leg 13, in 1970 (sites 120 to 134 on Figure 3), when samples of evaporites were obtained throughout the whole Mediterranean deep basin, thereby providing evidence of the widespread extension of the Messinian evaporites over the whole Mediterranean basin and its margins (Hsü, Ryan and Cita, 1973; Ryan, Hsu, and et al., 1973).

This discovery occurred in a context of growing international competition in exploring the oceans post World War II (Adler, 2019). In the 1960s, the

growing strategic importance of ocean exploration led some European countries to develop greater capacity in marine scientific research (Martínez-Rius, 2020). Almost synchronously with the discovery of the MSG, from 1969 to 1980, the first broad seismic exploration campaign of the Mediterranean Sea (MS) for scientific purposes was carried out by the OGS (Finetti and Morelli, 1972). The development of multifold acquisition and digital processing in the 1960s considerably improved the quality of the seismic images of the subsurface, leading to a boom of seismic acquisitions in the 1970s (Trabant, 1984). The pioneering MS survey allowed the acquisition of ~ 50,000 km of 2D seismic covering the entire deep Mediterranean, contributing to the discovery of the extent and the salt dome geometry of the MSG (Finetti *et al.*, 2005).
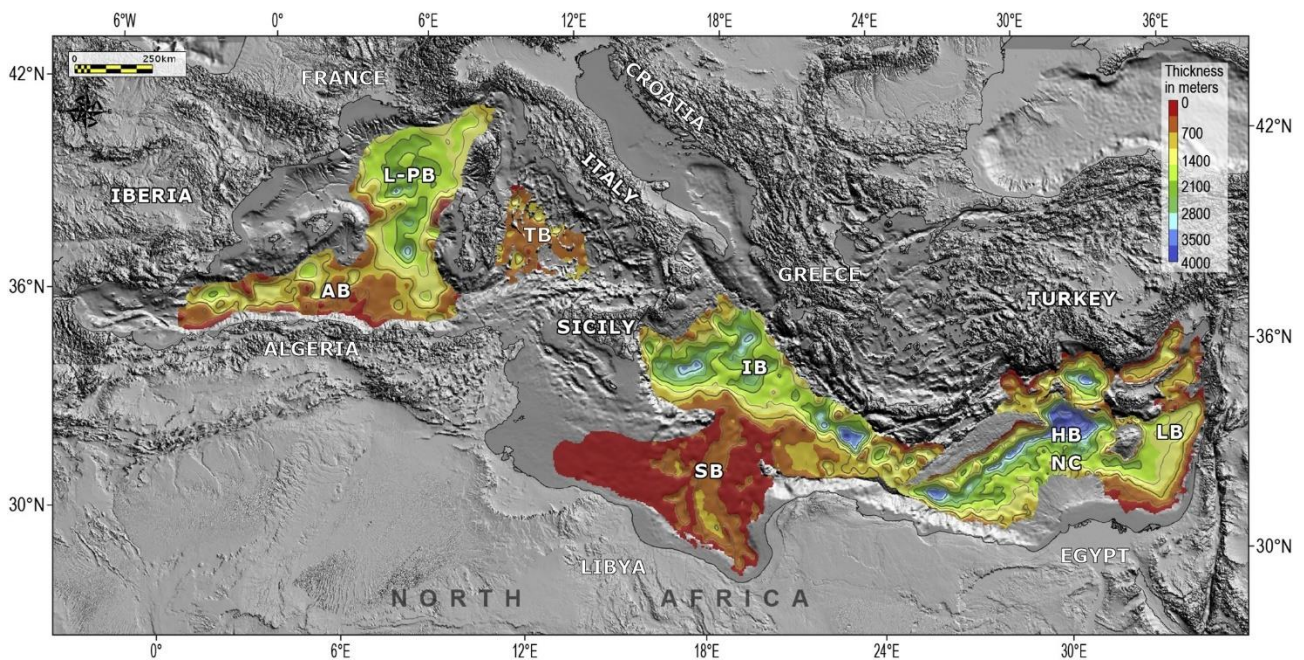
Figure 1 Isopach map of evaporites and Messinian Salinity Crisis-related sediments in the deep basins based on seismic facies analysis from the deep Mediterranean basins (modified from Haq *et al.*, 2020). L-PB: Liguro-Provençal Basin; AB: Algerian Basin; TB: Tyrrhenian Basin; IB: Ionian Basin; SB: Sirte Basin; HB: Herodotus Basin; LB: Levant Basin; NC: Nile Cone.

Nowadays, the extent of the MSG is relatively well constrained onshore and offshore (Figure 1, Figure 3). This is thanks to a much denser seismic covering the offshore basins driven by the oil and gas exploration (see section 1.1.3 and 1.2). Yet, due to a lack of sub-surface samples, particularly in the western and the central deep basins, little is known about its origin, the timing of its emplacement, and the correlation between the shallow and the deep evaporites (CIESM, 2008; Roveri, Flecker, *et al.*, 2014; Camerlenghi and Aloisi, 2019).

The CIESM consensual model of the MSG can be broadly described as a mobile wedge-shaped halite-rich layer encompassed in between two layers made of evaporite-terrigenous couplets on the marginal basins (Figure 2; the lower and the upper Evaporites, mostly gypsum-shale couplets referred to as the Primary Lower Gypsum and the Upper Gypsum), where they may pass landward into carbonate or evaporite-free terrigenous facies (Hsü, Ryan and

Cita, 1973; CIESM, 2008). Offshore, the nature and the thickness of the evaporite layers is not well constrained, notably because of the absence of samples in the deep Mediterranean (CIESM, 2008; Roveri, Flecker, *et al.*, 2014). Several studies based on uplifted outcrops and industrial wells showed that the layer underlying the deep-water halite is mostly made of evaporite-free shales (Figure 2b), questioning the timing of the onset of the MSC in the deep basins (Manzi *et al.*, 2007; Gvirtzman *et al.*, 2017; Manzi *et al.*, 2018; Meilijson *et al.*, 2018; V. Manzi *et al.*, 2021). No wells have yet sampled the pre-halite records elsewhere in the central and western Mediterranean. In the Levant basin, industrial wells have revealed that the deep halite yields internal interbeds of evaporites and clastic (Gvirtzman *et al.*, 2013, 2017; Feng, Steinberg and Reshef, 2017; Meilijson *et al.*, 2019).
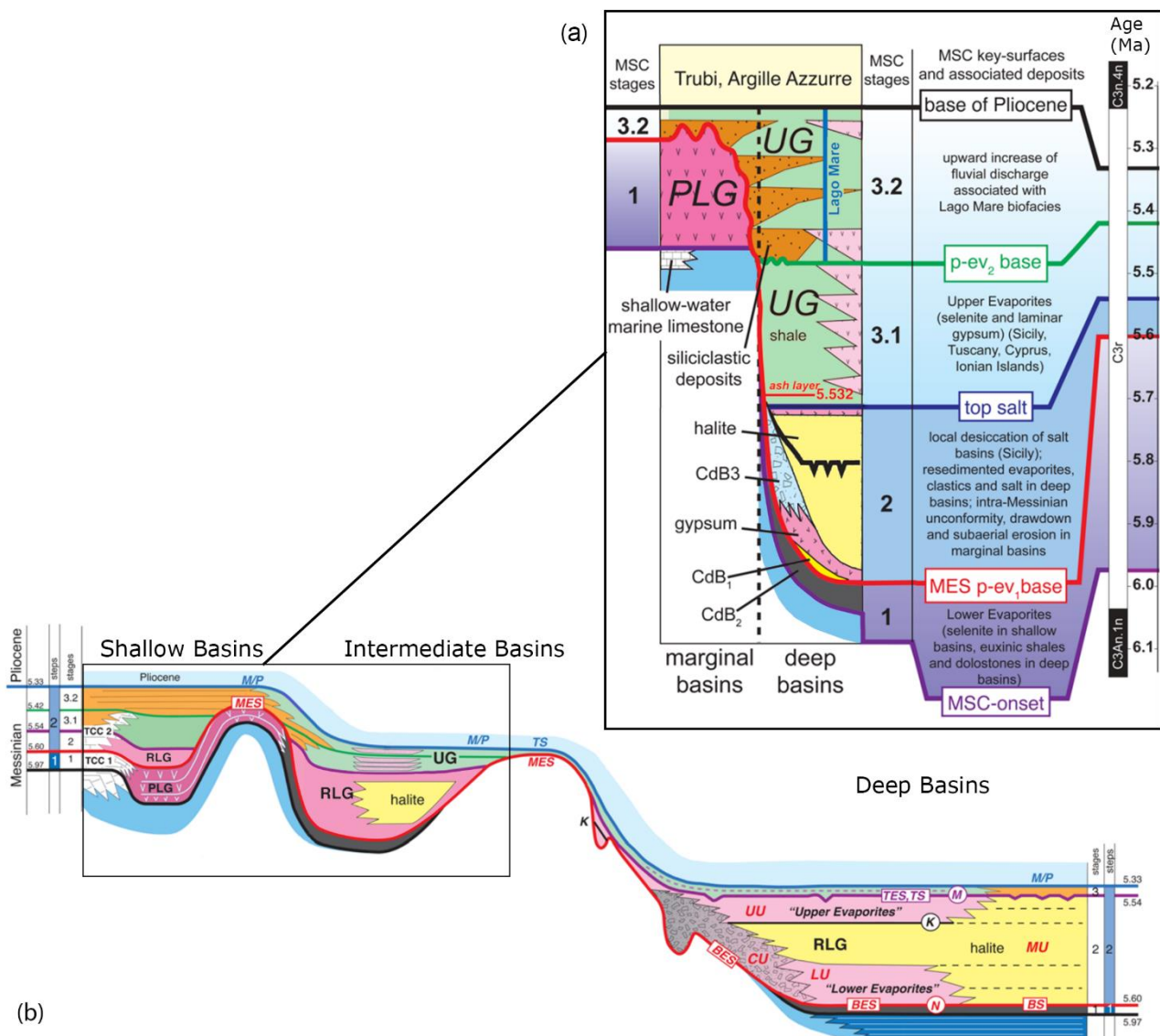
Figure 2 (a) Chronostratigraphy of Late Miocene to Early Pliocene with MSC events in the Mediterranean (modified from CIESM, 2008; Manzi *et al.*, 2013; Roveri, Flecker, *et al.*, 2014). (b) Stratigraphic model of the Messinian deep-basin deposits and their correlation with marginal basin successions (modified from Roveri, Lugli, *et al.*, 2014). PLG, Primary Lower Gypsum; RLG, Resedimented Lower Gypsum; UG, Upper Gypsum; CdB, Calcare di Base

DSDP-ODP cores and industrial wells that recovered the top-most MSG showed that it consists mainly of interbedded dolomitic clastics and evaporites, mostly gypsum or anhydrite, often with Lago-Mare fauna (Hsü, Ryan and Cita, 1973; Kastens and Mascle, 1990; Comas *et al.*, 1996; Lugli *et al.*, 2015; Gvirtzman *et al.*, 2017). This suggests that the presence of a possible deep-water equivalent of the stage 3 upper evaporites (Roveri, Lugli, *et al.*, 2014). Alternatively, this unit could be mainly made of fluvio-deltaic terrigenous sediments with a low fraction of evaporites, fed by massive input from Messinian rivers (Bache *et al.*, 2009; Bowman, 2012; Gorini, Montadert and Rabineau, 2015; Leroux *et al.*, 2017; Madof, Bertoni and Lofi, 2019). Industrial wells that penetrated the whole Messinian succession in shallow and intermediate basins in the western Mediterranean encountered mostly terrigenous and carbonate Messinian records, with occasional gypsum and anhydrite intervals (Habibas-1, Alger-1, Arzew-1; see section 1.6.3; Burollet, Said and Trouve, 1978; Medaouri *et al.*, 2012). This highlights the fact that the MSG must not be considered as a thick salt body only made of evaporites, but as an intertwined mixed of terrigenous clastics and evaporites, sometimes only made of siliciclastic sediments. This is an aspect of the MSG I have always kept in mind during the seismic depth imaging of Messinian record, by carefully investigating the veracity of velocities above 4000 m/s in the interval velocity model (Chapter 3).
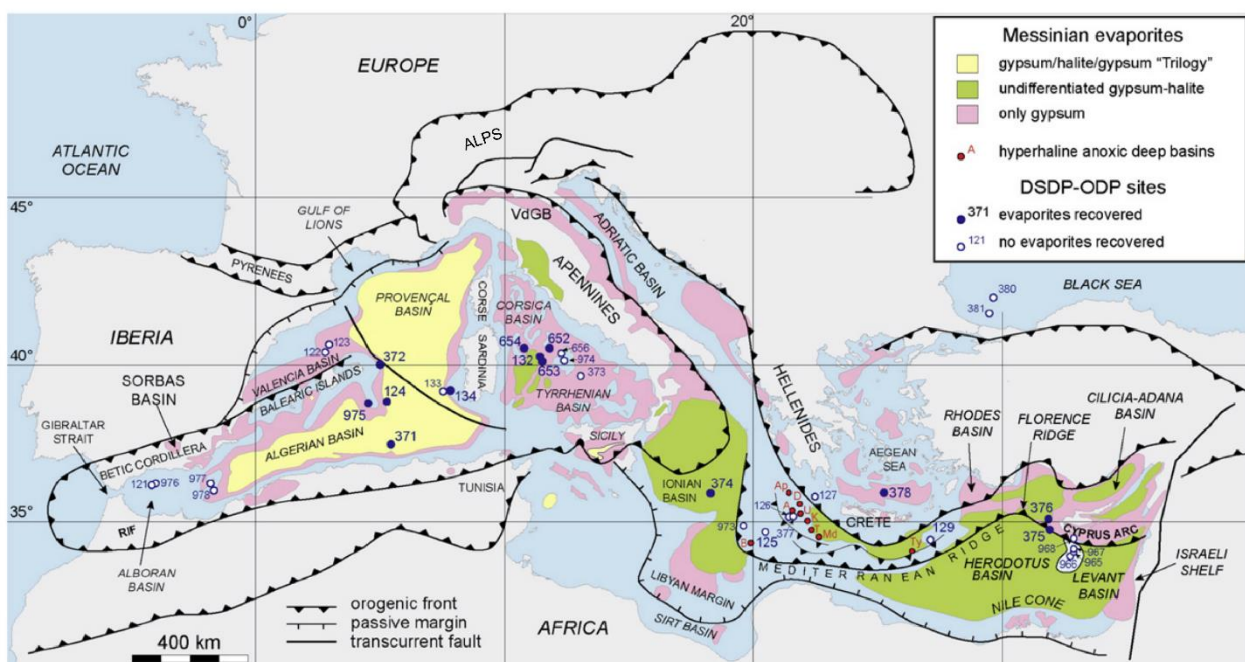
Figure 3 Distribution of Messinian evaporites and location of the DSDP-ODP boreholes which recovered Messinian deposits (modified from Roveri et al., 2014b and Lofi, 2018). Ap, Aphrodite; A, Atlante; B, Bannock; D, Discovery; K, Kryos; M, Medee; T, Thetis; Ty, Tyro; U, Urania.

1.1.2 The Messinian Salinity Crisis (MSC)

This section aims to briefly describe the context of this study and the SALTGIANT ETN. For a more exhaustive description of the MSC and the open key questions linked to it, one can read the reviews published by CIESM, 2008, Roveri et al., 2014c, 2016, Camerlenghi & Aloisi, 2019 and Andreetto et al., 2021b, that I used for writing this section.

The term MSC was introduced in the scientific literature by Selli, (1960) based on its study of the Apennine gypsum deposits on land. The discovery of the deep offshore MSG gave rise to a proliferation of studies, proposals, interpretations, and hypotheses on the origin of this deep-lying salt giant (Busson, 1990). The common trend was to envision a widespread evaporite deposition in desiccated Mediterranean, but the idea of precipitating salts in restricted deep-water bodies received increasing attention and is still debated today (Hsü, 1972; Hsü *et al.*, 1977; Manzi *et al.*, 2005; Roveri, Flecker, *et al.*, 2014; Lugli *et al.*, 2015; Camerlenghi and Aloisi, 2019).

The premises of the MSC go back to ~7.8–6.7 Ma (Tortonian to Messinian), with a worldwide global cooling (Tzanova, Herbert and Peterson, 2015; Herbert *et al.*, 2016; Holbourn *et al.*, 2018), an aridification on land (Blondel *et al.*, 2010; Edwards *et al.*, 2010; Pound *et al.*, 2012), combined with a gradual restriction from the Atlantic due to the uplift of the Gibraltar Arc (Krijgsman *et al.*, 1999; Martin, Braga and Betzler, 2001; Garcia-Castellanos and Villaseñor, 2011; Flecker *et al.*, 2015; Capella *et al.*, 2018, 2020; Bulian *et al.*, 2021), and from the Paratethys (Krijgsman *et al.*, 2010; Kontakiotis *et al.*, 2022). Predating the MSC, from ~7.17 Ma onward, progressive hydrological restriction of the Mediterranean changed the thermohaline circulation within the basin (Figure 4), with deep-water stagnation and oxygen depletion resulting in change in the marine biodiversity, the formation of cyclic sapropels and diatom-rich sediments (Bulian *et al.*, 2022). Because of the presence of the Sicily sill, that acts as a "dam" between the western and the eastern Mediterranean, the impact of stratification is first recorded in the central and eastern Mediterranean Basin (Krijgsman *et al.*, 1997; Seidenkrantz *et al.*, 2000; Kouwenhoven, Hilgen and van der Zwaan, 2003; Karakitsios *et al.*, 2017; Tzevahirtzian *et al.*, 2022) and then, from ~6.8 Ma, in the western Mediterranean Basin (Fortuin and Krijgsman, 2003; Sierro *et al.*, 2003; Krijgsman *et al.*, 2006; Ochoa *et al.*, 2015).

As the connectivity of the Mediterranean with the adjacent basins diminished, continuous evaporation drove the water salinity to rise until its saturation by salts, leading to the so-called MSC and the emplacement of the evaporites between ~5.97 and ~5.33 million years ago (Hsü, Ryan and Cita, 1973; Krijgsman *et al.*, 1999; CIESM, 2008; Manzi *et al.*, 2013). It resulted in the extraction of ~5% of the salts dissolved in the global ocean and had a permanent impact on both the terrestrial and marine ecosystems of a huge area surrounding the Mediterranean (Ryan *et al.*, 2009). A consensus

stratigraphic model for the MSC was defined by several MSC experts (CIESM, 2008; Roveri, Flecker, *et al.*, 2014 and referencees therein). The stages can be summarized as follows:

- stage 1 (5.97-5.60 Ma): evaporitic cycles, likely controlled by orbital variation, recorded by carbonate platforms and gypsum-shale and marine-shales couplets in shallow and intermediated depths marginal basins (Primary Lower Gypsum), while euxinic shales and dolostones prevails in the deep basins, where the absence of oxygen and sulfate oxidation prevents gypsum precipitation.
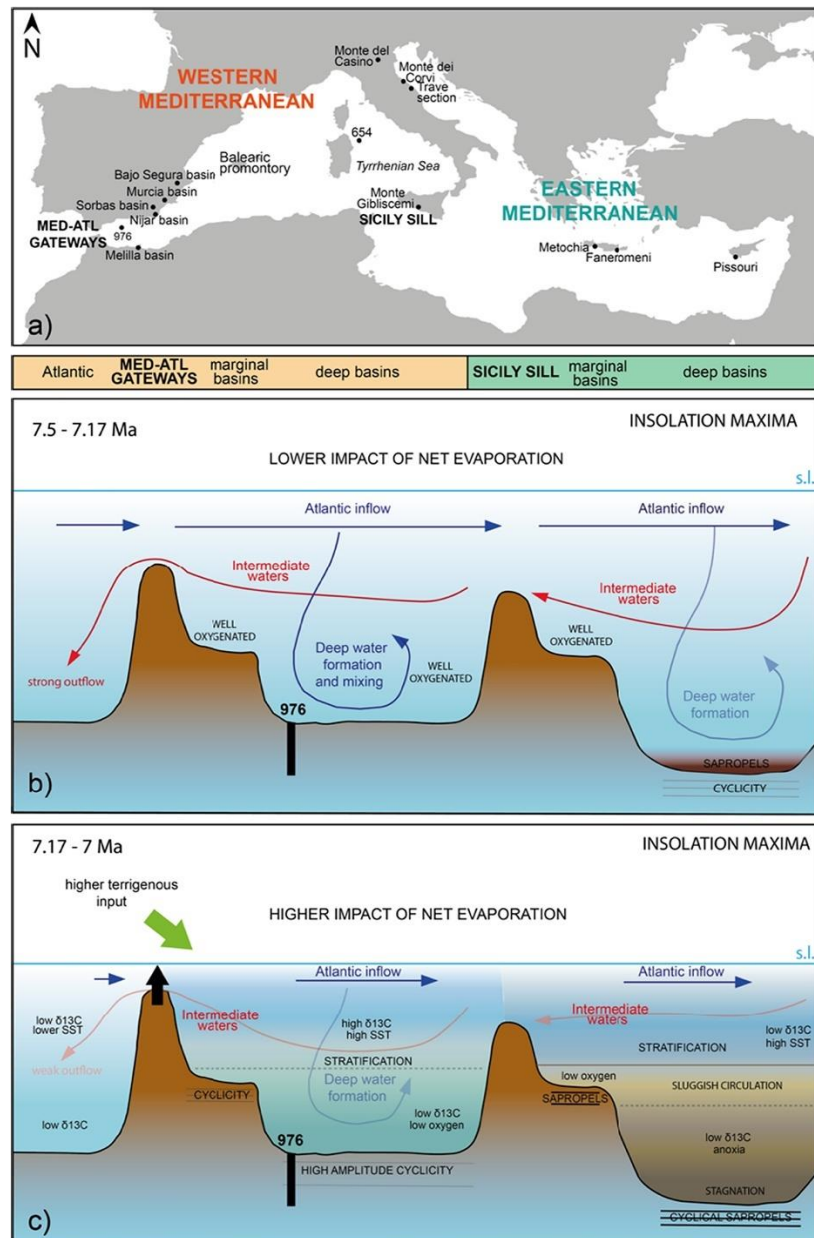
Figure 4 a) Generalized map of the Mediterranean Sea showing the basins, sections and ODP Sites mentioned in this section (from Bulian *et al.*, 2022). Cartoon showing the Mediterranean thermohaline circulation: b) before (from present circulation studies like Pinardi and Masetti, 2000) and c) after the 7.17 Ma event (Circulation patterns adapted from Alhammoud, Meijer and Dijkstra, 2010; and Topper and Meijer, 2015).

- stage 2 (5.60-5.55 Ma): high-amplitude base-level drop during glacial peaks, with widespread dominantly halite and potash salts precipitation, erosion in marginal basins, and clastic gypsum redeposition (Resedimented Lower Gypsum).

- stage 3.1 (5.55-5.42 Ma): evaporitic cycles, also likely controlled by orbitally driven base-level oscillations, recorded by mostly siliciclastic gypsum-shale couplets in shallow and intermediated depths marginal basins (Upper Evaporites) laterally turning into evaporite-free fluvio-deltaic deposits. Gypsum/Anhydrite-shale couplets are also present in the deep basins.

- stage 3.2 (5.42-5.33 Ma): Similar to Stage 3.1 but with an enrichment in siliciclastic deposits, brackish to fresh-water fauna and flora affiliated to the Paratethys/Black Sea, and a different isotopic composition.

The amplitude of the base-level variation and the understanding of geochemical conditions allowing evaporites precipitation are at the core of the MSC controversy (CIESM, 2008; Roveri, Flecker, *et al.*, 2014; Roveri *et al.*, 2016; Camerlenghi and Aloisi, 2019). During Messinian times, the paleogeography of the Mediterranean basins was close to the one observed today (Figure 5): The western Mediterranean was broadly similar to that of the present day, with an ongoing inversion along African margin, but the Tyrrhenian Basin was initiating its opening, the oblique rifting of the Sicily sill was not yet triggered, and the Eastern Mediterranean and the Adriatic Sea were wider and better connected to the Ionian Sea (Mascle and Mascle, 2019; Civile *et al.*, 2021). Flexural-isostatic reconstruction of the Western Mediterranean during the Messinian Salinity Crisis and analogue modelling experiments suggested at least a −1,500 m base level drop at the acme of the MSC (Heida *et al.*, 2021; Strzerzynski *et al.*, 2021). Other studies suggested a lower, but still high-amplitude, relative base-level drop between -800 and 1300 m (Urgeles *et al.*, 2011; Amadori *et al.*, 2018; Pellen *et al.*, 2019). The Messinian Erosion Surfaces (MES) is generally suggested as an evidence of a high amplitude drop, synchronous with an increase in terrigenous sediment input reflecting the enhanced fluvial erosion of the margins (Ryan and Cita, 1978; Bache *et al.*, 2009; Breda *et al.*, 2009; Lofi *et al.*, 2011; Gorini, Montadert and Rabineau, 2015; Leroux *et al.*, 2017; Madof, Bertoni and Lofi, 2019; Pellen *et al.*, 2019). Alternatively, some authors have argued for much smaller water level variations (+- 200m), with dense submarine water cascades responsible for the observed Messinian erosion on the margins (Roveri, Manzi, *et al.*, 2014; Lugli *et al.*, 2015; Vinicio Manzi *et al.*, 2021), comparable to what can be observed today locally along some margins of the Mediterranean (e.g. Gaudin *et al.*, 2006).

The relative base level during stage 3 is also debated. Some authors propose an isolated and desiccated Mediterranean studded with endorheic lakes (Figure 6a), where the Black Sea fauna is transported by migratory aquatic birds (e.g., Hsü, Ryan and Cita, 1973; Orszag-Sperber, Rouchy and

Blanc-Valleron, 2000; Stoica *et al.*, 2016; Kartveit, Ulsund and Johansen, 2019; Caruso *et al.*, 2020; Raad *et al.*, 2021). Other authors argue that stage 3 records a progressive Mediterranean sea-level rise resulting from river runoff and overspill from both the Atlantic and Paratethys (Flecker and Ellam, 2006; Marzocchi *et al.*, 2016; Vasiliev *et al.*, 2017; Grothe *et al.*, 2020). At the Lago-Mare stage 3.2, relative base-level fluctuated by several hundred meters with precessional periodicity, with an already relatively full Mediterranean during the wet precessional phases (Figure 6b)(Andreetto, Matsubara, *et al.*, 2021).
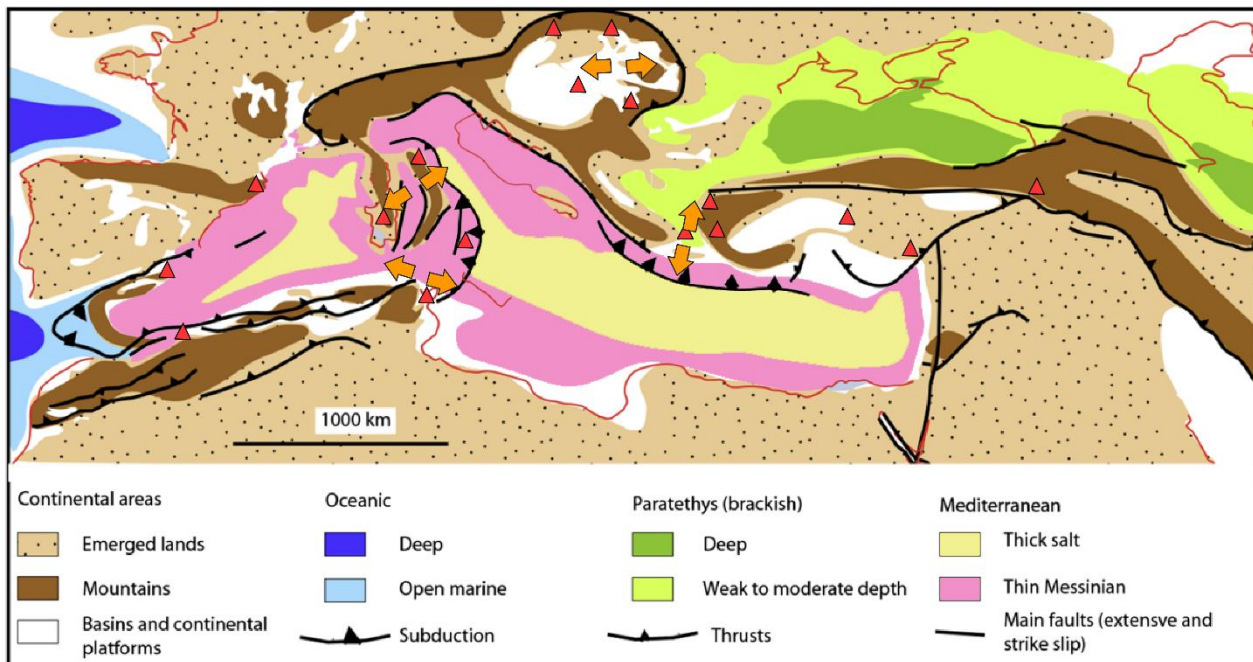
Figure 5 Paleogeography of the Mediterranean Sea and the Paratethys during Messinian (modified from Mascle and Mascle, 2019). Red triangles indicate active volcanic provinces, orange arrows indicate active back-arc extensional regions (from Faccenna *et al.*, 2014).

The MSC ended with the Zanclean flooding, when the Mediterranean basin was fully reconnected to the neighbouring Atlantic ocean via the Gibraltar Straight (Hsü, Ryan and Cita, 1973; Garcia-Castellanos *et al.*, 2009). This hypothesis is supported by the presence of long and deep erosion channel extending from the Gulf of Cádiz to the Algerian Basin (Ryan *et al.*, 2009; Bache *et al.*, 2012; Garcia-Castellanos *et al.*, 2020), as well as megaflood deposits at the Malta Escarpment (Micallef *et al.*, 2018). Some studies suggested that the Zanclean sea level rise has occurred in two phases, with a slow sea level rise preceding a later phase of rapid sea level rise (García *et al.*, 2011; Bache *et al.*, 2012).
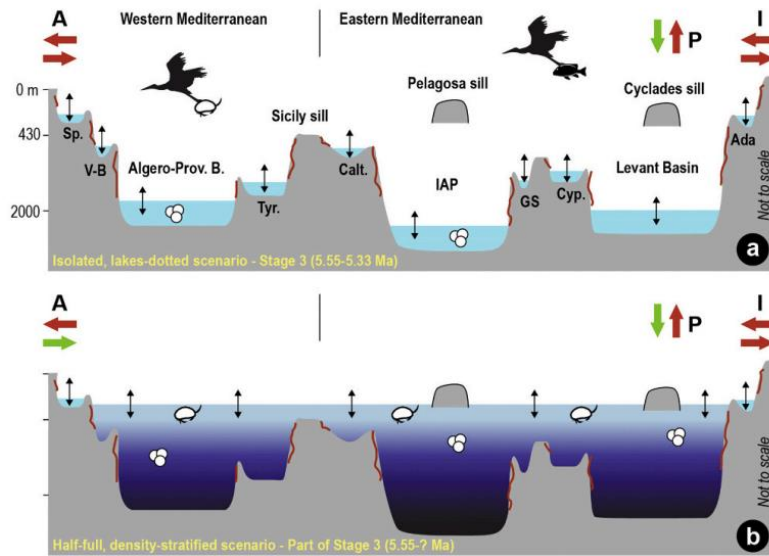
Figure 6 Schematic W-E profiles across the Mediterranean Basin showing the contrasting paleoenvironmental, palaeohydrological and paleoconnectivity interpretations between the isolated (a) and density-stratified (b) proposed for Stage 3 (modified from Andreetto, Aloisi, *et al.*, 2021). When a water flow is present (green arrow) from and/or to an extra-Mediterranean water mass (i.e., A: Atlantic Ocean; I: Indian Ocean; P: Eastern Paratethys), the direction of the arrow gives the direction of flow. For simplicity, water added by the major and local rivers is not shown, but it adds to the hydrological budget at any time in each scenario. Sp.: SE Spain; V-B: Valencia Basin; Tyr: Tyrrhenian Basin; Calt: Caltanissetta Basin; IAP: Ionian Abyssal Plain; GS: Gulf of Sirt; Cyp: Cyprus; Ada: Adana Basin.
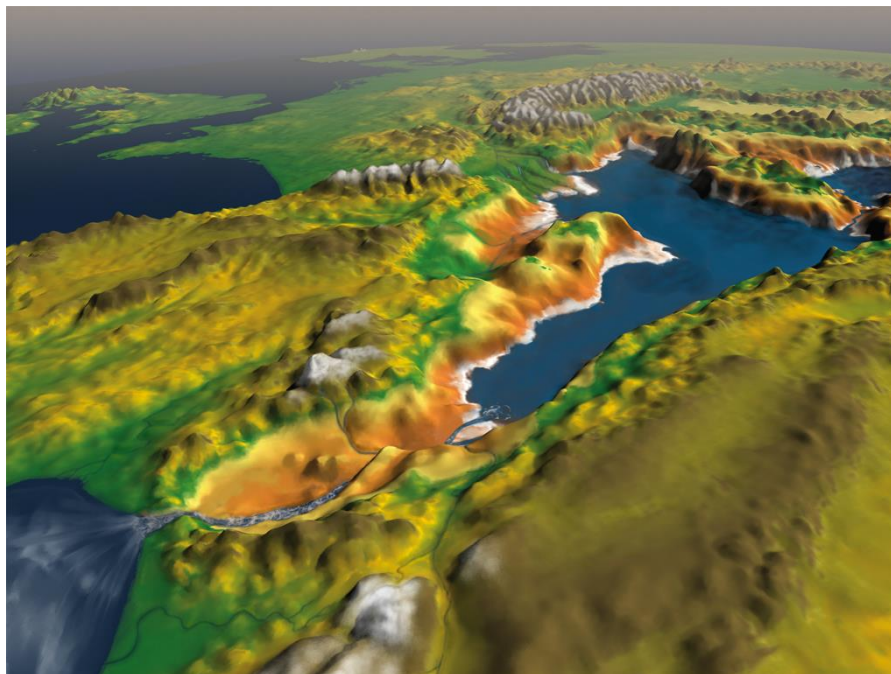
Figure 7 Illustration of the presumed Zanclean flood of the Mediterranean after its desiccation during the Messinian salinity crisis. The view in this image is from the southwest, with the future British Isles in the upper left-hand corner (image from Roger Pibernat under supervision of Daniel Garcia-Castellanos, based on Garcia-Castellanos et al. (2009); license: CC-BY, available at https://it.m.wikiversity.org/wiki/File:Messinian_Mediterranean_and_Gibraltar_-_reconstructed_landscape.jpg)

1.1.3 Economical and societal importance of the MSG

The initial interest in exploring the Mediterranean was not oceanography nor exploration, but exploitation of oceanic natural resources (oil, gas, manganese nodules, fish; Martínez-Rius, 2020). But within the context of global earth warming, the understanding of the MSG and the related MSC is not only of industrial interest. Several studies showed that it could also shed new light on the response of the Mediterranean basin to climate change (water level, ocean currents, precipitations, rate of erosion, fauna, flora etc. e.g., Fauquette *et al.*, 2006; Willett, Schlunegger and Picotti, 2006; Schneck, Micheels and Mosbrugger, 2010; Ivanovic *et al.*, 2014; Andreetto, Matsubara, *et al.*, 2021; Ng *et al.*, 2021; Trájer, Sebestyén and Padisák, 2021). This study of the latest MSC, where a climatic shift to warmer and wetter conditions occurred (Vidal *et al.*, 2002; Krijgsman *et al.*, 2010; Perez-Asensio *et al.*, 2013), could notably improve our models predicting the response of this enclosed environment to global warming (UNEP/MAP and Plan Bleu, 2020). The study of the deep life in the MSG could also span beyond the understanding of our Earth by providing an analogue to extreme environments on other planets (Oren, 2014). Yet, the study of the MSG remains financed and driven by its ability to store fluids underground.

During the 21st century, to address the challenge posed by global warming and climate change, salt also appears as one of the best geological media for geological storage of gas. This is because of: (i) its negligible porosity which ensures sealing to most fluids and gases and (ii) its visco-plastic creep deformation that allows salt to tolerate high levels of strain without developing structural damage and self-healing of cracks and faults (Costa *et al.*, 2015, 2020; Goulart *et al.*, 2020). Depleted oil and gas reservoirs can be re-cycled for CO_2 storage, hereby offsetting carbon dioxide emissions of offshore oil and gas production (Costa *et al.*, 2020). These properties that make salt a good seal are also responsible for the main risks encountered when drilling through salt. For long-term underground storage projects salt's mobility can endanger the reservoir's integrity: rising salt diapirs and gravity-driven gliding can deactivate the trap or trigger operational problems, such as stuck pipe and casing collapse (Costa *et al.*, 2010). Within the IODP 2013-2023 science plan, understanding the properties and processes that govern the flow and storage of carbon in the subseafloor is considered as one of the area of interests for which a scientific ocean drilling proposal could be submitted (Bickle *et al.*, 2011). Borehole experiments are needed to measure key subseafloor physical properties that control fluid migration (e.g., permeability, porosity, fracturation, storage properties, microbial processes) and assess the impacts of CO2 injection (see House *et al.*, 2006; Goldberg, Takahashi and Slagle, 2008; Kelemen and Matter, 2008).

Today, the exploration of the deep Mediterranean subsurface and the MSG remains dominantly driven by the exploration of oil and gas. Unlike other salt-

bearing basins (e.g., Gulf of Mexico, Atlantic margins), oil and gas production and exploration is not so important in the Mediterranean Sea (Kostianoy and Carpenter, 2018). Throughout the 20th century, oil and gas related activities were focused in the western Adriatic Sea (Italy), the Aegean Sea (Greece) and the Gulf of Gabès (Tunisia and Libya; Figure 8). But in 2010, after successful discoveries in the eastern Mediterranean, the Levant Basin and the Nile Delta Province were estimated to held 3.5 billion barrels of recoverable oil and about 381 trillion cubic feet (tcf) of recoverable gas, over 5 percent of the world's gas reserves (Kirschbaum *et al.*, 2010; Schenk *et al.*, 2010). The discovery of the Israel's Leviathan gas field in 2010 (22 tcf) and the Egypt's Zohr gas field in 2015 (30 tcf) confirmed the presence of some of the world's largest offshore fields in the Eastern Mediterranean (Zhang *et al.*, 2019). The location of these gas fields, adjacent to Europe, makes them strategic for the Europe Union in order to diversify their import sources of gas (Shin and Kim, 2021). The Zohr gas field evidenced the existence of isolated carbonate buildup reservoirs capped by Messinian salt, provoking a paradigm shift in East Mediterranean Exploration (Cozzi *et al.*, 2021). This focus in exploration can be seen as a major opportunity for the MSC researchers community; several studies presented major insights on the MSG and the MSC by using the borehole data of recent industrial wells (e.g., Gvirtzman *et al.*, 2017; e.g., Manzi *et al.*, 2018; Meilijson *et al.*, 2018, 2019) and high-resolution 3D seismic data (e.g., Bertoni and Cartwright, 2006; Bertoni, Cartwright and Hermanrud, 2013; Gvirtzman *et al.*, 2013; Kartveit, Ulsund and Johansen, 2019; Madof, Bertoni and Lofi, 2019).
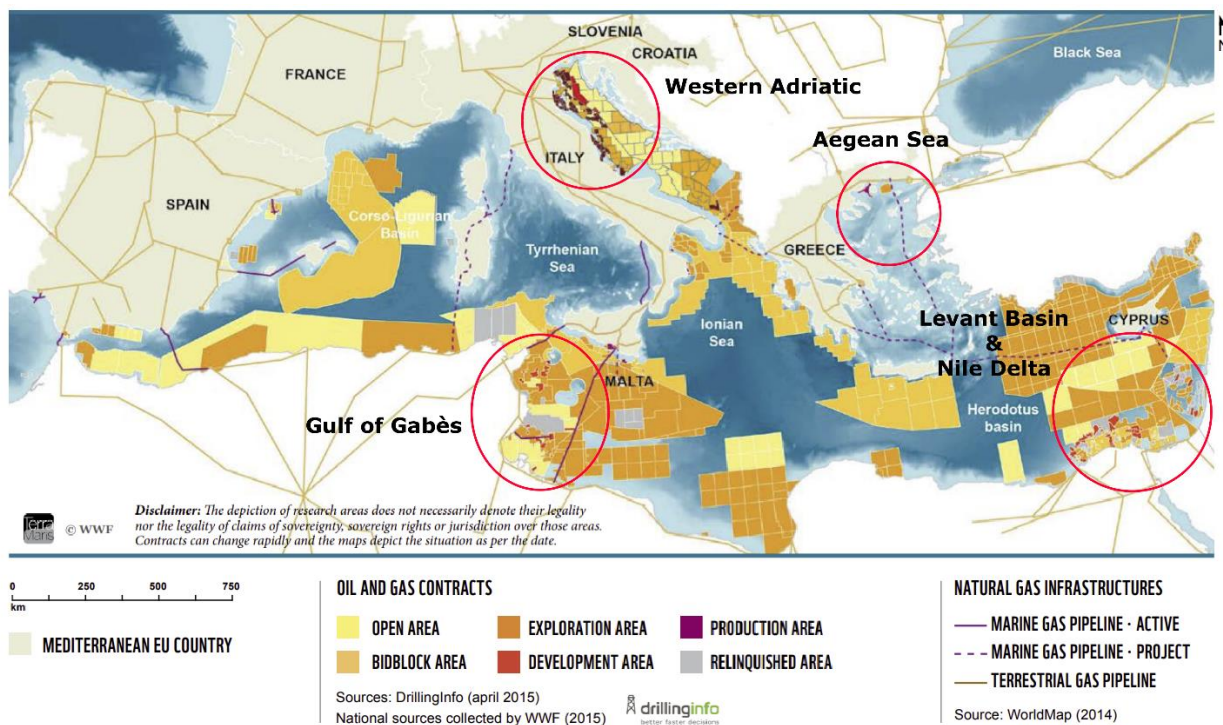
Figure 8 Offshore oil and gas exploration and production contracts and active and projected gas pipelines in the Mediterranean Sea in 2015 (modified from Piante, Ody and Roberts, 2015)

Paradoxically, the sudden attention to oil and gas exploration in the Mediterranean also proved to play in disfavour of the MSC community, by increasing public concerns on preserving the marine environment (Martínez-Rius and Herran, 2022). In 2016, a scientific marine geophysical survey designed to support the IODP proposal 857B in Spanish waters (Deep-Sea Records of the Messinian Salinity Crisis; DREAM; Lofi *et al.*, 2017) was prohibited. The controversy arose because it was perceived as an oil industry ploy to undertake hydrocarbon exploration activities in the Mediterranean, under the guise of scientific research (Martínez-Rius, 2022). Consequently, long-time prepared scientific data acquisition projects are nowadays still on hold or cancelled, and the MSC controversy remains unanswered. In addition to this, guidelines for site survey and safety of IODP proposals considers the potential presence of hydrocarbons as a main hazard that would seriously hinder the feasibility of IODP drilling (Graber, 2006). The presence of evaporites, diapirs, flowing fluids, gas hydrate zones, and any seal below which hydrocarbons may be trapped or where overpressured zones may be present, is considered as a main hazard in scientific ocean drilling with respect to pollution prevention and safety. Consequently, an IODP proposal targeting the drilling through the MSG should display a careful and in-depth study of these geological and social aspects to convince of the feasibility of the drilling.

1.1.4 Hazards related to drilling operations through salt

There are three main hazards associated with drilling operations through the MSG, and salt in general (Figure 9):

i.   the potential presence of microbially-generated hydrogen sulfide ("sour gas") within the extracted fluid (Machel and Foght, 2000): hydrogen sulfide is a hazardous toxic and corrosive gas that must be monitored and removed before gas can be commercialized;

ii.   instability of the drilling hole. The creeping movement of the salt or the dissolution of halite by circulating fluids can cause damage to the well during the drilling or during the production/injection life of the well (Dusseault *et al.*, 2004a; Weijermars and Jackson, 2014);

iii.   the presence of overpressured zones beneath the impermeable salt layers, with the risk that drilling could cause a blowout at the well-head (Luo *et al.*, 2015).

Whether it is for fossil energy extraction or geological capture and storage of fluids and gas, drilling through salt layers requires a precise knowledge of the subsurface to guarantee the project's safety and sustainability. Understanding the cause and nature of salt deformation and associated fluid flow is critical for mitigating the risks associated with drilling in salt-capped reservoirs, for guaranteeing the sustainability of long-

term underground fluid storage, and for the evaluation of potential related geohazards (e.g., salt-related landslide-induced tsunamis).
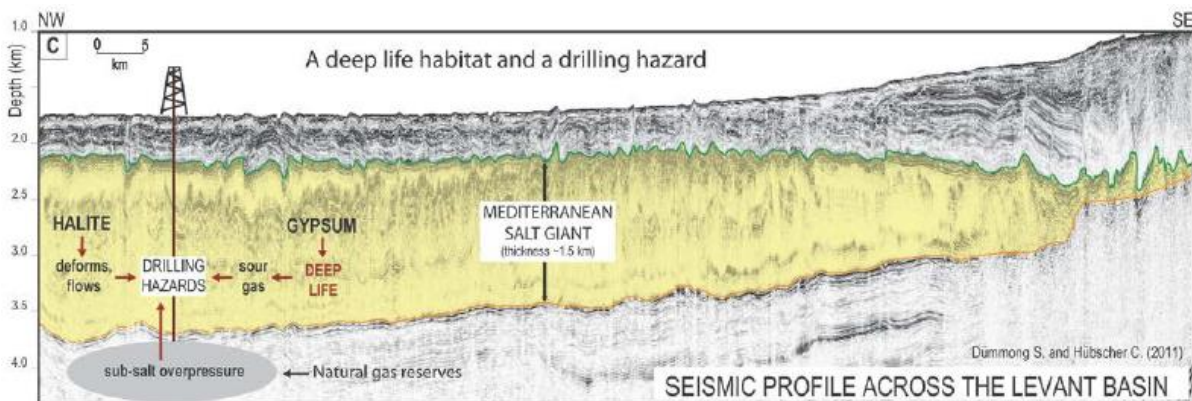
Figure 9 Interpreted seismic section across the Levantine basin showing the risks link to drilling through and around the Messinian Salt Giant (from EUROPEAN COMMISSION Research Executive Agency, 2017).

One of the main concerns is the potential presence of zones of high overpressure within the evaporites and throughout pre- and post-evaporites sequences. Salt is a viscous, low density, high velocity, and impermeable material that creeps under differential stress as a function of differential loading (Dusseault *et al.*, 2004b, 2004a). Around and below salt, a wide range of stress and pore pressure conditions can be encountered, including zones with open fractures, overpressured fluids or unusual horizontal stress regimes (Dusseault et al., 2004a). This can cause borehole closure through creep within the salt, borehole instability when exiting salt or in cases of sharp stress gradients or lithology contrasts, lost circulation, or sudden transition to overpressure beneath salt that could lead to a blowout at the well-head (Desbrandes, 1994; Farmer *et al.*, 1996; Dusseault *et al.*, 2004b). A wellhead blowout is a serious hazard to the environment because it would cause hydrocarbon spilling, which would have dramatic consequences in an environment as vulnerable as the Mediterranean Sea. This hazard is of paramount importance for IODP proposals in the absence of drilling riser to the surface, return circulation, or blowout preventers on the *JOIDES Resolution* (Graber, 2006)*,* automatically excluding the possibility to drill through the MSG with this ship, except if the absence of overpressured zones can be demonstrated. Conceptual models of stresses and material behaviour can be used to evaluate risks linked to the salt movement and the zone of overpressure. These models must account for many parameters such as the geological history of the salt structure emplacement, estimations of the pressure and temperature distribution in the sub-surface, or fracture pressures in non-salt rocks (Dusseault *et al.*, 2004a). The reliability of these models depends notably on our understanding of the processes of sub-salt overpressure development and the salt flowing behaviour in these systems.

Fluid flow and overpressure have been previously studied in Mediterranean, evidencing a high risk of overpressure development both in the

shallow and the deep sediments (Revil, 1999; Bertoni and Cartwright, 2015; Arab *et al.*, 2016). Recent models suggest that the rapid evaporite loading during the Messinian Salinity Crisis caused high overpressure within Messinian evaporites and the pre-Messinian sediments (Ducros and Nader, 2020; Dale *et al.*, 2021), thereby questioning the feasibility of drilling operations through the MSG without an adapted drilling rig. Locally, the development of overpressure also led to the fracturing of the salt, creating migration paths to the post-evaporitic overburden for hydrocarbons, where dissolution and seepage pipes are documented (Bertoni and Cartwright, 2015; Eruteya *et al.*, 2015; Cartwright *et al.*, 2018; Ducros and Nader, 2020; Dale *et al.*, 2021). These structures are an additional risk for drilling operations and question the ability of the MSG for storing fluids and gas. Studies of intrasalt structure in the eastern Mediterranean also evidenced brittle deformation and strain partitioning within the MSG that can affect the wellbore stability within the MSG, in response to the gravitational forces driving deformation (Feng, Steinberg and Reshef, 2017; Evans and Jackson, 2021). These studies highlighted that drilling through the heterogeneous MSG really is a hazardous operation that requires an in-depth understanding of the salt behaviour.

1.2 Objectives of the thesis

In the framework of the SALTGIANT ETN, this thesis aims to contribute to our understanding of the MSG and the related MSC, to investigate the factors controlling salt tectonics of the MSG, and to support safe offshore drilling proposals. The initial objective was to identify and classify salt structures in different geological environments of the Mediterranean basin. This was supposed to include a collaboration with ESR 12 at the National Oceanographic centre (NOC; UK), for exploiting the produced velocity sections to predict pressure conditions within the subsurface. However, due to the COVID-19 restrictions, I could not consult high-resolution data in the central and eastern Mediterranean at ENI (Italy) and I never went to the NOC. Based on the data at my disposition, I decided to focus my work on one of the area that was the less understood in the western Mediterranean: The Algerian basin.

1.2.1 Improving the resolution and the penetration of seismic images

The controversy surrounding the MSG and the MSC are related our lack of data on the composition of the offshore MSG (Section 1.1.1 and 1.1.2). To tackle this challenge, scientific drilling proposals of the MSG have been submitted to the IODP, but social, environmental, and political constrains are impending the realization of scientific data surveys (Section 1.1.3). Considering the difficulty and the costs for acquiring new data, the MSC community must explore new ways to investigate the offshore MSG and maximize the information they can extract out of legacy data.

Geophysical imaging is the most used method for exploring the offshore sub-surface. Reflection seismic methods plays a crucial role in the surveying of drilling operations by providing an image of sub-surface. Not only the location of the drilling is based on the accuracy of these images, but also it is used to build the models used for guiding and assessing risks associated with the drilling. But imaging the evaporites and the underlying sediments is not such an easy task, and most of the legacy academic data was acquired using old seismic acquisition techniques that are not well adapted to illuminate salt bodies (section 1.4.1). Yet, several studies showed that the application of modern processing methods, such as broadband processing and pre-stack depth imaging data, can successfully improve the quality of images from legacy data (e.g., Sargent, Hobbs and Gröcke, 2011; Chuan *et al.*, 2014; Tyagi *et al.*, 2016; Mahgoub *et al.*, 2017).

In Chapter 3, I develop a cost-effective reprocessing strategy to improve the seismic images of the MSG. To assess the value of the reprocessing, I also investigate if I can extract valuable new information on the MSG and the fluid flow out of the reprocessed datasets. To do so, I use legacy "dormant" public data acquired in the Algerian basin by the OGS. I design the processing flow by copying the strategies and the methods used in the industry. The goal is to design a robust and cost-effective reprocessing strategy, with velocity models accounting for the heterogeneity and internal structure of the MSG, to increase the resolution and the penetration of the final seismic images. At first, I have tried to apply this workflow using the Echos© software from Paradigm at the OGS. However, I have found it difficult to design a solid workflow with reliable quality check adapted to the software. This was also hindered by very limited computing power at the OGS (8 computing units). In 2020, just before the start of the COVID-19 pandemic, I have managed to find an agreement with Shearwater Geoservices for a free full license of their REVEAL© processing software for my research, at the University of Trieste. This was a game-changer in the strategy used for re-processing: not only the software was better fitted for the reprocessing strategy I was aiming for, but the Department of mathematics and geosciences of the University of Trieste donated a network of 64 computing units dedicated to my project. This allowed me to preform extensive testing on the parameters used for re-processing the data and in-detail depth-imaging I would have never been able to perform without such computing capacity.

1.2.2 Understand the evolution of the central Algerian basin salt system

Deciphering the tectono-sedimentary framework of salt basins is an arduous task because of the complex geometry resulting from salt tectonics. The structure of salt-bearing passive continental margins, such as the Gulf of Mexico (Diegel *et al.*, 1995; Peel, Travis and Hossack, 1995; Rowan, 2014)

and the south Atlantic margins (Marton, Tari and Lehmann, 2000; Hudec and Jackson, 2004; Kukla, Strozyk and Mohriak, 2018), is well-represented in literature thanks to their hydrocarbon prospectivity. But even in the most well imaged salt basins, there are still pending questions on factors controlling the style of the observed structures and their controls. The evolution of these old (i.e., pre-Cenozoic) and deeply buried salt giants can be puzzling because they typically experienced multiple phase of deformation, where one or several phases of deformation overprint the precursor structures (Warren, 2016). Because of its young age, the MSG is a unique field analogue for investigating early salt deformation within older salt basins. During its deposition, the paleogeography of the eastern and Mediterranean was relatively similar to the one we observe today (Figure 5), with a salt relatively uniformly deposited throughout the deep basins. The Mediterranean tectonic settings remained relatively steady until today, with north-westward regional shortening induced by the convergence between African and Eurasian plates (DeMets, Iaffaldano and Merkouriev, 2015). This suggests that salt structures of the MSG are hardly tectonically overprinted and can be considered as unique examples for studying early salt deformation. As such, salt deformation at the front Mediterranean collisional orogenic belts can provide a perfect field early-stage analogue for other salt-bearing orogenic fold-and-thrust belts.

In Chapter 2, I review the literature on the seismic expression of the offshore MSG and its salt tectonics. Then, using the newly produced seismic images that I describe in Chapter 3, I investigate the salt system in the central Algerian basin, which I suggest to be a good field laboratory for understanding early salt deformation in orogenic contractional settings. The objective is to assess why and when the salt start flowing, and how the intensity of salt-related deformation is distributed within the basin.

1.2.3 Fluid flow and mud diapirism in the central Algerian basin

Because of their low permeability, evaporites typically forms seal preventing fluid migration, which results in the accumulation of fluids in highly pressured rocks underneath (Warren, 2016). When planning the trajectory of am IODP drilling, areas and stratigraphic intervals containing fluids under greater than normal hydrostatic pressure should be avoided because of their common association with hydrocarbons and their tendency to cause blowouts (Graber, 2006; Section 1.1.4). A first assessment of the presence of fluid flow and overpressured zones can be done on seismic data, where they are observed by (Andresen, 2012; Bertoni and Cartwright, 2015): sand injection complexes, mud volcanoes, pockmarks, distorted or convoluted reflections, vertical or lateral amplitude anomalies (see previously mentioned studies for illustrations). Overpressure zones are also typically signalled by a decrease in interval velocities in the sub-surface.

Overpressured Mud volcanoes are abundant in contractional zones and areas with high sedimentation rates (e.g., accretionary complexes) and most often originate as a result of rapid overloading caused by structural or tectonic thickening (Dimitrov, 2002).

Mud volcanoes, deep sea pockmarks and gas chimneys are widespread in the Mediterranean (Figure 10) (Camerlenghi and Pini, 2009). Evidence of fluid circulation has been described in the Nile deep-sea fan and the Levant basin, along the Mediterranean ridge and the Calabrian trench, and in the Alboran basin (Camerlenghi *et al.*, 1995; Robertson, 1996; Kopf and Behrmann, 2000; Charlou *et al.*, 2003; Huguen *et al.*, 2004; Loncke and Mascle, 2004; Praeg *et al.*, 2009; Bertoni and Cartwright, 2015). Previous studies demonstrate that despite its low permeability, the MSG seal can allow pore fluid circulation, with gas exsolution caused by the base level drop, and disequilibrium compaction-related hydro fracturing due to high overpressure within the MSG and the underlying sediments (Bertoni and Cartwright, 2015; Eruteya *et al.*, 2015; Al-Balushi *et al.*, 2016; Zhang *et al.*, 2020; Dale *et al.*, 2021). Fluids can either migrate along salt-related extensional faults, escape from beneath the MSG and create mud volcanoes or dissolution craters (Bertoni and Cartwright, 2015). (Gradmann et al., 2005)

In the Algerian basin, circular flat-topped structures observed on the seabed were suspected to record the presence of mud volcanoes, by analogy with the other mud structures of the Mediterranean (Camerlenghi *et al.*, 2009). In the neighbouring Alboran sea (SW Mediterranean), there are large fields of pockmarks related to vertical and lateral fluid flow triggered by mid-Pliocene tectonically-driven diapirism of Lower Miocene shales (Sautkin *et al.*, 2003; Blinova *et al.*, 2011, 2011; Medialdea *et al.*, 2012; Somoza *et al.*, 2012). Models computed by Arab et al. (2016) and Dale et al., (2021) suggest high pore fluid pressure within and beneath the MSG, with potential gas emitting source rocks in pre-MSG sediments. This implies a high risk of overpressure beneath the MSG, with a potential source of overpressured shales similar to the ones observed in the neighbouring Alboran Sea. Along the Balearic margin, normal faults in the lower Pliocene and the UU have been interpreted as an overpressure-induced polygonal fault system caused by gypsum dehydration (Wardell *et al.*, 2014; Camerlenghi *et al.*, 2018) or by disequilibrium compaction-related hydro fracturing (Dale *et al.*, 2021). In Chapter 3, I use the reprocessed seismic images to assess the presence of fluid flow and mud volcanoes in the Algerian basin. In Chapter 4, I explore alternative interpretations of the aforementioned structures previously related to mud volcanoes or gypsum dehydration.

MUD VOLCANOES IN THE MEDITERRANEAN REGION
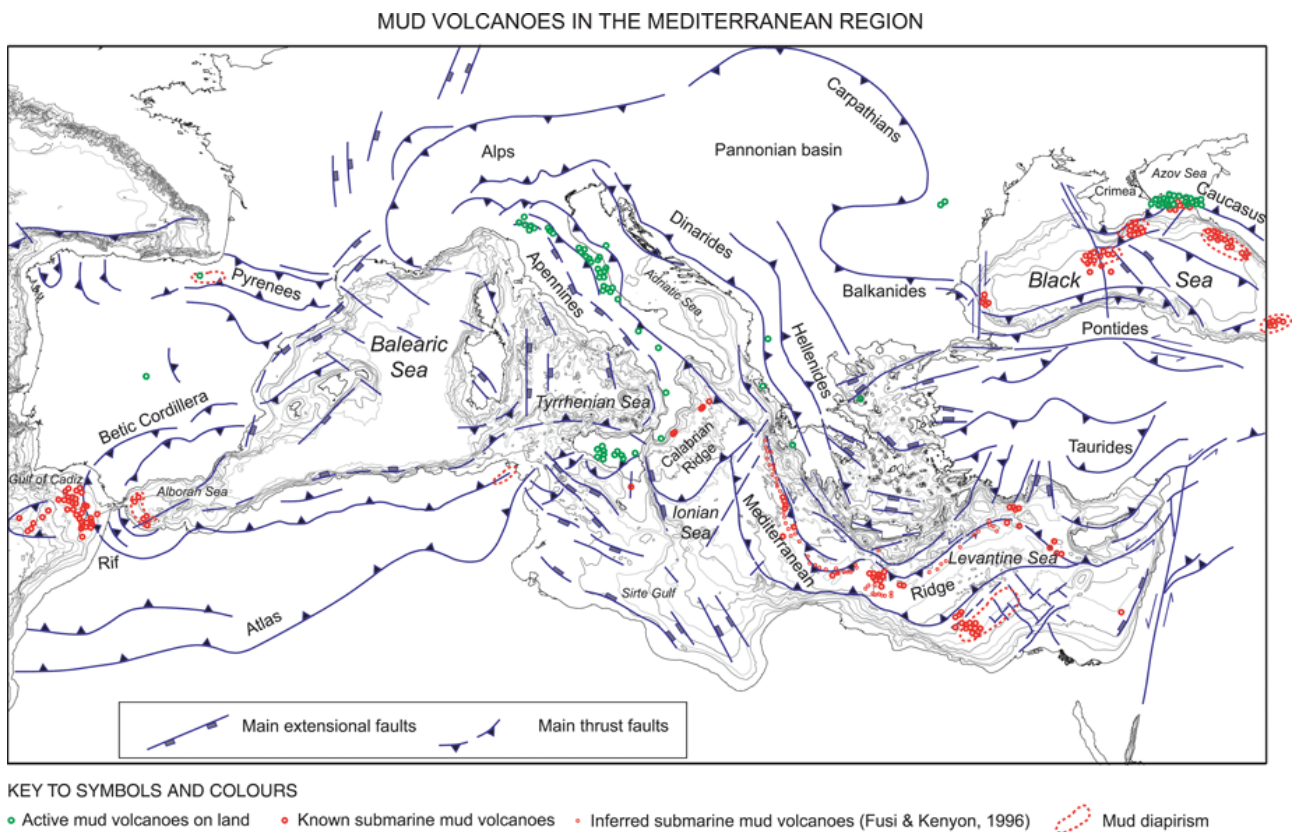
Figure 10 Distribution of mud volcanoes in the Mediterranean region (modified from Camerlenghi and Pini, 2009). The distribution of mud volcanoes is correlated with the Mediterranean ridges.

1.2.4 Summary

This thesis aims to address the following open questions in the field of seismic imaging of salt structures and salt tectonics applied to the MSG:

- Can we develop a robust and cost-effective strategy to reprocess legacy seismic reflection data?

- Is it worth investing time on reprocessing the legacy data? Does it provide new insights on fluid flow and on the salt tectonics of the MSG?

- What is the role of halokinesis in the structural and sedimentary development of a basin?

Acquiring offshore data is expensive and in the western Mediterranean, it has become more and more difficult to acquire new seismic data considering the environmental, societal and political constrains of the 21st century. It is therefore crucial to make the best use possible of the data we have. Seismic reflection data are fundamental tools for uncovering the controversy of the MSC and convince society and stakeholders of the safety of drilling operations. The overall objective of this thesis is to improve our knowledge of the MSG and salt basins through improved seismic imaging, to support the drilling through salt giants. Results should show an accurate knowledge of the salt structures geometry and their origin that contribute to our understanding of the salt-

related deformation of the MSG. To a broader extent, this study can also shed a new light on other salt basins, the MSC, and the geodynamics of the south-western Mediterranean basins.

1.3 Data

In this section I briefly present the data used during the thesis.

1.3.1 Multichannel reflection seismic

Figure 11 shows the location of the seismic lines used for this study. I distinguish between the data acquired and stored by the OGS (SALTFLU, SBAL-DEEP and MS) and the data consulted during the secondment at the Institut des Sciences de la Terre de Paris – ISTeP (MEDS and MAPS). The first category has been re-processed from the raw shot gathers during this work and is presented in more detail in Chapter 3. The second category of data were not reprocessed pre-stack because the raw field data is not available. They cannot be displayed within the thesis due to confidentiality agreements. They are all un-migrated post-stack data, with a low to medium signal-to-noise ratio. The data processing is unknown. Dominant frequency does not exceed 30 Hz at best, and their vertical is about 15 meters at best, in the shallowest and low-velocity sub-surface.

I also use the compilation of some of the main regional seismic stratigraphic markers throughout all the Western Mediterranean Sea published by Bellucci et al. (2021). It provides the interpretation, in two-way-time of the following horizons (Figure 12): i) Acoustic basement, ii) Base and Top of the MSG, iii) base Pliocene and iv) Seafloor. This compilation included our interpretations from SALTFLU and MS-046. The imported horizons were used as a guide for the interpretations and refined during this work on re-processed data. I also use the interpretations of the similar horizons on the SPIRAL profiles (Sismique Profonde et Investigation Régionale du Nord de l'ALgérie) from Leprêtre, (2012). This allows use to extend isochore surfaces to the Algerian margin, where there were no seismic data available for this study.

Color	Seismic Survey	Year	Provided by	Data used	Dominant Frequency	Resolution range
	SALTFLU	2012	OGS	PSTM and PSDM	60 Hz	6-25 m
	SBAL-DEEP	2005	OGS	PSTM	80 Hz	5-20 m
	MS-046	1972	OGS	PSTM	25 Hz	15-60 m
	MAP	1978	Data-Room	Post-stack migrated stacks	30 Hz	15-50 m
	MEDS	1976	Data-Room	Post-stack migrated stacks	30 Hz	15-50 m
	SH73	1974	Data-Room	Post-stack migrated stacks	30 Hz	15-50 m
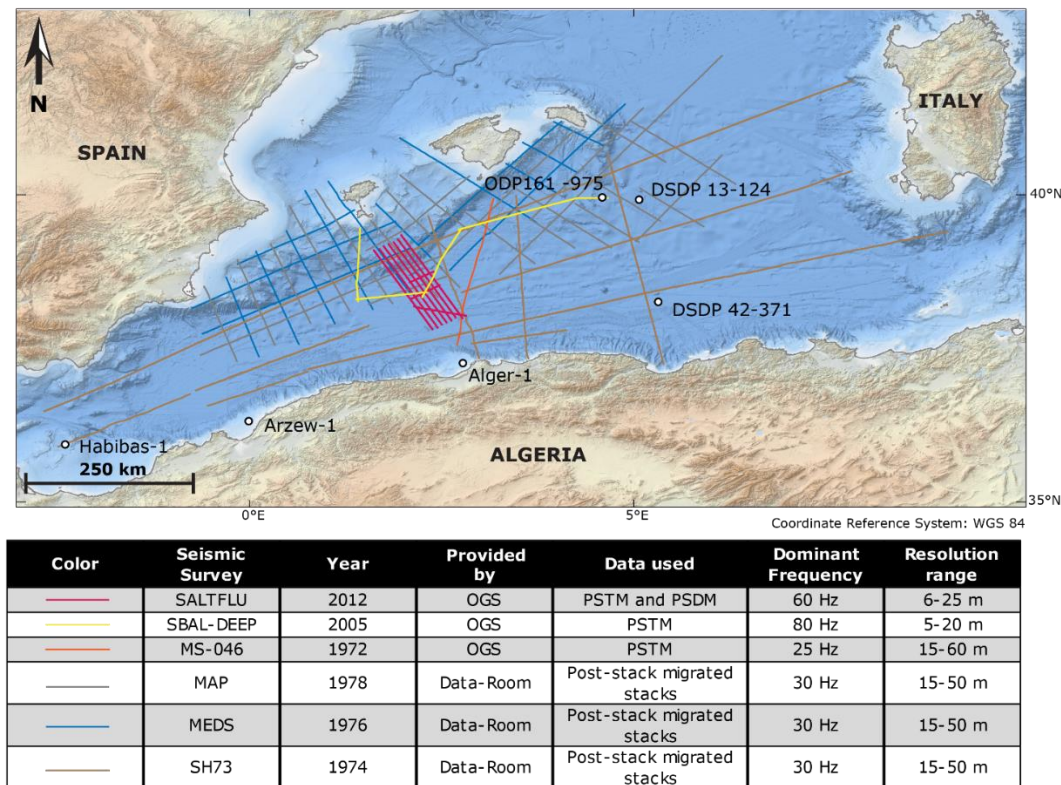
Figure 11 Map of the seismic dataset used in this study. The underlying table sums up their characteristics. The white dots represent the location of the boreholes described in section 1.6.3. The background bathymetry is the EMODnet 2020 bathymetric map (https://ows.emodnet-bathymetry.eu/wms).
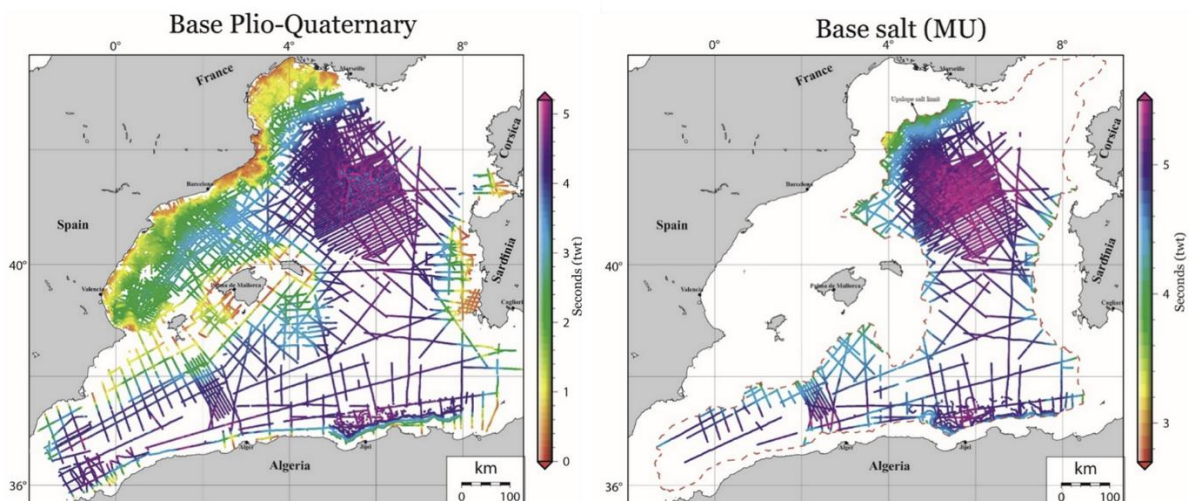
Figure 12 Base Plio-Quaternary (left) and Base salt (right) isobath map from Bellucci et al. (2021) **used to expand the isobath in this study. The NE Algerian margin interpretation comes from** Arab et al. (2016)**. Upslope salt (MU) limit is from** Bellucci et al. (2021a)

1.3.1.1   Other geophysical methods

I used the world gravimetry maps (Bouguer, isostatic and surface free-air; Figure 13) realized by the Bureau Gravimétrique International (Bonvalot *et al.*, 2012). I also use world magnetic map from Meyer et al. (2017). They allow the interpretation of structures larger than 5 arc-minutes (~6-10km). They are

used to constrain and extends the regional trends of the basement made and the crustal domains on seismic data (Find figure that explain anomalies).

Figure 13 World Gravity Maps 2012 (Bonvalot _et al._, 2012)
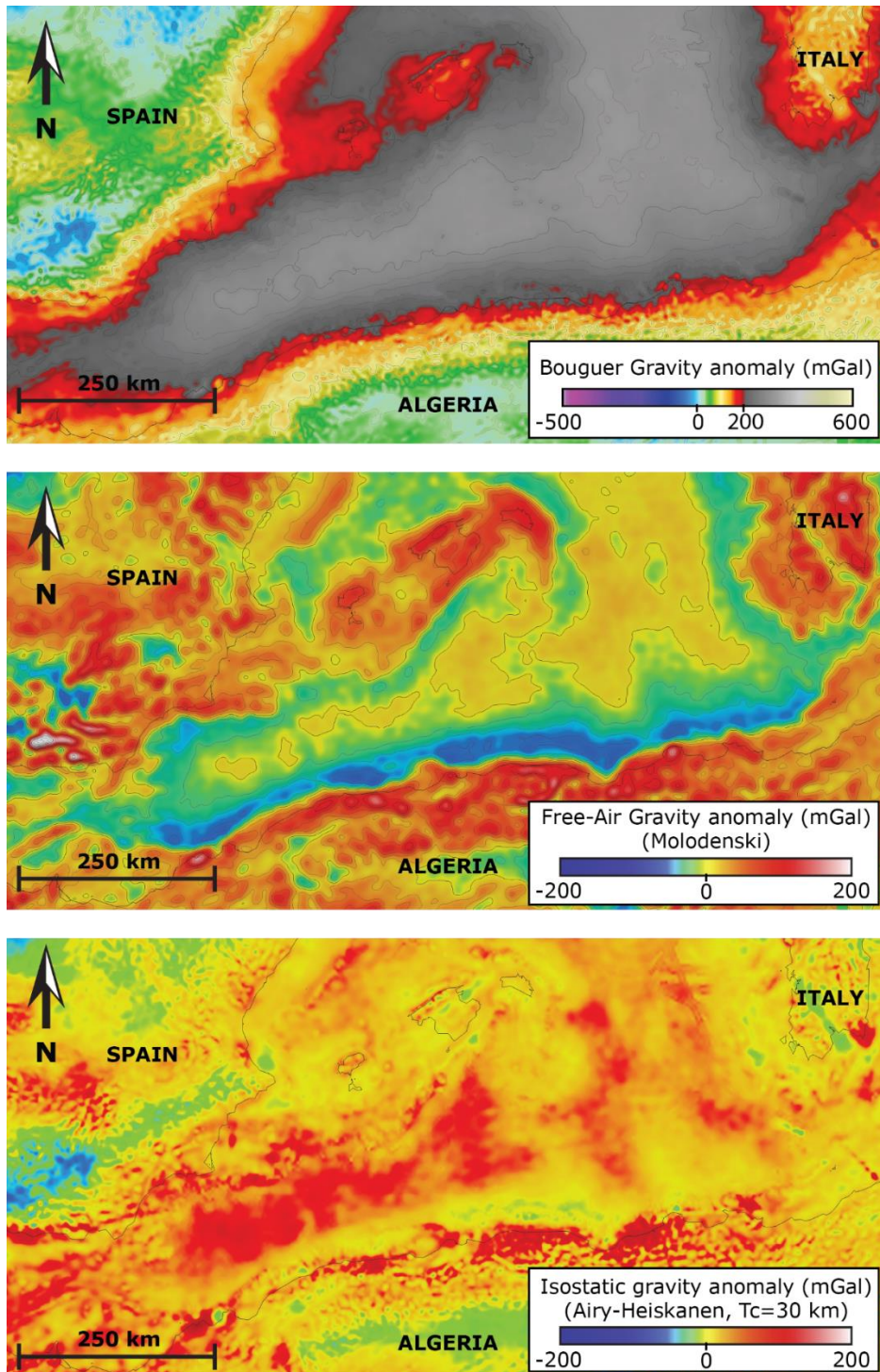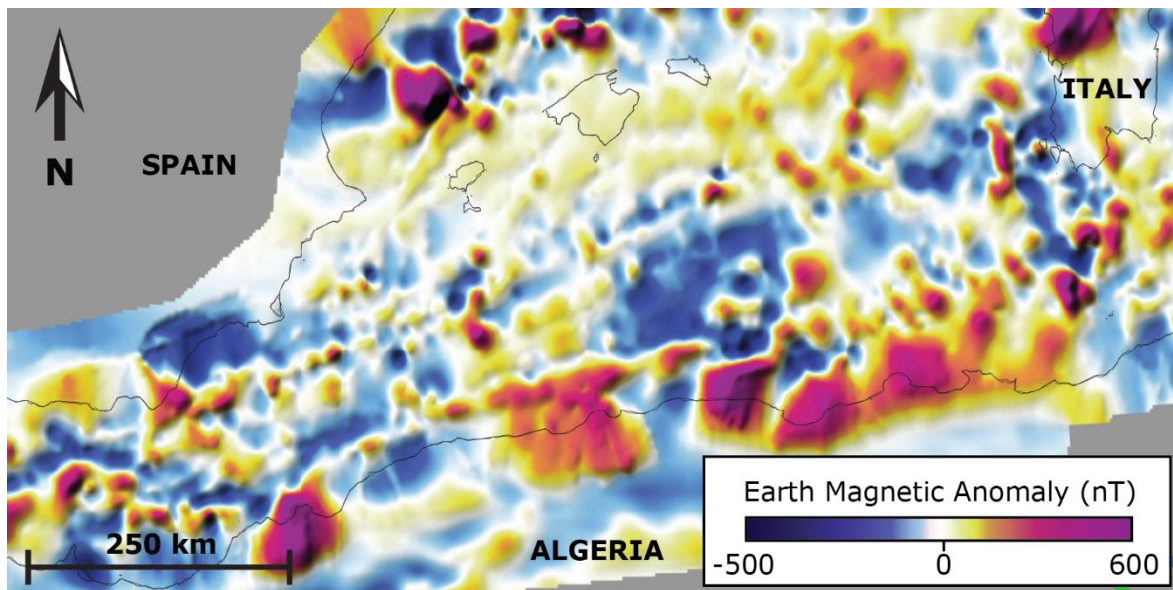
Coordinate Reference System: WGS 84 UTM 31N

Figure 14 EMAG2v3 Earth Magnetic Anomaly (Meyer, Saltus and Chulliat, 2017)

1.3.2 Seafloor imaging

I used the harmonised EMODnet 2020 Digital Terrain model (DTM; https://ows.emodnet-bathymetry.eu/wms). It already incorporates the multibeam bathymetry acquired during the SALTFLU and the SBALDEEP surveys, but with a grid resolution of 115x115m (Figure 15). The original multibeam data yield an original grid resolution of 50x50m (Figure 15). I use the original data during in-detail studies of the Formentera basin and the adjacent foot of the slope. It allows a better interpretation of the drainage pattern along the continental slope and the trend of the salt structures in the deep basin. For the computation of the regional isochore and thickness maps, I use the EMODnet grid.

1.3.3 Offshore borehole sampling

I used the summary of the borehole results published in litterature including (Figure 11): Habibas-1 (Medaouri *et al.*, 2012), Algers-1 and Arzew-1 along the Algerian margin (Burollet, Said and Trouve, 1978), ODP Site 975 (Comas *et al.*, 1996; Marsaglia, 1999) and DSDP site 124 (Ryan, Hsu, and et al., 1973) in the Balearic rise, DSDP site 371 in the Hannibal ridge (Hsü *et al.*, 1978). The wells on the Algerian margin were drilled through the whole Messinian evaporites but in intermediate or shallow depth basins where the mobile salt is absent. They do not provide good record analogue for the deep Algerian basin, but they could potentially be record analogues of the conjugated Formentera basin. The ODP and DSDP sites only sampled the top-most MSG and did not penetrate the mobile salt. They provide direct sampled

for the lithology of the uppermost Upper Unit in the Algerian basin. The results are summarized in Table 1.
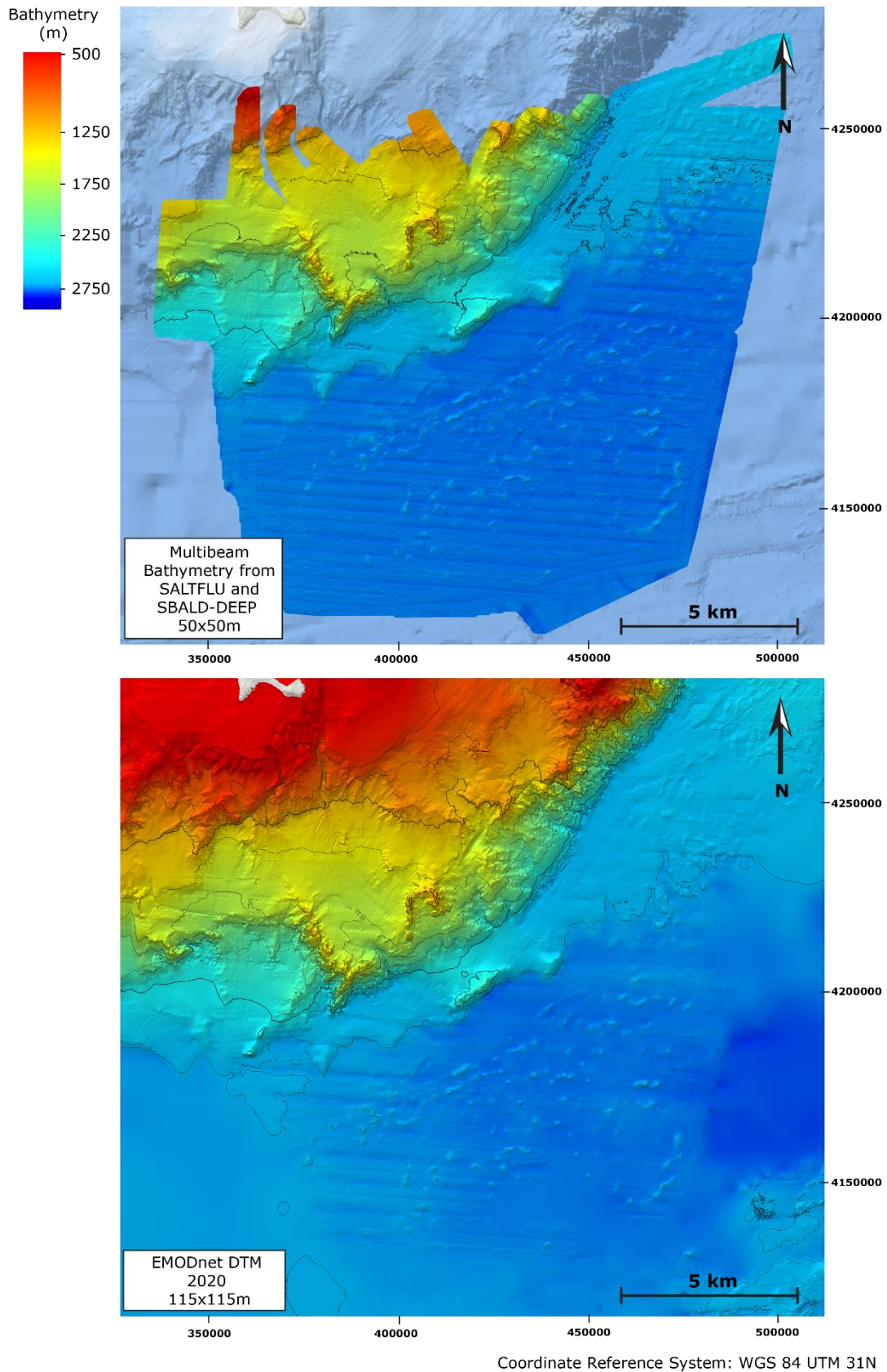
Figure 15 Bathymetry data used within this study. The original multibeam bathymetry reach a 50x50m resolution. The EMODnet yields a lower resolution (115x115 m) but covers the whole Mediterranean Sea.

33

Table 1 Summary of the borehole results in the Algerian basin (Hsü, Ryan and Cita, 1973; Ryan, Hsu, and et al., 1973; Burollet, Said and Trouve, 1978; Comas *et al.*, 1996; Marsaglia, 1999; Medaouri *et al.*, 2012)

	HABIBAS-1 (923m water depth)	ALGER-1 (100 meters water depth)	ARZEW-1 (127 meters water depth)	DSDP site 124 (2726 m water depth)	DSDP site 371 (2792 m water depth)	ODP site 975 (2415 m water depth)
Plio-Quaternary	Distal marls, clays, scarce interbedded sandstones (~1000m)	Sand and sandstone with marl intercalations (28 m, 137m below water bottom) shallow marine	Limestones with gray silty marl intercalations (153 m, 340 m below water bottom) Gray compact pyritic marls with reworked gypsum (49 m) Outer to deeper shelf	Marl/Mudstones nannofossil ooze with Turbidites and contourites (359 m) Open marine	Calcareous muds to mudstones, with nongraded and graded sandy beds and laminae (539 m) Open marine	Nannofossil to calcareous clay and silty clay and nannofossil ooze with local organic-rich layers (~305 m) Open marine
Messinian	Shallow_water siliciclastic or carbonate facies, with occasional gypsum and anhydrite intervals, rich OM (~1250 m)	Gray plastic marls, slightly gypsiferous, rich in planktonic foraminifera (176m) Outer shelf environment	Massive gypsum with rare marl intercalations (129 m) Gray marls and clays with some gypsum intercalations. Rare Pyroclastic material (ignimbritic) (147 m)	Layers of dolomitic marls, Organic and pyrite rich layers, anhydrite (63.2 m) Sabkha and lagoonal deposits	Thin calcareous sands (6m) Layers of dolomitic mudstone, more or less sandy/silty, and anhydrite Sabkha and lagoonal deposits (5 m)	Layers of micrite, micritic silty clay, calcareous volcaniclastic sand, gypsum and gypsiferous chalk (~7 m) Intertidal
Tortonian	Sinterbedded sandstone , claystone, silty clay (turbidites), Volcaniclastic levels (~250 m)	Gray plastic marls, slightly gypsiferous (294 m) Outer shelf environment	Gray marls with fine intercalations of pyroclastic material (204 m) Outer to middle shelf			
Serravalian	Sandy and silty turbidites Undercompacted shales at the base (1000m)	Gray plastic marls with fine limestone intercalations (427 m)				
upper Langhian to Serravallian		Calcareous Marls (121 m) Reworked volcano-clastics (12 m)				

35

Chapter 2

Review of salt tectonics in the Mediterranean

In this chapter, I present a succinct literature review on the seismic expression of the offshore MSG, the fundamentals of salt tectonics and the terminology used in this thesis, and the different salt systems of the Mediterranean.

1.4 Seismic expression of the Messinian Evaporites

1.4.1 Problems and pitfalls of reflection seismic methods for imaging the MSG

Salt basins are notoriously difficult places to explore because of the traditionally poor subsurface images around and below salt (Leveille *et al.*, 2011). Seismic imaging of evaporite bodies is challenging because of the steep, complex shapes of the salt bodies and the strong acoustic impedance contrast at the evaporite-sediment interface (Jones and Davison, 2014). This causes defocusing of the raypaths and complex wave propagation, with double bounces, turning-wave reflections and critical refractions (Hale, Hill and Stefani, 1992; Bernintsas, Sun and Sicking, 1997; Cavalca and Lailly, 2005). With conventional 2D acquisition methods, this results in illumination gaps where low primary signal is recorded. On the resulting images, this is expressed by a laterally disappearing base of salt and poor imaging of the evaporite-sediment interface (notably in case of allochthonous salt bodies or intra-salt sediments; Leveille, Larner and Higginbotham, 2005).

In the 2000s, significant improvements have been accomplished in the field of salt and subsalt imaging thanks to (Regone, 2006; Jones, 2008; Leveille *et al.*, 2011; Jones and Davison, 2014):

i) increasing computing capacities allowing an efficient use of accurate pre-stack depth imaging methods (e.g., full wave-form inversion and reverse-time migration; RTM)
ii) the development of new seismic acquisition techniques with far offset range (long cable length), multi-azimuth acquisition (e.g., wide and full azimuth acquisition), gun arrays with a low frequency content (3 to 7 Hz frequencies best penetrate salt bodies)
iii) New pre-processing methods (also arising thanks to increasing computing power) enhancing the low frequency content of the images (e.g., wide bandwidth processing, complex reverberations preservation)

There is little that we can do to compensate a poorly acquired conventional dataset, but we can try to investigate the feasibility of broadband reprocessing strategies and, where the quality of the acquisition and the computing resources allows it, the application of RTM approaches. RTM faithfully represents the propagation phenomena, handling both turning waves and multi-arrivals generated by the complex salt geometries and sharp velocity contrasts (Baysal, Kosloff and Sherwood, 1983; Farmer *et al.*, 1996; Jones *et al.*, 2007). It is not yet being used often for processing in academia, potentially because of its computing cost, a limited access to the RTM algorithms, and processors unfamiliarity with the specific processing that must be applied to preserve the lower part of the frequency band. New imaging strategies also

aims to account for spatial heterogeneity of the salt, leaving behind the homogeneous velocity salt layer assumption that can generate severe subsalt distortions (Haugen, Arntsen and Mispel, 2008). This is important to consider for the MSG because the presence of intrasalt complex structures and/or rapid velocity changes is proven in the Levant Basin (Feng and Reshef, 2016; Feng *et al.*, 2016), but it is difficult to include these velocity perturbations in our models if we only have a poor recording of the reflected 3D wavefield.

Except in the eastern Mediterranean, a wide range of seismic data in the Mediterranean consist of one direction/azimuth 2D-line acquired before the 2000s with narrow-azimuth and short-offset towed streamer. They poorly illuminate the complex geometry of the MSG, with coverage gaps in the subsurface resulting in poorly imaged data with greater noise content (Jones and Davison, 2014). The geophysical record of the MSG has been well investigated thanks to a good seismic coverage of the Mediterranean (Figure 16; Section 1.2), but studies are often limited to the definition of the main MSC seismic units (Figure 17a, b and c). Many uncertainties on the classification and the presence of some of the seismic units of the MSC (notable the LU) remain. In the Levant basin, driven by the discovery of new oil and gas resources, dense and high-resolution seismic data finally provided new insights on the nature and the tectonics of the MSG (Section 1.1.2 and 1.4; Figure 17d). By contrast, in the western and central Mediterranean Sea, 3D and high-resolution data are rare, and the seismic coverage is uneven (Figure 16, Figure 17a and b). Most seismic data consist of legacy data acquired and processed in the 20th century using narrow bandwidth processing, migrated post-stack (when migrated), where amplitude variations are not preserved. Typically, these legacy data poorly image the salt flanks, the pre-salt reflectors, the associated fault systems, and the indicators of fluids migration in the sedimentary sequence. Reprocessing these datasets could potentially provide brand new insights on the MSG and yet, there are not many studies that include the use of seismic data reprocessed using the methods (broadband processing, amplitude preservation, pre-stack imaging etc.). This could be due to a lack of access to these data, a lack of computing resources, or a lack of access to modern seismic processing and imaging algorithms in academia.
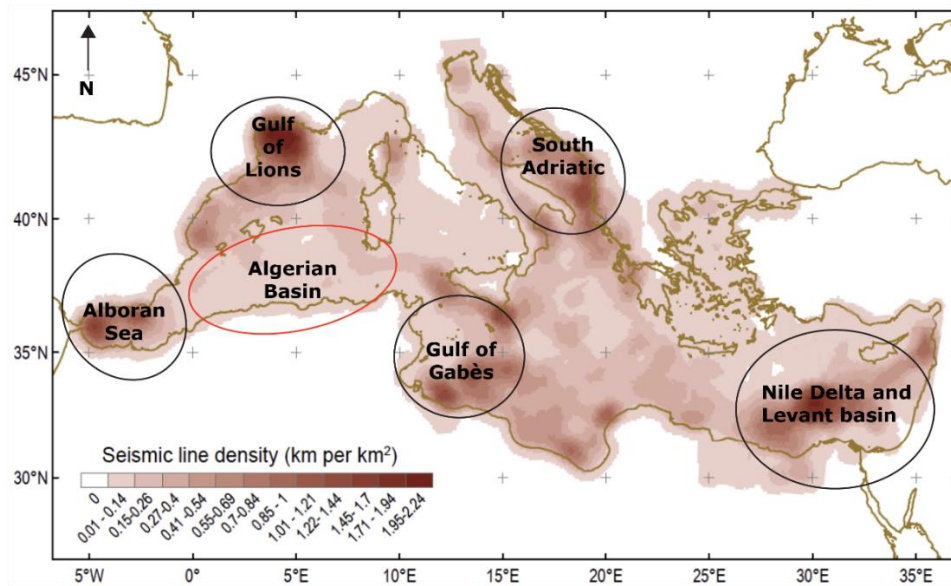
Figure 16 Approximated seismic data density (seismic lines/sq km) in the Mediterranean Sea (modified from Haq *et al.*, 2020). Black circles indicate region of high seismic density. The red circle indicate the underexplored Algerian basin studied in this thesis.

1.4.2 Seismic markers of the Mediterranean salt giant

Before describing the salt tectonics of the offshore MSG, I will present the seismic markers that are used to identify the seismic units of the MSG on seismic data (Figure 18). Throughout my work, I have based my seismic interpretations on the atlases of Lofi et al. (2011) and Lofi (2018) for the deep basins (e.g., Algerian, Liguro-Provençal, Ionian, Levant basins) and the recent study of Raad et al. (2021) on the Central Mallorca Depression for the intermediate depth basins (e.g., Balearic promontory, Valencia, East Corsica, Aegean basins). Detailed definitions and origins of these seismic markers can be found in the aforementioned atlas and study.

In the deep basins I used the so-called Messinian "trilogy" (Montadert *et al.*, 1970; Ryan, Hsu, and et al., 1973; Rehault, Boillot and Mauffret, 1984; Lofi *et al.*, 2011; Lofi, 2018). Based on the definition from atlases of the MSC markers (Lofi *et al.*, 2011; Lofi, 2018), it comprises (Figure 18, Figure 19):

- The Upper Unit (UU): High frequency and high amplitude reflections facies below the Plio-Quaternary and above the Mobile Unit (Figure 19a). It can be divided into a roughly bedded lower UU1 and a relatively well bedded Upper UU2, locally separated by an Intermediate Erosion Surface (IES) on the margins. Its top is bounded the by Top Surface (TS), conformable with the overlying Plio-Quaternary except along diapiric salt structures where it is an angular discordance. Towards the margins it becomes erosive or discordant (Top Erosion Surface; TES), with locally drainage pattern and valleys.
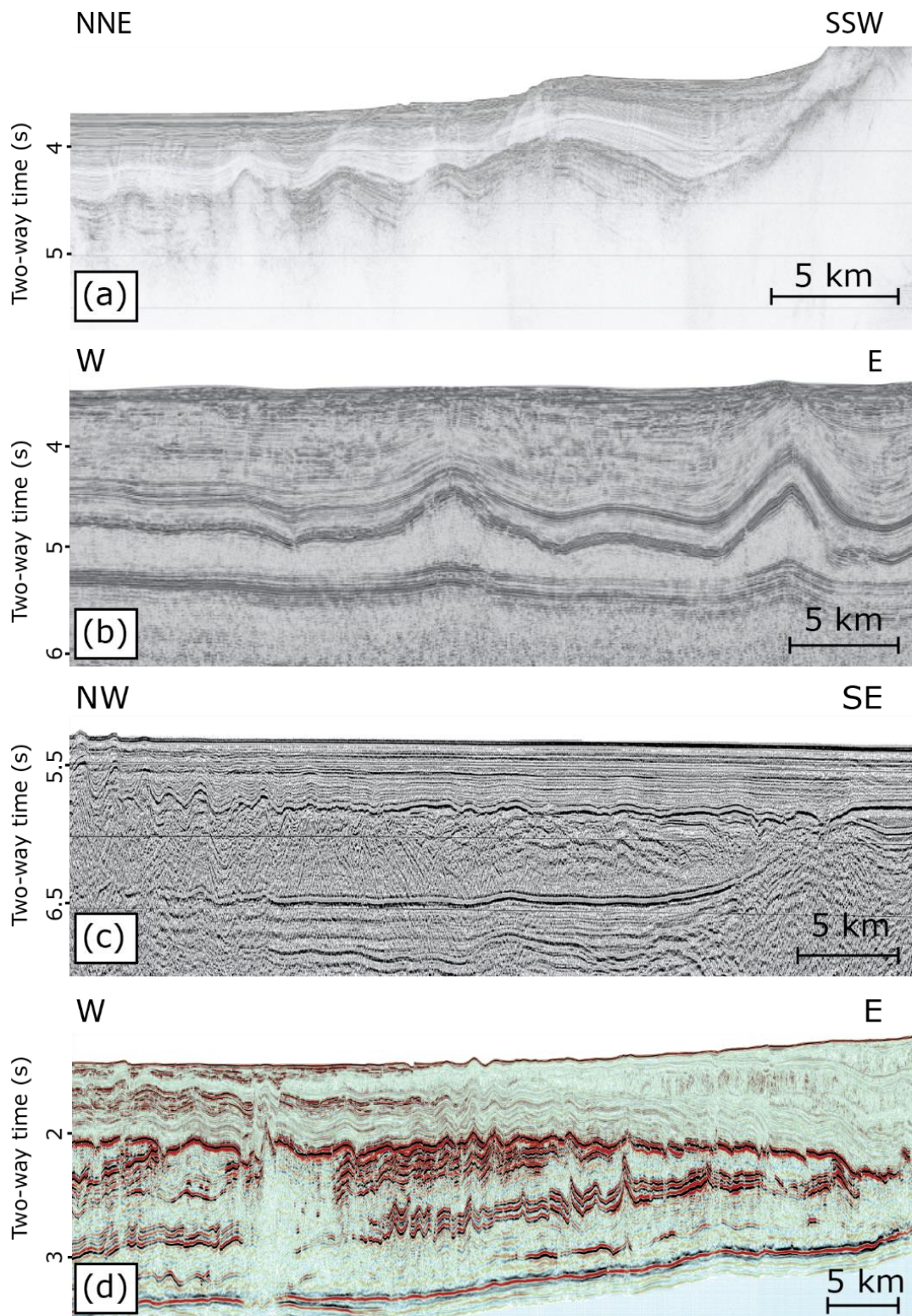
Figure 17 Various seismic sections throughout the Mediterranean showing the different quality and resolution of the seismic images (modified from Lofi, 2018 and references therein). (a) Migrated section of MDJ2-44 in the east Algerian basin, displaying a high resolution but a low penetration depth (b) Migrated section of MS-39 in western Sardinia, displaying a low resolution but a good penetration depth (c) Un-migrated section of Archimède-23 in the Ionian basin, displaying a low resolution but a good penetration depth. (d) Pre-stack migrated section from a 3D survey in the Levant basin, displaying a very high resolution (~6 m) and a good penetration depth.
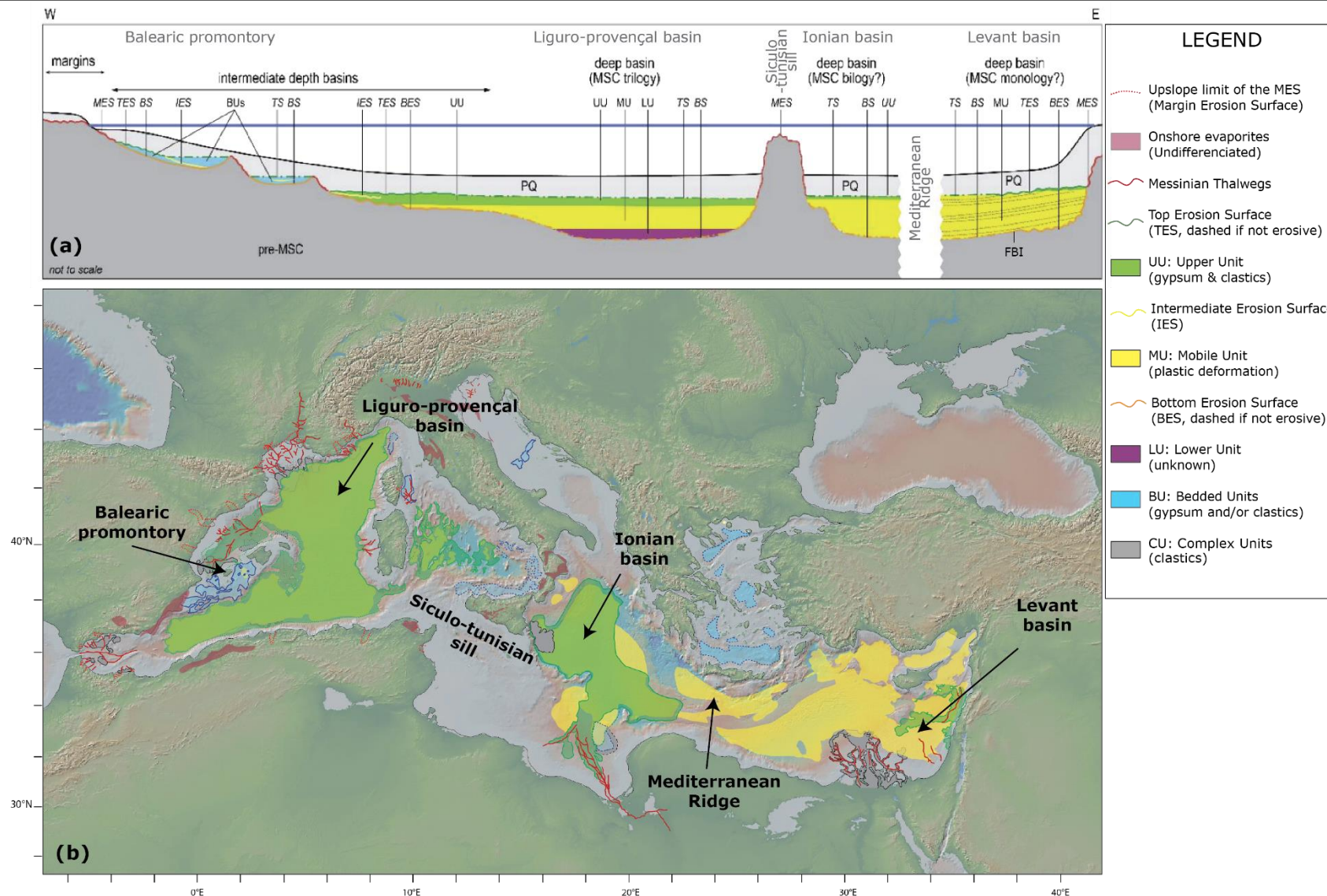
Figure 18 (a) Schematic cross section of the Mediterranean basin illustrating the present day distribution of the offshore MSC markers (modified from Lofi *et al.*, 2011; Lofi, 2018). (b) Relief map of the Mediterranean area (http://www.geomapapp.org, (Ryan *et al.*, 2009)) with the present-day spatial extent of the Messinian Salinity Crisis markers, excluding the Lower Unit (modified from Lofi *et al.*, 2011; Lofi, 2018).

It is made of clastics and evaporites that could be equivalent to the stage 3 Upper Evaporites. In the Levant basin, the UU is not widespread. Some authors suggest that it is recorded by vast fluvio-deltaic clastic deposits at the mouth of major Messinian rivers (Bowman, 2012; Radeff *et al.*, 2017; Madof, Bertoni and Lofi, 2019; Leila *et al.*, 2022). Elsewhere, the UU is absent: the stage 3 of the MSC is recorded by the topmost unit of the MU (unit 7), with its base bounded by the Intra-Messinian Truncation Surface (IMTS; Gvirtzman *et al.*, 2017);

- The Mobile Unit (MU): A highly deformed transparent seismic unit that may contain internal reflections (Figure 19a). Its base is commonly marked by a strong soft kick reflecting the strong acoustic impedance between the MU and the underlying units. Its top is conformable with the overlying UU except along intrusive diapiric structures. In the Levant basin, six distinctive internal units bounded by internal reflections (clastics and evaporites; Figure 19b) are defined within the MU (Netzeband, Hübscher and Gajewski, 2006; Gvirtzman *et al.*, 2013, 2017; Feng, Steinberg and Reshef, 2017). Its top is marked by the IMTS. It is considered to be predominantly made of ductile halite that could be equivalent to the stage 2 halite-rich unit onshore.

- The Lower Unit (LU): Low frequency, high amplitude and high continuity reflections seismic unit underlying the MU (Figure 19a). Its base is marked by the conformable Bottom Surface (BS) that can become erosive or discordant on the margins (Bottom Erosion Surface; BES), with gullied morphologies and a drainage pattern. It is absent in the eastern Mediterranean, where industrial wells evidenced the partial presence of a thin Foraminifer Barren Interval (FBI), that may record the onset of the MSC instead of the LU (Manzi *et al.*, 2018; Meilijson *et al.*, 2018, 2019; V. Manzi *et al.*, 2021). The LU could be an equivalent to the stage 1 PLG, but it has never been drilled in the western and central Mediterranean: its lithology and its Messinian age are speculative and it may contain a large part of clastic sediments (Lofi *et al.*, 2005; Bache *et al.*, 2009).

This "trilogy" can laterally pass into a chaotic, more or less transparent unit (the Complex Unit CUs), that is thought to represent clastics or mass transport deposits linked to the MSC thalwegs. In the proximal domains, along the upper margins and the steep slopes, the MSC is recorded only by the Messinian Erosion Surface (MES): an erosional or angular discordances, with subaerial drainage pattern topography and deep narrow incisions above pre-MSC deposits. Alternatively, some authors suggest that this is sub-aquatic erosion recording gravity flows or dense water cascading erosional flows (Lofi *et al.*, 2005; Roveri, Manzi, *et al.*, 2014; Lugli *et al.*, 2015; Vinicio Manzi *et al.*, 2021).
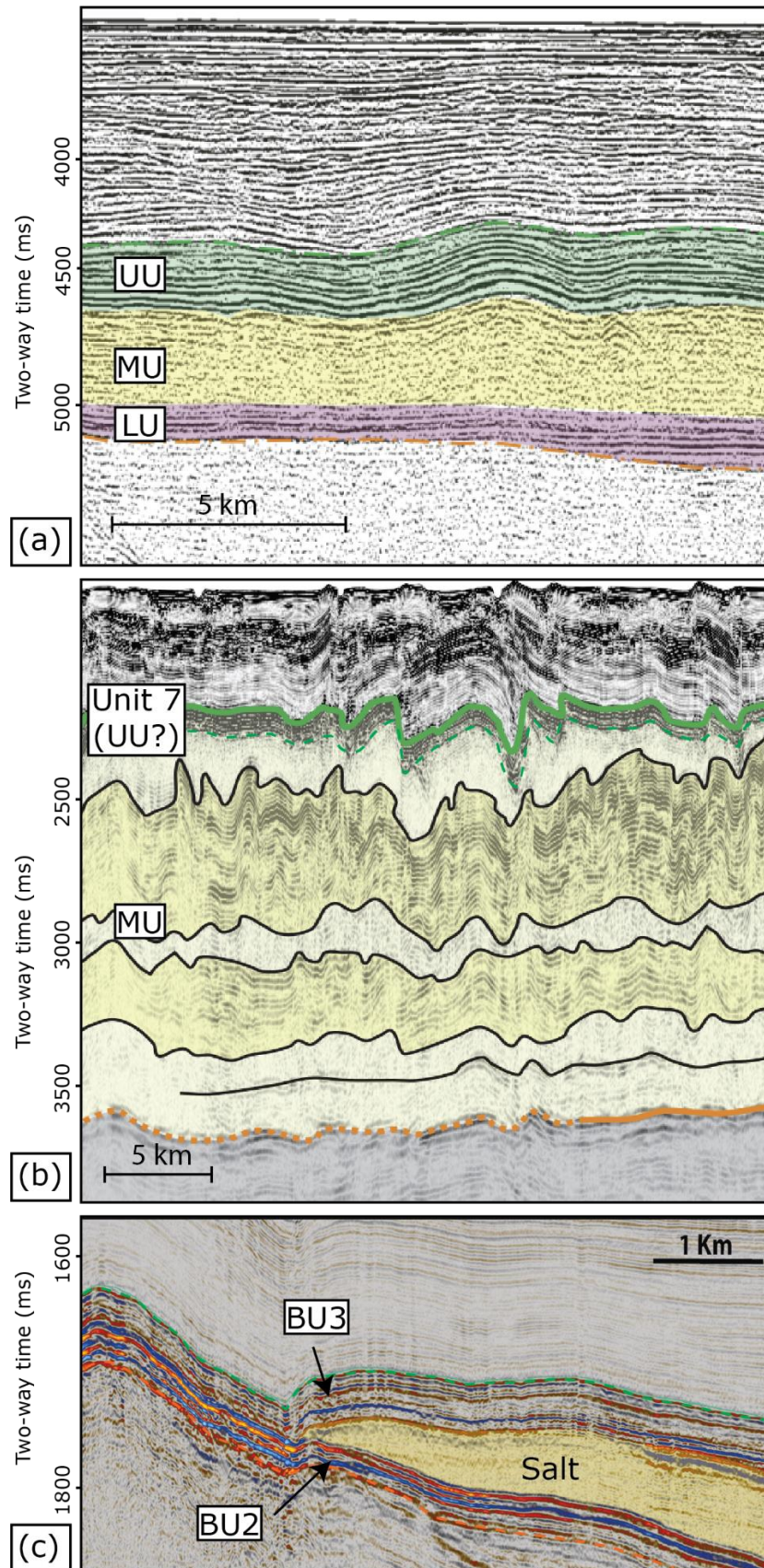
Figure 19 Seismic section of Messinian seismic records. (a) Section from the Gulf of Lion (West Mediterranean) showing the Messinian trilogy (UU: Upper Unit; MU: Mobile Unit; LU: Lower Unit; mofidied from Lofi et al., 2011). (b) Section from the Levant basin showing the Mobile Unit and the topmost Unit 7 that could be an equivalent of the stage 3 UU (modified from Lofi et al., 2011). (c) Section showing the Bedded Units (BUs), with the salt sandwiched between BU3 and BU2 (modified from Raad et al., 2021).

For the intermediated depth basins, I used the refined terminology of Raad et al. (2021) for the Bedded Units (BUs). They distinguish (Figure 19c):

- The BU3: low-to medium-amplitude, high frequency reflections conformably overlain by the Plio-Quaternary. Its base is marked by the IES   bounding above BU1/BU2 or the salt unit, or the MES. They interpret it as an equivalent of the Upper Evaporites.
- The salt unit: dominantly transparent with internal low-amplitude low-frequency continuous reflections sandwiched between BU3 and BU2. They interpret is as an halite-rich unit with K- and Mg-salts
- The BU2: parallel medium-to high-amplitude, relatively low frequency reflections, overlain conformably by the salt unit or by BU3. On the proximal zones its top is marked by an erosional surface. They interpret it as an equivalent of primary gypsum cumulates and clastics
- The BU1: medium to high-amplitude, relatively low frequency, bedded reflections unit overlain by the Plio-Quaternary or by BU3. Its top is marked by an erosive surface (TES or IES). It overlays the pre-MSC units. They interpret it as equivalent to the bottom growth selenitic PLG, as evidenced by nearby industrial wells on the Balearic promontory (Lanaja, 1987; Ochoa *et al.*, 2015).

Alternatively, one could have used the nomenclature of the offshore MSC records suggested by Gorini et al., (2015), with two megasequences:

- the Messinian Lower Megasequence (MLM), encompassing among others the LU and the CUs, composed by deeper evaporites and clastics deposits during the regression of the Mediterranean base level.
- the Messinian Upper Megasequence (MUM), encompassing the MU and LU units, composed by shallow water salt, aggradation sand and evaporites deposits during the lowstand and the transgressive rise of the Mediterranean sea level.

1.5 Salt deformation

The study of salt deformation aims to understand why, how, and when salt flows. Because of its mechanical weakness compared to other lithologies, salt deforms in a ductile way at the geological scale (Weijermars, Jackson and Vendeville, 1993; Jackson and Vendeville, 1994). Salt-bearing basins often display complex structures that influence the stress and strain distribution within the subsurface, presenting unique challenges for drilling operations (Section 1.1.4). Understanding salt kinematics and the factors that governs it helps determining the rules and the equations we use to model the salt movement and predict the subsurface properties (Weijermars and Jackson, 2014). These models are used to assess the objective and safest trajectory of

drilling to mitigate shear stress, and to guarantee the sustainable geological storing of gas and fluids.

In this chapter I present a succinct description of salt tectonics based on Jackson and Hudec, (2017). It does not aim to provide critical insights on salt tectonics. Instead, it aims to define the principles and the vocabulary I used to describe the salt structures and their evolution. This is followed by a brief overview of regional salt tectonics study of the MSG, before focusing on the Algerian basin, on which the work of my PhD is focused.

1.5.1 How salt flows

Halite-rich salt units are ductile rock that deforms like a viscous fluid on geological timescales (Ode, 1968; Jackson, Vendeville and Schultz-Ela, 1994). At this scale, salt deformation can be modelled based on laws of fluid dynamics and the Navier–Stokes equations, governed by the density and viscosity of the mobile salt unit, as well as the pressure and the shear stress in the medium (Nasir and Dabbousi, 1978; Woidt, 1978; van Keken *et al.*, 1993; Wagner and Jackson, 2011). Three principal types of deformation regime have been defined for salt (Figure 20) (Weijermars and Jackson, 2014; Fossen, 2016; Sarkarinejad, Sarshar and Adineh, 2018):

- the Poiseuille flow dominated by the pressure gradient and shear forces at its boundaries with a no-slip surface at the base and the top of the salt layer;
- the Couette flow dominated by the shear stress with a no-slip surface only at the base of the salt layer;
- a mixed of both (Hybrid flow) with a no-slip surface at the base of the salt layer.

At the regional scale, salt is frequently simplified as a single isotropic ductile layer primarily composed of halite (a one-layer model), following a unique dominant flow regime. But most evaporitic sequences, and the MSG in particular, are lithologically heterogeneous, anisotropic and multi-layered sequences comprising more brittle evaporitic or clastic lithologies (Cartwright *et al.*, 2012; Warren, 2016; Feng, Steinberg and Reshef, 2017; Rowan *et al.*, 2019; Evans and Jackson, 2021). Intrasalt layers will typically be more competent and brittle than halite, partitioning pressure and shear strain within the evaporitic sequence, and often decreasing the rate of lateral flow due to increased drag effects (Burliga, Koyi and Chemia, 2012). Typically, for the case of an overlying sliding overburden with a multi-layered salt unit, the salt layers above the basement will follow a Couette flow due to the induced shearing, but when the salt is not subjected to a gliding overburden the salt layers at the centre of the salt unit may follow a Poiseuille flow due to drag on the top salt surface (Fossen, 2016; Sarkarinejad, Sarshar and Adineh, 2018).
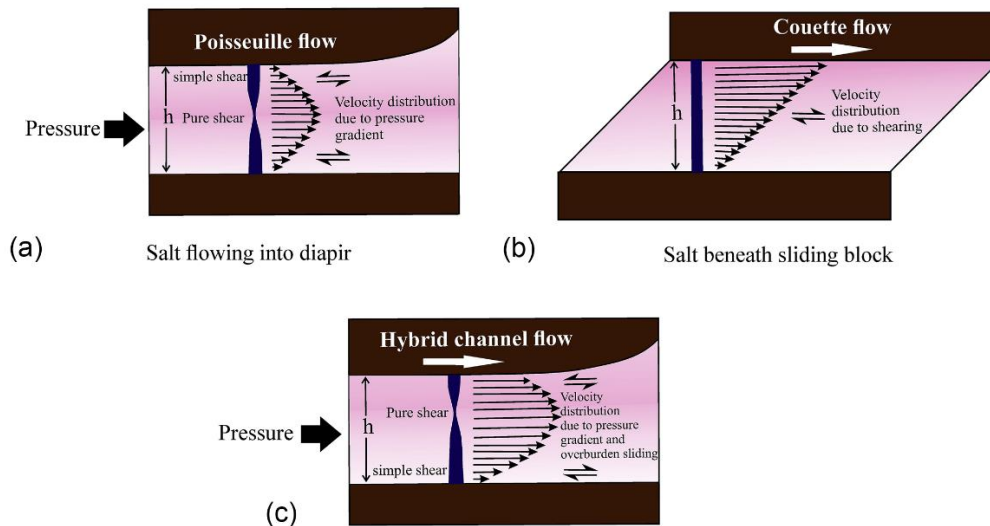
Figure 20 Idealized flow profiles through a salt sheet of width h. (a) Pure Poiseuille flow caused by pressure gradient within the salt, with maximum velocity at the center of the layer and no-slip surface at the base and top (b) Pure Couette flow caused by shear stress within the salt layer, with maximum velocity at the top of the salt velocity beneath sliding block and no-slip surface at the base. (c) Combination of Poiseuille flow and Couette flow, with maximum velocity in the upper salt layer and no-slip surface at the base (modified from Sarkarinejad, Sarshar and Adineh, 2018).

Advances in seismic imaging have unlocked new understanding on the intrasalt deformation and the structural evolution of layered evaporite sequences (Fiduk and Rowan, 2012; Raith *et al.*, 2016; Feng, Steinberg and Reshef, 2017; Rowan *et al.*, 2019; Evans and Jackson, 2021). However, the solely internal composition of the salt is just one of the many parameters that one must consider to understand and model salt deformation.

1.5.2 Why salt flows

Because salt is mechanically weaker than its encasement at the geological time scale, it readily responds to stress and accumulates most of the regional strain(Weijermars, Jackson and Vendeville, 1993; Jackson and Vendeville, 1994). Salt creeps primarily in response to differential loading: salt will flow away from areas where loading is the highest toward areas where it is the lowest (Hudec and Jackson, 2007). The strength of the overburden and the boundary friction at the edge of the salt rocks are the parameters inhibiting it. Three principal mechanisms of differential loading may act on a salt layer (Jackson and Hudec, 2017):

- Gravitational loading applied by the salt unit's weight itself and by the overburden.

- Displacement loading applied during tectonic extension, tectonic shortening or prograding sediments.

- Thermal loading caused by temperature changes. Higher temperatures cause salt expansion and increase its buoyancy.

Which loading is most important depends on the depth of salt burial, geometry of the salt body, tectonic setting, and thermal conditions of the salt. Gravitational loading can be subdivided into two sub-categories:

- Gravity spreading: when salt moves by sedimentary differential loading (Jackson and Talbot, 1986; Ge, Jackson and Vendeville, 1997; Vendeville, 2005)
- Gravity gliding: when the salt and its overburden slide down-dip an inclined base relief (Cobbold, Rossello and Vendeville, 1989; Demercian, Szatmari and Cobbold, 1993; Fort, Brun and Chauvel, 2004)

Many parameters drive and influence these mechanisms. Their relative role on salt tectonics is not easy to comprehend, yet is essential to correctly interpret salt kinematics and the resulting distribution of strain within salt basins. The key parameters include (Jackson and Hudec, 2017):

- The composition and the heterogeneity of the salt (Section 1.2.1).

- The competing syn-kinematic sedimentation and diapir rise rate. High rate of regional aggradation increases sediment loading on the salt, but if aggradation is too fast, it can also bury the diapirs under a stiff and thick overburden (Fernandez *et al.*, 2019).

- The thickness ratio between salt and overburden influences the wavelength and the amplitude of the salt structures (e.g., Hughes and Davison, 1993). If the salt is thin, the drag effects can resist salt flow and the salt supply can be quickly exhausted, slowing down diapirism.

- The pre-salt topography can facilitate gravity-gliding or inhibit lateral salt flow (e.g., Dooley *et al.*, 2017; Pichel, Finch and Gawthorpe, 2019)

- The presence of pre-kinematic salt-structures that will focus the strain (Hudec and Jackson, 2007; Duffy *et al.*, 2018)

- The regional geological setting (extension, compression, strike-slip) during and after the deposition of the salt generates lateral forces that can create new salt structures and/or rejuvenate pre-existing ones (e.g., Uranga *et al.*, 2022)

- The thermal gradient, that affects the density and the buoyancy of the salt, and potentially triggers thermal loading (e.g., Bellucci, Aslanian, *et al.*, 2021).

These variables are inter-dependant, highly heterogeneous in space and time, and it is expensive to collect enough data to measure their evolution accurately. For example, salt related structures can form highs blocking sediment transport, with lows accumulating syn-kinematic sediments in halokinetic minibasins (e.g., Venus, Mountney and McCaffrey, 2015; Hartley and Evenstar, 2018; Cumberpatch *et al.*, 2021; Uranga *et al.*, 2022).

Halokinetic sequences that form in minibasins around salt structures highs can provide insights on the complex interplay between salt rise, diapir geometry, roof thickness and sediment accumulation (Giles and Rowan, 2012; Pichel and Jackson, 2020). These new highs can in turn be eroded or provide substrate for reef development, increasing the sediment supply that loads the salt (e.g., Yohann *et al.*, 2016).

The time scale of these processes spans far beyond humans' range and many salt giants underwent multi-phase deformation, resulting in a mosaic of salt structures complicating the estimation of the significance of the key parameters that governed salt tectonics. This translates to a complex, and still debated, terminology for salt structures.

1.5.3 Salt structures terminology
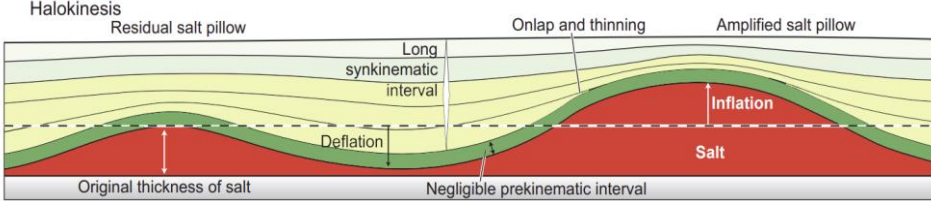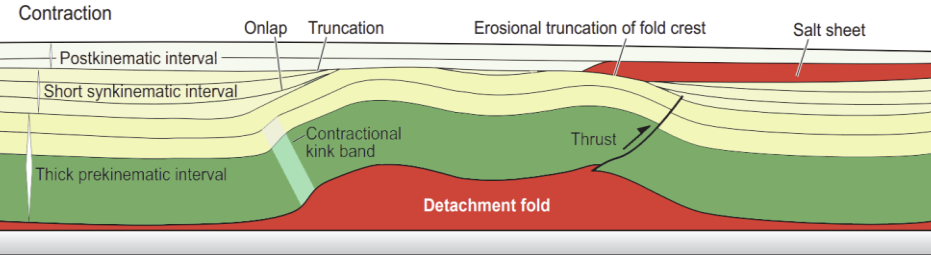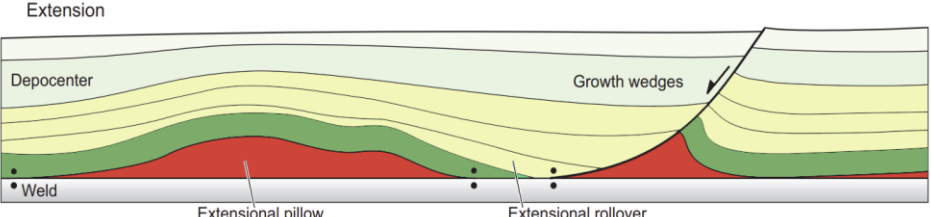
In the previous section, I described that salt flows principally in response to differential loading applied by gravitational and tectonic forces. Salt structures that result formed by the flowing salt are described in terms of shape (diapirs, turtle-back, canopied etc…), depth, heights, length, setting, and if we possess rock samples, composition. The type and the distribution of structure structures observed is an indicator of the intensity and the history of the salt-related deformation. In my work, the identification of salt structures is based on the classification and the terminology presented by Jackson and Hudec, (2017) and by Rowan and Giles, (2021).
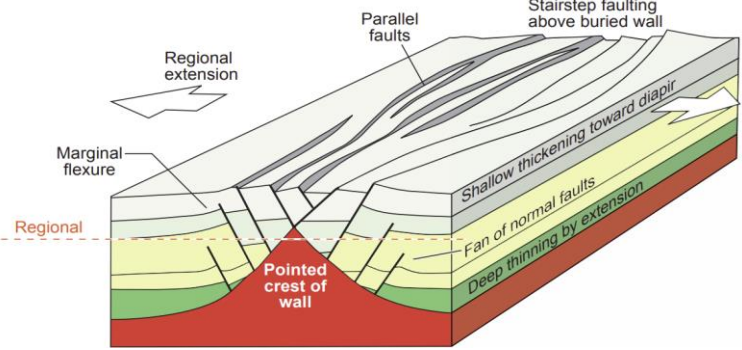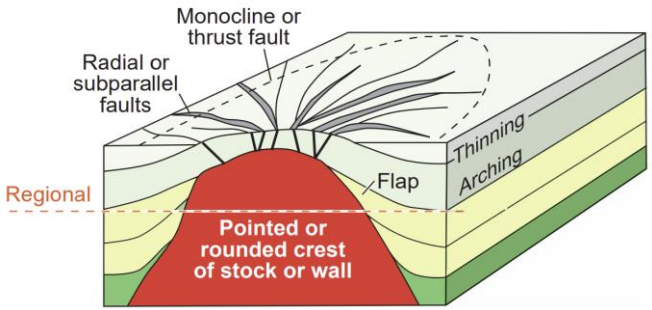
I distinguish between structures having a concordant contact with their overburden (salt pillows and anticlines) and those that don't (salt diapirs). Salt units that are resting above younger strata (i.e., Latest Messinian to present) are identified as allochthones salt sheets. Based on the salt structures identified, the thickness of the overburden and the deformation of the pre-salt basement, I then delimit zones of extension, contraction or strike-slip, and the transitional zones in between. Table 2 succinctly presents the terms used in Chapter 4. This is not an exhaustive glossary of salt tectonics, and some terms are still debated in literature.

1.6 Geological settings and salt-tectonic systems of the MSG
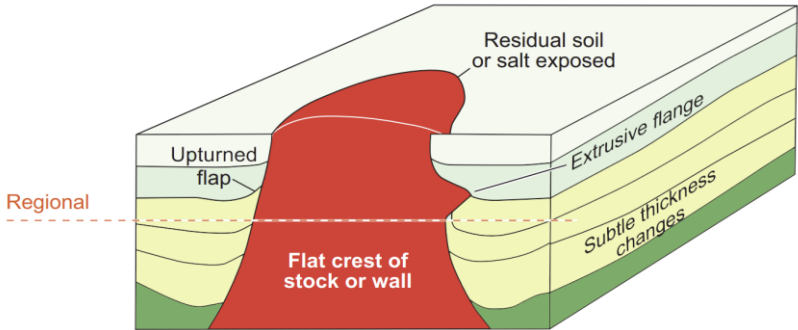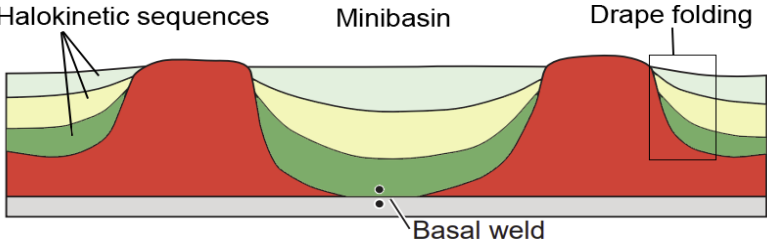
In this section, I aim to provide the tectonic context in which the MSG evolved (Messinian to present) and delimit the regions of extension, contraction, and strike slip. First, the terminology of the Mediterranean basins and the dynamics of the Mediterranean is briefly presented. I focus on the geodynamics of the southwestern Mediterranean because I did not study data in the central and eastern Mediterranean. Second, I present an overview of the salt tectonics of the Mediterranean. A more detailed description of the Algerian basin settings is presented in Chapter 4.
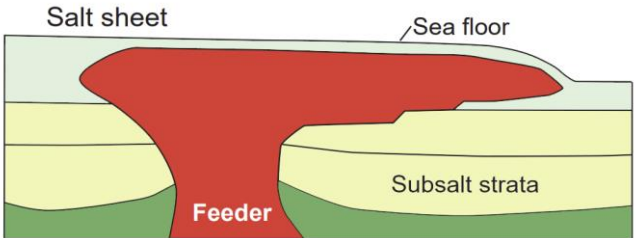
Table 2 Terminology, description and conceptual models of salt structures used in this study (modified from Jackson and Hudec, 2017; Rowan and Giles, 2021)
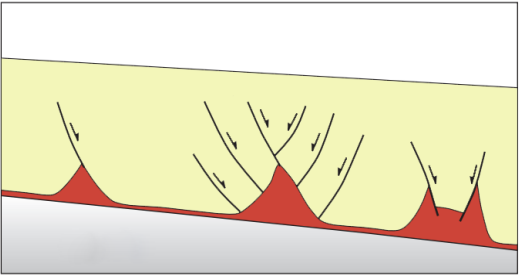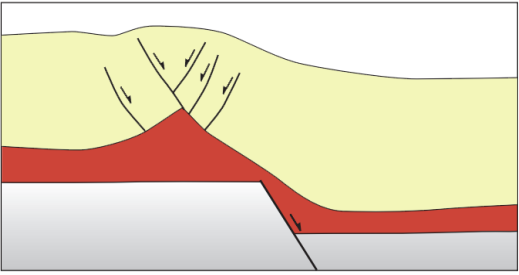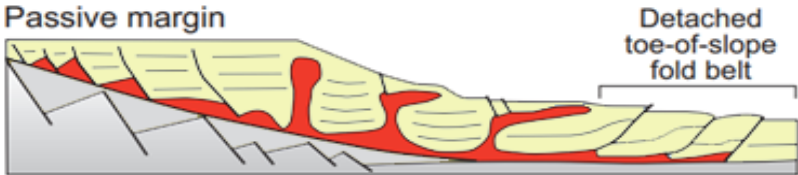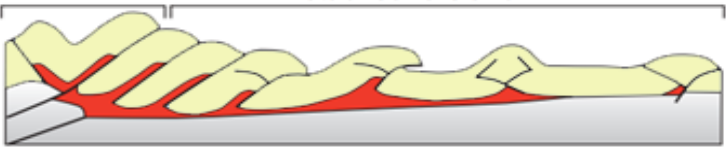
Name	Mechanism	Diagnostic features	Model
Salt Anticlines and Salt Pillows	Salt structures having concordant contacts with their overburden. Salt pillows are subcircular while salt anticlines are elongated. Most form by halokinesis or buckling, but some form by extension		
Halokinetic (gravity-driven) salt-cored folds	Salt flows driven by differential loading applied by lateral variations in density or thickness in the overburden	Long synkinematic growth interval, stratal thinning over the crest, thin prekinematic interval, limbs of halokinetic folds need not be the same age (Diachronous sedimentation)	Modified from Jackson and Hudec, 2017
Contractive salt-cored folds	Salt fills the core of buckle folds formed in response to regional compression	Long-lived prekinematic arched roof, short synkinematic period, crestal thrusts or contractional kink bands, top erosional unconformities, synkinematic sediments thinning onto contractional folds should be the same age on both sides of the fold crest, pre-existing diapirs to expel salt sheets at the level of the synkinematic section	Modified from Jackson and Hudec, 2017
Extensive salt-cored folds	Salt is expelled by sagging rollover	Associated to rollover on one flank	Modified from Jackson and Hudec, 2017

Salt Diapirs	Diapiric salt structures having discordant contacts against their overburden. Salt stocks are pluglike bodies having equant planforms, whereas salt walls are more elongate.		
Reactive Diapirs	Diapirs emplaced in space created by the stretching of the overburden	triangular shape, pointed crest, crestal graben or half-graben, associated to salt rollers and salt-detached growth faults	Modified from Jackson and Hudec, 2017
Active Diapirs	Rising salt structure arches, uplifts, or shoulders aside its overburden, driven either by gravity-loading or by compression	Overburden arched above regional, large flaps of the overburden tilting outward, complex crestal extension, thinning and onlap of the roof toward the crest	Modified from Jackson and Hudec, 2017
Passive Diapirs	Pressurized salt flows upward until the near surface, syndepositionally with sediment accumulation, while its base is sinking. The diapir is flanked by Halokinetic	Salt emergent at the surface or partially or completely covered by a thin (less than ~300 m) roof, upturned stratal cutoffs against the diapir flanks (halokinetic sequence), sometime extrusive salt on the flanks	

	sequences	 Modified from Jackson and Hudec, 2017
Diverse Salt-related structures		
Halokinetic sequence	Succession of strata upturned and thinned by drape folding near a passive diapir, bounded by angular unconformities that become conformable away from the diapir	 Modified from Jackson and Hudec, 2017
Drape folding	Fold of roof and diapir-flanking strata adjacent to a diapir due to the relative rise of the salt and the subsidence of the adjacent minibasin.	
Minibasin	Small basin adjacent to salt-related structures, with accommodation generated by subsidence into underlying flowing salt and/or growth of flanking salt structures	
Flap	Wedge of sediment upturned against the flanks of a diapir. A thick kilometric basal flap folded to near vertical or overturned that lie immediately above the source layer is known as a basal megaflap.	

Salt Sheet	Allochthonous salt sourced from a single feeder whose breadth is several times greater than its maximum thickness	 Modified from Jackson and Hudec, 2017
Salt roller	Low-amplitude, gravity-driven asymmetric salt structure	
Rollover	Stratal interval that thickens and bends downward toward a normal fault, diapir, or salt weld .	
Salt weld	Surface or fault joining strata originally separated by salt	
Thick-skinned deformation	Deformation where the pre-salt basement is involved, the strain is accommodated by the salt and its overburden above a salt décollement	
Thin-skinned deformation	Deformation where the pre-salt basement is not involved, the strain affects both the basement and its cover	
Salt systems	Regional or local system comprising a source layer of salt, its sedimentary overburden, and the presalt rocks below the salt. The salt typically acts as a broad sub horizontal décollement accommodating the strain. The strain generated by regional lateral forces will also be focused in salt-structures but can also create new structures and/or trigger thick-skinned deformation	
Extensional Salt-Tectonic Systems	Regional or local salt deformation in response to gravity- or tectonically-driven stretching. Key features include salt rollers and stratal rollovers along basinward dipping growth faults. Diapirism dominantly reactive or passive, with short episode of gravity-driven active diapirism	

Basement-detached extension

Basement-involved extension

Modified from Jackson and Hudec, 2017

Contraction al Salt-Tectonic Systems	Regional or local salt deformation in response to gravity- or tectonically-driven contraction. Key features include contractive or halokinetic salt-cored folds, salt-detached thrusts, active diapirs squeezed diapirs, salt sheets. Contractional deepwater fold belts are typically gravity-driven on a basinward tilted passive margin. Orogenic and inverted margins are typically tectonically driven on landward or multi-strike base.	 Modified from Jackson and Hudec, 2017

Strike-Slip Salt-Tectonic Systems	Regional or local salt deformation in response to tectonically driven transpression, transtension or pure strike slip. Strike slip can have barely visible effects in profile. In 2D profiles, key features include flower structure, steep strike-slip faults with limited visible throw, or oblique normal faults	 Modified from Jackson and Hudec, 2017
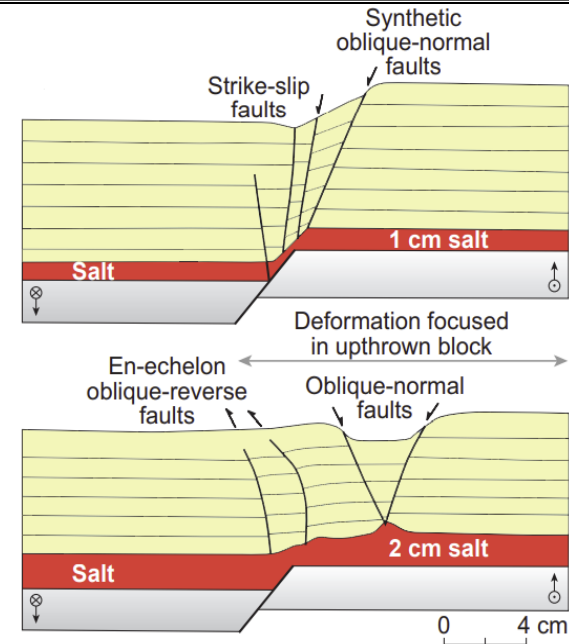
The geodynamics of the Mediterranean is linked to the Tertiary Alpine–Himalayan orogenesis, that initiated ~65 Ma, framed within the subduction of the Mesozoic Tethys Ocean and the Africa-Eurasia convergence (Smith, 1971; Dewey *et al.*, 1973; Ben-Avraham *et al.*, 2006; Carminati, Lustrino and Doglioni, 2012). In the Alpine Tethys, the collision was centred around the Alps and the Adria plate in the centre of the Mediterranean (Figure 21), with two large trenches flanking the Alpine collision: the western Mediterranean (Liguro-Provençal, Tyrrhenian, and Algerian basins) on one side and the Dinarides-Hellenides on the other side (Faccenna *et al.*, 2014). This resulted in a complex configuration of subduction zones that shaped the relief of today's Mediterranean, with regional fold-and-thrust belts at the boundaries of progressive arcs of, for instance, the Apennines, Alps, Carpathians, Dinarides, and Hellenides (Figure 21) (Biju-Duval, 1978; Jolivet and Faccenna, 2000; Faccenna *et al.*, 2001; van Hinsbergen *et al.*, 2005; Schmid *et al.*, 2008; Handy *et al.*, 2010).
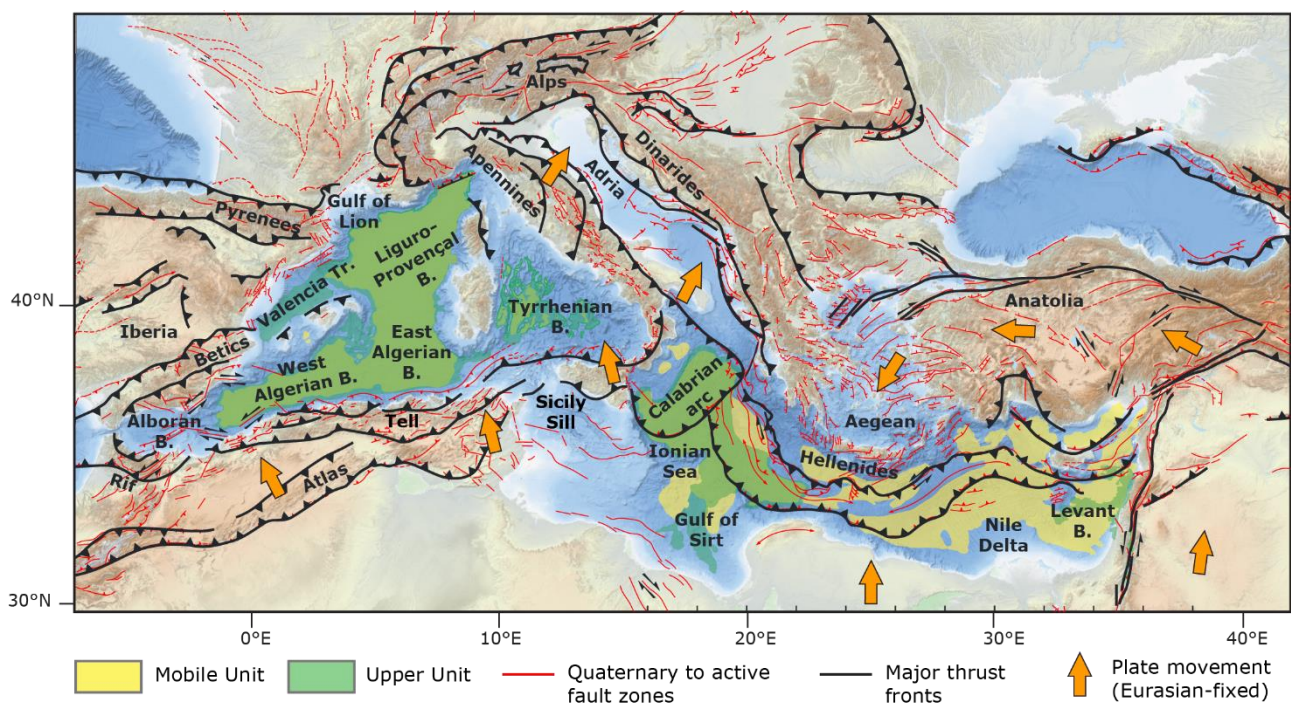
Figure 21 Geodynamic settings of the Mediterranean Salt Giant (MSG). The extent of the MSG is from Lofi, 2018. Quaternary to active fault zones and are modified from Barrier et al. (2004). Major thrust faults and gps-derived plate motions arrows are modified from Faccenna et al. (2014). Background bathymetry if from EMODnet (https://ows.emodnet-bathymetry.eu/wms)

The central to eastern Mediterranean is considered to be a relic of the Alpine Tethys Ocean, subducting northward beneath the Anatolian-Aegean plate along the Hellenic-Cyprian trench, and north-westward beneath Adria-Eurasian plates along the Calabrian trench (Biju-Duval, 1978; Ben-Avraham *et al.*, 2006; Carminati, Lustrino and Doglioni, 2012; Dellong *et al.*, 2018). The relief is dominated the fold-thrust belts of the Mediterranean Ridge that runs along the Hellenides, from the Calabrian to the Cyprus Arc, at the plate boundary between the Eurasian and African plates (Kahle and Mueller, 1998;

Vidal, Alvarez-Marrón and Klaeschen, 2000; Hall *et al.*, 2005). In these setting, the Ionian sea is postulated to represent a relic of the Triassic or pre-Triassic oceanic Tethys crust (Catalano, Doglioni and Merlini, 2001; Speranza *et al.*, 2012; Gallais *et al.*, 2013; Polonia *et al.*, 2016; Gutscher *et al.*, 2017; Maesano, Tiberti and Basili, 2017). A late Miocene-Pliocene, a new phase of oblique convergence between the Eurasian and the Arabian plates generated a series of folds, thrusts, and sinistral transpressional strike-slip fault movements along the Levant Margin, with associated transtension in the Aegean behind the Hellenides (Jackson and McKenzie, 1988; Litak *et al.*, 1997; Hall *et al.*, 2005; Hawie *et al.*, 2013; Nader *et al.*, 2018).

In contrast, the Western Mediterranean Sea is as a succession of late Oligocene to Neogene diachronous back-arc basins (~30 to present), formed by extensions behind the Apennines-Maghrebides trenches (Figure 21, Figure 22)(Rehault, Boillot and Mauffret, 1984; Robertson and Grasso, 1995; Gueguen, Doglioni and Fernandez, 1998; Jolivet *et al.*, 2006). It includes the Liguro-Provençal, the Valencia, the Algerian, the Alboran and the Tyrrhenian basins. The extension was generated by an eastward Alpine Tethys slab roll-back below an ancient Alboran-Balearic-Sardo-Corsican arc (Figure 22a, b, c), with rifting and drifting that propagated from the Liguro-Provençal to the Alboran basin (Auzende, Bonnin and Olivet, 1973; Olivet, 1996; Vergés and Sàbat, 1999; Rosenbaum, Lister and Duboz, 2002; Spakman and Wortel, 2004; Carminati, Lustrino and Doglioni, 2012; Faccenna *et al.*, 2014; Dannowski *et al.*, 2020). A first early Oligocene to early Miocene phase of NW-SW extension led to the opening of the Liguro-Provençal basin and the Valencia rift (~32 to 16 Ma, Figure 22a), with intense arc alkaline magmatism and a 30° counter-clock rotation of the Balearic-Sardo-Corsican block, accommodated by NNW-SSE to NW-SE dextral transfer faults (Rehault, Boillot and Mauffret, 1984; Mauffret *et al.*, 1995, 2004; Rollet *et al.*, 2002; Carminati, Lustrino and Doglioni, 2012; Etheve *et al.*, 2016). Extension shifted progressively to the southwest and initiated a second phase of NW-SE to W-E strike-slip opening (Figure 22a and b). The opening direction and timing of this second phase are not yet constrained, with one school of thought assuming a 16–8 Ma E-W extension (Rosenbaum, Lister and Duboz, 2002; Mauffret *et al.*, 2004; Spakman and Wortel, 2004) and another school assuming a 25-16 Ma NW-SE extension (Gueguen, Doglioni and Fernandez, 1998; Vergés and Sàbat, 1999; Faccenna *et al.*, 2004; Schettino and Turco, 2006). These different scenarios for the opening of the Algerian basin are reviewed in more details by Van Hinsbergen et al., (2014) and Chertova et al., (2014). Haidar et al., (2022) recently suggested a mid-Miocene fan-shaped opening of the East Algerian basin, followed by a lower W-E opening of the western Algerian basin similarly Medaouri et al. (2014). In both cases the opening of the Algerian basin was associated with the counter-clockwise rotation of the Kabylides away from the Balearic, which eventually led to their oblique collision with the North African margin and the Tell Fold-and -thrust belt. This ends the extensional

phase in the southwestern Mediterranean, with a migration of the extension in the Tyrrhenian basin (Figure 22c), shortly before the deposition of the Messinian evaporites (Kastens and Mascle, 1990; Sartori, 1990; Serpelloni *et al.*, 2007).
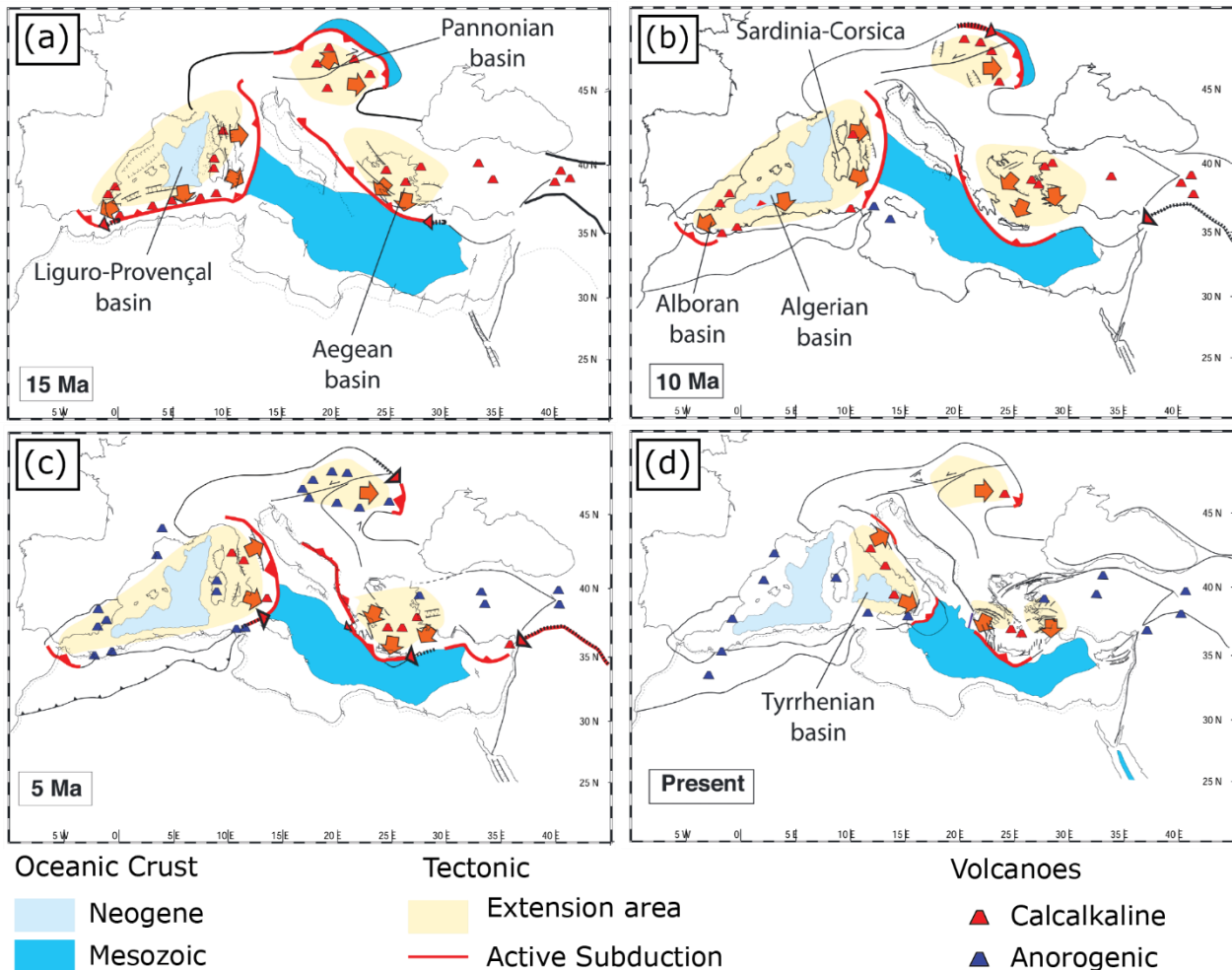
Figure 22 Evolution of the Mediterranean from mid-Miocene (a and b) to present (d), with one step at the earliest Pliocene (c), right after the deposition of the Messinian salt giant (modified from Faccenna *et al.*, 2014).

From mid-Miocene to today (Figure 22c and d), slab rollback is associated with major block rotations, a progressive bending and arching of the subduction fronts, and lateral tearing of the subducted slabs (van Dijk and Scheepers, 1995; Faccenna *et al.*, 2004, 2014). In some places, this lateral tear is recorded by Subduction-Transform Edge Propagator (STEP) faults separating the subducting lithosphere from the continental plate (Govers and Wortel, 2005). Such STEP faults have been described in the Calabrian trench (Carminati *et al.*, 1998; Govers and Wortel, 2005; Del Ben, Barnaba and Taboga, 2008; Rosenbaum *et al.*, 2008; Wortel, Govers and Spakman, 2009; Gallais *et al.*, 2013; Gutscher *et al.*, 2016; Polonia *et al.*, 2016; Maesano, Tiberti and Basili, 2020), the Hellenic trench (Govers and Wortel, 2005; Özbakır, Govers and Fichtner, 2020), or along the limits of the south-western internal Alpine thrusts (Betics and North African margin; Carminati *et al.*, 1998; Badji *et al.*, 2015; Mancilla *et al.*, 2018; d'Acremont *et al.*, 2020;

Negredo *et al.*, 2020; Haidar *et al.*, 2022). This tearing is also marked by a strong strike-slip component and by a surge of Na-alkaline anorogenic volcanism (Faccenna et al., 2014).

For the study of the MSG tectonics, the previously described complex evolution of the Mediterranean can be simplified to the quieter Messinian to present day geodynamics. In this study, I consider that the MSG evolved in an overall frame of steady and oblique convergence between the African and Eurasian plates until today. This implies that along inverted margins (i.e. the North African margin) and at the Alpine subduction fronts (Calabrian and Hellenic trenches), a strong shortening and strike-slip displacement loading component must be applied to salt.

1.6.1 The MSG in the Levant basin and the Nile deep-sea fan

From the Nile Delta to the Levant Basin, the MSG is emplaced on a stretched relic passive margin of the Mesozoic Neo-Tethys (Figure 23a and d)(Dewey *et al.*, 1973; Biju-Duval, 1978; Hirsch *et al.*, 1995; Netzeband, Hübscher and Gajewski, 2006; Nader *et al.*, 2018). The MSG tectonics is dominantly thin-skinned and gravity-driven with (Gaullier *et al.*, 2000; Loncke *et al.*, 2006; Allen, Jackson and Fraser, 2016):

(i)   differential loading (i.e. gravity spreading) in response to the prograding Plio-Quaternary sediments from the Nile fluvio-deltaic system

(ii)   gravity gliding on a tectonically tilted margin, with a secondary pre-salt relief influence on the deformation

Changes through time and space in the relative contribution of differential loading and margin tilting influences the salt flow regime (Evans, Jackson and Oppo, 2021). It displays a typical structural segmentation of salt-bearing passive margins (Figure 23a), with (Tibor *et al.*, 1992; Gradmann *et al.*, 2005; Bertoni and Cartwright, 2006; Cartwright and Jackson, 2008; Allen, Jackson and Fraser, 2016; Evans, Jackson and Oppo, 2021):

(i) an updip extensional domain with listric growth faults, salt rollers, and ramp syncline basins

(ii) a downdip contractional domain thrusts and pop-up structures

Two phases of deformation have been described with:

(i) A Messinian pre-Nile deformation phase of salt gliding in response to the tilting of the margin uplift (Bertoni and Cartwright, 2006; Netzeband, Hübscher and Gajewski, 2006; Reiche, Hübscher and Beitz, 2014)

(ii)A Messinian to present phase with additional gravity spreading and outward radial expulsion of the MSG (with a thickness up to ~2km

in the Levant), in response to the Nile progradational-aggradational wedge since Pliocene (Tibor *et al.*, 1992; Gradmann *et al.*, 2005; Loncke *et al.*, 2006; Haq *et al.*, 2020)

Zucker *et al.* (2019) argue that downslope gliding is dominant on the western side of the Nile delta, where the deep-sea fan do not reach the deep-basin salt. By contrast, they suggest that gravity spreading played a major role on the salt tectonics in the Levant basin, where the Nile delta front reach the MSG. In the northern Levant, the Messinian Nahr-Menashe fluvio-deltaic sequence might have applied an early south-directed sediment loading on the mobile salt (Madof, Bertoni and Lofi, 2019).

The eastern MSG consists of six to seven sequences reflecting the presence of intrasalt heterogeneity strongly affects that affects the salt flow (Bertoni and Cartwright, 2006; Netzeband, Hübscher and Gajewski, 2006; Hubscher *et al.*, 2007; Feng *et al.*, 2016). Salt deformation is recorded by intrasalt reflectors folding and faulting, where both a pressure-induced Poiseuille flow and a drag-induced Couette flow have been interpreted (Cartwright *et al.*, 2012, 2018; Kirkham *et al.*, 2019). Evans and Jackson (2021) suggest that both regimes have been cumulatively recorded with a first phase of Poiseuille and a later phase of Couette flow.

1.6.2 The MSG in the Mediterranean ridge and Cyprus Arc

From the Calabrian to the Cyprus arc (Figure 24), most of the MSG is poorly imaged, highly deformed, and partly incorporated in the Calabrian and Mediterranean accretionary wedges (Reston *et al.*, 2002; Westbrook and Reston, 2002; Kopf, Mascle and Klaeschen, 2003; Polonia *et al.*, 2016). In the Ionian sea, from Messinian to present, the salt acts as a décollement in a contractional setting, facilitating the advance of SSE directed Calabrian wedge and the W-SW directed Mediterranean wedge (Figure 24a and b), reducing the size of the abyssal Ionian plain (Del Ben, Barnaba and Taboga, 2008; Gutscher *et al.*, 2016; Camerlenghi *et al.*, 2020). Salt is partly incorporated and expelled outward from both the wedges, forming low tapered imbricated thrusting and back thrusting on the wedge (Reston *et al.*, 2002; Polonia *et al.*, 2011). In the abyssal Ionian plain, at the front of accretionary wedge units, the MSG is cornered between the strike-slip Malta escarpment and the Medina ridge (Figure 24d), forming a thick, coherent salt unit, without much diapirism (Gutscher *et al.*, 2016; Camerlenghi *et al.*, 2020).

To the east, the NW-SE Mediterranean Ridge accretionary wedge is relayed by the Florence Ridge accretionary wedge and the Cyprus arc (Figure 23c and d), where an arcuate and south-verging fold and thrust belt delineate piggy-back basins in which the MSG was deposited (Biju-Duval, 1978; Woodside, 2000; Sellier *et al.*, 2013).
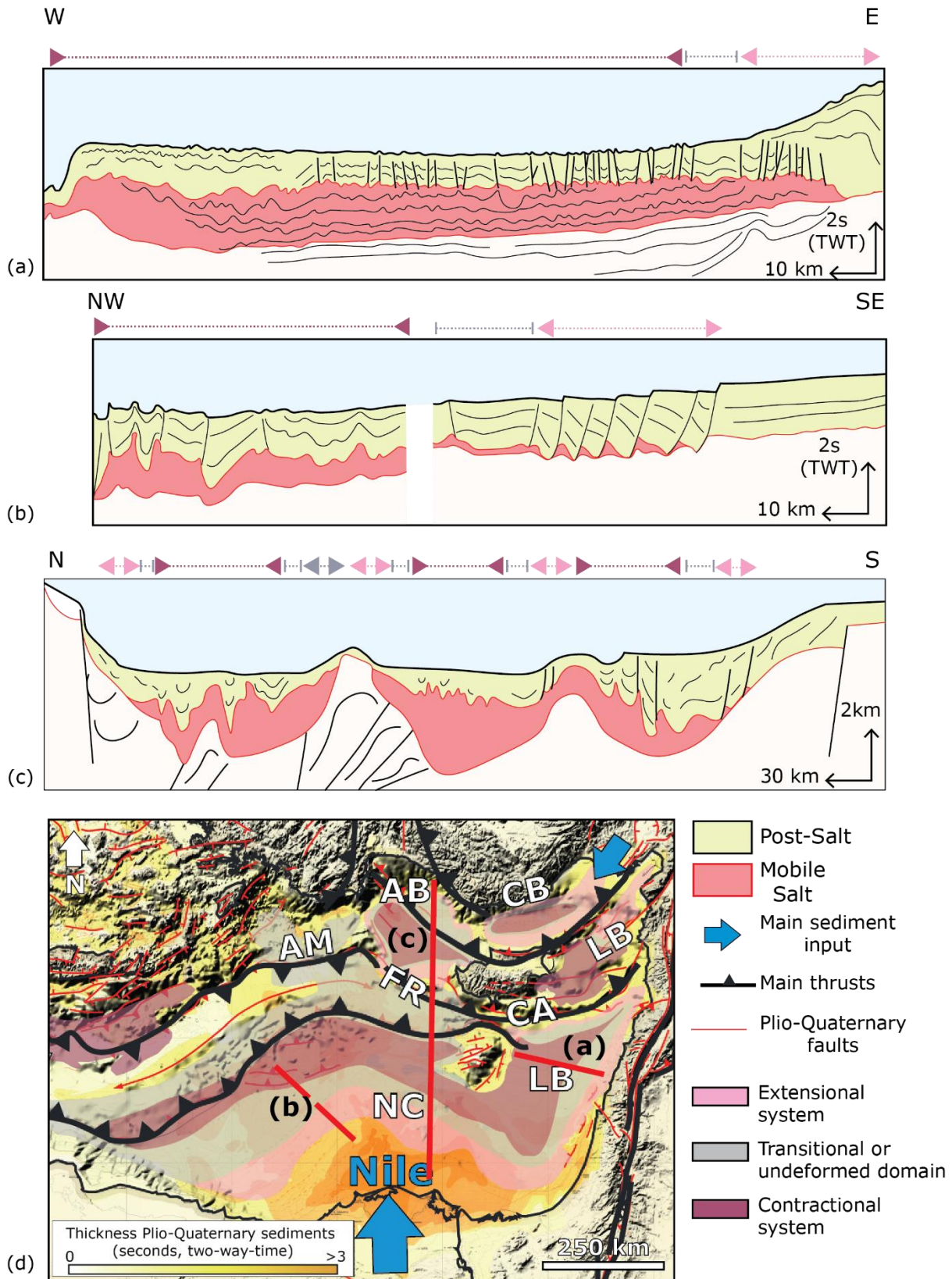
Figure 23 Seismic schemes showing the domains of salt tectonics in (a) the Levant basin, (b) the Nile Delta and (c) the Florence Ridge/Cyprus Arc (modified from Sellier *et al.*, 2013; Allen, Jackson and Fraser, 2016). Panel (d) shows the tectono-stratigraphic settings of the eastern MSG and salt-related tectonic domains distributions. The background Plio-quaternary thickness map is from IBO, (1981). The pinch-out of the salt is modified from Lofi, (2018). The Plio-quaternary faults are modified from Barrier *et al.* (2004). Major thrust faults are modified from Faccenna *et al.* (2014). AB: Antalaya Basin; AM: Anaximander Mountains; CB: Cilicia Basin; LB: Latakia Basin; FR: Florence Rise; CA: Cyprus Arc; LB: Levant Basin; NC: Nile Cone.
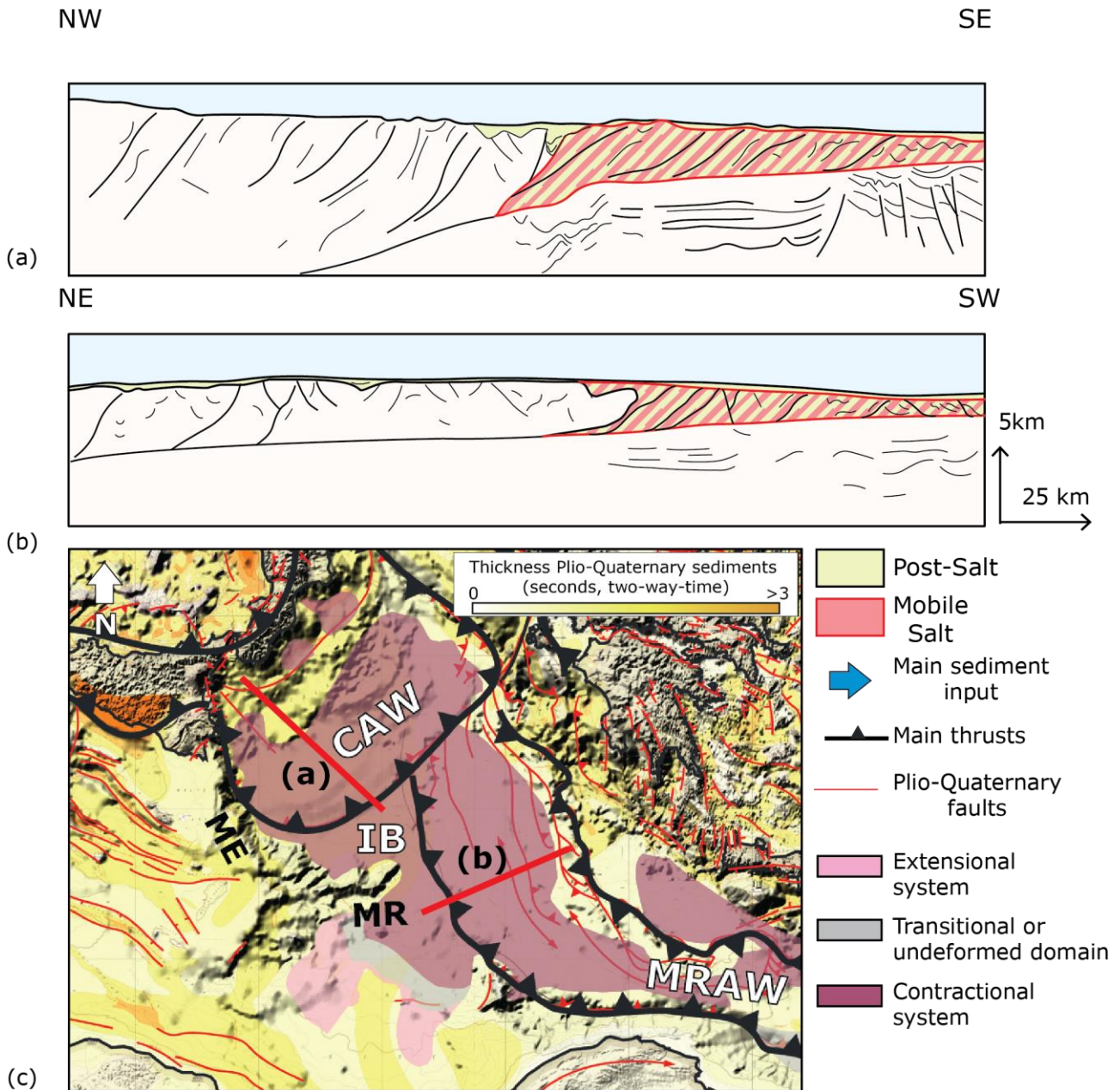
Figure 24 Seismic schemes showing the domains of salt tectonics in (a) the Calabrian accretionary wedge and (b) the Mediterranean accretionary wedge (modified from Westbrook and Reston, 2002; Kopf, Mascle and Klaeschen, 2003; Polonia *et al.*, 2011). Panel (c) shows the tectono-stratigraphic settings of the central MSG and salt-related tectonic domains distributions. The background Plio-quaternary thickness map is from IBO, (1981). The pinch-out of the salt is modified from Lofi, (2018). The Plio-quaternary faults are modified from Barrier et al. (2004). Major thrust faults are modified from Faccenna et al. (2014). CAW: Calabrian Accretionary Wedge; MRAW: Mediterranean Accretionary Wedge; IB: Ionian Basin; ME: Malta Escarpment; MR: Medina Ridge.

From Messinian to present, the region underwent a transpressional regime (Bridge *et al.*, 2005; Hall *et al.*, 2005; Işler *et al.*, 2005; Aksu *et al.*, 2014). The strain is partitioned into morphotectonic domains parallel to the arc, with extension on tectonically tilted inner slopes (e.g., Antalya, Latakia, Cilicia), alternating with contraction and strike slip within the basins and along the reactivated pre-existing ridges (e.g., Florence rise, Kyrenia range, Anaxagoras Mountains; Aksu *et al.*, 2014; Güneş, Aksu and Hall, 2018).

Studies distinguish between (Bridge *et al.*, 2005; Işler *et al.*, 2005; Maillard *et al.*, 2011; Sellier *et al.*, 2013; Güneş, Aksu and Hall, 2018):

- multi-directional gravity driven and thin-skinned deformation, with salt gliding along the slopes of the tilted basins, salt spreading beneath the basins depocenters, and contractional salt-cored fold belts where both salt flows converge
- tectonically driven and thick-skinned deformation, with transtension and transgression recorded by ramp anticlines along sub-vertical strike-slip faults and positive flowers structures arching the whole sedimentary sequence

1.6.3 The MSG in the northwestern Mediterranean (Gulf of Lions, Liguro-Provençal basin, and western Sardinia)

The Liguro-Provençal basin is bordered by passive margins, with the Gulf of Lions to the north-west and the Corsica-Sardinian margins to the east (Figure 25). It is characterized by a high subsidence and a high sedimentation rate, with sediments converging from the Rhône, the Var and the Ebro systems (Gorini, Le Marrec and Mauffret, 1993; Lofi *et al.*, 2003, 2005; Migeon *et al.*, 2006; Leroux *et al.*, 2017; Mianaekere and Adam, 2020).

Like the Levant basin and the Nile margin, the Gulf of Lion displays a characteristic passive salt-bearing margin tectonic segmentation (Figure 25e), with (Gorini, Le Marrec and Mauffret, 1993; dos Reis, Gorini and Mauffret, 2005; Estelle Leroux *et al.*, 2015; Ferrer *et al.*, 2017):

- an upper thin-skinned extensional domain, accommodated by basinward-dipping listric normal faults
- a weakly-deformed midslope domain
- a lower contractional domain that accommodates upslope extension by folding, salt inflation, or diapir squeezing

The deformation is essentially gravity-driven, with salt gliding and spreading radially, in response to a tilted margin and sediment loading from the Rhône deep-sea fan (dos Reis, Gorini and Mauffret, 2005; Gorini *et al.*, 2005; E Leroux *et al.*, 2015). If the processes and the segmentation are comparable to the Levant, salt structures differ from the eastern Mediterranean, particularly in the contractional domain where high amplitude diapirs are numerous.

Eastward, along the Provençal and Ligurian sections (Figure 25d), the margins are reactivated by ~N-S Mio-Pliocene compression since at least the Messinian: they gradually steepen, the extensive domain narrows, and the translated province seems to be short or even absent (Rehault, Boillot and Mauffret, 1984; Gueguen, Doglioni and Fernandez, 1998; Maillard *et al.*, 2003; Obone-Zue-Obame *et al.*, 2011). Active thrust faults and folds have previously
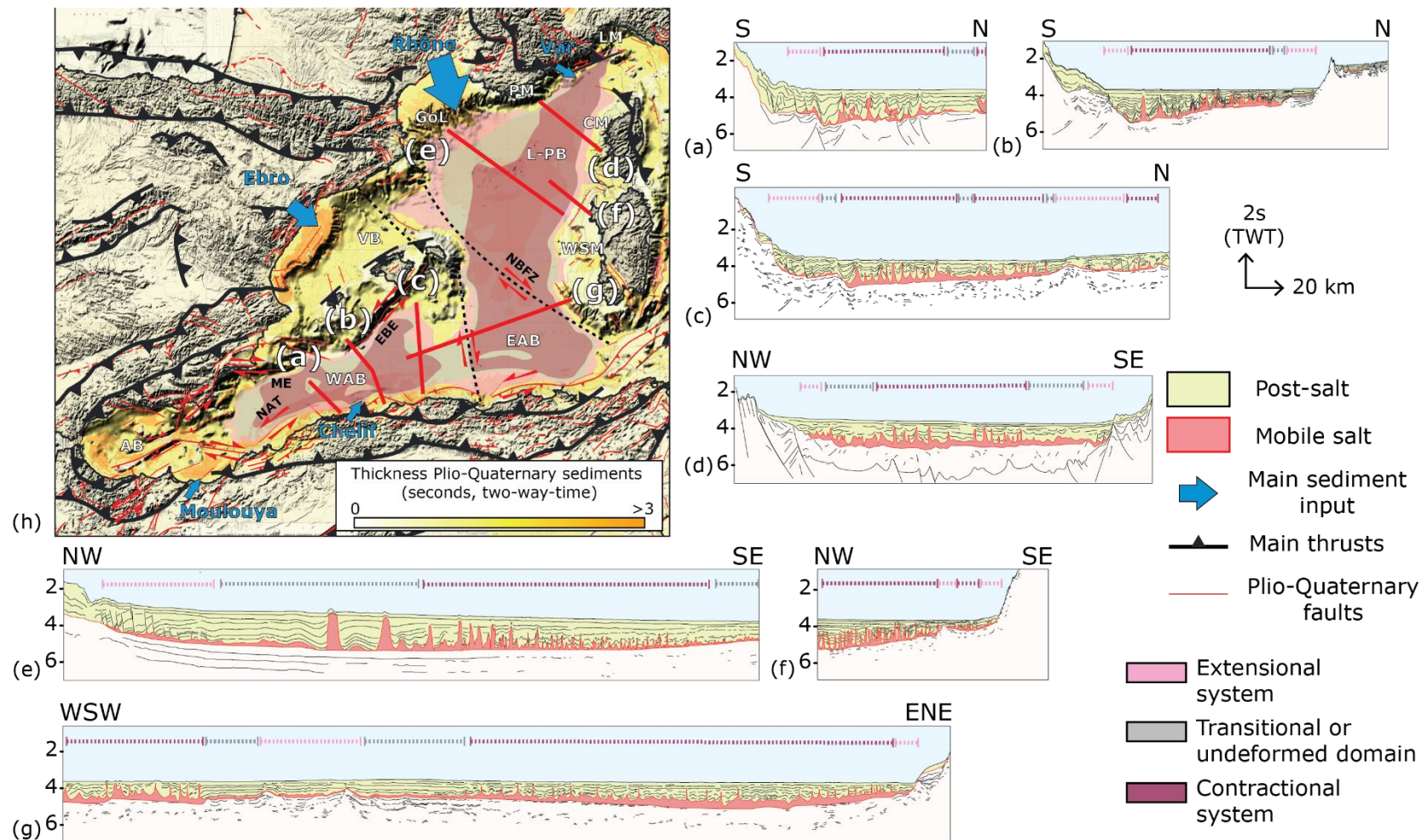
Figure 25 Seismic schemes showing the domains of salt tectonics in (a) the western Algerian margin, (b) the central Algerian, (c) the edge of the central Algerian, (d) The northern Liguro-Provençal, (e) The Gulf of Lions, (f) the Sardinian margin, and (g) the eastern Algerian (modified from Rollet *et al.*, 2002; Soto *et al.*, 2019; Bellucci, Aslanian, *et al.*, 2021). Panel (h) shows the tectono-stratigraphic settings of the western MSG and salt-related tectonic domains distributions. The background Plio-quaternary thickness map is from IBO, (1981). The pinch-out of the salt is modified from Lofi, (2018). The Plio-quaternary faults are modified from Barrier et al. (2004). Major thrust faults are modified from Faccenna et al. (2014). AB: Antalaya Basin; LM: Ligurian Margin; PM: Provençal Margin; GoL: Gulf of Lions; L-PB: Liguro-Provençal basin; VB: Valencia Basin; CM: Corsica Margin; WSM: West Sardinia Margin; EAB: Eastern Algerian Basin; WAB: Western Algerian Basin; AB: Alboran Basin: ME: Mazarron Escarpment; EBE: Emile-Baudot Escarpment; NAT: North African Transform.

been identified below the margin, uplifting and tilting parts of the margin, triggering late salt gliding and arching of the overburden above salt-cored anticlines (Chaumillon *et al.*, 1994; Bigot-Cormier *et al.*, 2004, p. ; Soulet *et al.*, 2016).

Similarly, the conjugate Corsica-Sardinian margins display steep slopes (Figure 25f), but they are still passive and stable since the Messinian time (Guennoc *et al.*, 1998). By contrast with the northern margins, they display a lower overburden/salt thickness ratio, testifying to a lower aggradation rate, with a higher rate of sediment supplied mainly from the Gulf of Lions than that of the Sardinian Isle (Sage *et al.*, 2005). They also display Late Messinian to present thin skinned and gravity-driven salt deformation, with a narrow extensional and transition zone where the MSG is relatively undeformed, except for nearly vertical salt-detached faults, with low to medium amplitude salt rollover (Sage *et al.*, 2005; Geletti *et al.*, 2014; Dal Cin *et al.*, 2016). The relative absence of an undeformed transitional domain can be related to the aforementioned low sedimentation rate, a heterogeneous sedimentation pattern, or pre-kinematic cover thickness (Ge *et al.*, 2019).

In western Sardinia, the salt is interpreted to be gliding as a consequence of margin uplift and tilting of the margins, with a peak of deformation during the Early Pliocene (Dal Cin *et al.*, 2016). From the Messinian to the Pleistocene, the Sardinian margins were affected by a diffuse alkaline basaltic volcanic related to the opening of the Southern Tyrrhenian basin (Beccaluva *et al.*, 1977; Lustrino, Melluso and Morra, 2000). The magmatic structure seems to have at least partially deformed and uplifted the margin, with a probable re-activation of the fault system of the rifting phase which would have favored gravity gliding (to my knowledge no studies have mentioned a potential tectonic loading of the salt; Geletti *et al.*, 2014)

1.6.4 The MSG in the southwestern Mediterranean (Algerian basin)

The south-western Mediterranean opened in the middle Miocene as a string of back-arc marginal seas (Figure 25), in response to the westward retreat and tearing propagation of the Tethys slabs (Dewey *et al.*, 1973; Carminati *et al.*, 1998; Rosenbaum *et al.*, 2008; Van Hinsbergen, Vissers and Spakman, 2014; Haidar *et al.*, 2022). The Algerian basins display steep "STEP" (Subduction-Transform Edge Propagator) margins (The Emile Baudot and Mazarrón escarpment to the north and the North African Transform to the south), with limited continental shelves along which a strong Miocene to Plio-Quaternary magmatic activity has been recorded. Since at least Tortonian, their Algerian margin is under inversion, with a NW-SE directed shortening (Stich *et al.*, 2006; Serpelloni *et al.*, 2007). The two basins are separated by a basement high referred to as the Hannibal high (Figure 25g), where salt thins down, with no or weak salt deformation (Mauffret *et al.*, 2004; Bellucci, Aslanian, *et al.*, 2021). The basin is asymmetrical, with preferential subsidence

and sediment accumulation along the southern Margin, mainly sourced from the Moulouya and Chelif rivers today, with a low input from the Balearic margin (Struglia, Mariotti and Filograsso, 2004; Leroux, 2019).

To the south, along the Algerian margin, salt tectonics show contrasting structural style, alternating between contractional, extensional and transtensional salt deformation (Soto *et al.*, 2019). Salt partly accommodates the late Miocene to present convergence, with diapir squeezing, suprasalt folding and even allochthonous salt sheets inflation above the UU (Figure 25a and b). The extensional and transitional domains are generally narrow or absent. Locally, the contractional tectonics is thick skinned and the salt is uplifted on growing piggy back basins, above south-dipping blind thrusts (Déverchère *et al.*, 2005; Kherroubi *et al.*, 2009; Bouyahiaoui *et al.*, 2015). In that scenario, the salt starts gliding along the steepened flanks of the perched basins. Toward the west, salt thins down and salt structures are dominantly gravity-driven, with a narrow extensional domain, but a wider transitional domain with low amplitude salt-cored folds (Bellucci, Aslanian, *et al.*, 2021).

To the north, on the Balearic margin, previous studies described gravity-driven salt structures formed by basinward gravity spreading and gliding along a gently dipping base-salt surface (Mocnik *et al.*, 2014; Wardell *et al.*, 2014; Dal Cin *et al.*, 2016). Dal Cin et al. (2016) suggest that salt deformation started in the late Messinian, during the deposition of the top-most Messinian evaporites, with a peak during the Early Pliocene. They also pointed out that extensional deformation was not well expressed, with a quick transition from extensional to contractional salt tectonics basinward. Further away in the Algerian basin, Camerlenghi et al. (2009) described tectonically driven salt-cored anticlines and pillows, responding either to the reactivation of underlying faults, or by the northward propagation of the compressional stress identified along the Algerian margin.

1.6.5 Summary

After this review I distinguish six regional salt systems in the Mediterranean:

- **The Nile Cone and Levant basin** (Figure 23b and c): Passive margins with strong sediment loading. Salt deformation is comparable to other worldwide passive margins, with an up dip extensional domain and a down dip contractional domain. Salt deformation is thin skinned, and gravity driven with divergent radial salt gliding and spreading. They display a high thickness ratio between the salt and the overburden. Salt accommodates high rates of contractional strain internally. The overburden and the intrasalt reflectors are folded and thrusted, with rare and low amplitude truncating diapirs in the contractional domain.

- **The Gulf of Lions** (Figure 25e): Similar to the Levant and the Nile systems, but with a lower thickness ratio between salt and overburden (a large portion of the MSG is made of more brittle evaporites in the west). It displays different contractional salt structures, with high frequency and high amplitude intrusive diapirism (locally up to the water bottom), as well as arching and folding of the overburden.

- **The Cyprus Arc** (Figure 23a): Fold-and-thrust belts with a strong strike-slip component pre-dating the deposition of the salt, and still active today. Salt flow is both gravity and tectonically driven. It displays gravity-driven convergent radial salt flow, locally disturbed by the direction of prograding sediments coming from the margins. Perched basins display a narrow extensional domain with salt gliding and spreading on the steepened flanks. They display wider contractional domain, with arching, thrusting and squeezing, where the salt flows converge. The deformation can be thick-skinned above active transtensional or transpressional faults.

- **The southern Algerian margin** (Figure 25a, b, c and g): Growing salt-bearing fold-and-thrust belts. The processes are comparable to the Cyprus Arc, with thick-skinned tectonics above active faults. However, the inversion is not as advanced, and perched basin are not enclosed. Along the steepening structures, the salt flow is multi-directional and is not confined to isolated sub-basins. The margin is landward dipping, with thick Plio-Quaternary depocenters flanking the Algerian margin. There are competing forces driving salt flow, with salt gliding along the landward tilted base, up-dip basinward salt spreading beneath the thick overburden, and north to north-westward transpression. Extensional domains are narrow, except on perched basins, with a quick transition to the contractional domain. Salt accommodates the contraction through high amplitude intruding, squeezing, arching, and upturning the overburden. Allochthonous salt sheets lying above the UU are not rare.

- **The Sardinian, Balearic and Provençal margins** (Figure 25d and f): Steep margins with low sedimentation rate, narrow or inexistant extensional and transitional domains, and low amplitude salt rollers. They display a medium to low thickness ratio between salt and overburden. Local perched basins can display larger extensional domains with multi-directional gravity-driven flows. I suspect a strong strike-slip component, although it is hard to assess without 3D seismic data. However, low-throw vertical faults and transtensional/transpressional reactivated structures are often observed.

- **The Calabrian and Mediterranean wedges** (Figure 24): Accretionary wedge units where salt lubricates the accumulation of the overburden against wide accretionary units. Salt structures are

intensely folded and thrusted, imbricated within the accretionary prism, and are not well imaged.

I did not consider the passive margins for this study of early salt deformation. I did not have much seismic data available in these areas, and they are well represented in literature. I could not consult the data in the Cyprus Arc due to COVID-19 restrictions. Considering the amplitude and the maturity of the deformation in the central Mediterranean, I believe that they are not a good analogue for early salt deformation. Based on the data available at the OGS, only the western Sardinia margin and the Balearic margin could be considered. A lot of seismic data has been acquired by the OGS on the Algerian margin, but except Dal Cin et al. (2016), who already compared the Sardinian and Balearic margins, the salt tectonics is poorly described and the factors and the style of the deformation are poorly known. In this study I have decided to focus on the under-explored Balearic margin of the Algerian basin.

Chapter 3

Improving images of the Algerian Basin

This Chapter is a modified version of Blondel et al., (under review).

1.7 Introduction

The poor understanding of the MSG and the related MSC is in large part due to a lack of data in the deep-water offshore domain, which represents more than 80% of the volume of MSC-related sediments, emphasizing the need for new and improved offshore data to better constrain the MSC (Roveri, Flecker, *et al.*, 2014). Multi-channel seismic reflection profiling is the most common geophysical method applied to image the architecture of offshore basins and to prospect for potential drilling sites. Acquiring new marine seismic data, however, is challenging due to high acquisition costs associated with marine operations. Numerous offshore seismic datasets have been acquired in the last decades in the Mediterranean Sea, providing countless 2-D profiles that could no longer be acquired today because they cover areas that are currently subject to restrictions related to obtaining exploration permits (Diviacco *et al.*, 2015). Many of these datasets are currently poorly exploited due to lack of public data access or poor-quality seismic processing. Reprocessing legacy data, therefore, is a potential source of new geological information that could be extracted from these dormant datasets, directly contributing to a better understanding of the MSG and the MSC.

Goals of reprocessing are to improve the data bandwidth, the spatial resolution, the signal-to-noise ratio, the reflector continuity and, where relevant, the seismic-borehole correlations (Sadhu *et al.*, 2008; Lille *et al.*, 2017). In this chapter, I aim to better image the salt structures, particularly the base salt. Due to the complex overburden geology and the short far-offset (between 650 and 3100m for the different surveys reprocessed) with respect to the target depth, the main imaging challenges include accurately resolving velocity variations, eliminating multiples and improving the signal-to-noise ratio at depth. I confront these challenges by outlining three key stages: i) 'broadband' processing, ii) multi-domain denoising and demultiple, and iii) geologically guided velocity model building using iterative pre-stack migration and travel-time tomography.

Compared to traditional 'narrowband' seismic processing, 'broadband' processing aims to improve the spectral accuracy by expanding the data bandwidth and restoring frequency content attenuated by the source- and receiver-side 'ghost' effect and by seismic absorption (Masoomzadeh, Woodburn and Hardwick, 2013; Lille *et al.*, 2017). High frequencies are most strongly affected by seismic absorption, which preferentially attenuates the highest frequency parts of the spectrum (Futterman, 1962; Sams *et al.*, 1997). Recovering this information improves the resolution and results in more accurate true amplitudes, improving the performance of other data processing steps such as velocity model estimation and migration, and quantitative interpretation such as amplitude variation with offset (AVO) analysis, impedance inversion, and attribute analysis (Chopra and Marfurt, 2007; Mavko, Mukerji and Dvorkin, 2009; Amundsen and Zhou, 2013; Lille *et al.*,

2017). Conversely, lack of low frequency signal commonly results in poor focusing in the deep part of the section, as low frequencies suffer less from scattering and absorption, so they penetrate deeper and display a better trace-to-trace moveout coherence, allowing us to build a more accurate velocity model (ten Kroode *et al.*, 2013).

In marine seismic data acquired with an airgun source, the source signature is a combination of a relatively broad impulsive signal (approximately a minimum-phase wavelet), periodic oscillations caused by the so-called 'bubble pulse' and an inverted polarity 'ghost' multiple, caused by the time-delayed reflection of the signal from the sea surface (Ziolkowski, 1970; Sheriff and Geldart, 1995; Hegna and Parkes, 2011; Watson, Werpers and Dunham, 2019). The data bandwidth is principally widened by performing a source designature, whereby the primary airgun impulse and the bubble pulse are collapsed into a sharp, zero-phase wavelet (Sheriff and Geldart, 1995; Amundsen and Zhou, 2013; Baldock *et al.*, 2013; O'Driscoll *et al.*, 2013; ten Kroode *et al.*, 2013). Deterministic deconvolution, where the operator is designed using an estimated source wavelet, can yield geological imaging superior to traditional statistical deconvolution methods, particularly for recovery of low frequencies and the preservation of amplitude information (Yilmaz, 2001; Sargent, Hobbs and Gröcke, 2011; Davison and Poole, 2015; Scholtz, Masoomzadeh and Camp, 2015). Deghosting, instead, aims to deconvolve both the source- and receiver-side ghosts from the wavefield, further sharpening the wavelet and removing the frequency 'notches' associated with the ghost effect (e.g., Sargent, Hobbs and Gröcke, 2011; Chuan *et al.*, 2014; Davison and Poole, 2015; Tyagi *et al.*, 2016; Willis *et al.*, 2018).

The quality of the bandwidth enhancement depends on the signal-to-noise ratio (S/N) of the input data (Amundsen and Zhou, 2013). It is therefore essential to attenuate as much as possible the low frequency noise (e.g., reverberation from the direct arrival, 'swell' noise caused by pressure fluctuation near the sea-surface) beforehand, because any remaining low frequency noise not correlated with the source pulse may be artificially boosted by the source deconvolution and deghosting filters (Yilmaz and Baysal, 2015). Thanks to lower computational costs in recent decades, multi-channel filtering and analysis in transform domains has become routine for noise reduction (Schultz, 1985). For example, 'swell' noise can often be better attenuated by predictive filters in the frequency-space (F-X) domain than by a simple time domain low-cut filter that results in loss of the low frequency signal along with the attenuated noise (Liu and Goulty, 1999; Schonewille, Vigner and Ryder, 2008). Multiple attenuation is also better tackled by move-out discrimination techniques in the parabolic Radon domain rather than by traditional statistical deconvolution based methods, for example (Basak *et al.*, 2012; Verschuur, 2013). A 'broadband' processing flow combined with an efficient multi-domain noise separation can improve the signal-to-noise ratio in the deep part of the

section (in our case below the MSG), allowing considerable improvements in velocity model building (Chuan *et al.*, 2014).

Seismic imaging restores the correct geometry of seismic reflectors and requires an accurate velocity model of the subsurface (Jones and Davison, 2014; Jones, 2015). Time domain migrations are relatively robust to errors in the velocity model but are only well-suited to imaging geology containing weak lateral velocity variation (i.e., approximately 'layer cake' geology), as they do not properly account for ray path refraction. This can lead to degradation in image quality in time domain images of complex geology such as salt diapirs. Depth domain migrations, instead, can more accurately reproduce the ray paths of reflections in the subsurface, but the image quality is more sensitive to velocity errors (Sheriff and Geldart, 1995; Yilmaz, 2001; Jones and Davison, 2014). Migration velocities are generally estimated based on the flatness of reflections on common midpoint gathers after migration (Tsvankin and Thomsen, 1994; Jones, 2015). In depth domain, the process of picking reflectors is often automated and used as input to travel-time tomography. Iterative rounds of analysis of the residual curvature of reflectors on depth migrated gathers followed by travel-time tomography to calculate model updates (Jones, 2015).

In this chapter, I aim to showcase a 'broadband' reprocessing strategy designed to improve imaging of the MSG. I demonstrate multi-domain de-noising, deghosting and a source designature using a seabed reflection derived operator. I then perform multiple attenuation and geologically driven iterative migration velocity analysis. The results include pre-stack time and depth migrated images, which I compare to the legacy 'narrowband' processing. With these reprocessed images I highlight some new geological insights that these new results provide on the salt system of the Algerian basin, the seismic expression of the MSC and the basement structure of the study area.

1.8 Geological setting

The datasets were acquired south of the Balearic Islands (Spain) with water depths between 1000 and 2800 m (Figure 1). They cover the transition from the Balearic Promontory to the deep Algerian basin, which is marked by the steep NE-SW Emile-Baudot Escarpment (EBE), a NW-SE volcanic transform fault system (Acosta *et al.*, 2001). The Algerian basin has previously been described as a Neogene back-arc oceanic basin that opened in response to the roll-back of the subduction of the Alpine–Maghrebian Tethys (Rehault, Boillot and Mauffret, 1984; Vergés and Sàbat, 1999; Mauffret *et al.*, 2004).

There are no boreholes within the study area to tie to the seismic profiles or to constrain the velocity model. The nearest borehole, Alger-1, is located 60 km to the south-east, in a perched basin, at only 100 m water depth, in a different geological setting (Burollet, Said and Trouve, 1978). The closest

borehole located in the deepwater Algerian basin is the ODP Site 975, more than 200 km away from the line, that penetrated only the uppermost Messinian sediments(Comas *et al.*, 1996).

Previous studies based their geological interpretation on the comparison with the analogous western Mediterranean margins, describing an Oligo-Miocene to Plio-Quaternary sediment cover, with the presence of thick (locally up to 2 km) Messinian evaporitic units both on the Balearic Promontory and in the deep offshore Algero-Balearic basin (Wardell *et al.*, 2014; Dal Cin *et al.*, 2016; Driussi, Briais and Maillard, 2015; Camerlenghi *et al.*, 2018; Raad *et al.*, 2021). The Mobile salt Unit (MU) is identified in both the deep Algerian basin and the intermediate depth Formentera basin. In the Formentera basin, it separates the Bedded Unit 2 (BU2) from the Bedded Unit 3 (BU3; Raad *et al.*, 2021). Laterally, when the salt pinches out, the BU2 turns into the Bedded Unit 1 (BU1) and/or the BU3. In the deep basin, the MU is highly deformed, with complex and steep salt structures locally deforming the seafloor, and separates the Messinian Upper Unit (UU) from the pre-salt unit (Camerlenghi *et al.*, 2009, 2018; Dal Cin *et al.*, 2016).

1.9 Datasets

1.9.1.1   SALTFLU

The "Salt deformation and sub-salt Fluid circulation" (SALTFLU) 2-D multi-channel seismic reflection dataset was acquired in June-July 2012 by the R/V OGS-Explora, Eurofleets Cruise No. E12. The survey was planned to study the influence of the MSG on pore fluid circulation during basin evolution since the post-Messinian. Participants included staff from the Institut de Ciències del Mar (Spain), the Universitat de Barcelona (Spain), the Istitució Catalana de Recerca i Estudis Avançats (Spain), the Istituto Nazionale di Oceanografia e di Geofisica Sperimentale (Italy), the Università di Trieste (Italy) and the FUGRO (Italy). The survey parameters for the seismic profiles are summed up in Table 3. Ten multichannel reflection seismic profiles were acquired (Figure 26). The data acquisition occurred mostly in optimal weather and sea conditions, with no relevant problems. The data contains a spectrum of frequencies spanning from a few Hz to about 200 Hz. They cover the transition from the Formentera basin, at about 1.5km water depth, to the deep Algerian basin, at 2.8 km water depth, where a thick layer of mobile Messinian salt lies down (Figure 1b).

The legacy SALTFLU processing followed a 'narrowband' approach, without deghosting, using narrow bandpass filters coupled with a source designature based on statistical deconvolution and no zero-phasing of the target wavelet. The filtering eliminated much of the low frequency signal (below around 6 Hz), whilst the source designature boosted the high frequency noise and produced a mixed-phase wavelet that has inconsistent phase across

the survey. The wavelet also contains strong residual energy (likely from the bubble pulse) that overprints and obscures the primary signal, particularly the shallow geology close to the waterbottom (Jovanovich, Sumner and Akins-Easterlin, 1983; Sheriff and Geldart, 1995; Yilmaz, 2001).

Table 3 Survey parameters for seismic survey Salt deformation and sub-salt Fluid circulation (SALTFLU) 2012

	SALTFLU 2012
Source	2 x 4 GI guns, 2940 cubic inch air-gun array (140 bar)
Shot Interval	25m
Source Depth	3m ± 0.5 m
Streamer Length	3000m
Near offset	100m
Number of Channels	240
Group Interval	12.5m
Streamer Type	Sercel Sentinel 428
Streamer Depth	4m ± 0.5 m
Record Length	8000ms
Sample Interval	2ms
Field filters	3 Hz - 200Hz
Nominal CMP interval	6.25 m
Nominal Fold	60
Coordinate Reference System	WGS84 UTM Zone 31N
Acquired By	OGS and Fugro
Vessel	OGS Explora
Acquisition Date	2012
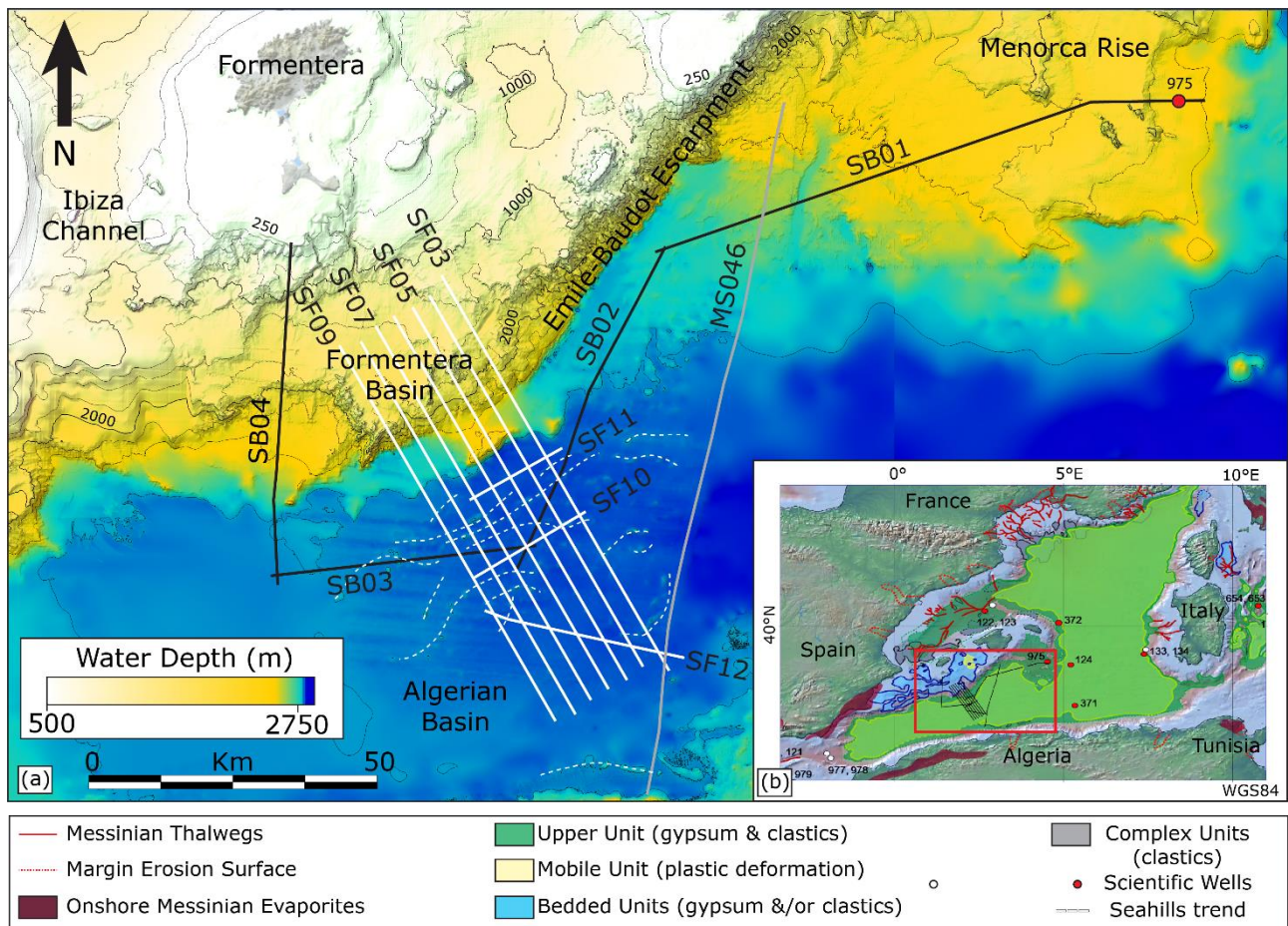
Figure 26 Location of the reprocessed seismic profiles. (a) Seismic lines acquired during the SALTFLU and SBAL-DEEP surveys, as well as line MS046, superimposed on the EMODnet bathymetric map (https://ows.emodnet-bathymetry.eu/wms). (b) Seismic lines superimposed on the extension map of the Messinian salinity crisis markers (modified from Lofi, 2018), with DSDP and ODP drillsites (sites sampling MSC evaporites in red). Profiles from the SALTFLU 2012 survey (in white) are prefixed with SF. SB refers to the SBALDEEP 2005 seismic acquisition (in black). MS refers to the Mediterranean Survey 1976 (in grey).

1.9.1.2   SBAL-DEEP

The Deep Sedimentary Environment of the South Balearic Margin (SBAL-DEEP) seismic dataset was acquired in 2005 by the R/V OGS-Explora, Cruise No. E12. The objective of the cruise was to identify the Plio-Quaternary pathways of sediment transfer from the conjugate margins of Algeria and of the Balearic to the Algerian basin. Participants included staff from the the Universitat de Barcelona (Spain), and the Istituto Nazionale di Oceanografia e di Geofisica Sperimentale (Italy). The survey parameters for the seismic profiles are summed up in Table 4. Four multichannel reflection seismic profiles were acquired (Figure 26). The data acquisition occurred in optimal weather and sea conditions but suffered from a lot of periodic noise and many missing channels. The data contains a spectrum of frequencies spanning from a few Hz to about 400 Hz but with a low S/N. It draws a transect that starts at the IODP site 975 and goes along the Emile Baudot escarpment in the deep Algerian basin, until the continental shelf of the Formentera Island (Figure 26).

Table 4 Survey parameters for seismic survey Deep Sedimentary Environment of the South Balearic Margin (SBAL-DEEP) 2005

	SBAL-DEEP 2005
Source	2 GI guns, 710 cubic inch air-gun array (140 bar)
Shot Interval	18.75m
Source Depth	6m
Streamer Length	600m
Near offset	52m
Number of Channels	48
Group Interval	12.5m
Streamer Type	OYO GEOSPACE DAS-1
Streamer Depth	3m
Record Length	5500ms
Sample Interval	1ms
Pre-amplitude Gain	24 db
Field filters	3 Hz – Anti Alias
Nominal CMP interval	6.25 m
Nominal Fold	16
Coordinate Reference System	WGS84 UTM Zone 31N
Acquired By	OGS
Vessel	OGS Explora
Acquisition Date	2005

1.9.1.3 MS-046

The Mediterranean Sea (MS) survey was acquired between 1969 and the end of the 1980s by the OGS, with the support of the Centro Nazionale di Ricerca (CNR). Line 046 was acquired in 1972. The survey parameters for the seismic profile are summed up in Table 5. The data contains a spectrum of frequencies spanning from 2 Hz to about 70 Hz, with a dominant frequency of

~25 Hz. It draws a 214 km transect within the Algerian basin, from the Balearic to the Algerian margin (Figure 26).

Table 5 Survey parameters for seismic survey Mediterranean Sea 46 (MS-046)

	MS-046
Source	Dynamite
Shot Interval	100m
Source Depth	~15m
Streamer Length	2400m
Near offset	~300m
Number of Channels	24
Group Interval	100m
Streamer Type	X
Streamer Depth	~25m
Record Length	10000ms
Sample Interval	4ms
Pre-amplitude Gain	?
Field filters	10 Hz – 52 Hz
Nominal CMP interval	50 m
Nominal Fold	12
Coordinate Reference System	WGS84
Acquired By	OGS
Vessel	Marsili
Acquisition Date	1972

1.10 Methods

I describe the methods by focusing only on the SALTFLU dataset. This is the dataset that has been used to define reprocessing strategy showed on Figure 27. It is also the one yielding the best resolution and S/N, hereby allowing a more in-depth study of the processing methods that can be used for enhancing legacy images. I also consider that the processing for SBAL-DEEP and MS046 do not show yet considerable improvements with legacy processing. Thei quality could be improved to better account for the specificities of each survey,

but I did not spend more time on this during my PhD. The differences are presented in section 1.10.6 for SBAL-DEEP and 0 for MS046.

Quality Check	Processing Step	Navigation Processing
	Input Field Data	**Import raw navigation**
Cross-plot maps	**Geometry merging**	**Edit Navigation** Match FFID numbers to the corresponding shot numbers based on observer's logs
Fold distribution, Stack	**CMP Binning**	
Output difference, Stack	**1st pass Low Frequency Noise Attenuation on shot gathers** Butterworth filter 2/30dB/Oct - 110/96dB/Oct	
Time direct wave first break on near channel	**Recording delay shift statics** Shift statics of -40 ms	
Visual checking	**Resampling to 4 ms**	
Output difference, Stack	**FX Prediction Filtering (CRG)** Run 1: 0-125Hz, 20 traces x 500ms windows, amplitude threshold > 8 Run 2: 0-125Hz, 11 traces x 500ms windows, amplitude threshold > 8 Run 3: 0-3Hz, 31 traces x 1000ms windows, amplitude threshold > 1 Run 4: 0-5Hz, 11 traces x 1000ms windows, amplitude threshold > 4 Run 5: 6-12Hz, 11 traces x 500ms windows, amplitude threshold > 5	
Visual checking	**Missing shot interpolation** Sorting to Common shot gathers 1st small gap interpolation in the F-K domain using patches of 500 ms x 21 traces 2nd big gap interpolation in the F-K domain using patches of 300 ms x 125 traces	
(**Output difference, Stack**)	**Linear Radon Filtering** Passing P range -0.35 to 0.7ms/m	
(**Output difference, frequency spectrum, Stack**)	**Deghosting in FK domain** Zero padding to left and right of shot gathers Extrapolation to left and right of shot gathers Receiver-side deghost, patch 2000 ms x 21 traces, reflection coeff -0.95, Regularization 0.05 Shot-side deghost, patch 1400 ms x 240 traces, reflection coeff -0.95, Regularization 0.1	**Stacking velocity analysis** 500m CMP interval for every line
Visual checking, frequency spectrum	**Signature Estimation** Align water bottom trim corrections base on max cross-correlation peak of traces Stack	
Visual checking, frequency spectrum	**Designature operator estimation** Design matching filter between water-bottom derived signature and a targeted band limited Zero-phase Ormsby wavelet 4-8-40-120	
Output difference, Stack	**Designature Application**	
Output difference, Stack	**Low-Frequency attenuation** Ormsby low-cut filter 3-7 Hz	
Visual, Frequency spectrum	**Inverse Q correction (phase)** Q =120 below seabed, reference frequency = 50 Hz	
Residual move-out, stack	**Isotropic Pre-Stack Time Migration, then velocity refining every 250 CDP (~1.5km)** Offset regularization	
Visual	**Radon Demultiple Model** Parabolic radon transform from -200ms to 500ms (reference offset= 2500m) with an AGC wrap of 500ms Left mute (Decreasing from 100 to 30 ms depending on iterations)	
Output difference, Stack	**Multiple substraction** Data - Radon Model	- OUT: Pre-migration final demultiple data - OUT: Stack & Migration RMS velocity
Output difference, Stack	**10 CDP (~50m), Automated residual velocity analysis** Auto-picking +- 10% velocity, every 25 ms Pick smoothing (51 CDPs)	
Visual, Frequency spectrum	**Inverse Q correction (amplitude)** Q =120 below seabed, reference frequency = 50 Hz	
Stack	**Stack** Angle mute 48deg Stack Waterbottom mute	- Processed Migration stacks

Figure 27 Time domain reprocessing sequence and parameters applied to the SALTFLU dataset

Reprocessing of the datasets is based on the following major processing stages:

1. Noise attenuation

2. Bandwidth enhancement, including source designature and source- and receiver-side deghosting.

3. Multiple attenuation, pre- and post-migration.

4. Iterative pre-stack migration and velocity model building in time and depth domains.

5. Post-migration processing, including seismic attenuation compensation.

Processing is performed using the REVEAL software from Shearwater Geoservices.

After loading, raw data are checked for integrity using header values (Field File Identification Number (FFID), shot point number, channel number) and cross-checked with the observer logs to assess FFID-shot point integrity. Near-trace plots are visually analysed to identify any problems with the source array (e.g., misfires, missing shots) and receiver channels (e.g., noise bursts, electrical interference). The acquisition setup did not record information on the positioning of the streamer, preventing accurate location of the common mid-points (CMPs). Instead, I use the ship positioning GNSS data and project the streamer along the smoothed ship track, resulting in CMP locations that roughly honour the ship track and likely feathering of the streamer. For SALTFLU the CMP binning is done using 6.25 m bins along the profile, giving a nominal fold of 60. After merging the navigation geometry into the trace headers, I subtract the recording time shift (40 ms), calculated as the average zero-offset time delay of the direct arrival (linearly extrapolated from the recorded data with a water velocity of 1511 m/s).

1.10.1   Noise attenuation

This stage aims to attenuate noise that could affect the deghosting and the estimation of the source signature. Firstly, data are resampled from 2 to 4 ms. A 3 Hz/30 dB-110 Hz/96 dB Butterworth bandpass filter is applied in the frequency domain (Figure 28b). The low- and high-cut values are chosen after analysis of the octave panels to ensure no elimination of signal (Figure 28a). The 3 Hz low-cut attenuates the very low frequency (1-3 Hz) part of the swell noise caused by pressure variations along the streamer (Bedenbender, Johnston and Neitzel, 1970; Dondurur, 2018). The 110 Hz high-cut filter is an anti-aliasing filter for later re-sampling to 4 ms.

The remaining low frequency part of the 'swell' noise is addressed by several iterations of frequency-space (F-X) domain prediction filtering (Hornbostel, 1991; Schonewille, Vigner and Ryder, 2008). I perform up to 5 iterations on common-receiver gathers, followed by 5 iterations on common-shot gathers. The first two iterations target broad noise bursts at all,
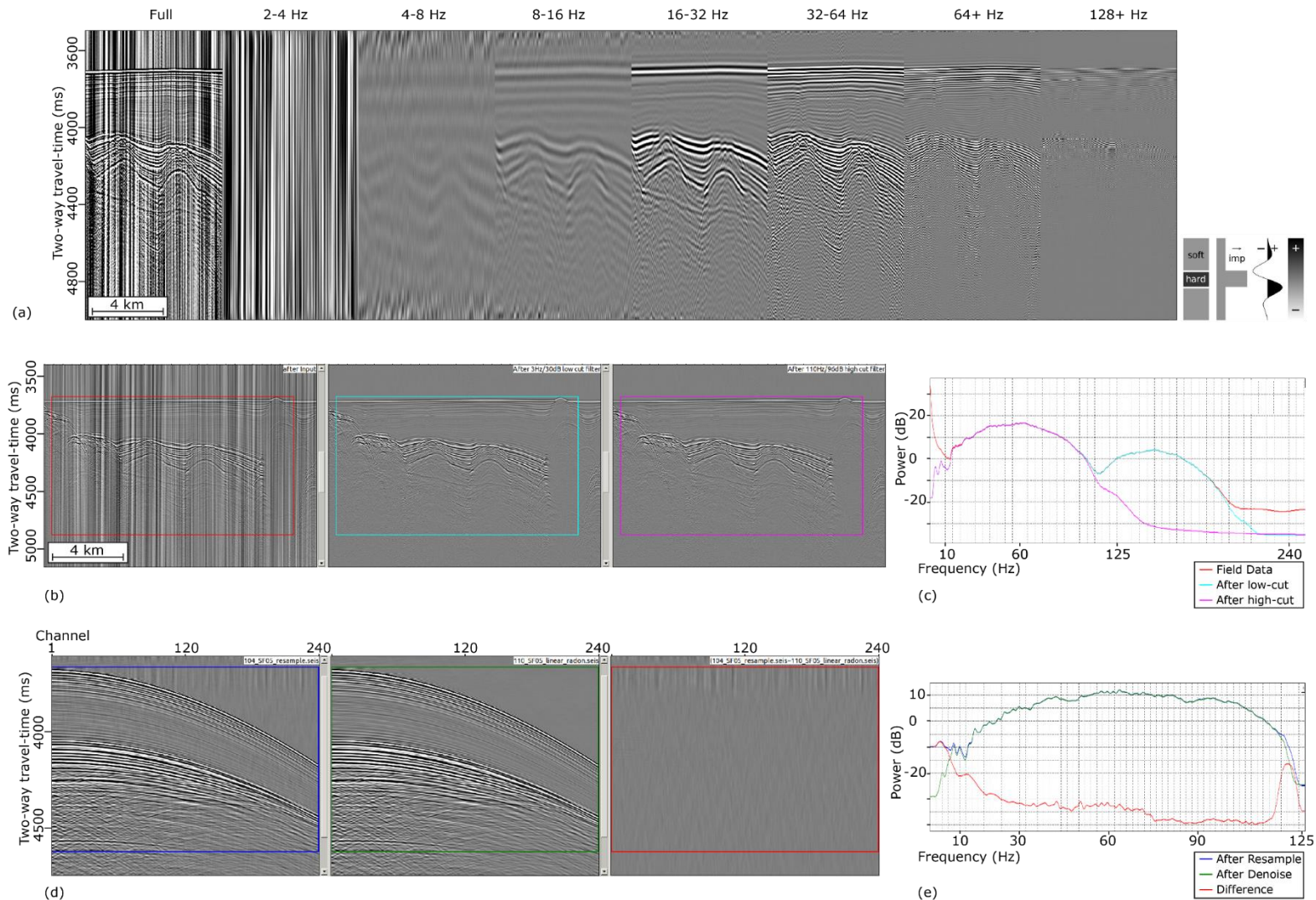
Figure 28 Seismic sections of part of the SF05 line illustrating the results at different steps of the noise attenuation stage (a) Frequency panels at different octaves of raw field data; (b) Input near-trace-plot (left), outputs after low-cut filter (middle) and high-cut filter (right); (c) Frequency spectra corresponding to (b); (d) Input shot gather after resampling to 4 ms (left) versus after linear low-frequency noise removal steps (middle), and difference panel between the two (right); (e) Frequency spectra corresponding to (d).

frequencies, while later iterations target local noise bursts with frequencies between 0-3 Hz, 0-5 Hz and 6-12 Hz respectively. The total number of iterations depends on the amplitude of the 'swell' noise for each individual profile. The F-X prediction filtering has the secondary effect of attenuating amplitude spikes present in the dataset (e.g., from electrical interference).

After this initial filtering and resampling, missing shots and traces removed during shot and channel edits (Section 2) are interpolated on common-receiver gathers. This is performed by frequency-wavenumber (F-K) domain interpolation in two steps: 21 traces x 500 ms patches to target small gaps, then 125 traces x 300 ms patches to target larger gaps. Finally, forward and inverse linear Radon (τ-p) transforms are performed on shot gathers to further reduce the remaining 'swell' and random noise (Figure 27).

1.10.2   Deghosting and source designature

Deghosting is performed on shot gathers in the F-K domain to attenuate the source- and receiver-side 'ghost' effect resulting from sea surface reflections. Shot gathers are transformed into the F-K domain, where the notch location varies as a function of frequency and horizontal wavenumber, illustrating that the ghost time-delay is dependent on the emergent angle (Amundsen, 1993; Day *et al.*, 2013). The optimal deghosting operators for each frequency and wavenumber are estimated through a least-squares inversion scheme, minimizing the error between the model and the recorded data, parameterized based on the acquisition and medium parameters (i.e. receiver depth, water velocity, sea surface roughness). An inverse two-dimensional (2D) Fourier transform is then performed to return the deghosted data in the time-space domain. The deghosting is window based to account for the non-stationary nature of the ghost in time and space. Prior to deghosting, shot gathers are padded by inserting 30 near-offset traces (362.5 m) and 10 far-offset traces (112.5 m) to prevent amplitude leakage from the forward and inverse transforms (Yilmaz, 2001). The receiver-side ghost is estimated in local patches (500 ms x 11 channels), and the source-side ghost is estimated in broader time patches (1000 ms x 240 channels). After deghosting, a further F-K filter is applied to remove artefacts that may be introduced during the deghosting, particularly at the edge of the gathers. A regularization parameter is applied (0.01 for the receiver side, 0.001 for the shot side) to prevent the amplification of low frequency noise (Wang, Wu and Chen, 2017; Denisov, Egorov and Burtsev, 2018)After deghosting, I apply a deterministic source designature to collapse the bubble pulse, sharpen the wavelet and zero-phase the data (Figure 29a). I follow the workflow of Sargent et al. (2011), where the far-field source signature is derived from the flattened and stacked water-bottom reflection (Figure 29d). A matching filter is then designed to convert the estimated far-field source signature to a zero-phase band-limited Ormsby wavelet (4-8-70-120 Hz). Using a single deterministic operator yields better
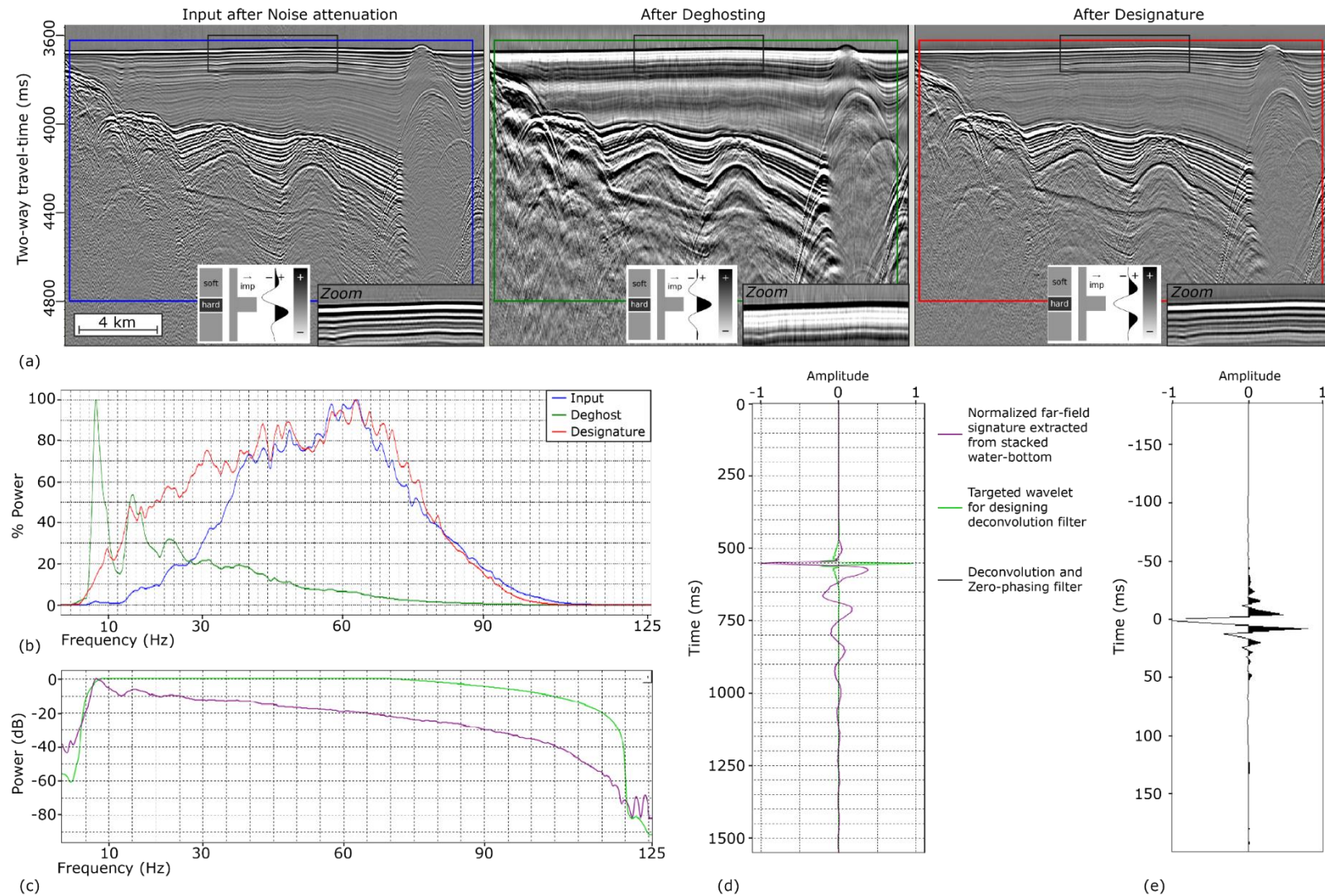
Figure 29 Results from the bandwidth enhancement stage. (a) Near-trace gather before deghosting (left), after deghosting (middle) and after source designature (right); (b) Frequency spectra corresponding to (a); (c) Far-field source signatures estimated from the stacked seabed, overlain with the target Ormsby wavelet used for designing the   source designature (debubble and zero-phasing) operator.; (e) The resulting source designature operator

sub-seabed consistent, imaging and low frequency recovery superior to probabilistic methods (e.g., surface-consistent spiking and predictive deconvolution) and modelled source methods (Sargent, Hobbs and Gröcke, 2011; Davison and Poole, 2015; Maunde *et al.*, 2017). Converting the seismic data to zero-phase tends to improve temporal resolution and lowers interference between closely spaced reflectors, allowing for better delineation of the stratigraphy, and is a necessary pre-condition for Kirchhoff-type migrations (Sheriff and Geldart, 1995).

Finally, an inverse-Q filter (phase only) is applied immediately before migration to compensate for dispersion effects caused by seismic attenuation (Sams *et al.*, 1997). Dispersion introduces a phase-shift with increasing propagation depth. Compensating for this is necessary to ensure that the wavelet remains zero-phase with increasing propagation depth (Wang, 2006). A two-layer Q model is used, with $Q = 1000$ in the water layer (essentially non-attenuating). I choose a value of $Q = 70$ in the subsurface, based on a constant single value that best flattens the frequency spectrum and balances amplitudes with depth across all the profiles in the survey.

1.10.3   Multiple attenuation

The water depth exceeds 1500 m in the survey area and the free surface 'waterbottom' multiples generally arrive later than most of the reflected primary signal at the target depths. High amplitude short period internal multiples are, however, observed throughout the survey, generally linked to the strong impedance contrasts associated with the salt (Fig. 5). I therefore attempt to attenuate both long and short period multiples using moveout discrimination techniques.

Before migration, I perform multiple attenuation in Radon domain (Figure 30). Normal moveout (NMO) correction is performed using the RMS velocity model (Section 1.10.1) to flatten primary energy, and the CMP gathers are transformed into the Radon domain using a least squares parabolic Radon transform (Sacchi and Porsani, 1999). The Radon domain multiple model is defined by a time-varying inner moveout mute (Figure 2). A top mute is applied at 200 ms below the water bottom to avoid attenuating primary energy in the shallow Plio-Quaternary (largely free of internal multiples). I then perform the inverse Radon transform on the multiple model and subtract from the original data.

I perform a second pass of Radon multiple attenuation post-migration, with a similar workflow to the pre-migration demultiple. For the depth domain processing (Section 1.10.2), the depth migrated CDP gathers are first converted to time domain using the time migration velocities, the Radon demultiple is applied, and the CDP gathers are converted back to depth domain using the same velocity field.
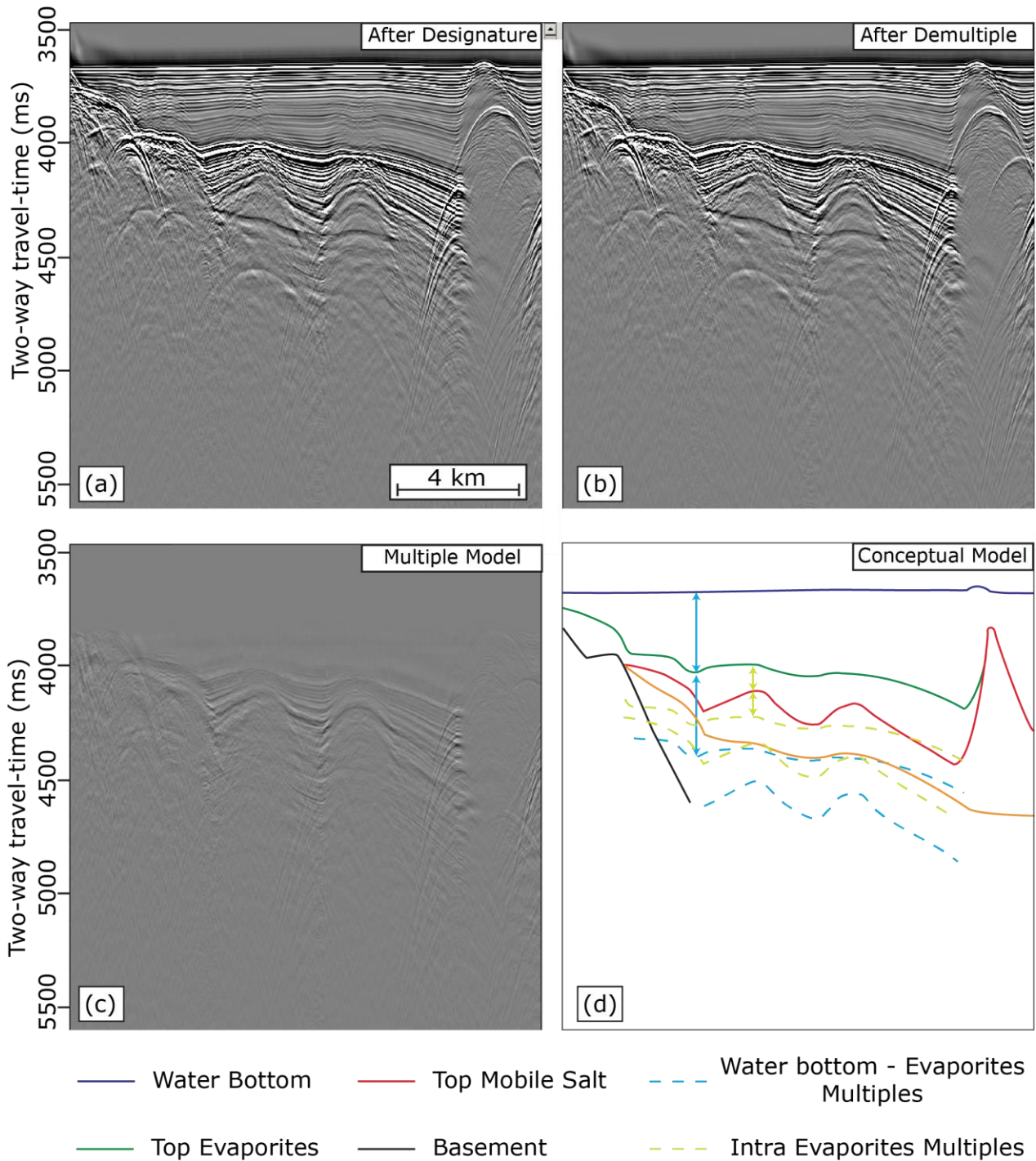
Figure 30 Stacked sections after Radon demultiple. (a) Input data; (b) Demultipled data; (c) Difference between (a) and (b), i.e., the modelled multiples; (d) Sketch cartoon of the major multiple generating horizons and corresponding multiples. Due to the water depth water-bottom (blue) related multiples are not superimposed on the primary reflections in the target geology and are not an issue for the deep-water Algerian basin. Most multiples are observed below the Top Evaporites (green).

1.10.4 Iterative migration and velocity model building

1.10.4.1 Time domain

Our approach to velocity model building in the time domain involves picking RMS velocities on semblance panels on migrated CMP gathers. I perform several iterations of migration velocity analysis, gradually refining the velocity field.

A sparse initial velocity model is picked from semblance analysis of unmigrated CMP gathers every 500 CDP (~3km). This initial velocity model is primarily used as a stacking velocity to quality control intermediate processing stages, and for the initial pre-stack time migration.

I use a Kirchhoff pre-stack time migration to image the data. Before migration, the data are regularised into evenly spaced offset bins of 50 m using a partial NMO correction. The migration aperture is parameterised by analysing the migration impulse response (Figure 31). Aperture is broadened from 1500m at 1500ms to 3500 m at 5000ms. After the migration, I perform Radon domain multiple attenuation (Section 1.8) with broad parameters (minimum moveout -100 ms, maximum moveout +300 ms) to avoid attenuating primary reflections for the following velocity analysis.
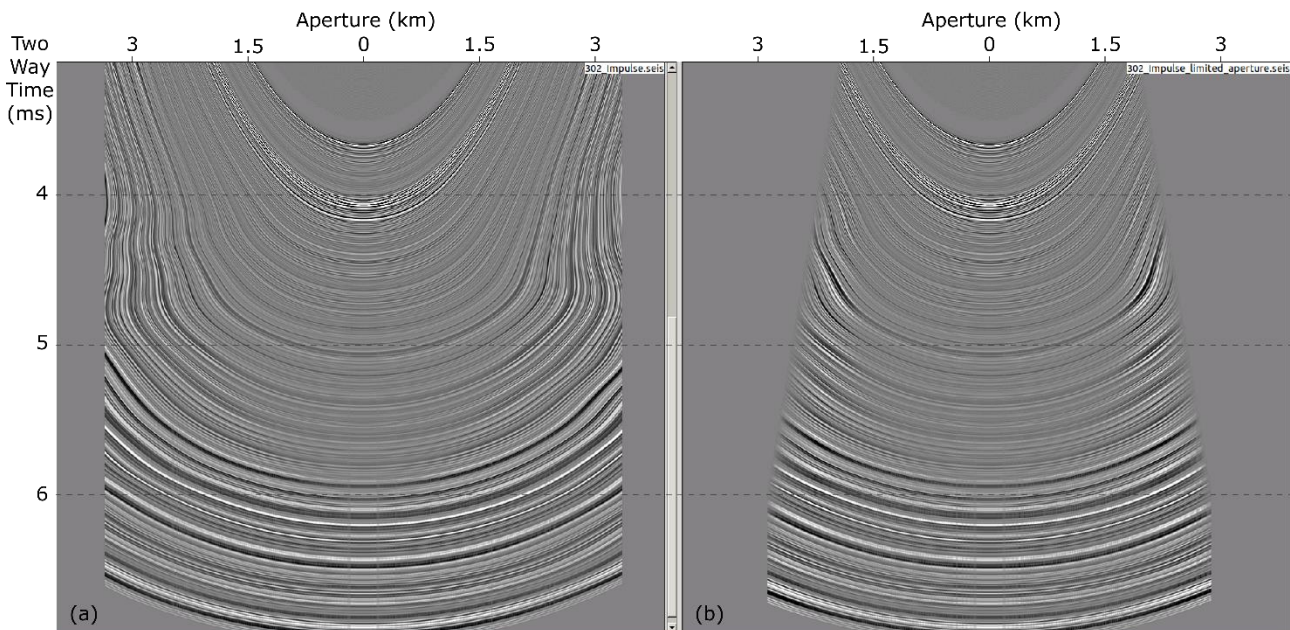
Figure 31 Impulse response of the Kirchhoff Pre-Stack time migration in the deep Algerian basin, without (a) and with an angle aperture (b).

I perform migration velocity analysis on the migrated CMP gathers every 250 CMP (~1.5 km). The migration followed by velocity analysis is repeated three times until the primary reflections are flattened on the migrated gathers.

1.10.4.2   Depth domain

Depth domain processing aims to estimate an interval velocity model and produce depth migrated seismic images. Similar to the time domain model building, I use an iterative approach by repeatedly performing velocity analysis on migrated gathers, gradually refining the velocity field. Our criteria for a successful velocity model are that the primary reflections are flat after depth migration.

I use a Kirchhoff pre-stack depth migration to migrate the data in depth domain. The input data to the migration are the regularised CMP gathers (after Radon demultiple and phase-only inverse-Q filtering) as were used in the pre-stack time migration (Section 1.10.1). The parameters used for travel-time computation are detailed in Table 6.

Table 6 List of the parameters used for the Kirchhoff pre-stack depth migration

PSDM Parameters	
Ray Tracing	
Gridding	2 CMP x 5meters
Number of rat takeoff angles	25
Maximum takeoff angle	60°
Stepper type	adaptive
Error tolerance	0.0004 m
Mimimum step	4 ms
Maximum step	10 ms
Wavefront step	10 ms
Coincident ray selection	minimum traveltime
Maximum ray separation	100 m
Maximum ray normal divergence	10°
Interpolate rays using	wavefront reconstruction
Maximum ray angle to vertical	90
Maximum travel time	3500 ms
Maximum ray generation	7
Maximum shot time	120 s
Gaps filling	Fast sweeping method for eikonal equations
Kirchhoff prestack depth migration	
Depth increment	5 m
Aperture (Depth/Radius)	1000-1500 /3250-3100/4500-4000
Angle limit to aperture	70°
Trace interpolation factor	8
CMP bin patch size	3
Antialisaing filter increment	2.5 Hz
Antialisaing filter roll-off	20 db/octave
Pad Fast Fourrier Transform	500 samples
Amplitude scaling	2D
Derivative filter	2D

The initial velocity model is built using a water velocity (which I assume to be constant) and sediment velocities derived from the time domain velocity analysis (Section 1.10.1). The water velocity is estimated by performing a range of constant-velocity depth migrations (1450-1550 m/s). I choose a constant water velocity of 1525 m/s, which best flattens the waterbottom reflection across the different SALTFLU profiles. To derive the interval velocity

model for an initial migration, I first flatten the RMS velocity models (Figure 32a) along the waterbottom (in time, (Figure 32b). The RMS velocity models are then converted to interval velocity models (in depth, (Figure 32c) using a Dix conversion (Dix, 1955). Then, the resulting interval velocities are smoothed (100 m x 500 CDP), before shifting back to the original waterbottom depth (Figure 32d). The initial depth migration is performed using this initial velocity model and the input gathers to the final pre-stack time migration.
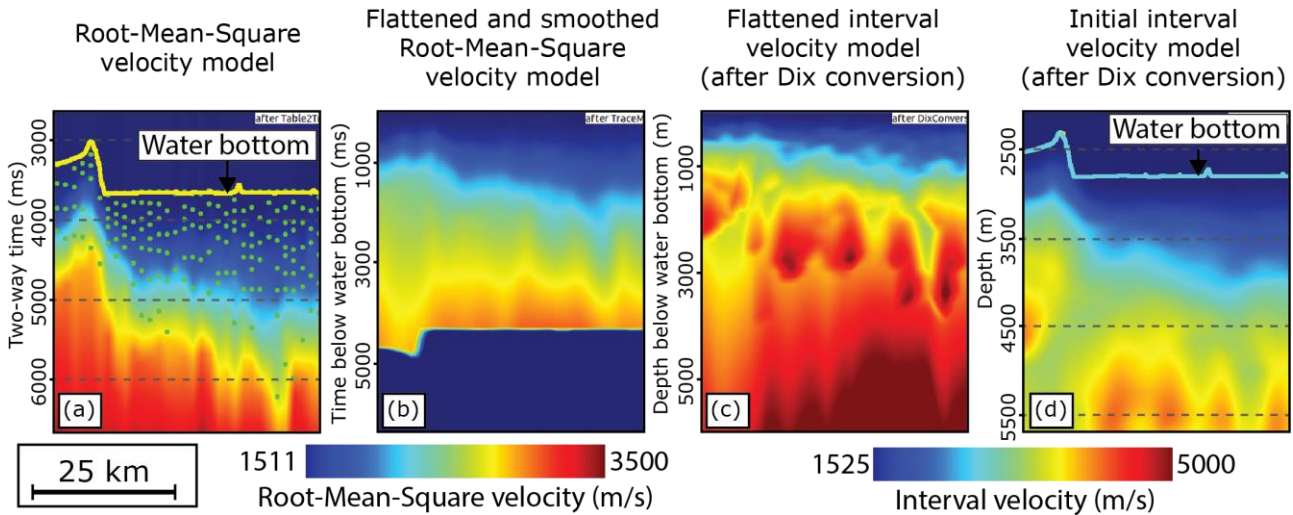
Figure 32 Velocity models during the Dix conversion. The root-mean-square velocity model (a) is flattened along the water bottom (in time) and smoothed (b) before the Dix conversion to the interval velocity model (c) and the shift back to the water bottom in depth (d).

Following this initial pre-stack depth migration, I obtain velocity updates using a global tomography procedure comprising automated offset-dependent residual moveout picking, ray tracing and travel-time tomography. The velocity update in each iteration is limited to -10% and +20% of the input velocity, respectively. The automated picks are quality controlled by visually checking that the picks correlate with major reflectors, eliminating picks with low trace-to-trace correlation and eliminating picks with anomalously high moveout correction. Travel-time tomography is then used to compute model updates from these edited picks. The parameters used for tomographic updates for each velocity model building iteration are detailed in Figure 33. I consider that the velocity model is good enough when most reflectors appear flat on migrated gathers. The first two iterations are performed only for the post-salt sediments, updating only between the interpreted water bottom and the top salt horizons. Initially, the top salt horizon is interpreted from the time domain data and converted to depth using the initial velocity model. The picking of the top salt horizon is refined for each velocity updates to fit the new depth image and limit the tomographic iteration to the post-salt.

The sediment model (Figure 34a) is then flooded with salt velocity from the top salt horizon to the base of the profiles (Figure 34b). The velocity used for the flooding is chosen by migrating profiles with the salt flood models with a range of salt velocities and observing the flatness of the base salt reflector.

Iteration 1 and 2		Iteration 3 and 4		Iteration 5 and 6	
L-Matrix Building		**L-Matrix Building**		**L-Matrix Building**	
CMP griding	every 2 CMP (12.5m)	CMP griding	every 2 CMP (12.5m)	CMP griding	every 2 CMP (12.5m)
Depth griding	5 m, from 0 to 5 km	Depth griding	5 m, from 0 to 7 km	Depth griding	5 m, from 0 to 7 km
Raytracing options		**Raytracing options**		**Raytracing options**	
surface tolerance	50 m	surface tolerance	50 m	surface tolerance	50 m
stepper type	adaptive	stepper type	adaptive	stepper type	adaptive
error tolerance	0.0004 m	error tolerance	0.0004 m	error tolerance	0.0004 m
mimimum step	4 ms	mimimum step	4 ms	mimimum step	4 ms
maximum step	10 ms	maximum step	10 ms	maximum step	10 ms
maximum traveltime	3.5 s	maximum traveltime	3.5 s	maximum traveltime	3.5 s
number of ray pairs traced per event	20	number of ray pairs traced per event	20	number of ray pairs traced per event	20
Max takeoff angle	50°	Max takeoff angle	50°	Max takeoff angle	50°
Inversion options		**Inversion options**		**Inversion options**	
Stopping criterion solver	1%	Stopping criterion solver	1%	Stopping criterion solver	1%
Maximum number of iterartions	200	Maximum number of iterartions	200	Maximum number of iterartions	200
Smoothing preconditionner	500m (x) x 10 m (y)	Smoothing preconditionner	1250 (x) x 50 m (y)	Smoothing preconditionner	1500m (x) x 50 m (y)
Mask	Seabed to Top Evaporites	Mask	Seabed to Top Salt	Mask	Seabed to bottom line
Maximum update	-10% to +15%	Maximum update	-10% to +15%	Maximum update	-5% to +15%
Laplacian Regularisation	2500 at top, 6000 at bottom	Laplacian Regularisation	5000 at top, 8000 at bottom	Laplacian Regularisation	5000 at top, 8000 at bottom

Evaporites Flooding

From top evaporites to bottom line

2500+0.6(|z-z0|) m/s

Salt Flooding

4300 m/s, First from Top salt to Bottom line to pick the base salt

Secondly from Top to Base salt

Pre-salt Flooding

2700+1.2(|z-z0|) m/s

From Base Salt to Basement or Bottom line (when no basement visible)

Figure 33 Depth imaging flow and list of the parameters used for the different tomographic inversion and velocity updates during the velocity model building

86

Figure 34 Pre-stack depth migration sections and velocity models after 3 iteration of tomographic velocity updates in the post-salt (before salt velocity flooding) (a); after salt velocity flooding until the bottom of the sections in order to pick the base salt horizon (b); and after salt velocity flooding between top and base salt horizons and two iterations of tomographic velocity updates post flooding (c).

I find that a salt velocity of 4300 m/s best flattens this reflector for survey profiles. The transition from the sediment velocity to the salt velocity is Gaussian smoothed (50 x 50 m) to enable projected rays to pass through the sharp velocity contrast during travel-time computation for the migration and tomography. The base salt horizon is interpreted on the depth migrated stacks after salt flooding, and a new velocity model is built with a salt velocity flooding that stops at this newly picked base salt (Figure 34c). The pre-salt is also flooded with a velocity gradient starting from the base salt horizon. I test the velocity gradient with a range of starting velocities and velocity gradients and assess the overall flatness of reflectors in the pre-salt. After testing, the best results were obtained with a gradient of 2700 m/s + 1.2 (m/s)/m. Finally, two more iterations of tomographic velocity updates are performed following the pre-salt flooding. After the final depth migration, Radon domain demultiple is performed as previously described for the time domain processing (Section 1.9).

1.10.5   Post-migration processing

After the final migration, residual moveouts are automatically picked every 4 CDP (~20m) using semblance velocity spectra. The residual moveout analysis is limited to 5% change, and the resulting picks are smoothed spatially (25 ms x 200 CMP). The residual moveout field is applied to the migrated CMP gathers before stacking. Additionally, I apply an inverse-Q filter (amplitude only) to compensate for the frequency-dependent amplitude attenuation caused by seismic absorption. The Q model is the same as was previously for the phase-only inverse-Q filter (Section 1.8). I then apply an inner angle mute (at 1.2°) to target near-offset residual multiples and an outer angle mute (at 48°) to remove far-offset refractions and data affected by wavelet stretching. The CMP gathers are stacked, and a low-cut frequency filter is applied (Ormsby, 500ms, 4-12 Hz) in a short 400ms window below the seabed to target residual bubble energy.

1.10.6   Processing for SBAL-DEEP

I tried to apply a similar strategy that the one previously presented for SALTFLU for SBAL-DEEP, with a few additional steps (Figure 35). The downside of SBAL-DEEP is a very low S/N and very low fold due to bad channels records (Figure 36, Figure 37). I could not find an optimal trade-off between noise attenuation and low-frequency preservation, and resulting images still display a medium S/N (Figure 38). To attenuate the very strong noise, I had to apply high low-cut filters (up to 24 Hz). Even after this, the S/N is low. Consequently, the benefit of bandwidth enhancement is limited. I only apply channel-side deghosting and designature based on the water-bottom signature. I did not yet attempt the PSDM. Because of the very short far offset (~600 m) and the low S/N (particularly for frequencies below 24 Hz), I

consider that the SBAL-DEEP survey can image the base of the MSG only where salt is thin and not highly deformed. Therefore, it shows limited interest for the study of the MSG tectonics. I did not invest more time into it for this work, but the high resolution of SBAL-DEEP could potentially be valuable for studying the expression of the MSC in details.

Quality Check	Processing Step	Navigation Processing
	Input Field Data	**Import raw navigation**
Cross-plot maps	**Geometry merging**	**Edit Navigation** Match FFID numbers to the corresponding shot numbers based on observer's logs
Fold distribution, Stack	**CMP Binning**	
Output difference	**Auto-zero high amplitude burst** Zero traces where amplitude is 10 times higher than the gather average	
Output difference, Stack	**1st pass Low Frequency Noise Attenuation on shot gathers** Butterworth low-cut filter 6/30dB/Oct	
Output difference, Stack	**100 Hz Notch filter on shot gathers**	
Time direct wave first break on near channel	**Recording delay shift statics** Shift statics of -10 ms	
Visual checking	**Resampling to 2 ms**	
Output difference, Stack	**Local RMS based Time-Frequency Domain filtering (CRG)** 1st run: Transform length 240 ms, noise threshold 2, statistics window 25 ms x 3 traces	
Output difference, Stack	**FX Prediction Filtering** Run 1: CRG, 0-6Hz, 11 traces x 1000ms windows, threshold > 1.5 Run 2: CRG, 8-12Hz, 21 traces x 500ms windows, threshold > 1.6 Run 3: CSG, 4-24Hz, 21 traces x 500ms windows, threshold > 6 Run 4: CSG, 4-12Hz, 21 traces x 500ms windows, threshold > 2.5	
Output difference, Stack	**Local RMS based Time-Frequency Domain filtering (CRG)** 2nd run: Transform length 240 ms, noise threshold 2, statistics window 25 ms x 3 traces	
Output difference, RMS map	**Surface Consistent Amplitude Corrections**	
Visual checking	**Missing channel interpolation** small gap interpolation in the F-K domain using patches of 100 ms x 13 traces	
(**Output difference, Stack**)	**Parabolic Radon Filtering** Passing moveout range 10 to 200ms	**Stacking velocity analysis** 500m CMP interval for every line
Visual checking, frequency spectrum	**Deghosting in FK domain** Zero padding to left and right of shot gathers Extrapolation to left and right of shot gathers Receiver-side deghost, patch 500 ms x 3 traces, reflection coeff -0.95, Regularization 0.05	
Visual, Frequency spectrum	**Inverse Q correction (phase)** Q =120 below water bottom, reference frequency = 80 Hz	
Residual move-out, stack	**Isotropic Pre-Stack Time Migration, then velocity refining every 250 CMP (~1.5km)** Offset regularization	
Output difference, Stack	**10 CMP (~50m), Automated residual velocity analysis** Auto-picking +- 10% velocity, every 25 ms Pick smoothing (51 CDPs)	- OUT: Stack & Migration RMS velocity
Visual, Frequency spectrum	**Inverse Q correction (amplitude)** Q =120 below seabed, reference frequency = 80 Hz	
Stack	**Stack** Stack	
Output difference	**Post-Stack Processing** Ormsby low-cut filter 4-12 Hz Waterbottom mute	- Processed Migration stacks

Figure 35 Time domain reprocessing sequence and parameters applied to the SBAL-DEEP dataset

In total, 21 out of 48 channels did not function properly and did not record any signal (Figure 36, see d for example). The amplitude level is not consistent between the channels, with some channel displaying a much dimmer signal with a strong noise compared with the rest of the others (compare the power level difference between frequency spectra on Figure 36 c and e).
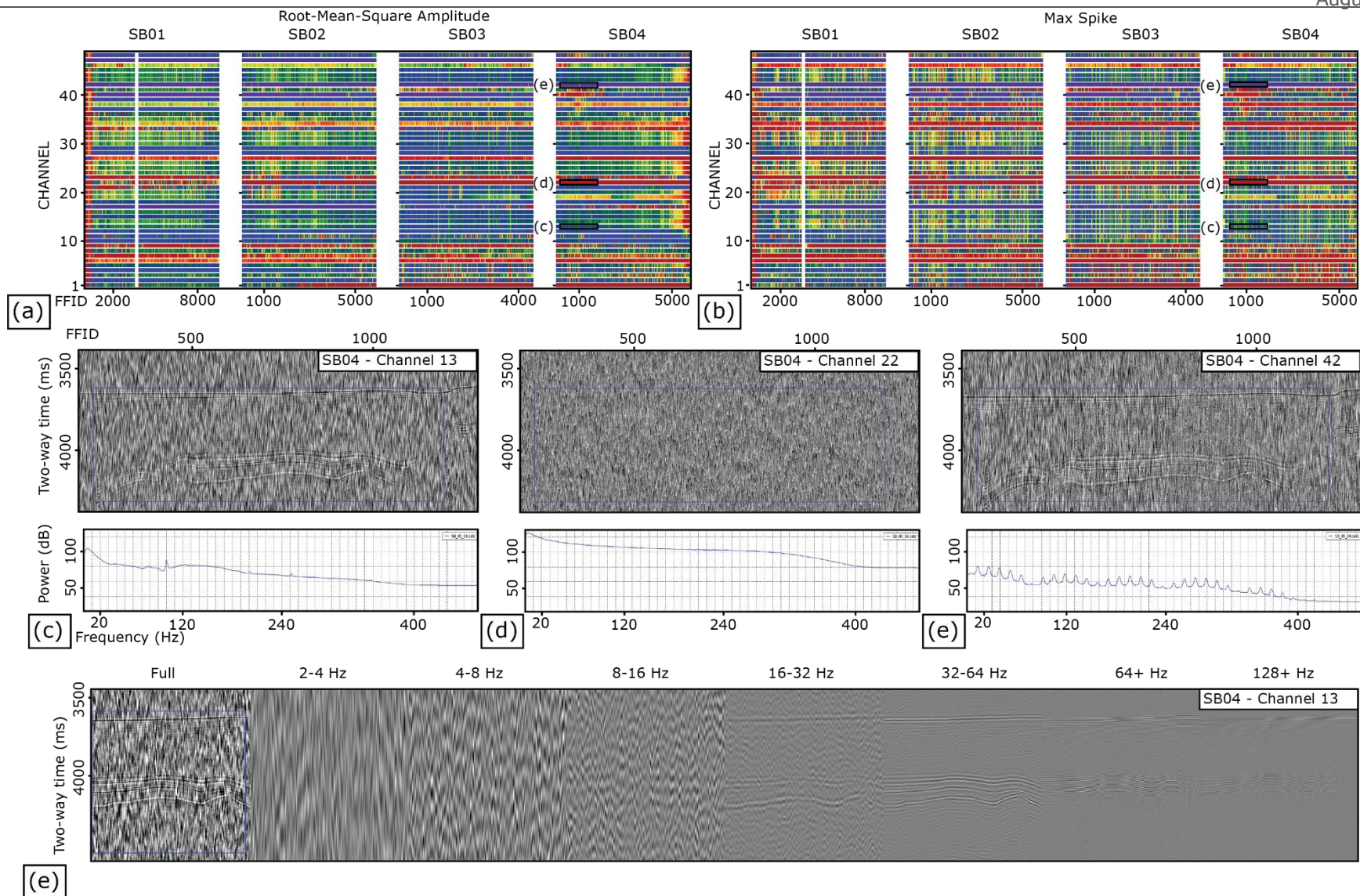
Figure 36 Overview of the raw field data for survey SBAL-DEEP. Cross-plots of the Root-Mean Square amplitude (a; from the water bottom, window length of 2s) and maximum amplitude for the SBAL-DEEP profiles (from the water bottom to the end of the records). Sections of common channels gathers and their corresponding frequency spectra for channels 13 (c), 22 (d) and 42 (e) of profile SB04. (e) Frequency panels at different octaves of a section of SB04.
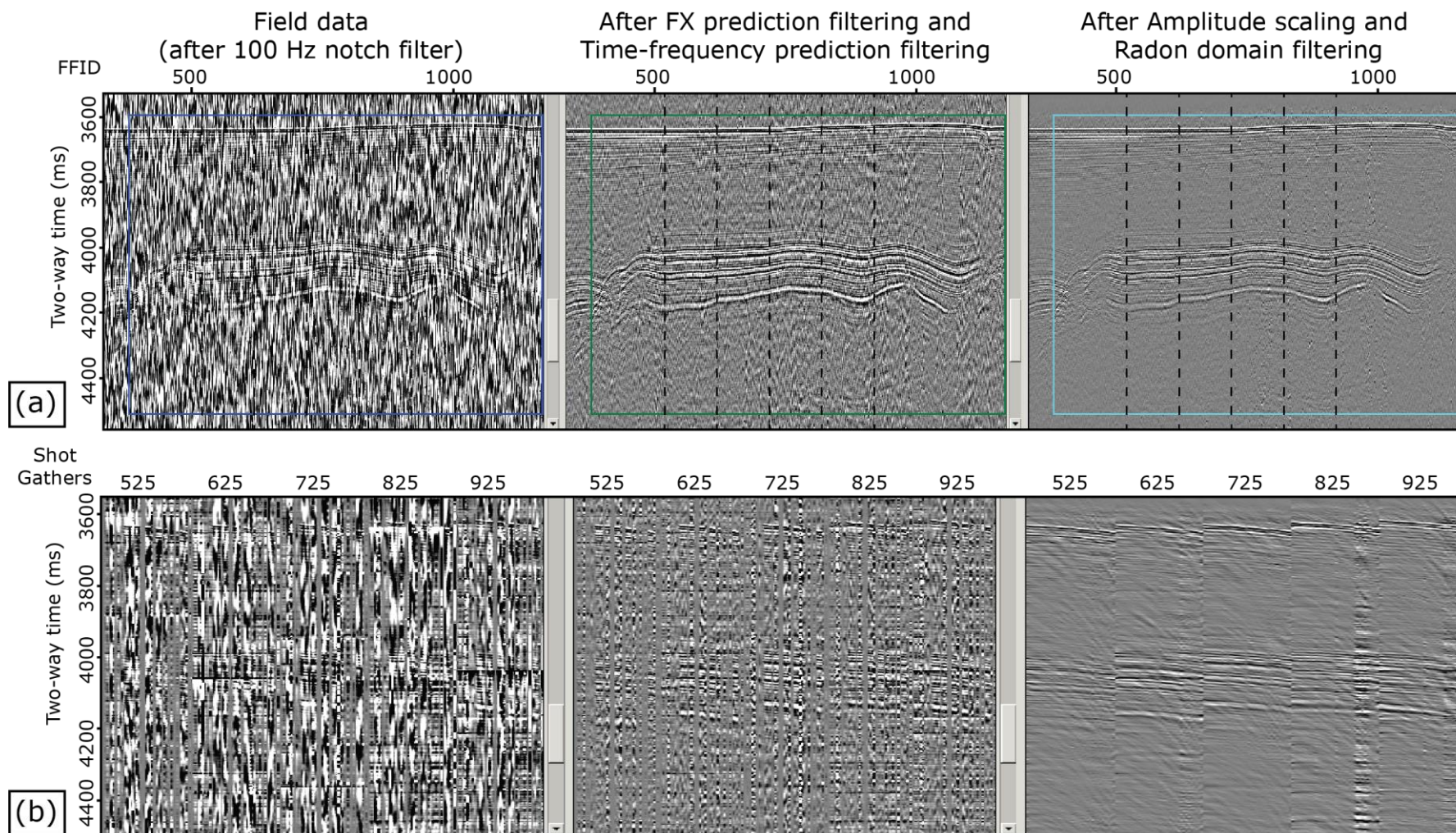
Figure 37 Gathers showing a section of SB04 through the denoising. (a) Near-trace-plots after 110 Hz notch filter on field data (left), after two iterations of FX prediction filter and Time-Frequency prediction filtering (middle) and after amplitude scaling and radon domain filtering (right). (b) Corresponding shot gathers (location illustrated by dashed lines on (a)) through the same denoising steps

All the bad channels that did not record any signal are zeroed post denoising. First channels 1 to 11 record no to very low signal and are eliminated, shifting the nearest recorded offset from 52m to 190m. Channels 2and 5 did record some signal but with a strong noise component. They could be kept but it would leave a large channel gap in shot gathers that could not be interpolated with confidence. The last three channels 46 to 48 are also eliminated, shifting the maximum recorded offset from 640 to 602m. This also results in a disparate and low fold (12 traces per CMP gather on average). With such a low fold, stacking itself does not attenuate well incoherent noise.

The SBAL-DEEP field data is also characterized a very low S/N ratio. Noise sources include (Figure 37, Figure 37):

- high amplitude horizontal noise on shot gathers (Figure 37b),

- Amplitude spike bursts,

- spikelike amplitudes at 100Hz and its harmonic multipliers in the amplitude spectra,

- swell noise

A notch filter is applied at 100 Hz before resampling to attenuate the spikelike amplitudes. The higher frequency harmonics produce negligible ringing and could not be attenuated without attenuating primary signal. The processing flow includes several iterations of RMS based Time-Frequency (TF) domain filtering, on common channel gathers. It aims at eliminating the amplitude bursts and the high amplitude horizontal noise. On channel gathers, the horizontal noise observed in shot gathers appears as point like amplitude bursts (Figure 37a). Channel gathers are transformed in the TF domain, and RMS amplitude is calculated in windows of 25 ms x 3 traces. If one of the traces yields an outlying RMS_amp (3 times superior to the RMS-amp of the window), then its amplitude is attenuated by 100. That way outlying amplitude bursts are attenuated without zeroing the whole trace. The resulting dataset after denoising display a better but still low S/N (Figure 37). Amplitude is scaled using a method similar to Taner and Koehler, (1981), in the channel domain.

A satisfying noise attenuation could be achieved only by considerably attenuating the low-frequency band of the data. Consequently, bandwidth enhancement shows limited recovery of the low frequencies: Deghosting is limited to the cable-side because I could not make it stable on the source-side. I interpret this to be due to the high remaining presence of noise, and the 100Hz notch in the spectrum that disturb the inversion in the FK domain. Nonetheless, the resulting images display a clearer base salt (Figure 38).
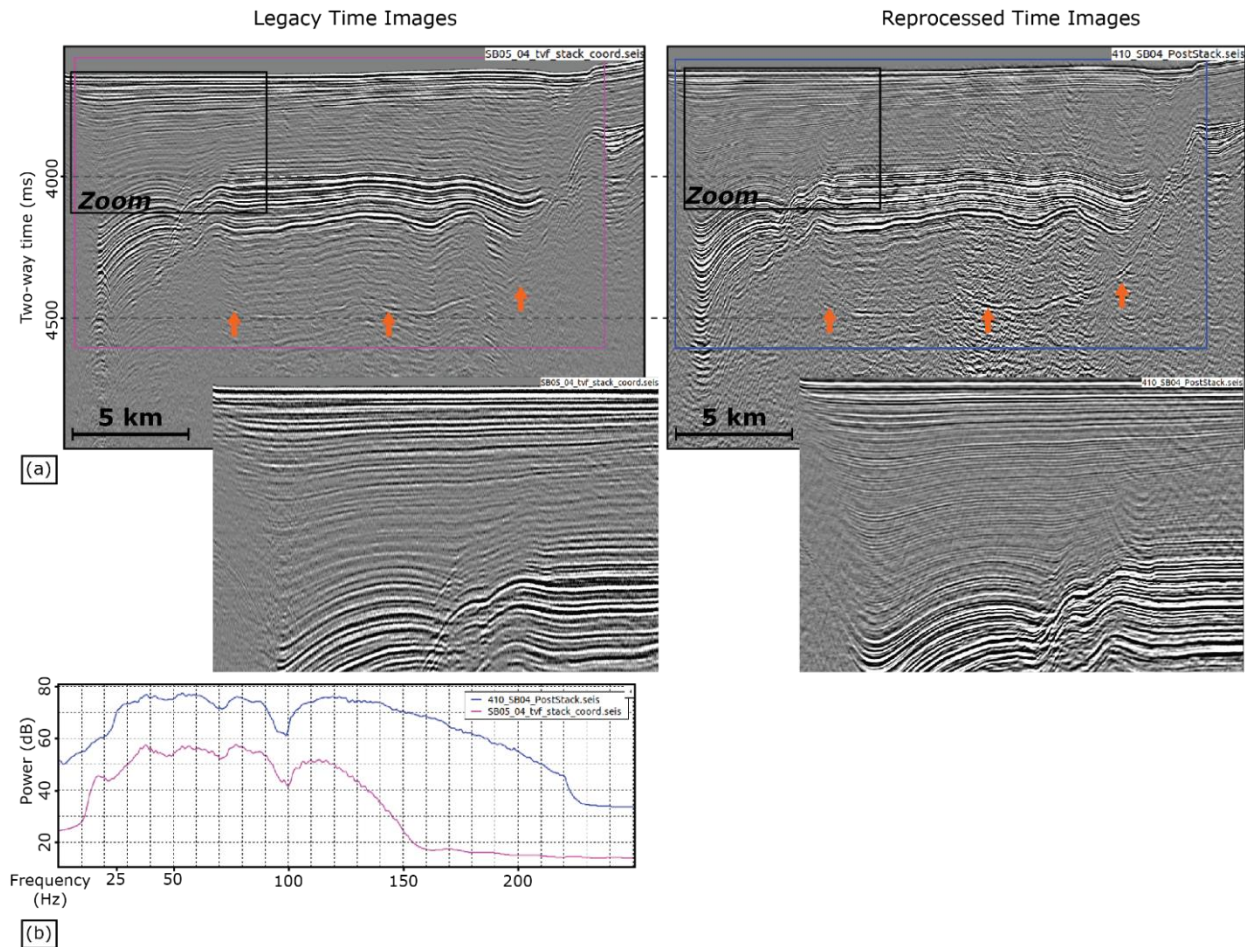
Figure 38 (a) Comparison between the legacy time images and the newly reprocessed time images, with zoom sections showing the improving resolution and continuity of reflectors. (b) Corresponding frequency spectra for (a). Orange arrows points the base of the high velocity mobile salt.

The new images show a higher resolution and, locally, a better continuity of reflectors (Figure 38a). The processing of the legacy data is unknown, but the spectrum of the stacks show that a bandpass filter was applied (~8-30-90-140; Figure 38b) to deal with the strong low-frequency noise and attenuate high-frequencies. The low-frequency enhancement of the new images result in a lower attenuation of the noise compared to the legacy data (high amplitude migration "smiles" on Figure 38a), but it improves the imaging of the base salt (Figure 38a). Further improvements might be achieved to improve the S/N of the images (e.g., deghosting, low frequency preserving noise attenuation, amplitude balancing) but I did not take the time to invest more time into this.

1.10.7 Processing for MS-046

MS046 displays a good S/N compared to SALTFLU and SBAL-DEEP and requires less denoising (Figure 39). This is thanks to the deeply towed dynamite source (~30m) and cables (~20M), preserving the records from low-frequency swell noise. Deeply towed source and streamers also generated several ghost notches that destructively interfere with the signal, notably the

one at ~27 Hz (Figure 40c). The downside of MS046 is the 100 m channel and receiver spacings, which results in a large spatial under sampling and relatively low fold (Figure 40b). It cannot image well the steep flanks of diapiric structures, but MS046 is of great value for imaging the base salt and the pre-salt where salt is not too deformed.

Quality Check	Processing Step	Navigation Processing
	Input Field Data	**Import raw navigation**
Cross-plot maps	**Geometry merging**	**Edit Navigation** Match FFID numbers to the corresponding shot numbers based on observer's logs
Fold distribution, Stack	**CMP Binning**	
Visual checking	**Correct for local time shifts** Automatic detection of shifts based on the water bottom continuity and constant shift of 110ms	
Output difference, Stack	**FX Prediction Filtering (CRG)** Run 1: 0-12Hz, 11 traces x 1000ms windows, amplitude threshold > 2 Run 2: 0-8Hz, 24 traces x 500ms windows, amplitude threshold > 2 Run 3: 0-12Hz, 7 traces x 500ms windows, amplitude threshold > 10	
Visual checking	**Missing shot interpolation** Sorting to Common shot gathers 1st small gap interpolation in the F-K domain using patches of 200 ms x 7 traces 2nd big gap interpolation in the F-K domain using patches of 500 ms x 50 traces	
Visual checking, Stack	**Triple Channels (100 to 25 m spacing)** Interpolation in the FX domain 1st round: 13 traces x 201 ms window, max dip 35 ms/trace 2nd round: 25 traces x 301 ms window, max dip 35 ms/trace	
(Output difference, frequency spectrum, Stack)	**Deghosting in FK domain** Zero padding to left and right of shot gathers Extrapolation to left and right of shot gathers Shot-side deghost, patch 251 ms x 95 traces, reflection coeff -0.95, Regularization 0.05 Receiver-side deghost, patch 201 ms x 12 traces, reflection coeff -0.95, Regularization 0.05	**Stacking velocity analysis** 500m CMP interval for every line
Output difference, Stack	**Low-Frequency attenuation** Ormsby low-cut filter 3-7 Hz	
Residual move-out, stack	**Isotropic Pre-Stack Time Migration, then velocity refining every 250 CDP (~1.5km)** Offset regularization	- OUT: Stack & Migration RMS velocity
Output difference, Stack	**10 CDP (~50m), Automated residual velocity analysis** Auto-picking +- 10% velocity, every 25 ms Pick smoothing (51 CDPs)	
Stack	**Stack** Angle mute 48deg Stack Waterbottom mute	- Processed Migration stacks

Figure 39 Time domain reprocessing sequence and parameters applied to the MS046 dataset

There are statics variations both on shot and channel gathers. On channel gathers this is illustrated by sudden 110 ms shift in the water bottom (Figure 40a). To correct this, I align the water bottom and I calculate the root mean square amplitude (RMS_amp) in a 100 ms window above the water bottom. If the RMS_amp of one trace exceed by a factor of 10 the average RMS_amp of the survey, I apply a -110 ms shift to the trace.

The new processing flow include a channel-interpolation step to tackle the low spatial resolution of the data and improve the migrated section (Figure 39, Figure 41a). This is done by interpolating trace in the frequency space (F-X) domain (Figure 41c), where aliasing does not affect the components of the spatial prediction filter, using the method described by Spitz (1991). A prediction filter is formed at each frequency, in small patches, to predict new
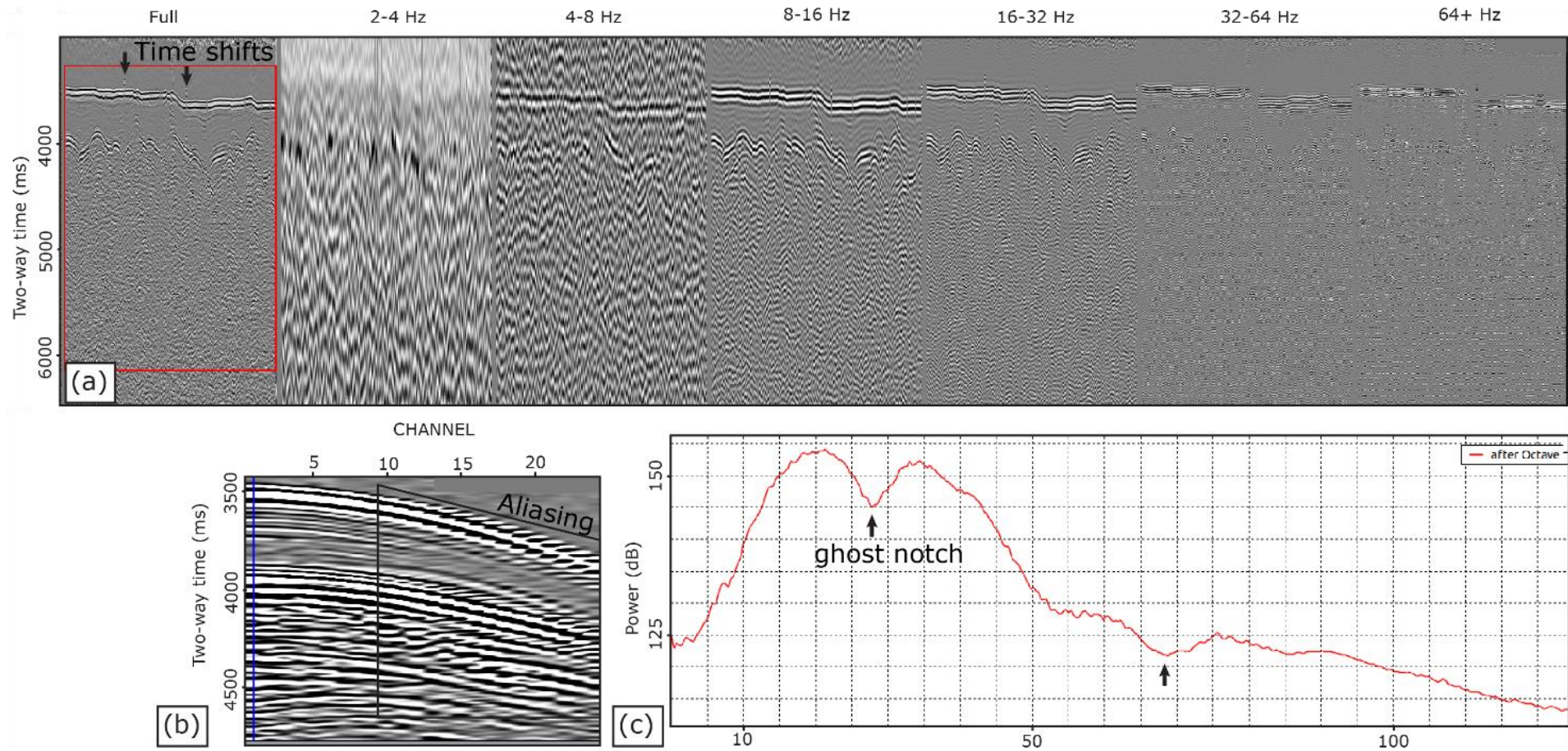
Figure 40 Overview of the MS046 field data. (a) Octave panels on a section of a near-trace-plot. (b) Example of a shot gather. (c) Frequency spetra corresponding to the raw near-trace-plot section.
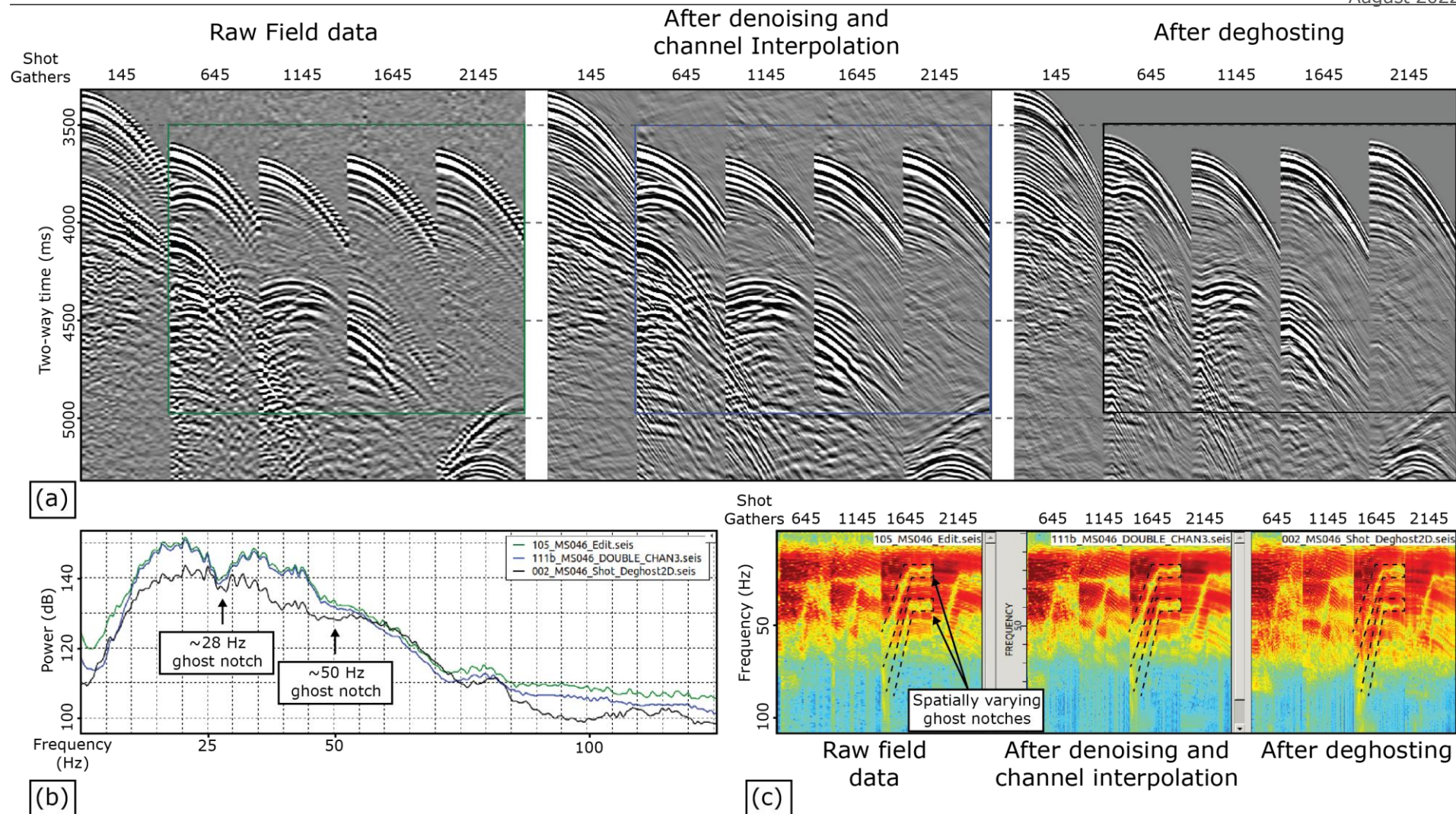
Figure 41 Panels showing the results obtained during the new processing of MS046 before migration. (a) Panels showing different raw shot gathers of MS046 and the resulting gathers after denoising, channel interpolation and deghosting. (b) Frequency spectra corresponding to (a). (c) Frequency-space spectra corresponding to (a) showing the varying ghost notch in the data.

traces at a finer trace spacing. This method is robust in presence of random noise and it correctly handles curvatures and lateral amplitude variations (Spitz, 1991). The resulting gathers after the inverse transform are not aliased anymore (Figure 41a) and show similar events than the initial data without artefacts.

The F-X spectras after deghosting still show notches, showing that I did not yet perform well deghosting (Figure 41c). This step is challenging for MS046 because the frequency of the notch decreases along the channels. For the lowest frequency notch (~28 Hz, Figure 40b, Figure 41b), F-X spectras show that it actually varies from ~53 Hz on channel 1, to ~22-26 Hz toward the far offsets (Figure 41c). Using a shallow water velocity of 1511 m/s, this corresponds broadly to a towing depth of the cable varying from ~15 to ~30m. The higher frequency notch (from ~110 Hz to 48 Hz) is interpreted to represent the same effect for the source ghost. These notches also vary along the survey (compare the notches in shot gathers 1645 and 2145 on Figure 41c for example). To tackle this, instead of the constant cable depth of 25 m stated in the acquisition report, I use a varying cable depth based on the observed notches for the initial model of the deghosting (15m at channel 1, increasing gradually until 30 at channel 85, then constant at 30 m). During deghosting, also search for the best depth for filling the frequency notches, with a variability of ±40% of both the source and cable depth from the initial model. Within the tool, it is determined as the depth yielding the primary with minimal L1 norm in time. The estimated best cable depth varies from 21 to 28 m, from the near- to the far-offset. However, the notches are not completely compensated, showing that more testing must be performed. The non-hyperbolic reflection of the water bottom due to the slanted cable might affect the estimation of the deghosting operators (Figure 42a).

The first break of the amplitude, that should represent the water bottom, do not align along a hyperbola and are not flat after normal moveout correction with the deep water velocity (1530 m/s; Figure 42a). I have tried to correct this by using the residual statics of REVEAL after deghosting to calculate the shifts to apply to the data. I did not manage to obtain good results through that approach. Alternatively, assuming the deghosting do correctly assume the best cable depth, it could be used to calculate the time shifts to apply. This has an impact on the expression of the water bottom on the time images with a diffuse first peak reflector for the water bottom (Figure 42b).

The new images display a better S/N ratio and a better imaging of the diapirs flanks thanks to the channel interpolation (Figure 43). However, it suffers from a loss of the high frequencies because of geometry issues post channel interpolation. I believe that there is also a lot of room for improvement for the deghosting considering that there is recorded signal in the 2-4Hz band (Figure 40a). I have performed only two rounds of RMS velocity picking so

there is also potential for improving the velocity model for time migration. With such a low frequency signal implies that with the right processing to compensate for the low spatial sampling, this dataset could provide great results in the depth domain. Because of their good S/N and penetration depth, the MS lines can provide a good image of the pre-salt where the MSG is not too deformed. However, to define the optimum processing sequence for this type of lines (notably the bandwidth enhancement) is yet to be defined. It would be better to test the processing flow on a MS line where the MSG is less deformed. I did not attempt the PSDM. This is a work yet to be done.
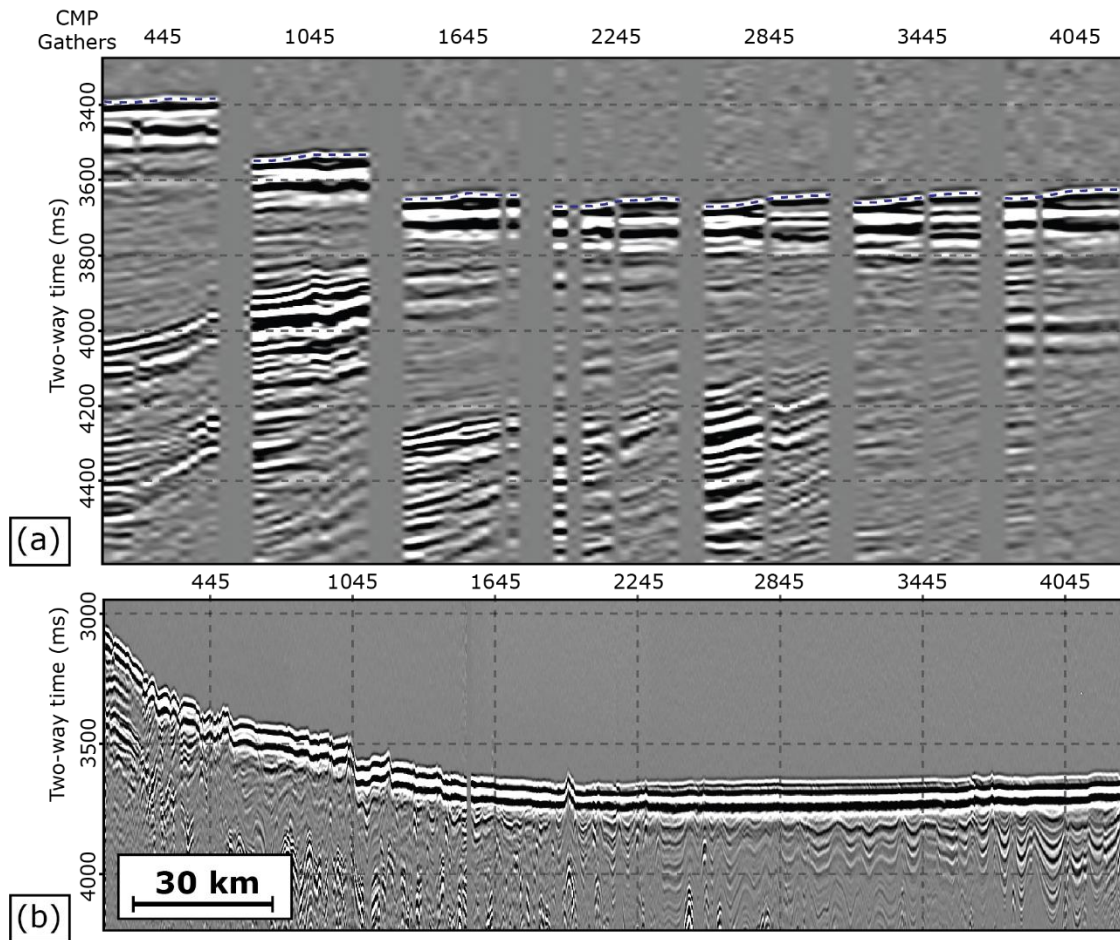
Figure 42 Panels showing the time variations due to the cable's depth variation in survey MS046. (a) Commom Midpoint (CMP) gathers after normal moveout correction using a constant velocity of 1530 m/s (estimated deep water velocity). (b) Resulting image after normal moveout at 1530 m/s and stacking. The blue dashed lines represent the first break of amplitude, interpreted as the water bottom.

1.11 Results for SALTFLU

I focus on the results for SALTFLU. As stated before, I consider that the images I produced for SBAL-DEEP and MS046 do not yet surpass enough the legacy images and require more work. Furthermore, the study of the salt tectonics in Chapter 4 is mainly focused on SALTFLU.
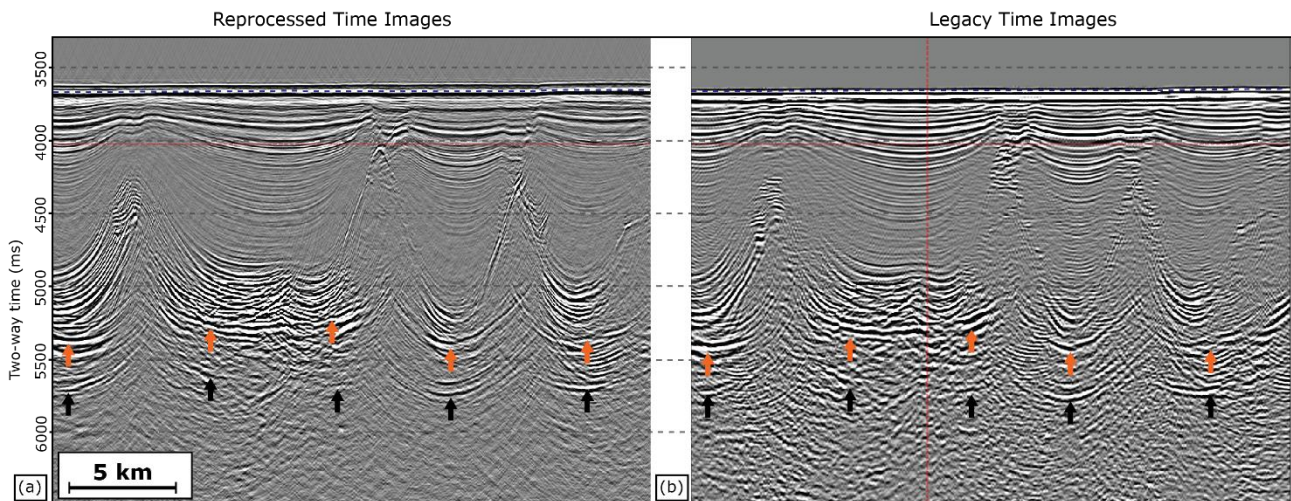
Figure 43 Comparison between the newly reprocessed time image (a) and the legacy image (b) of seismic profile MS046. Orange arrows point the interpreted base salt. Black arrows point an interpreted pre-salt reflector.

The initial bandpass filter eliminates the lowest frequency 'swell' noise and prepares the data for resampling from 2 ms to 4 ms by removing high frequency data (>125 Hz) that would become aliased (Figure 28b). The filter parameters are designed based on visually inspecting octave panels showing different frequency bands of the raw field data (Figure 28a). The 2-4 Hz octave panel is dominated by 'swell' noise and can be filtered out without losing significant primary signal. The 125-250 Hz octave panel shows that there is primary signal above 125 Hz. This implies that some high frequency signal is lost by resampling. The data are resampled both for computational efficiency and to ensure that any spatially aliased high frequency signal is removed before further processing stages, meaning that no trace interpolation is needed for 2-D transforms in channel domain. This results in a considerable decrease in computing time for the most computationally intensive processing steps (e.g., deghosting, Radon de-multiple and pre-stack migration), at the cost of removing some high frequency primary signal. I consider this to be an acceptable trade-off for this study because the main objective is to better image the base salt, primarily by recovering the low frequency part of the data.

Following F-X prediction filtering and linear Radon filtering, most of the low frequency noise is removed without attenuating primary signal or introducing artefacts (Figure 28d and 3e). Some of the noise remains between 8 and 16 Hz, but it could not be eliminated at this stage without filtering out primary signal and is cancelled out after stacking.

The deghosting sharpens the seabed and enhances the lower frequencies, highlighting the base salt, but also boosting the residual 'swell' noise and the low frequency bubble pulse (Figure 29a), with peaks at the harmonics of the bubble pulse frequency at 7 Hz, 15 Hz and 23 Hz (Figure 29b). The bubble oscillation is contained within the far-field source signature estimated from the stacked seabed reflection (Figure 29d). The matching filter

between the far-field source signature and the targeted band-limited and zero-phase Ormsby wavelet (Figure 29c, d) successfully sharpens the source wavelet and eliminates the bubble oscillations (Figure 29a) thereby improving the balance of the frequency spectrum (Figure 29b).

Radon demultiple attenuates the internal multiples observed below the salt but does not completely eliminate them (Figure 30). The multiple model also contains a weak component of the primary signal, but this 'primary leakage' is considered acceptable as it does not significantly alter the amplitude of the reflectors after stacking.

Based on RMS velocities and dominant frequencies ranging from 1511 m/s and 60 Hz at the seabed to 5500 m/s and 10 Hz at the pre-salt, the nominal maximum vertical resolution of the new results varies from approximately 6.3 m to 137 m. Based on the same velocities, the legacy time migrated stacks display a slightly higher dominant frequency of 65 Hz, hence they have very slightly higher vertical resolution (5.8 m) at the water bottom. The legacy processing, however, did not include deghosting, a robust source designature or zero-phasing, so the effective vertical resolution of the legacy data is in fact much lower than this nominal resolution. The amplitude content of the new pre-stack time migrated stacked sections appears better balanced than the vintage dataset, particularly for the low frequencies (Figure 44a, b). The wider bandwidth of the reprocessed data better highlights the impedance contrasts and improves the interpretability of the data, particularly for the base salt and the pre-salt reflectors. The reprocessed new dataset displays lateral amplitude variations within the Plio-Quaternary and the Upper Unit that were not clearly visible before (see Section 4.3.2).

The pre-stack depth migration corrects for geometrical distortions linked to the strong lateral velocity variation between the evaporites and the encasing sediments (Figure 34). The 'pull-ups' of the pre-salt beneath the salt structures seen in the time migrated section are flattened after depth migration with an average velocity of 4300 m/s. Tomographic updates performed after salt flooding resolve velocity variation within the salt. The pre-salt reflectors are not always clearly visible on the final sections, thereby limiting the reliability of the velocity model beneath the salt.

1.12 Discussion

1.12.1   Limits of the pre-processing strategy

The chosen pre-processing strategy for SALTFLU is determined by the computing costs and our ability to separate noise from primary signal. The time resampling from 2 to 4 ms eliminates the frequencies above 125 Hz and attenuates the frequencies from 90 Hz. This is due to the smooth roll-off of the applied filter, that is necessary to avoid ringing. By doing so, the highest
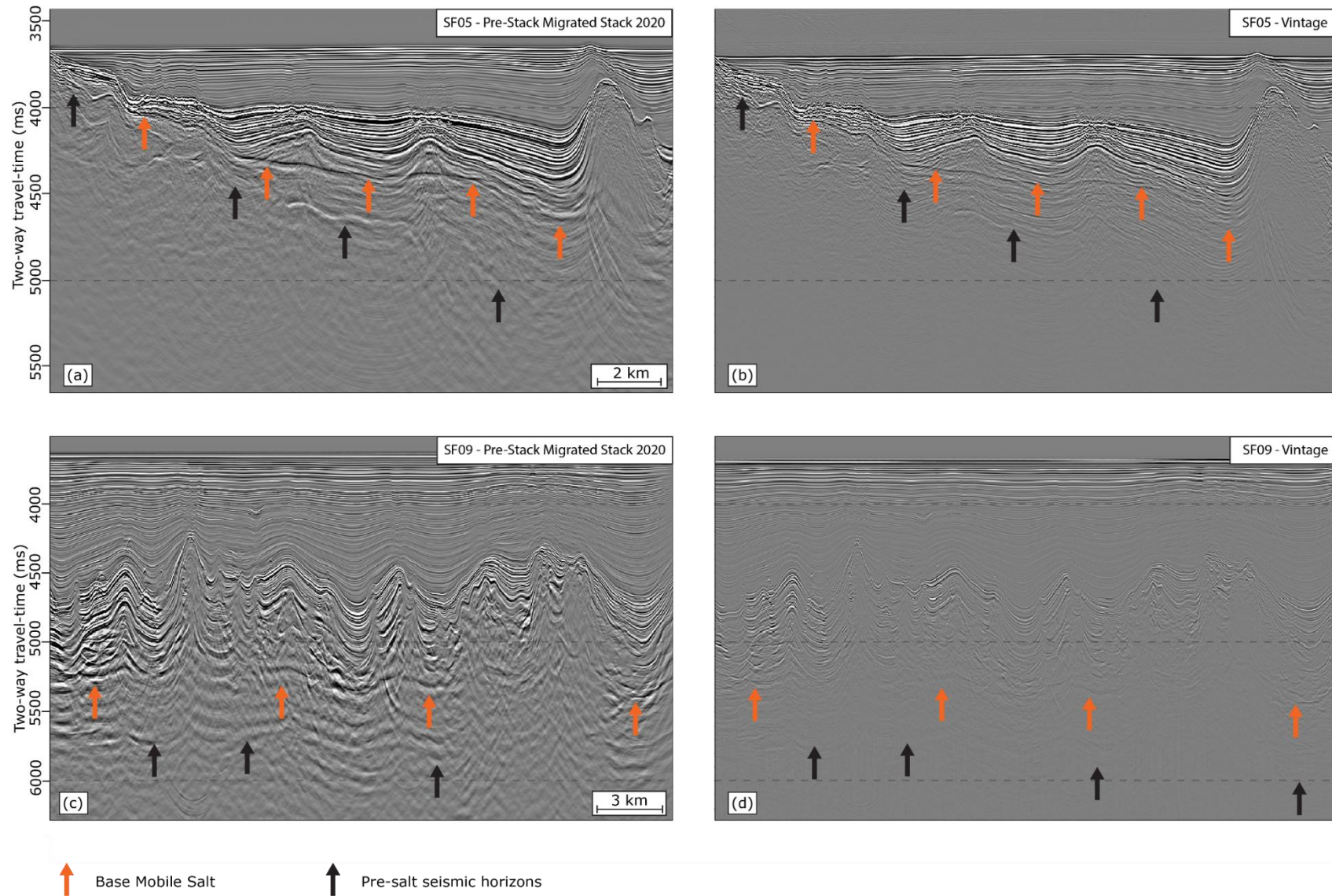
Figure 44 Comparison between the newly re-processed sections (left; a and c) and the vintage sections (right; b and d) in time domain, for sections of lines SF05 (a and b) and SF09 (c and d). Bandwidth enhancement and Radon demultiple allow better imaging of the base salt horizon (orange arrows) and pre-salt horizons (black arrows)

resolution part of the data is lost but this allows a significant reduction of computing times. Resampling divides by two the size of the dataset and lowering the Nyquist frequency to 125 Hz filters out frequencies that would otherwise become aliased after resampling. That way, spatial transforms (e.g. F-K, Tau-P and Radon filters) can be performed without further trace interpolation to unwrap the aliased energy. This avoids multiplying the size of the dataset by at least a factor of 2, therefore the resampling reduces data size by 4, improving the computing times. The aim of this reprocessing is to improve the image of the evaporites and the salt generally lying below a thick Plio-Quaternary cover, therefore I consider this resolution loss an acceptable trade-off. A future study focusing on the shallower sub-surface could benefit from the preservation of these higher frequencies by processing the dataset at 2 ms sample rate.

During the acquisition of SALTFLU, the source array and streamer were For a water velocity of 1511 m/s at the surface (based on previous water velocity measurements and direct arrival slopes), the first frequency notch should appear around ~252 Hz for the source-side 'ghost', ~189 Hz for the receiver-side 'ghost', and ~108 Hz for the combined source and receiver 'ghost'. In the data, the 'ghost notch' varies between approximately 118-150 Hz on near-trace gathers (offset 100m) depending on the lines, and it gradually shifts towards higher frequencies along channels until it disappears above filtered frequencies after the 10th receiver (offset 325 m). Such values broadly correspond to the combined source and receiver 'ghost' and might reflect a varying depth of the towed source or poor depth control along the streamer during the acquisition. With a Nyquist frequency of 125 Hz after resampling, the source- and receiver-side 'ghost' notches are mostly outside the data bandwidth (Figure 28c), but deghosting still helps to extend the lower part of the bandwidth and removes the interference of the 'ghosts' with the primary wavelet in time domain (Raj *et al.*, 2016). A deeper towing depth would have been desirable to improve the recording of the lower frequencies and to attenuate the 'swell' noise, which is particularly strong and dominates the low frequency part of the data. It could not be fully eliminated pre-stack without attenuating some primary signal. The best results were obtained with iterative F-X prediction filtering, which better preserved the low frequency primary signal compared to the low-cut filter applied to the vintage dataset, but it required many iterations with different sliding windows on both common-shot gathers and common-receiver gathers. Other approaches tested include F-K filtering and time-frequency filtering, but these were either unsuccessful at separating the noise from the primary signal, or too computationally expensive. Tau-P domain filtering is also an efficient way to separate noise from primary signal (Basak *et al.*, 2012). Here, I apply a shot domain forward and inverse Tau-P transform, with a limited slowness range, without further muting in the Tau-P domain. The 'swell' noise is incoherent enough to not sum constructively during the transform and is therefore well attenuated. The

remaining noise embedded in the data is low amplitude enough to ensure a stable deghosting operator estimation, but it is boosted after the deghosting stage and an additional denoising step is required after bandwidth enhancement (Figure 2).

The pre-processing strategy did not function so well for SBAL-DEEP and MS046 and need further adjustments. SBAL-DEEP suffers from a very low S/N ratio which is hard to compensate for without hitting the primary signal. Pre-processing for MS046 include an additional step for increasing the spatial resolution of the images, and specific parameters during deghosting to account for spatially varying ghost notches. For MS046, I did not take the time to further work on this because the line was mostly outside the study area (see Chapter 4). But I believe that if the aliasing is well tackled, the large bandwidth of the recorded signal of the MS lines can be valuable for the MSG imaging.

1.12.2 Limits of the multiple elimination and accuracy of the velocity models

As the water depth exceeds 1500 m in the survey area, long period surface-related multiples are not superimposed on the target primary signal. Therefore, surface-related multiple elimination (SRME; Verschuur, 2013) is not applied, and all multiples (long and short period) are attenuated solely by move-out based methods. However, short period internal multiples are present and not fully eliminated (Figure 30). They are generated by strong acoustic impedance contrasts either within the Upper Evaporites, or between the waterbottom and the Top Evaporites. They prevent the resolution of velocity variations below and within the evaporites and can be misinterpreted as primary signal. During the processing they are only partially attenuated by move-out discrimination on CMP gathers, likely because they are generated by a high velocity layer (the upper Messinian unit above the salt). With a maximum offset of 3100 m, they only yield a small move-out difference compared to the primary reflections. Other approaches for attenuating multiples include boundary-related internal multiple method (Verschuur and Berkhout, 1996), data-driven internal multiple removal method (Jakubowicz, 1998) and inverse scattering internal multiple removal (e.g. Araújo *et al.*, 1994). The second method has been tested but it was not applied in the final flow due to significantly increased computational times (16 hours for 5000 shots, while the survey consists of more than 170 000 shots).

The presence of remnant multiple can lower the accuracy of the time and depth domain velocity analyses. The time domain velocity model is built through several iterations of semblance-based migration velocity analysis (with a pre-stack Kirchhoff time migration, and Radon multiple attenuation). The remaining multiples and the out-of-plane reflections can generate high semblance values that can be wrongly picked. Consequently, automatic picks

had to be carefully quality controlled during the residual move-out analysis stage after both the time and depth migrations.

Internal multiples generated within the Upper Evaporites can also be wrongly picked as the top salt horizon used for the velocity flooding. Two reflectors R1 and R2 could be interpreted as the top of the salt (Figure 45). The top of the salt is difficult to follow laterally because of the complex salt structures and the presence of several reflectors within the salt that could represent residual internal multiples, out-of-plane reflections or the presence of internal clastic beds within the salt. The transition from the Upper Evaporites seismic facies to the 'transparent' salt seismic facies is gradual. The impedance contrast between the base of the Upper Evaporites and the salt is not clearly marked. Based on the strength of the amplitude and the lateral continuity of the reflectors, R2 seems to be the most likely horizon marking the top of the ductile salt. However, despite the likely presence of internal multiples below R2, some reflectors are believed to represent geology. I interpret them as intrasalt reflectors generated by the presence of clastic beds with the mobile salt. Intrasalt reflectors have already been observed in the eastern Mediterranean, where they lower considerably the average salt velocity to ~4260 m/s (Feng and Reshef, 2016). On CMP gathers, these reflectors align at a velocity of ~3250 m/s and would be over migrated if salt flooding was performed from R2 (Figure 46). To preserve them from the post-migration Radon demultiple, the salt flooding is performed starting from reflector R1. This choice has a strong control on the velocity used for the flooding to flatten the base salt (a lower top salt implies a higher flooding velocity to flatten the base salt), the resulting geometry of the salt structures on the stacked sections, and the depth of the base salt and pre-salt units. A better identification of the top salt could be guided by drilling through the UU until the top of the salt in the Algerian basin.

The final interval velocity models used for Kirchhoff depth migration are sampled every 12.5 meters laterally and 5 meters vertically. Tomographic updates were considerably smoothed and regularized to avoid velocity 'bulleyes'. In the absence of nearby wells, the only quality check on the interval velocity model is whether the reflectors in common reflection point gathers are flat or not after migration. However, considering the limited offset of 3.1 km compared with the depth of the target and the strong velocity variations, the gathers get flattened under a substantial range of velocities. This implies that there are large uncertainties in the velocities, particularly for the evaporites and the pre-salt, where the residual internal multiples and the lack of strong pre-salt reflections makes it difficult to constrain the velocity model.

The ray-based Kirchhoff migration is not the best suited strategy for salt imaging du to (Leveille *et al.*, 2011): (i) a limited ability to handle steep and large velocity variations which requires a smoothing velocity model and limit
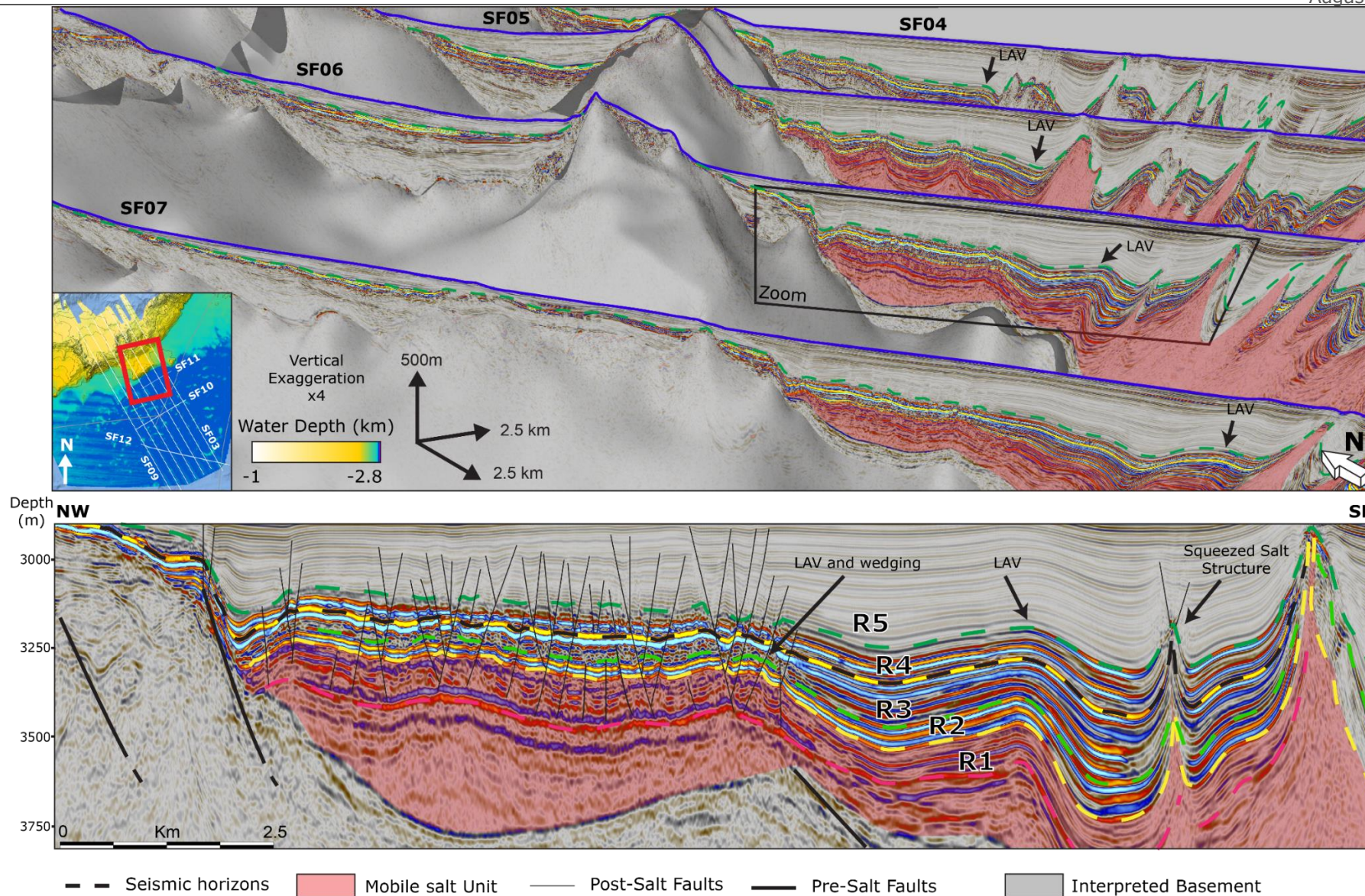
Figure 45 3D view of the SALTFLU seismic profiles along the Balearic margin of the Algerian basin, with a zoomed section along line SF06 showing the post-salt Messinian seismic facies. R1, R2, R3 and R4 represents the four seismic horizons observed regionally in the Algerian basin within the evaporites. Vertical exaggeration x5.
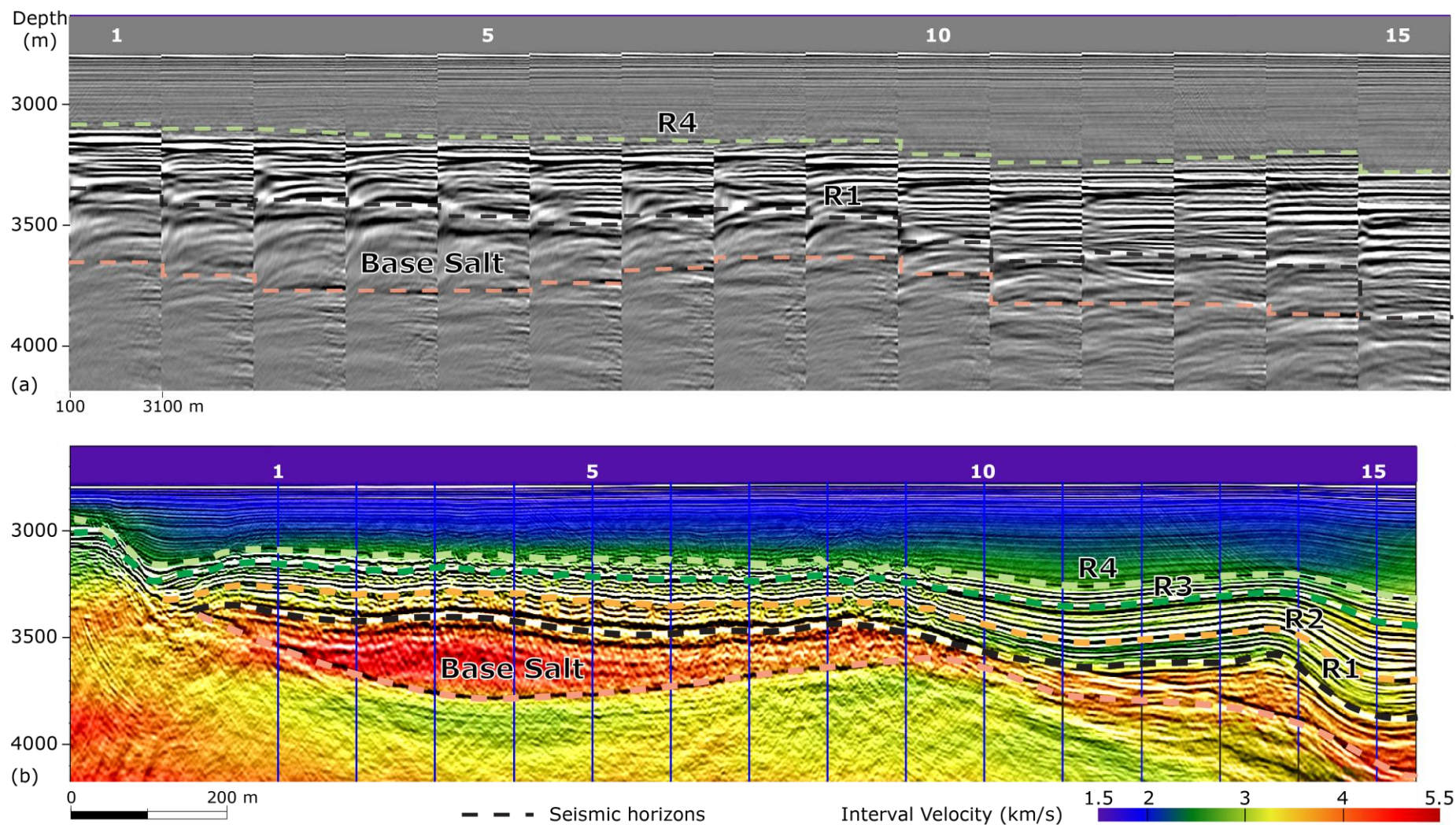
Figure 46 A section of line SF06 after pre-stack depth migration: (a) common reflection-point gathers with interval velocity overlay; (b) a single migrated offset plane (offset 1063 m) with interval velocity overlay (positions of gathers in (a) marked). The velocity of the upper evaporites increases downward from 2500 to 3500 m/s. The mobile salt unit was flooded with 4200 m/s. Two rounds of tomographic velocity updates were performed in the pre-salt sediments after salt velocity flooding.

the quality of the output images and (ii), the apparition of migration "swing" artifacts in poorly illuminated zones under or near salt bodies due to limitations of the assumption of the ray-based scheme. More advanced migration techniques (e.g., anisotropic migration or reverse time migration) have not been tested. They are more costly and are accurate with sufficiently detailed velocity models, thus they require corresponding higher resolution velocity estimation techniques (e.g., waveform inversion or anisotropic model building; Jones, 2015). These techniques require dense and long-offset recording of the reflected wave field, a good knowledge of the geology and petrophysics distribution within the medium, with ideally nearby well control, and good computational power (Virieux and Operto, 2009). SALTFLU data is sparse (~6 km spacing between the lines), with no nearby wells, and the maximum offset recorded is ~3.1 km, while the local subsurface is known to include a highly deformed and deep (>4 km) salt (Camerlenghi *et al.*, 2018). For these reasons, the Kirchhoff migration is preferred (Yilmaz, 2001; Vardy and Henstock, 2010; Dondurur, 2018). In practice, it remains a flexible and robust approach where the velocity model is not well constrained and the objective is primarily the imaging of salt structures, not the subsalt imaging, but reverse time migration could potentially improve the imaging of the salt structures.

1.12.3 Area of interest within the central Algerian basin observed on the reprocessed data

The newly reprocessed data better image the pre-salt reflectors, allowing an improved understanding of the salt tectonic system from late Miocene to today in the central Algerian basin (Blondel *et al.*, 2022), with a peak of contractional salt deformation at early to mid Plio-Quaternary. This peak could be linked to an important episode of shortening of the Tell-Atlas fold-and-thrust belt, along the Algerian Margin. A contemporaneous tectonic event has been also identified along the Balearic margin, with a regional unconformity, and the reactivation of pre-existing faults leading to the uplifting and the tilting of the Balearic slope (Blondel *et al.*, 2022).

SALTFLU is one of the highest seismic resolution datasets available in the Algerian basin. It allows detailed study of the late Miocene seismic facies, the acoustic basement in the Formentera basin, and faulting within the Plio-Quaternary that could provide new insights on the geological evolution of the region. Combined with other neighbouring datasets, regional sections extending from the Mallorca shallow basins to the Algerian margin through the Formentera basin and the deep Algerian basin could be drawn.

1.12.3.1 Mud volcanoes and fluid circulation

The presence of mud volcanoes in the Algerian basin has previously been suggested by Camerlenghi et al. (2009). In salt basins, shale diapirs are

common in areas of shortening, which can pressurize and mobilize shale, as can vertical loading (Jackson and Hudec, 2017). Mud volcano systems have been recognized in the neighbouring Alboran sea, where they are sourced by pre-Messinian sediments (Aquitanian–Burdigalian in age; Sautkin *et al.*, 2003; Blinova *et al.*, 2011; Medialdea *et al.*, 2012; Somoza *et al.*, 2012). I observe several weakly reflective diapir contacts, with no underlying velocity pull-up but with a narrow dimming zone instead (Figure 47d). Migrating this structure with a high salt velocity result in over-migration artefacts, suggesting that either (i) they are not made of high velocity material, but could be made of low velocity mud; (ii) the structures are are out-of-plane with respect to the 2-D seismic profiles; or (iii) the salt is allochthonous and too thin to generate a pull-up. They could testify to an active mud volcano system, but the evidence is too poorly constrained to verify this hypothesis.

I observe several low amplitude anomalies with accompanying push-down and dimming along the Balearic margin (Figure 47a, b) and in the south-central Algerian foredeep (Figure 47c, d). In the Algerian foredeep I interpret these as gas chimneys, which supports the presence of an active fluid migration system. They are systematically located above a pierced UU, suggesting they need a migration path through the UU to escape vertically into the Plio-Quaternary. Somehow, they do not migrate further up dip along the Plio-Quaternary strata (Figure 47d), suggesting the potential presence of stratigraphic traps. It is not known if this gas is thermogenic or biogenic in origin. Previous studies in the Mediterranean sea have shown that cross-evaporite fluid flow through an hydro-fractured MU is likely, implying that the gas observed in the SALTFLU profiles could potentially be sourced from a pre-salt source rocks (Dale *et al.*, 2021; Oppo *et al.*, 2021). A thermal modelling study in the eastern Algerian basin from Arab et al. (2016) favours the pre-salt Oligo-Miocene sourcing, with the Messinian shale as a possible biogenic gas source. In the Algerian foredeep, seismic fluid indicators are only observed in the western part of the study area, which is characterized by relatively undeformed Plio-Quaternary deposits, and less deformed salt compared to the eastern part (Blondel *et al.*, 2022). The absence of gas chimneys in the eastern part could be due to the absence of traps, and/or migration pathways, and/or the immaturity or absence of a source rock. If there were fluids migration but no traps, I would expect to see evidence of fluid escape features, such as pockmarks, at the seabed. Arab et al. (2016) conclude that discharge and accumulation of the pre-salt thermogenic fluids is limited to the Algerian margin or beyond the slope toe (60 km from the coastline), with some structural traps associated with the Quaternary north-verging thrust ramps. Further eastward, the basin widens and the thrust ramps are located further away from the seismic data (Blondel *et al.*, 2022). I speculate that the fluids may not be able to migrate far enough within the basin to be observed locally of the eastern lines. The western part of the Algerian basin also displays a higher heat flow than the eastern part (Poort *et al.*, 2020), this spatial
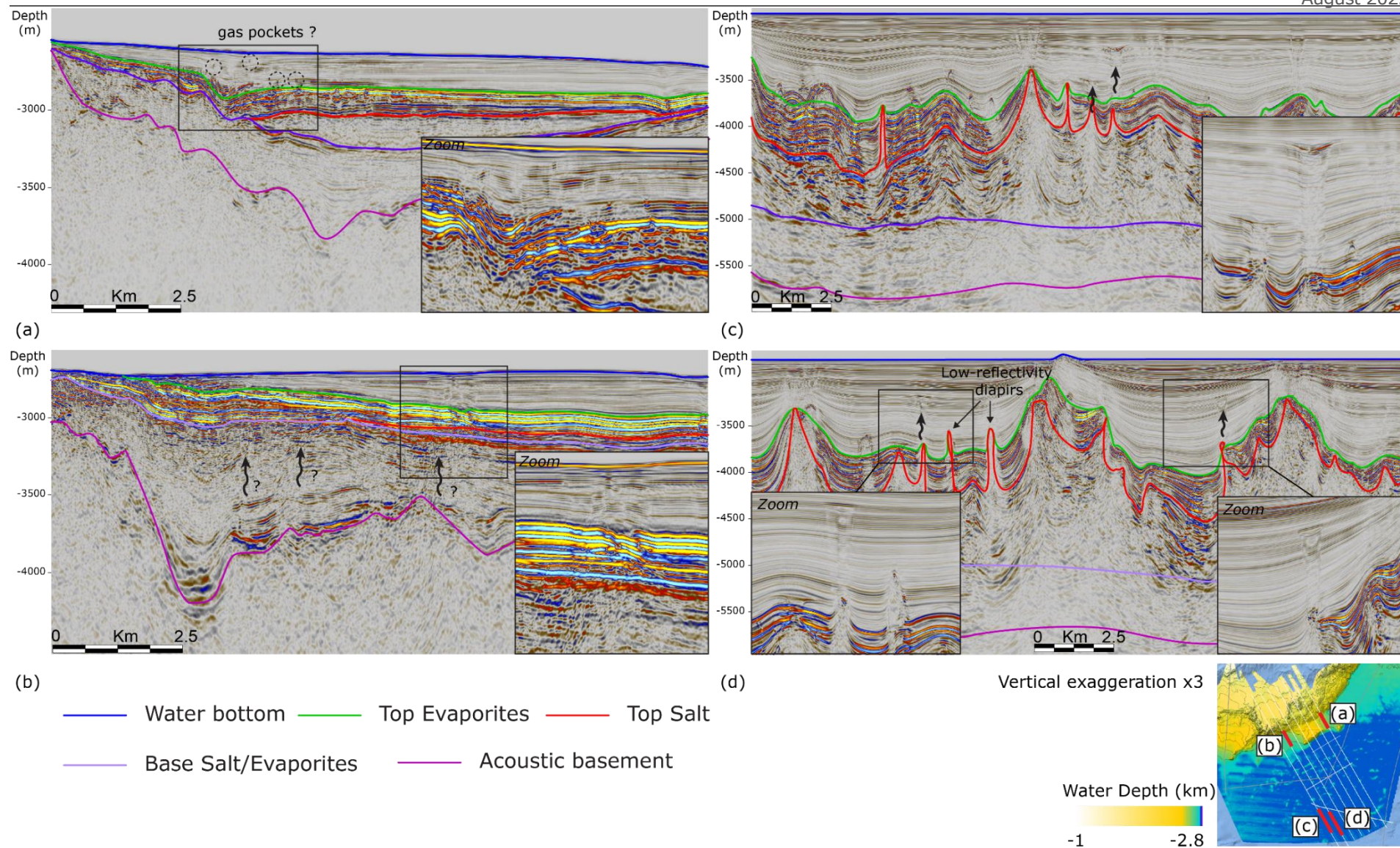
Figure 47 Sections in depth of lines SF03 (a), SF08 (b and d), and SF09 showing amplitude anomalies and disturbed bedding that may indicate the presence of fluid migration. Arrows indicate areas of blanking and/or disturbed bedding, representing possible fluid migration pathways. Vertical exaggeration x3.

variation could have had an impact on the production of fluids, whether biogenic or thermogenic.

Along the Balearic margin, fluid indicators are observed locally when salt is absent (Figure 47a, b). The nature and the source of these fluids are also unknown. Previous studies link these seismic amplitude anomalies and the normal faulting on the Balearic margin to hydrofracturing induced by the fluid circulation (Urgeles *et al.*, 2013; Wardell *et al.*, 2014; Del Ben *et al.*, 2018; Dale *et al.*, 2021).

1.12.3.2 Seismic facies variations within the Messinian seismic units

Along the Balearic margin, the Upper Unit is interpreted as an evaporite-rich layer, with two subunits UU1 and UU2 separated by an intra-UU unconformity, and possibly, an intra-UU salt layer (Dal Cin *et al.*, 2016; Camerlenghi *et al.*, 2018). The reprocessed SALTFLU profiles show that the UU can be divided into more than two units (Figure 45). These units display a cyclicity in amplitude strength that could be linked to changes in lithology or depositional environment. The lowermost seismic unit of the UU, between reflectors R1 and R2, is characterised by relatively discontinuous medium amplitude reflectors embedded in a low amplitude seismic background 'matrix', with a velocity comparable with the overlying units (3000 +/- 250 m/s; Figure 45). This unit could represent a transition facies from the ductile salt (dominantly halite with poor clastic content) to more brittle Upper Evaporites, richer in clastic and gypsum evaporites. Many faults can be tracked up to the reflector R1 which attests to brittle behaviour (Figure 45). Whether it is part of the UU or the MU, this unit pinches out before the overlying units.

The presence of an intra-UU salt layer and of an intra-UU erosion surface is questioned. Reflector truncations are only visible on SF03 at the outlet of a canyon of the EBE and are not visible elsewhere (Figure 45, Figure 48). Velocity profiles do not show any high velocity layer in the UU (Figure 46). On the contrary, the average velocity of the UU is low: it increases downward, from ~2500 m/s at R4 to ~3250 m/s at R1. These values cannot be associated to high velocity evaporites such as gypsum and/or anhydrite (~5000-6000 m/s; Schreiber, Fox and Peterson, 1973; Mavko, Mukerji and Dvorkin, 2009) or halite. This could indicate a clastic-rich layer, with an increase in the proportion of low-velocity material, where the last unit of UU is predominantly made of clay, such as in the Unit 7 of the Levant Basin (Gvirtzman *et al.*, 2017). The scientific wells that penetrate the topmost UU in the Algerian basin confirm the presence of a sequence of mud and marls, interbedded with evaporites (dolomites, gypsum and anhydrite) that are possibly rich in organic matter (ODP-975, DSDP-124, DSDP-371; Ryan, Hsu, and et al., 1973; Hsü *et al.*, 1978; Comas *et al.*, 1996).

The Reflector R4, separating the UU1 from the UU2, is the strongest amplitude reflector observed within the whole survey (Figure 45 and 11). This

regional strong impedance contrast could mark the part of the UU containing the largest proportion of evaporites and could record a climax for the UU stage.

The shallowest Upper Unit, between R4 and R3, exhibits lateral amplitude variation, both toward the Algerian and the Balearic margin, on all profiles (Figure 45 and 11). The reflectors of this unit lose their high amplitude expression toward the nearest Balearic margin and toward the deepest Algerian basin. This loss of amplitude could result from a variation in the acoustic impedance contrast, that could be related to a change in lithology or pore fluid content. This uppermost unit of the UU also thins down toward the margin. It nearly falls below the seismic resolution (Section 3) and is then expressed as a medium to strong amplitude reflection with negative polarity compared to the water bottom. It is not clear where it pinches out, but it appears to do so before the underlying unit, between R3 and R2. This last underlying unit also displays a sudden lateral variation (Figure 45, Figure 48), pinching out towards the margin. The point where most reflectors onlap the R3 reflector could coincide with the point where the overlying unit falls below the seismic resolution. These sudden changes could indicate a different depositional environment, either due to local variation in accommodation space, sediment supply and/or salinity.

1.12.3.3 Seismic expression of the Messinian Lower Unit in the central Algerian basin

The absence of a high amplitude LU below the salt, as it is expressed in the Provençal basin (Lofi *et al.*, 2011), could indicate the absence of the LU in the Algerian basin; that the LU is much thinner than the vertical resolution of the data; or that there is an absence of strong impedance contrasts within this unit and within the pre-Messinian units. In the Levant basin, in the eastern Mediterranean Sea, the LU is also absent and the onset of the Messinian Salinity Crisis is marked by the Foraminifers Barren Interval (FBI), a 10s-of-meters thick, evaporite-free, shale unit that records the entire duration of the first stage of the crisis (V. Manzi *et al.*, 2021).

It could be that the record of the onset of the MSC along the Balearic margin of the deep-water Algerian basin is similar to the record of the MSC in the Levant basin. Toward the southern Algerian margin, however, the expression of the pre-salt units changes laterally and displays a set of continuous low amplitude and low frequency reflectors that could record the LU (Figure 48). Such seismic facies have been associated with the LU in previous studies, where it would be made of 100-200 meters of plastic grey marls and gypsum based on nearby industry wells (Burollet, Said and Trouve, 1978; Medaouri *et al.*, 2014). However, they seem difficult to differentiate from the Tortonian underlying units (Leprêtre, 2012a). This could confirm a lack of impedance contrast between the two. Nearby wells showed that the underlying
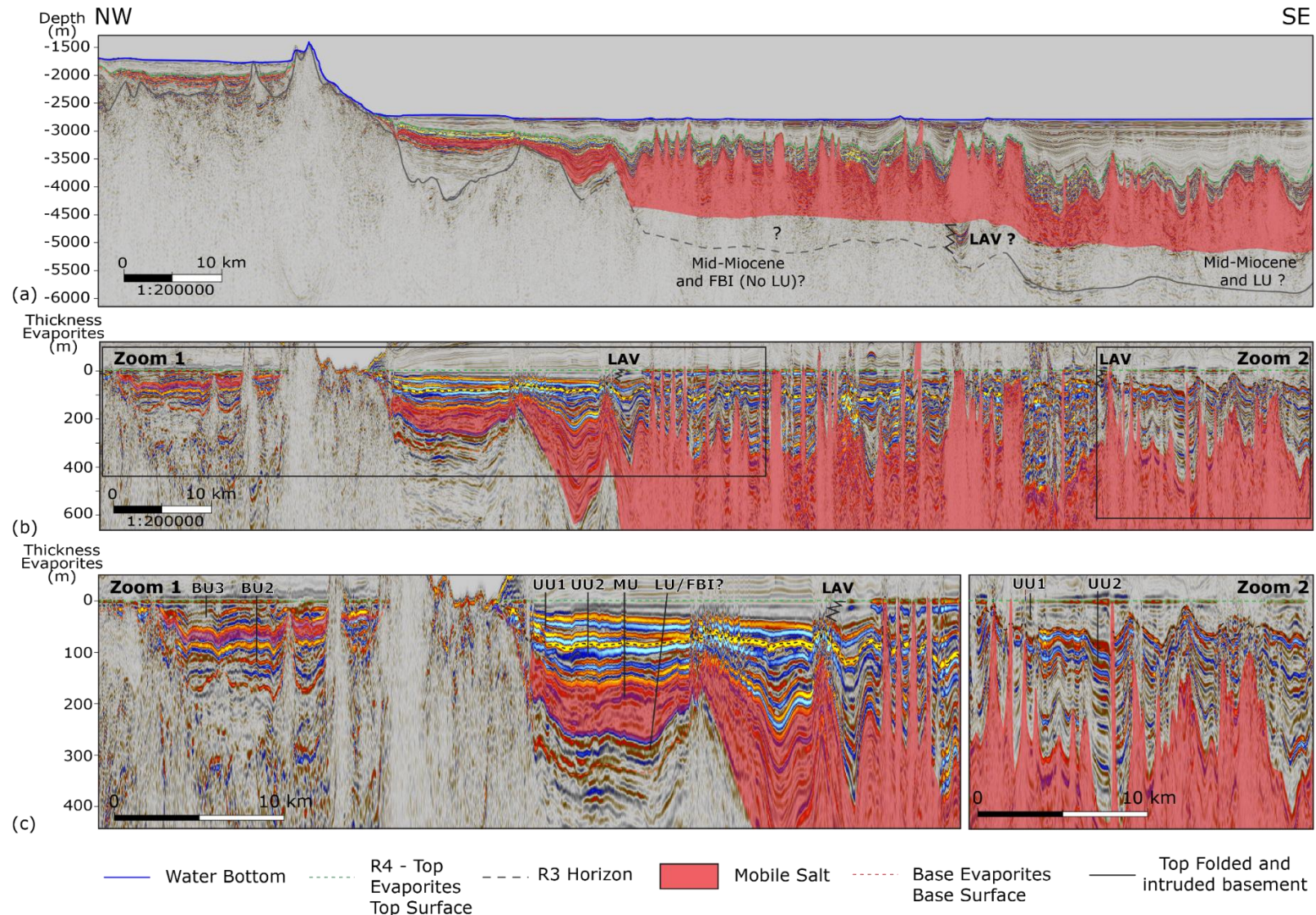
Figure 48 Pre-stack depth migrated line SF09 before (a) and after flattening (b) along seismic horizon R5 (interpreted as the top of the Messinian evaporitic sequence). The two zoomed sections (c) along the flattened line illustrate the comparison between the Bedded Units of the Balearic promontory with the units of the Algerian basin, and the variation in seismic facies within the Messinian Upper Unit in the Algerian basin. Vertical exaggeration x8 for the original line, x20 for the flattened line

Tortonian and Serravalian units were also made of grey marls, with intervals of pyroclastics sands or limestones (Section 1.6.3, Table 1) suggesting that in the Algerian basin, the LU, when present, is not as rich in evaporites as in the Provençal basin. In that case, the LU could be a lateral equivalent of the FBI, deposited preferentially in the deepest part of the Algerian basin. Alternatively, contemporaneously with the deposition of the LU in the Provençal basin, MU is already being deposited in the Algerian basin, and LU is a lateral equivalent of the lower MU (Roveri *et al.*, 2019).

1.12.3.4   Insights on the tectonic setting of the Balearic promontory

The new SALTFLU sections also provide improved imaging of the Formentera basin, which could allow better stratigraphic correlation with the Messinian units from the Mallorca depression and the deep-water Algerian basin and a better understanding of the tectonic history of the Balearic promontory (Figure 48and Figure 49).

When aligning the seismic data to the top surface of the evaporites (Figure 48), it seems straightforward to correlate the BU3 with the UU above the salt. Following the interpretation of Raad et al, (2021), if the BU1/BU2 (contemporaneous in age) are equivalent to the Stage 1 primary Lower Gypsum, according to the correlation suggested by Roveri et al, (2019), the

equivalent of the BU1/BU2 in the deep offshore is the thin FBI (likely below the seismic resolution). This could explain why a pre-salt evaporitic unit is not observed in the deep basin, while it is recorded by the BU1/BU2 in the intermediate depth basin.

Collapse structures are observed at the top of the BUs, in the deepest part of the Formentera basin (Figure 49). The top surface of the BU3 unit is generally conformable with the Plio-Quaternary in the Balearic promontory (Raad *et al.*, 2021) and is erosive only on topographic highs, not in the depressions where salt is preferentially accumulated. This suggests that the depressions were never aerially exposed to erosion or dissolution. Instead, the collapse features could be due to the circulation of undersaturated fluids or diagenesis, similar to features observed in the Messinian evaporites in the eastern Mediterranean (Bertoni and Cartwright, 2015) . Below the collapse structures, there seems to be a vertical dimming of the image that could be related to escaping fluids from the underlying pre-Messinian units or the basement itself attenuating the seismic amplitudes (Figure 49). Heat flow measurements on the Balearic promontory record anomalously low values that support the presence of groundwater fluid circulation (Poort *et al.*, 2020).

In the reprocessed SALTFLU dataset, the pre-salt basement appears highly variable, containing several sharp and high-relief structures inferred to be of volcanic origin (Figure 49). These structures match the geometry and the seismic expression of igneous bodies in volcanic provinces, such as the

Taranaki basin Infante-Paez and Marfurt, (2017). I interpret several magma conduits beneath the Miocene to the current sedimentary cover of the Formentera basin (Figure 49). They are overlain by a highly deformed unit, that is onlapped by pre-Messinian reflectors wedging towards the top of the magma conduits. These wedges indicate that the volcanoes were already present during the deposition of these pre-Messinian units. Extensive faults within the Plio-Quaternary cover suggest that the Formentera is still actively deformed (Figure 49).

1.13 Conclusions

I present the reprocessing of 2-D airgun seismic reflection data acquired offshore the Balearic Islands in the Algerian Basin. The goal is to improve the imaging of the Messinian evaporites and the overall basin architecture. The reprocessing strategy is designed to better image the pre-salt reflectors in an amplitude-preserving manner, attempting to overcome the challenges of imaging complex sub-surface geology using short-offset seismic data. This has been done using a 'broadband' processing strategy, multiple attenuation and an imaging approach that integrates geophysics and geological interpretation to iteratively build the velocity model. The resulting pre-stack migrated images, in depth and time, display improved reflector continuity and amplitude preservation, particularly for the pre-salt. The processing flow presented here was applied to other short offset (<3 km) legacy airgun reflection seismic datasets in the Mediterranean Sea. The efficiency and efficacy of the workflow strongly depends on the original acquisition parameters: the limited offset of most vintage data (often <3 km) compared with the depth of the salt structures (the base salt lies in between 3.5 and 5.5 km) inhibits our ability to separate signal from noise and to accurately resolve the subsurface velocity distribution using moveout-based processing techniques. The reprocessed data reveal several fluid indicators, amplitude variations, salt structures and volcanic structures. These new results provide insights into the evolution of the under-explored Algerian basin and the Messinian Salinity Crisis. These outcomes highlight the value of reprocessing legacy academic seismic data, particularly when considering how challenging acquiring new seismic and borehole data has become in the western Mediterranean Sea.
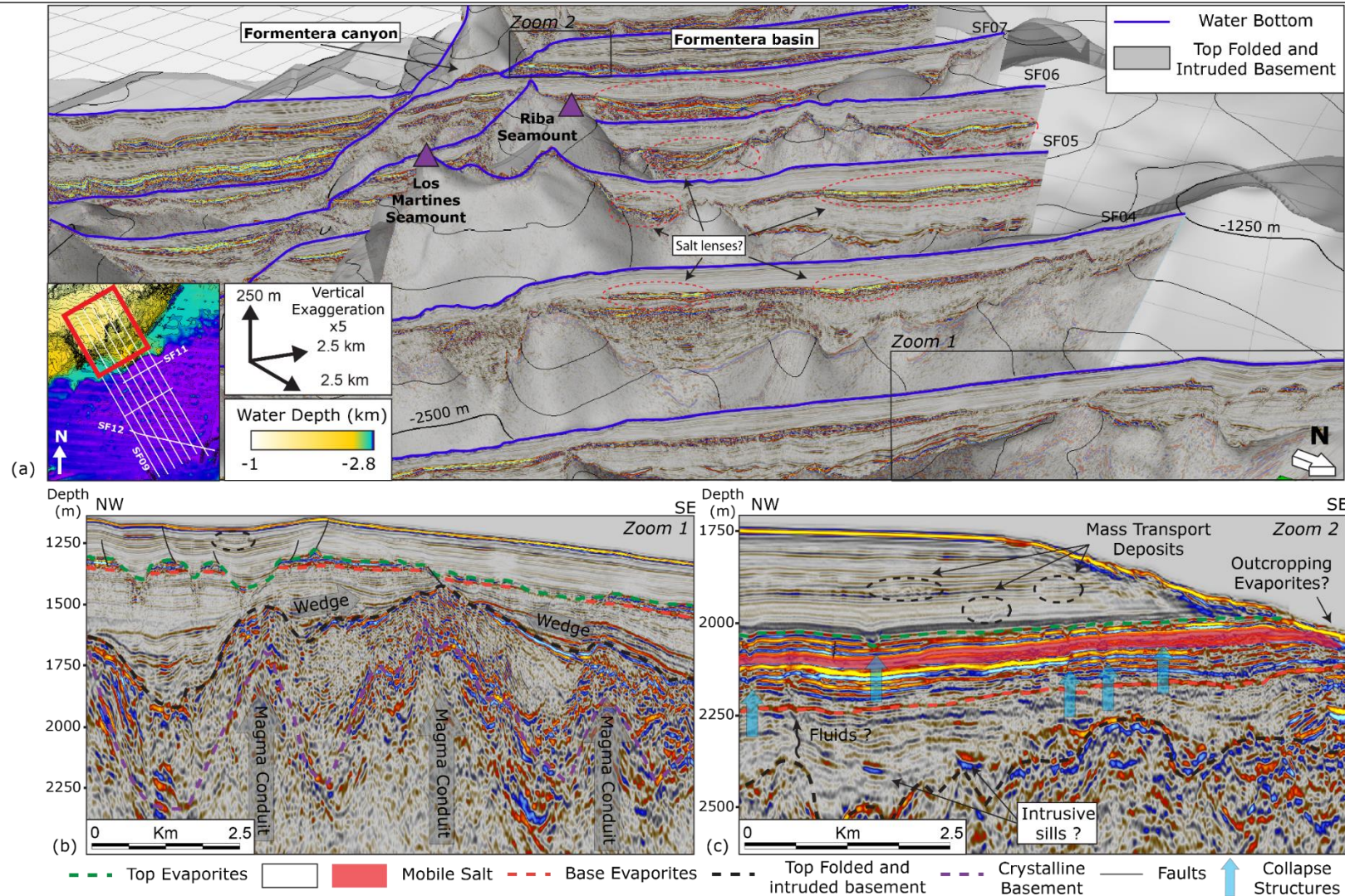
Figure 49 3-D view of the SALTFLU seismic profiles along the Balearic promontory. Zoom 1 along line SF03 (zoom 1) shows the eroded and incised Messinian evaporites and the underlying volcanic basement, with onlapping wedges at both sides of the volcano. Zoom 2 along line SF08 shows the Messinian evaporites in the Formentera sub-basin, with several depressions at its top that suggest the presence of collapse structures, chaotic seismic facies in the Plio-Quaternary that suggests the presence of mass transport deposits, and disturbed signal below the Evaporites that could indicate fluid circulation. Vertical exaggeration x5

Chapter 4

The Central Algerian Basin Salt System

This chapter is a modified version of Blondel et al. (2022).

Blondel, S., Bellucci, M., Evans, S., Del Ben, A. and Camerlenghi, A. (2022), Contractional salt deformation in a recently inverted basin: Miocene to current salt deformation within the central Algerian basin. Basin Res. Accepted Author Manuscript. https://doi.org/10.1111/bre.12673

2.1 Introduction

Contractional salt tectonic systems encompass settings where widespread shortening is applied to a salt layer (Jackson and Hudec, 2017). They are commonly described within three distinct geological settings (Letouzey *et al.*, 1995; Jackson and Hudec, 2017): (i) gravity-driven deformation on a continental margin; (ii) thick-skinned inversion of an extended intracratonic basin and (iii) orogenic shortening on a convergent or collisional margin driven by subduction. While gravity-driven, salt-detached deep-water fold belts are well-documented (e.g. Lundin, 1992; Rowan, Peel and Vendeville, 2004; Davison, Anderson and Nuttall, 2012; Quirk *et al.*, 2012; Jackson, Jackson and Hudec, 2015), thick-skinned contractional salt systems are not as well imaged and relatively less-understood.

Thick-skinned, orogenic fold belts display similar salt structures to thin-skinned, gravity-driven fold belts, such as salt-cored anticlines, box folds, squeezed diapirs, salt-detached thrusts and extruded salt sheets, with tens of kilometres of lateral displacement driven by horizontal tectonic loading (Davis and Engelder, 1985; Granado *et al.*, 2018). This style of deformation is due to the mechanical weakness of salt compared to most lithologies (Weijermars, 1988; Jackson and Vendeville, 1994), thus its presence yields a large influence on the structural development of fold-and-thrust belts (Duffy *et al.*, 2018). The weak salt layer acts as a décollement surface, decoupling the thin- and thick-skinned deformation and allowing the horizontal strain to propagate far out into the basin with a low-angle taper (Davis and Engelder, 1985; Letouzey *et al.*, 1995). Parameters influencing the localisation of deformation include: the relative thicknesses of overburden and salt, the strain magnitude, the base-salt relief, and the presence and distribution of pre-existing structures prior to the onset of shortening (Letouzey *et al.*, 1995; Dooley, Jackson and Hudec, 2009; Jackson and Hudec, 2017; Duffy *et al.*, 2018; Pichel *et al.*, 2019; Li *et al.*, 2021; Uranga *et al.*, 2022).

Natural examples of thick-skinned, salt-detached fold-and-thrust belts are dominantly long-lived systems, where the orogenic shortening was applied to an already deformed basin with heterogeneously distributed salt. Known field examples include: the south-western subalpine French Alps (Graham *et al.*, 2019), the Rif-Betics (Flinch and Soto, 2017), the Atlas mountains (Vergés *et al.*, 2017), the Pyrénées (Sans and Vergés, 1995), the Zagros (Najafi and Lajmorak, 2020), the offshore Morocco (Pichel *et al.*, 2019; Uranga *et al.*, 2022) or the North American Rocky Mountains foreland (Trudgill, 2011). The complexity that results from these mature, poly-phased systems makes it difficult to determine the tectono-stratigraphic history of the basin, especially in its early stages. For this reason, our current understanding of salt-influenced contractional systems has relied heavily on analogue and numerical modelling.

The Mediterranean Salt Giant (MSG) is a relatively young wide and thick salt layer deposited during the latest Miocene (Messinian stage ~5.96- 5.32

Ma; Krijgsman *et al.*, 1999), at the convergence between the African and Eurasian plates. In the south-western Mediterranean sea, in the Algerian basin (Figure 50), the MSG was deposited in an already inverted system, after a short extensive rifting and drifting stage (~8-6 Ma; Vergés and Sàbat, 1999; Rosenbaum, Lister and Duboz, 2002; Mauffret *et al.*, 2004; Déverchère *et al.*, 2005; Domzig *et al.*, 2006; Booth-Rea *et al.*, 2007; Serpelloni *et al.*, 2007). This implies that the salt system of the Algerian Basin evolved in a regional contractional setting since its deposition. It provides a unique opportunity to analyse contractional salt deformation during the early stages of shortening at the front of an incipient collisional fold-and-thrust belt.
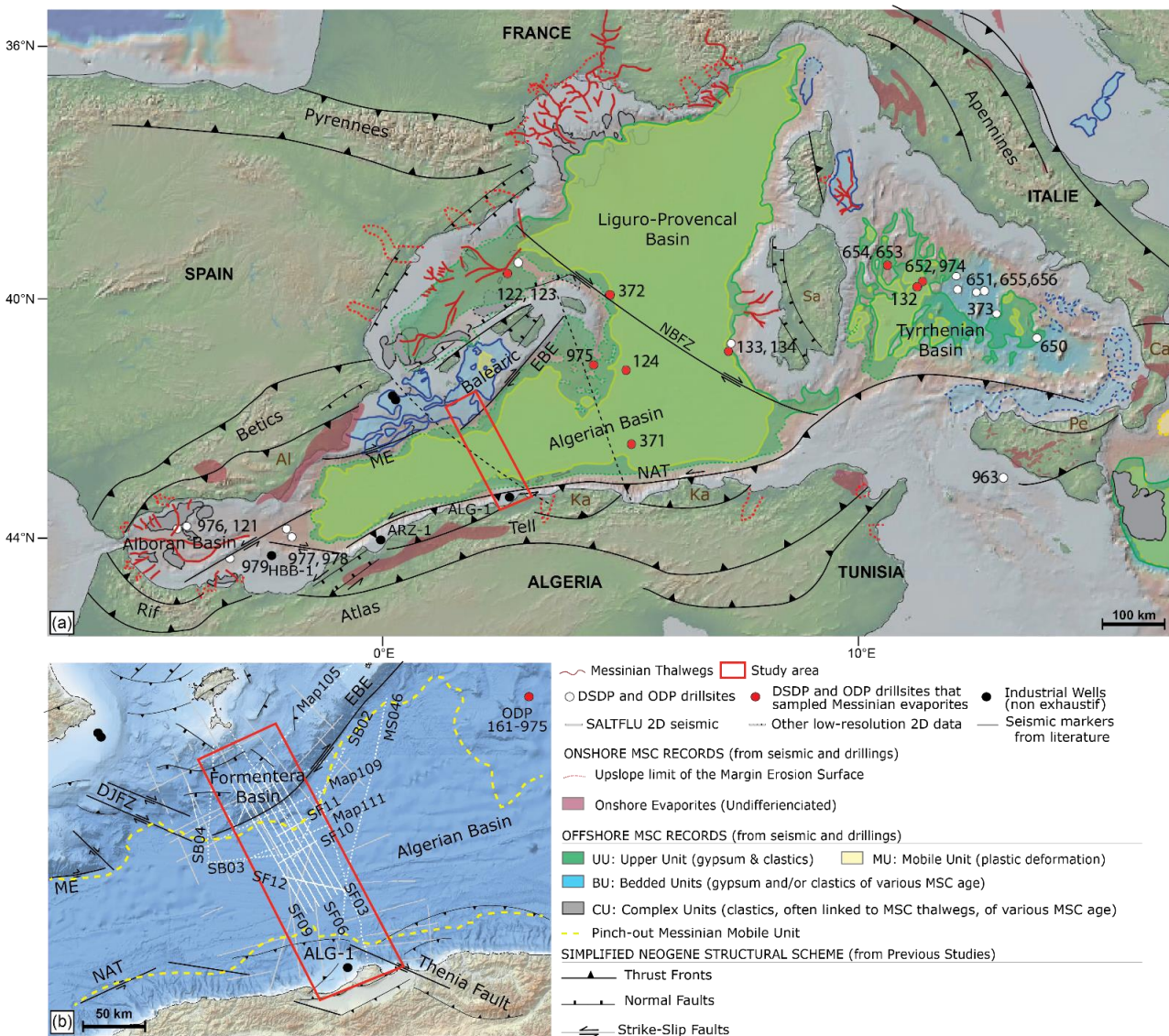
Figure 50 a) Relief map of the Western Mediterranean sea (http://www.geomapapp.org; Ryan et al., 2009) with the present-day spatial extent of the MSC markers (modified from Lofi, 2018) and the general structural setting (modified from Roure, Casero and Addoum, 2012; Van Hinsbergen, Vissers and Spakman, 2014; Etheve et al., 2016; Arab et al., 2016). b) Relief map of the study area in the central Algerian basin (https://ows.emodnet-bathymetry.eu/wms) showing the location of seismic lines used in this study (2D data interpretations from literature refer to Bellucci et al. 2021), the pinch-out of the MU (Lofi, 2018) and the detailed structural setting (Déverchère et al., 2005; Domzig et al., 2006; Yelles et al., 2009; Driussi, Briais and Maillard, 2015; Acosta et al., 2013; Etheve et al., 2016). EBE = Emile Baudot Escarpment, NBFZ= North Balearic Fault Zone, ME= Mazarron Escarpment,

DJFZ= Don Juan Fault Zone, NAT=North African Transforms, Ka=Kabylies, Pe= Peloritan, Ca= Calabria, DSDP= Deep Sea Drilling Program, ODP= Ocean Drilling Program, MSC=Messinian Salinity Crisis.

The study area is located in the central Algerian Basin, in the south-western Mediterranean Sea. I investigate the salt deformation at the front of a recently inverted salt-bearing passive margin. A reprocessed pre-stack depth migrated 2D seismic reflection dataset allows us to examine the early spatial distribution of salt structures in a contractional system. I use structural maps of key horizons, thickness maps and stratigraphic relationships, in association with global gravity and magnetic maps, to investigate the relationship between salt morphologies, pre-salt segmentation and relief, distance from the active margin, and the variations in salt and overburden thickness.

2.2 Geological setting

The Western Mediterranean Sea comprises a series of diachronous late Oligocene to Neogene (~30 – 6 Ma) back-arc basins that formed during the north-westward subduction of the Tethys ocean until the collision of Africa with Europe (Figure 50a; Rehault et al., 1984; Robertson and Grasso, 1995; Gueguen et al., 1998; Jolivet et al., 2006). The Algerian deep basin is situated in the south-western Mediterranean Sea, between the Balearic Islands (Spain) to the North and Algeria to the South (Figure 50a). Its northern and southern margins are marked by the transform zones of the Emile Baudot (EBE) – Mazarron (ME) escarpments and the North African transforms (NAT), respectively (Acosta *et al.*, 2001; Mauffret *et al.*, 2004; Booth-Rea *et al.*, 2007). The EBE and ME escarpments are offset by the Don Juan Fault Zone (DJFZ; Acosta *et al.*, 2013), which is interpreted by Vergés and Fernàndez, (2012) as the north-western end of a dextral transform fault that runs until Algiers (Algeria), near the Thenia Fault on the conjugate Algerian margin (Figure 50b).

The basin inversion initiated during the Tortonian, with a general N-S to NW-SE shortening and sinistral strike-slip movement (Vergés and Sàbat, 1999; Rosenbaum, Lister and Duboz, 2002; Déverchère *et al.*, 2005; Stich *et al.*, 2006). After the inception of the Algerian margin inversion, during late Miocene (from ~5.97 to ~5.33 Ma), the Messinian Salinity Crisis (MSC) led to the deposition of the MSG (Hsü, Ryan and Cita, 1973; Krijgsman *et al.*, 1999; CIESM, 2008; Manzi *et al.*, 2013), resulting in the deposition of 500 m to 1.5 km of salt in the western Algerian basin (Haq *et al.*, 2020). During the Plio-Quaternary, significant tectonic shortening along the Algerian margin generated a set of north-verging transpressional underthrust fronts, combining thin-skinned and thick-skinned tectonic styles (Frizon de Lamotte *et al.*, 2000; Déverchère *et al.*, 2005; Domzig *et al.*, 2006; Leprêtre, 2012b; Recanati *et al.*, 2019; Leffondré *et al.*, 2021; Strzerzynski *et al.*, 2021). These thrusts likely signal early-stage subduction of the Algerian oceanic crust below Africa

(Gueguen, Doglioni and Fernandez, 1998; Billi *et al.*, 2011; Roure, Casero and Addoum, 2012; Hamai *et al.*, 2018; Recanati *et al.*, 2019; Leffondré *et al.*, 2021).

GPS-derived velocities show that today, the displacement rate increases westward but is highly variable laterally, with an average shortening of 1.5 ± 0.5 mm year^{-1} at the central Algerian Basin (Serpelloni *et al.*, 2007; Bougrine, Yelles-Chaouche and Calais, 2019). North-westward Nubia-Eurasia plate motion has been shown to be relatively steady during the past ~13 Myr (DeMets, Iaffaldano and Merkouriev, 2015). Assuming a constant rate of shortening since the onset of the MSC, the Algerian Basin should have accommodated approximately 8 km of shortening. For the Algerian margin and the coastal domains at the Algiers longitude, Strzerzynski et al. (2021) proposed a higher cumulated crustal shortening of 11 ± 3 km since the Pliocene.

Despite this, contractional deformation features have rarely been described in the Algerian Basin. Previous studies concluded that thin-skinned deformation started in the late Messinian, with a peak during the Early Pliocene, driven by salt-detached gravity spreading and gliding along a gently dipping base-salt surface (Mocnik *et al.*, 2014; Wardell *et al.*, 2014; Dal Cin *et al.*, 2016). They suggested that the development of salt structures was controlled by the availability of salt and by the steepening of the base-salt due to the basin's thermal subsidence and the sedimentary loading. However, Camerlenghi et al. (2009) described salt-cored anticlines and pillows that lie too far from the continental slope of either side of the Algerian basin to be generated by the compressional stress induced by gravity gliding. They suggested they were tectonically-driven, either by underlying extensional or strike–slip faults, or by northward propagation of the compressional stress identified along the Algerian margin. Soto et al. (2019) also described contractional salt structures adjacent to the Algerian margin driven by the thick-skinned, tectonically driven shortening. They suggest that the Messinian salt layer acts as a décollement accommodating part of the thick-skinned shortening via thin-skinned diapir squeezing and folding, above a partially inverted half-grabens in the pre-salt sequence.

2.3 Dataset and Method

I used several 2D time-processed multichannel seismic reflection datasets acquired over the central Algerian Basin. The interpretation is focused on the Eurofleets project 'Salt deformation and sub-salt Fluid circulation' (SALTFLU) dataset, acquired in 2012 by the R/V OGS-Explora and recently re-processed in time and depth using the software REVEAL® by Shearwater Geoservices®. Velocities used for the migration were estimated via ray-based tomography during the depth imaging processing. The maximum resolution varies from 7 to 80 m downward from the seabed to the pre-salt, with interval velocities

ranging from 1511 to 5000 m/s, and a dominant frequency ranging from 15 to 55 Hz. The streamer was 3km long, with a source consisting of two groups of four 210 cubic inch GI guns (the base-salt target in the abyssal basin was estimated at about 5 km below sea-level).

Other datasets I have used consist of low-resolution seismic reflection data provided by the Instituto Geologico y Minero de Espana (IGME) and by the National Institute of Oceanography and Applied Geophysics (OGS). The processing flow applied to these data is not always known and their vertical resolution is at least 10m. World gravity (Bonvalot *et al.*, 2012) and magnetic anomaly maps (Meyer, Saltus and Chulliat, 2017) were also used during the interpretation. All data are displayed with the Society of Exploration Geophysicists (SEG) 'normal' polarity convention, where a downward increase in acoustic impedance is represented by a positive reflection (yellow to red).

The interpretation of the seismic profiles was performed using the software Petrel® by Schlumberger®. Mapped seismic units are characterised by their seismic facies and seismic-stratigraphic relationships (as described in the following section). Terminology for the Messinian seismic units is derived from Camerlenghi et al. (2018), in the atlas of the "Seismic Markers of the Messinian Salinity Crisis" from Lofi (2018), including: the Upper Unit (UU), the Mobile Unit (MU) and the Lower Unit (LU). In the intermediate depth Formentera Basin and the EBE, two other units are defined: the Bedded Units (BUs) and the Complex Units (CUs). In this study, these two units are not described further and are assimilated to the UU (see Driussi *et al.*, 2015; Raad *et al.*, 2021).

Mapping is performed in the time domain because only the SALTFLU data has been processed in depth. As the interpretation is based on 2D seismic data, the steep flanks of the diapirs are not well imaged, particularly where overhanging salt is present. Out-of-plane reflections may also be present in the 2D seismic sections presented. The spacing of the 2D lines is sparse with respect to the 3D geometry of salt structures, which may change abruptly over short distances. This makes the interpolation of the top salt surface between lines challenging. To aid the interpolation, the structural trends of bathymetric features observed on the seabed are used to guide the subsurface interpretation between lines. Time surfaces are then converted to depth based on the velocity gradients obtained through the depth imaging of the SALTFLU data. The parameters used for the conversion from time to depth are presented in Table 1. Seismic markers published by (Bellucci, Pellen, *et al.*, 2021) are also included as input for computing the isochore maps.

2.4 Results

2.4.1 Seismic Facies

Seven horizons defining six seismic units have been mapped across the study area (Figure 51). From oldest (deepest) to youngest (shallowest) the mapped units comprise: the Pre-salt unit, the Mobile Salt Unit (MU), the Upper Unit (UU), the lower Plio-Quaternary unit (PQ1), the middle Plio-Quaternary unit (PQ2) and the upper Plio-Quaternary unit (PQ3).

2.4.1.1   Pre-Salt unit

The pre-salt unit is the oldest and deepest mapped seismic unit. It comprises low amplitude and low frequency reflections, apparently continuous but generally poorly imaged (Figure 51). The pre-salt is best imaged along the basin margins (Figure 51a), where it is fan-shaped and onlaps the acoustic basement (interpreted as the post-rift unconformity). The unit is thickest along the Algerian Basin margin to the south (700 to 900 m), where the base is observed down to ~5.8 km below sea-level (Figure 52, Figure 53b). Previous studies by Leprêtre et al. (2013) and Medaouri et al. (2014) associated the pre-salt unit with gray plastic marls, middle to late Miocene in age, drilled in the wells Algers-1 (ALG-1) and Arzew-1 (ARZ-1), on the Algerian shelf (Burollet, Said and Trouve, 1978).

2.4.1.2   Mobile Salt Unit (MU)

The highly deformed MU overlies the pre-salt unit. It is characterised by semi-transparent and chaotic seismic facies (Figure 51). The upper MU exhibits low frequency and low amplitude internal reflections, particularly toward its top, making recognition of the top salt difficult. Locally, it forms diapiric structures and can appear at an allochthonous stratigraphic level (Figure 52). The regional base-salt is defined by a strong soft-kick in the deep basin. There is little to no evidence supporting the presence of the LU described by Lofi et al., (2011) in the study area (Figure 51). A maximum salt thickness of 1.8 km is observed within the diapirs in the deepest part of the basin, while its average thickness is estimated around 600 to 800 m (Figure 54a). The unit thins towards the margins of the basin where it pinches out (Figure 52, Figure 55). No wells have ever been drilled through the MU in the Algerian basin. However, its seismic facies and diapiric geometries are characteristic of dominant halite composition and dirty salts (Medaouri *et al.*, 2014).
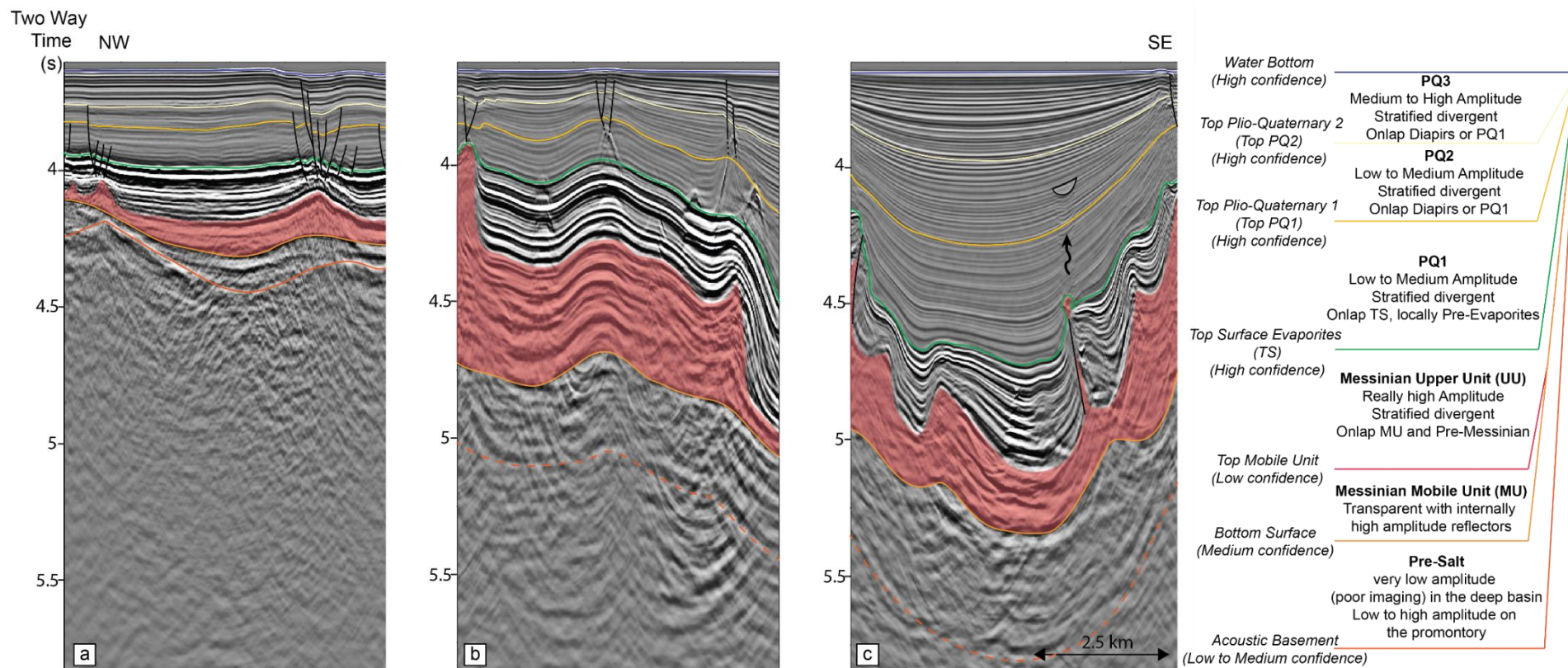
Figure 51 Seismic horizons interpreted within the deep Algerian basin along the seismic line SALTFLU 08. (a) Seismic profile 18 km southeast of the EBE illustrating a salt-cored anticline/pillow, with its faulted overburden (UU + PQ 1-3 units) and a landward dipping pre-salt; (b) Seismic profile 40 km southeast of the EBE illustrating wider salt-cored anticlines/pillows, with faulted overburden that thickens between salt structures (c) Seismic profile 80 km southeast of the EBE, 34 km from the North African escarpment, with salt diapirs piercing up to TOP PQ1 associated with amplitude anomalies and pull-downs, suggesting the presence of gas chimneys (indicated by a wiggling arrow on c)
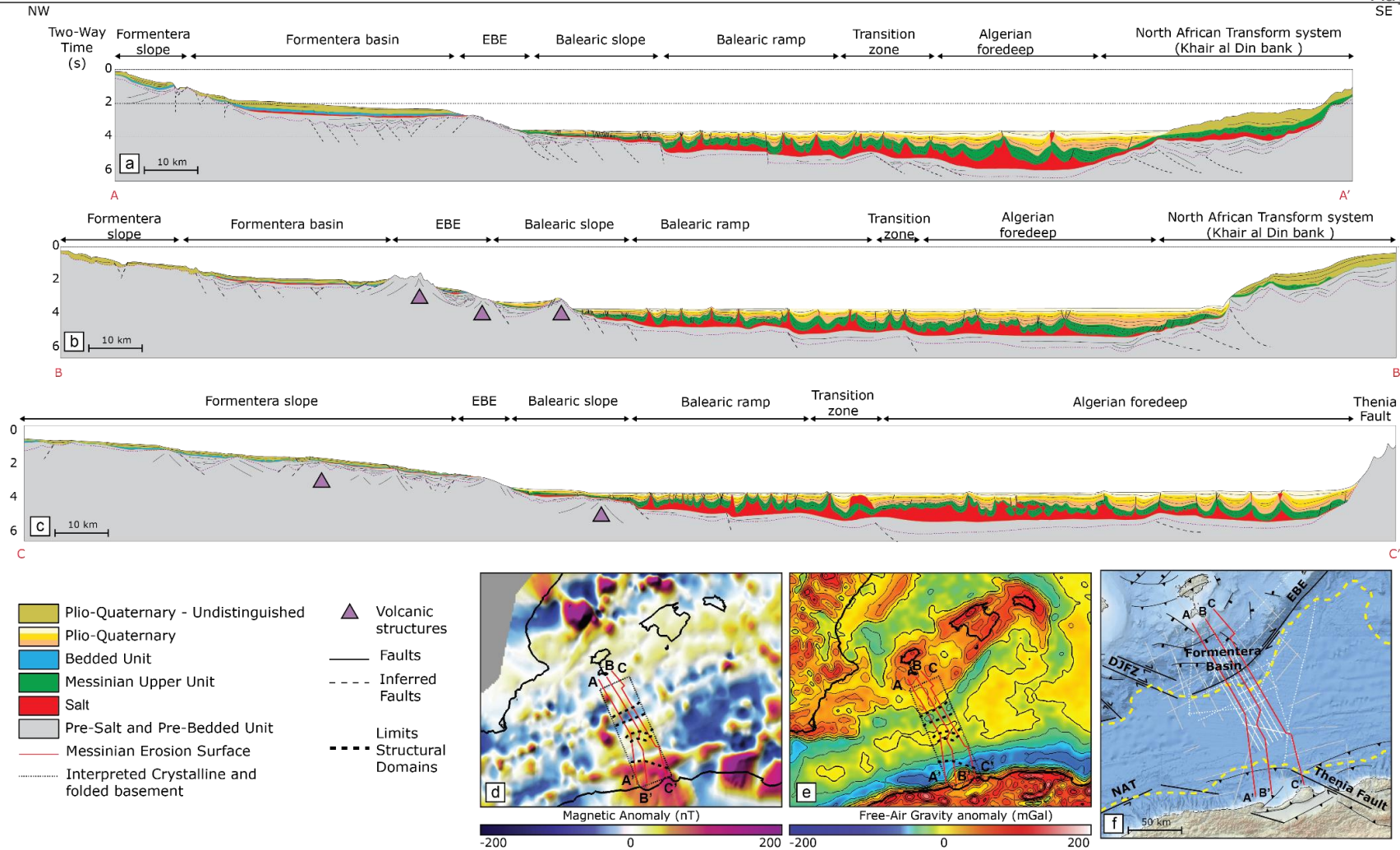
Figure 52 Schematic cross sections from the Balearic margin to the North African margin. To the west (a and b), the Algerian basin is narrower, the Emile Baudot escarpment is faulted, the Balearic slope uplifted, and the North African transform (NAT) is marked by thick-skinned thrust fronts. To the east (c), the Algerian basin is wider, the Emile-Baudot is less steep but the Algerian margin is more abrupt, without visible thrust fronts. The salt deformation appears more intense in the east, with several allochthonous salt sheets. The base-salt is not flat throughout the whole basin, with marked base-salt steps along the Balearic slope and the transition zone. This drop is aligned along WSW-ENE positive gravimetric (Bonvalot *et al.*, 2012) and magnetic anomalies (Meyer, Saltus and Chulliat, 2017)
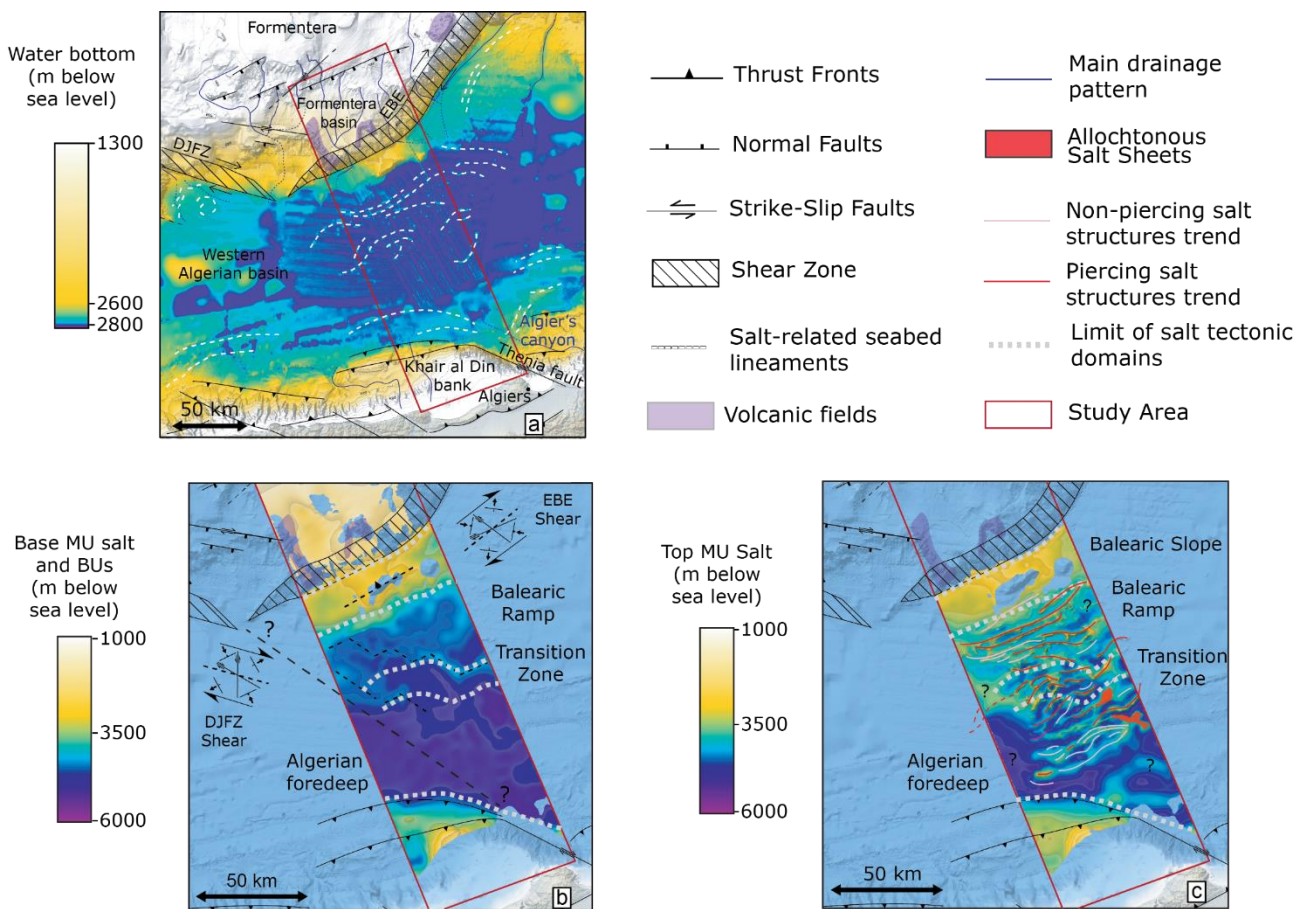
Figure 53 Depth maps from the sea level of (a) the seabed with key structural features (modified from Domzig _et al._, 2006; Acosta _et al._, 2013) and interpreted salt-related deformation trends, (b) the top salt with interpreted salt-related structural trends and (c) the base-salt with interpreted structural trends. Dashed lines show the limits of the main structural domains. Background bathymetry from _https://ows.emodnet-bathymetry.eu/wms_

2.4.1.3   Upper Unit (UU)

The UU is characterised by a continuous, stratified, divergent seismic facies with high amplitude and high to medium frequency reflections. The overall amplitude and frequency of the reflections decrease with depth (Figure 51). The UU reflections onlap the underlying MU within the basin, and the pre-salt unit along the margins where the MU is absent (Figure 52). The contact between the UU and MU is poorly defined due to: (i) the lithological transition is gradational, (ii) the edges of the complex structures formed by the deformed MU are poorly imaged by 2D seismic data, and (iii) internal multiples of the UU interfere with the potential presence of intrasalt reflectors. The base of the UU

is therefore defined as the youngest continuous high amplitude reflection onto which the UU reflections onlap. At the top, the unit is bounded by a continuous high amplitude reflection that strongly contrasts with the overlying unit, whether it is a hard or a soft kick.

The deformation of the UU is concordant with the underlying MU, although locally truncated by it where diapiric structures penetrate the overburden (Figure 12). The average thickness of the UU is about 400m. It thins across the structures formed by the MU, with an observed maximum of 600m between salt diapirs (Figure 11b). It thins towards the basin margins where it pinches out (Figure 45). Based on scientific wells that penetrated the uppermost UU in the Algerian Basin, it is thought to comprise evaporites such as dolomites, gypsum and anhydrite, interbedded with mud and marls, and possibly rich in organic matter (ODP-975, DSDP-124, DSDP-371; Ryan, Hsu, and et al., 1973; Hsü *et al.*, 1978; Comas *et al.*, 1996).
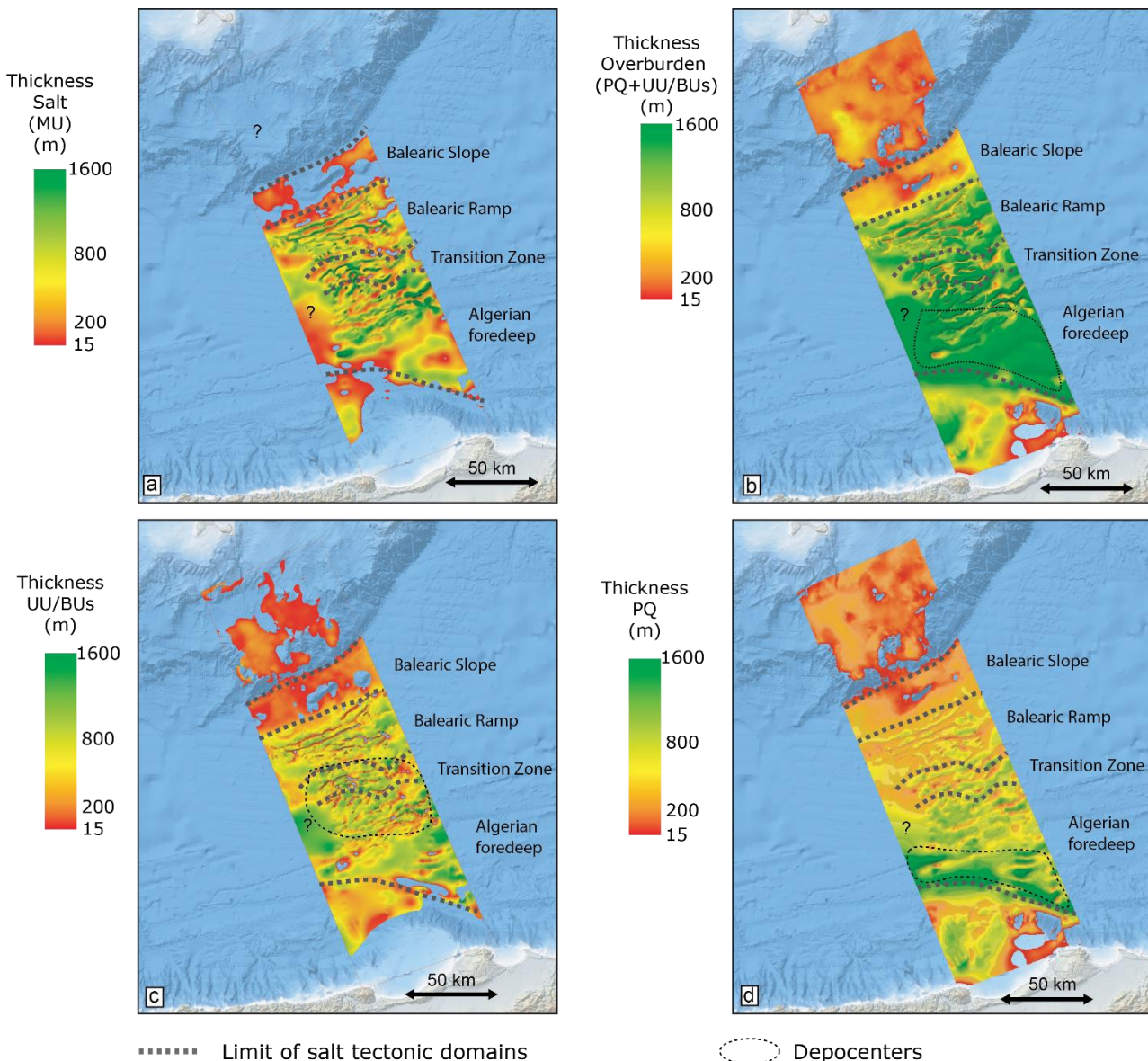
Figure 54 Thickness maps of (a) the salt unit, (b) the total overburden (PQs + UU/ BUs), (c) the Upper Unit and Bedded Units (UU/BUs) and (d) the Plio-Quaternary (PQ). These maps show an asymmetric distribution of the overburden with thickest deposits along the North African thrust front during the Plio-Quaternary. Dashed lines show the limits of the main structural domains (see text). The base-salt map reveals the base-salt relief with structural trends parallel to the synthetic and antithetic conjugate faults of the EBE shear zone. DJFZ: Don Juan Fault Zone; EBE: Emile Baudot Escarpment. Background bathymetry from *https://ows.emodnet-bathymetry.eu/wms*
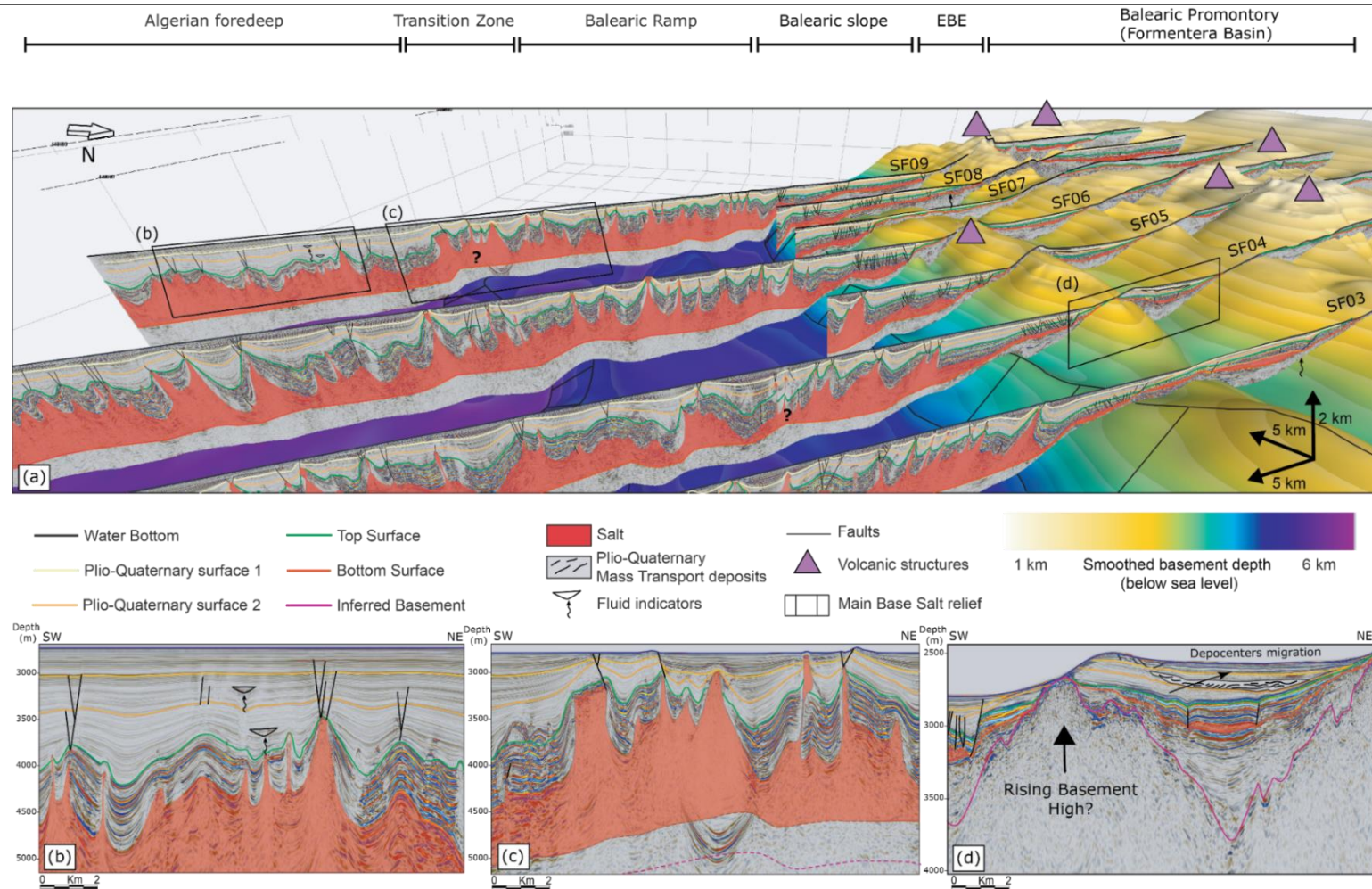
Figure 55 3D view of the interpreted basement along the north-western Balearic margin and interpreted SALTFLU 2D seismic sections. The basin is divided into five structural domains based on the thickness of the overburden, the thickness of the salt (i.e. MU), the base-salt relief and the style of the salt structures. The NE-SW trending Emile-Baudot escarpment is bordering the northern margin of the Algerian basin, with at least two volcanic pinnacles groups (presumably early Pleistocene to recent, according nearby dating performed by Acosta et al. (2004)). Another NE-SW trending topographic high is dividing the deep Balearic slope in two, with Plio-Quaternary mass transport deposits on its landward north-western flank. Wiggling arrows indicate areas of amplitude blanking, amplitude anomalies, pull-downs and/or disturbed bedding, representing possible fluid migration pathway.

2.4.1.4   Plio-Quaternary overburden

The Plio-Quaternary overburden is divided into 3 sub-units of similar seismic frequency but with different amplitudes. It locally onlaps the underlying UU, the basement or the allochthonous MU (Figure 51, Figure 55). The deepest Plio-Quaternary sub-unit, PQ1, is characterised by a low to medium amplitude and high frequency seismic facies, with continuous, divergent reflections. The overlying PQ2 displays a similar facies, but with slightly higher amplitude reflections. The contact between PQ1 and PQ2 is

defined by a regional high amplitude and low frequency soft kick (TOP PQ1), onto which the PQ2 reflections onlap.

The youngest and shallowest sub-unit, PQ3, is comparable and conformable with the PQ2 facies, but with much higher amplitude reflections (Figure 51). The contact between PQ2 and PQ3 is defined by a regional high amplitude and low frequency reflection (TOP PQ2), which marks the contrasting amplitudes between PQ2 and PQ3. Along the basin margins, PQ3 directly onlaps TOP PQ1 or the TOP Evaporites.

The thickness of the Plio-Quaternary unit shows an asymmetrical distribution, with the main depocenter along the southern Algerian margin (up to 1.4 km; Figure 52, Figure 54d). Its thickness is influenced locally by the salt structures, with local maxima in between salt highs. The lithology of the Plio-Quaternary unit is inferred from scientific wells in the Algerian Basin, where it consists of pelagic oozes with sandy intercalations with a downward increasing carbonate content (Ryan, Hsu, and et al., 1973; Hsü *et al.*, 1978; Comas *et al.*, 1996). Although these wells are located more than 100 km away from the study area, they are assumed to be deposited in a similar deep-water setting, where the sedimentary record should be comparable at a basin scale.

2.4.2 Interpreted structural domains

I define five structural domains in the deep Algerian Basin, classified according to the thickness of the overburden (UU + PQ units), the thickness of the salt, the base-salt relief and the type of salt structures observed. From the northern margin moving south I distinguish: (i) the deep Balearic slope, (ii) the Balearic ramp, (iii) the transition zone, (iv) the Algerian foredeep, and (v) the North African thrust front (Figure 52, Figure 53, Figure 55).

2.4.2.1   Balearic slope

The Balearic slope domain is bordered by the EBE to the northwest and a 500 m base-salt step to the southeast (Figure 55a). It is internally segmented by a local topographic basement high that separates two gently landward-dipping ramps (Figure 52b, Figure 55d). In this domain the overburden is relatively

thin (up to 700 m) with a broadly uniform thickness. Likewise, the thickness of the salt remains broadly constant and below 300m. The salt pinches-out against the topographic high or the EBE, with small salt-detached normal faults and associated rollovers at its edges (Figure 55, Figure 56a).

The salt-detached deformation in this domain is characterised by salt anticlines/pillows with a relatively small vertical amplitude (<150 m) and a short wavelength (1 to 2 km) (SP1, SP2 in Figure 56a). The crests of the structures are populated with small normal faults (Figure 51). Most faults terminate at TOP PQ1, but some also penetrate up to PQ2, PQ3 and the seabed (Figure 56a). Within the perched basin between the EBE and the basement high, depocenters progressively migrate away from the basement high from the pre-salt unit to PQ3 (Figure 55d), with locally chaotic intervals that are interpreted to represent Mass Transport Deposits (MTDs).

2.4.2.2   Balearic Ramp

The Balearic ramp extends from the previously described base-salt step at the end of the Balearic slope, to a zone of complex and poorly imaged salt structures where another base-salt step has been identified (Figure 55). In this domain the base-salt is mainly flat or landward dipping, and maintains a relatively constant depth of 4500m below sea level (Figure 56a, Figure 57a). The overburden here is significantly thicker, up to 1.7 km between salt structures, half of which is UU and half PQ.

The salt is also thicker and more deformed than on the Balearic slope, with an average thickness of 800m and a local maxima up to 1.5 km within diapirs (Figure 56a, Figure 57a). Salt anticlines are common and larger, with medium to high amplitudes (250 to 600 m) and medium to long wavelengths (1.5 to 3 km). They seem to be aligned along an arcuate ENE-WSW trend, parallel to the EBE (Figure 53b).

Diapiric structures are common, notably at the base of the Balearic slope step. They generally reach to the TOP PQ1 seismic horizon, with a PQ2-PQ3 roof (SW2 in Figure 56a and "SW1", "SW2", "SW3, "SW4" in Figure 57a). In some cases, they reach the seabed where they are locally extruded (SS1 in Figure 57a). Some diapirs are flat-topped ("SW2" in Figure 56a, "SS1" on Figure 57a). The UU to PQ1 units show minimal thickness variations with a relatively uniform thickness of 500±100 m (Figure 56a and 8a). They are thining and strongly upturning (>45º) within ~300 m of the diapir contact, where the strata become thin or absent (<100 m). Wide (>10 km) and steep UU to PQ2 panels adjacent to squeezed diapirs are also present ("SW1" and "SW2" in Figure 56a, "SS1" in Figure 57a). Near the top of the diapirs, these upturned limbs are delimited by crestal normal faults. They are often observed at the borders of the Balearic margin (i.e. where the base salt drops), at the
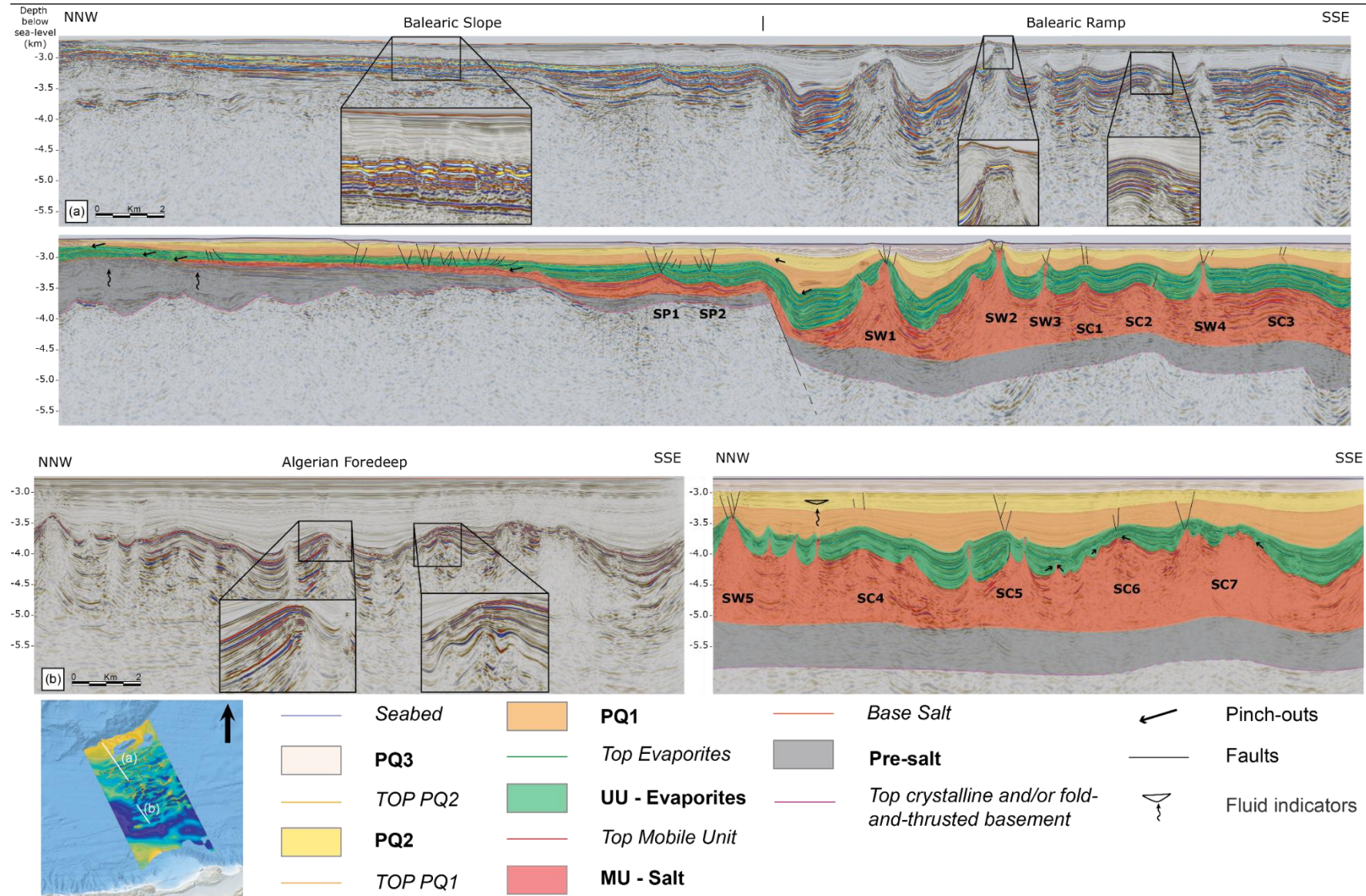
Figure 56 Dip-oriented seismic profiles showing non-piercing salt structures (anticlines as SCs, salt pillows as SPs, salt walls as SWs) in the northern Balearic margin (a; SF08) and in the Algerian foredeep (b; SF09). Location map shows the top salt from Figure 53b. Vertical exaggeration x2
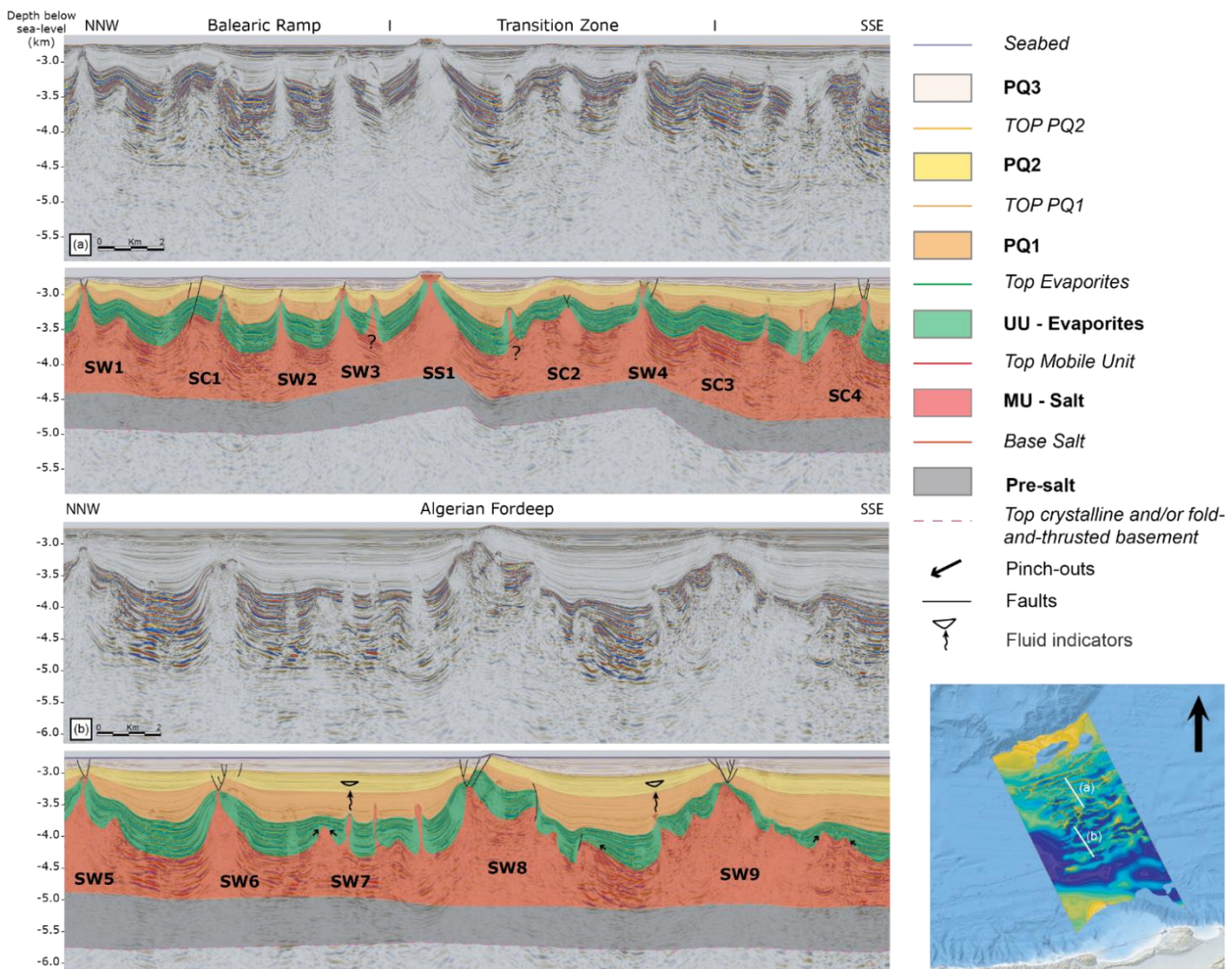
Figure 57 Dip-oriented seismic profiles showing piercing salt structures within the central Algerian basin (anticlines as SCs, salt walls as SWs, salt stocks as SS), in the northern Balearic margin (a; SF06) and in the foredeep of the Algerian basin (b; SF08). Most structures appear to be squeezed by a post-Messinian shortening episode that seems to be ongoing at present. The vertical flanks are not properly imaged by the 2D seismic data, particularly when the top of the diapirs is wider than its stem. SS1 is well imaged by several 2D seismic lines that allow us to discern it as a salt stock. Location map represents the top salt from Figure 53b. Vertical exaggeration x2

Balearic slope and the Transition zone. Two trends of salt walls can be distinguished (Figure 53c):

i) ENE-WSW trending salt walls located at the foot of the base-salt step, parallel to the EBE, that are expressed at the seabed by two belts of NE-SW elongated sea hills (Figure 53a, "SW1" and "SW2" on Figure 56a). They display strongly rotated flanks, with inward-dipping salt-detached normal faults immediately above their crests. Most often the landward limb is slightly more upturned than the seaward limb, forming the sea hills observed on the seabed (Figure 53a) rather than the salt diapir itself ('SW2' in Figure 56a).

ii) iWNW-ESE trending salt walls (Figure 53, Figure 57a), generally associated with salt-detached faults above their crests. They typically appear to be squeezed, with a narrow diapir stem or secondary weld separating the head of the wall from its triangular

shaped pedestal (Figure 57a, "SW2", "SW3", "SW4"). Locally, small salt-detached thrust faults seem to be present, but their offset are not well imaged to confirm their throw ("SC2" in Figure 56a). The PQ2 and PQ3 units thicken between these structures and drape their crests.

2.4.2.3   Transition domain

The transition domain separates the Balearic ramp, where the base-salt stands at a depth of 4.5 km below sea level, from the Algerian foredeep, where salt stands a depth of 5 km below sea level (Figure 57a, Figure 52c). In this domain the base-salt relief is generally poorly imaged due to the presence of large, complex salt structures, but generally presents a steep basinward slope. Salt structures are tall (up to 1.7 km) and squeezed (Figure 55a, Figure 55c), with thick accumulations of Plio-Quaternary sediments (up to 2 km) in halokinetic mini-basins (~1.5 to 3.5 km wide).

When a very weak signal is recorded below some structures, the presence of allochthonous salt sheets is suggested (Figure 58). The 4.5 km wide salt sheet SH1 lying above the UU is relatively well imaged (Figure 58a, SH1), with a salt stem connecting it to a triangular salt pedestal. The overburden is uplifted and faulted above the sheet, with moderately upturned strata. The PQ units onlap and thin across the sheet.

2.4.2.4   The Algerian foredeep

The Algerian foredeep extends from the transition zone to the southern basin margin, bounded by the North African transform margin (Figure 52, Figure 53). In this domain the base-salt appears sub-horizontal, at a constant depth of 5 km below the sea level (Figure 52, Figure 56b, Figure 57b). Contrary to the rest of the deep Algerian Basin, the pre-salt here displays a good signal-to-noise ratio, with flat parallel low-frequency and medium amplitude reflections suggesting either (i) a better penetration of the emitted seismic signal or (ii) stronger acoustic impedance contrasts, notably at the base of the pre-salt. The Plio-Quaternary is thickest in this domain (Figure 54c), where it makes up approximately 60 % of the total overburden. Diapirs rarely penetrate or deform the PQ overburden or seabed in this domain, but they commonly penetrate the UU (Figure 55, Figure 56b, Figure 57b). The UU reflections steepen toward and onlap the salt structures. In the south-western part of the study area, strong amplitude anomalies are observed within the PQ, with a dimming of the amplitude and a "pull-down" effect underneath (Figure 51c, Figure 55b, above SW7 in Figure 57b).

Salt structures are aligned along an arcuate ENE-WSW trend, above a nearly flat-lying pre-salt (Figure 53). Salt anticlines display a large amplitude (400 to 800 m) and a medium to long wavelength (1.5 to 3.5 km; Figure 56b,
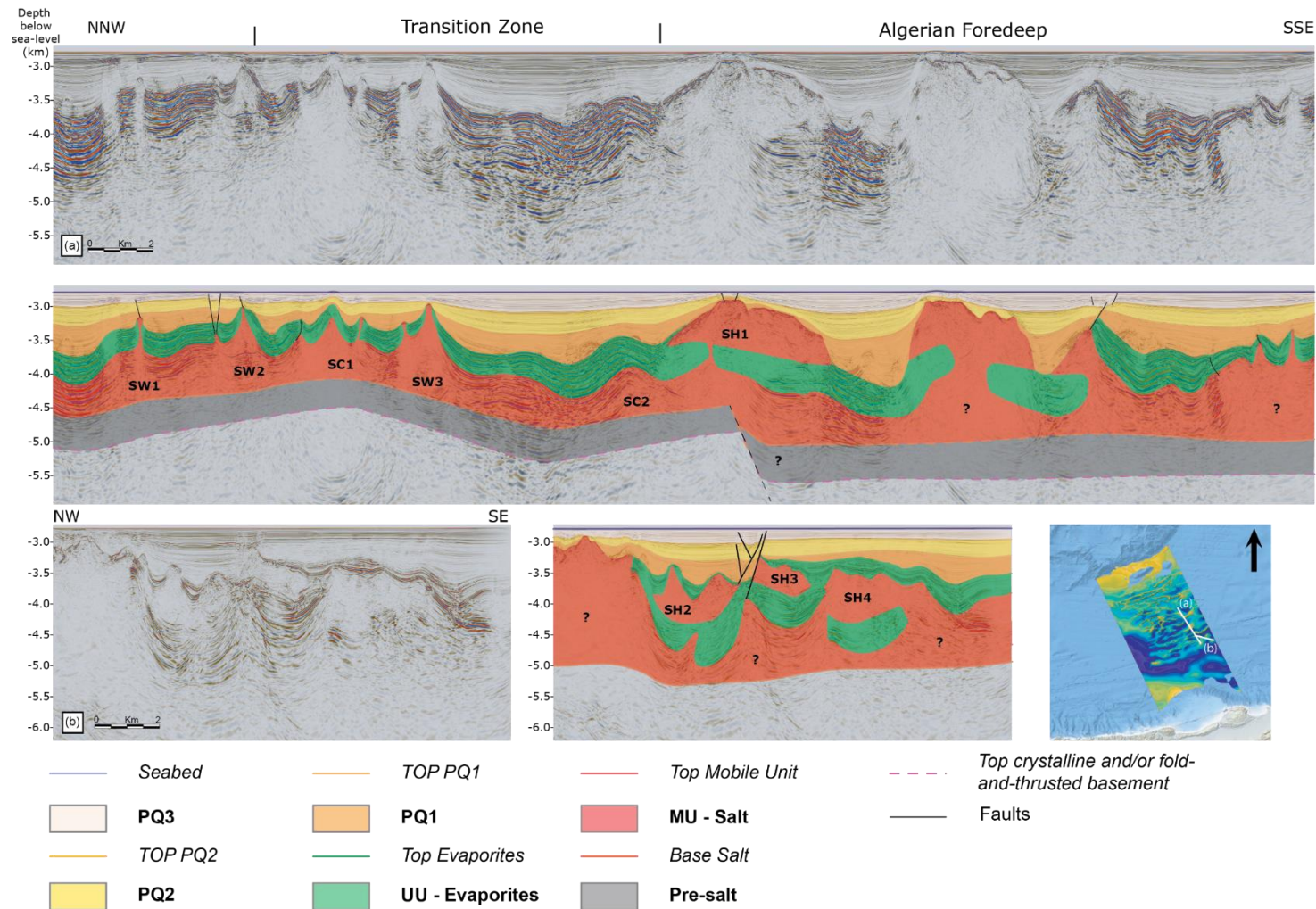
Figure 58 Seismic profiles showing salt sheets within the central Algerian basin (anticlines as SCs, salt walls as SWs, salt sheets as SH), in the foredeep of the Algerian basin along seismic profiles SF04 (a) and SF12 (b). Salt Sheets are located in the Algerian foredeep and along the transitional slope. They are poorly imaged on the available 2D seismic data, with very limited signal below the salt. Some important transparent salt structures could potentially be salt sheets because internal reflections are overmigrated if flooded with salt (in this case the available data do not allow us to distinguish them from a wide piercing diapir). SH1 seems to be located above a faulted basement. Location map represents the top salt from Figure 53b. Vertical exaggeration x2

Figure 57b). The folding mainly affects the UU and lower PQ1, while the upper PQ1 and overlying units are relatively undeformed. Locally, at the top of the salt, shorter wavelength and lower amplitude polyharmonic folds are observed (SC6 to SC7 in Figure 56b), which are onlapped by UU reflectors. Diapiric salt structures are complex with squeezed salt walls and minibasins uplifted above regional ("SW8" in Figure 57). Salt-detached thrust faults are locally observed between the salt structures (right-flank of "SW8" in Figure 57b, between "SC1" and "SW3" in Figure 58a). I observe an increased intensity of the salt-related deformation toward the north-eastern part of the study area, with wide allochthonous salt sheets within the UU and the early PQ (Figure 58).

2.5 Discussion

Since its deposition, the Messinian salt in the Algerian Basin has been in a basin under inversion, with thick-skinned thrusting and possible initiation of subduction of the Algerian oceanic crust beneath the North African margin (Frizon de Lamotte *et al.*, 2000; Recanati *et al.*, 2019; Strzerzynski *et al.*, 2021). In this discussion, I assess how this shortening has been recorded by salt tectonics adjacent to the Algerian margin. I first discuss whether the development of salt structures in the previously described structural domains is predominantly driven by gravitational forces or by lateral forces related to regional tectonics, and how the dominant drivers vary through time and space. Secondly, I focus on the Balearic margin, speculating its influence on the salt tectonic system.

2.5.1 Salt tectonics along the Balearic ramp

The stratal onlapping geometries of the UU to PQ1 units, with thinning and upturned strata in the vicinity of the diapirs, are characteristic features of halokinetic sequences deposited during near surface growth of load-driven passive diapirs (Jackson and Hudec, 2017; Rowan and Giles, 2021). This suggests that along the Balearic ramp, the early stage of the deformation was marked by load-driven passive diapirism, synchronous with deposition of the UU and early PQ1 sequences. Along the Balearic slope, where the salt thins and pinches out, normal faults record some extension in the overburden (Figure 55a, Figure 56a). These faults show relatively small displacement, recording a minor gravity-gliding of the salt along its base (see section 5.5). Furthermore, even though the pre-salt imaging is poor, the base salt relief is either flat or landward dipping, which would imply low basinward gravity gliding.

During the deposition of PQ1 the stratal geometries change. The thick UU-PQ1 strata are folded above salt-cored anticlines, elevating their roof above regional (Figure 55a). Most diapirs observed are squeezed in between UU to PQ1 rotated limbs. The TOP PQ1 horizon marks a regionally discordant surface

which is onlapped by PQ2 strata. The wide steeply upturned limbs often observed at the borders of the Balearic margin (i.e. where the base salt drops) are interpreted as megaflaps (Rowan *et al.*, 2016; Rowan and Giles, 2021). These features are commonly observed in contractional salt systems (Jackson and Hudec, 2017; Rowan and Giles, 2021). Because there is little evidence of gravity gliding, this contraction is interpreted to be tectonically driven.

I suggest the shortening initiated during PQ1 and peaked around TOP PQ1, generating the structures onto which the PQ2 strata onlap. The pre-existing passive diapirs were squeezed, and the overburden buckled, with PQ1 to PQ2 growth strata recording syn-shortening folding of the overburden. At the edges of the Balearic ramp, basement-involved normal faults (Figure 56a) and a rising basement high (Figure 55d) suggest the deformation is locally thick-skinned. Basinward, the pre-salt imaging is not good enough to discern whether the salt deformation involved the basement.

After Top PQ1, there seems to be a change in salt kinematics. Most diapirs do not rise above Top PQ1, and a PQ2-PQ3 roof is draping the diapirs crest (Figure 56). The burial of the diapirs results from the aggradation rate of the overburden out-competing the rise rate of the diapirs (Jackson and Hudec, 2017). This could be due to either an increase in sedimentation rate or decrease in the rate of diapiric rise. I suggest that the decreasing rise rate of the diapirs could be related to a diminishing regional shortening following the peak at Top PQ1, combined with an increased sediment supply from newly formed topography at the basin margin. This is also supported by growth strata above salt-cored anticlines: the PQ2 unit appears slightly folded, but the overlying PQ3 unit is relatively undeformed.

Though most become buried, some diapirs manage to continue rising actively and penetrate the younger PQ2-PQ3 units ("SW1" and "SW2" in Figure 56a). Recent crestal faults are present above the diapirs, with uplifted and upturned PQ2-PQ3 sequence at their flanks, suggesting ongoing active salt diapirism. At the foot of the base salt drop delineating the Balearic slope and the Balearic ramp, they form ENE-WSW trending salt walls, whose uplifted limbs form seahills on the current seabed (Figure 53a). At present the diapirism seems dominantly load-driven, with thick subsiding minibasins expelling salt into the precursor structures. Some salt-cored anticlines are also still inflating, arching their overburden ("SC1" in Figure 57a). Passive diapirism resumes locally where the overburden is not too thick ("SS1" in Figure 57a).

2.5.2 Salt tectonics along the Algerian foredeep

In the Algerian foredeep, the UU to PQ1 interval is not as uniformly distributed. Short wavelength buckle folds at the base of the UU suggest an early UU phase of contraction ("SC6" in Figure 56b, "SW9" in Figure 57b). It is

not clear whether this contraction was driven by thick-skinned, tectonic shortening or local thin-skinned, gravitational instability. Early thin-skinned, gravitational salt deformation during deposition of the UU is observed on other Western Mediterranean margins, such as in the Gulf of Lion (Mianaekere and Adam, 2020; Bellucci, Aslanian, *et al.*, 2021), the Western Sardinian (Del Ben *et al.*, 2018), but also along the Levant margin in the eastern Mediterranean (Gvirtzman *et al.*, 2013). The small magnitude of the folds and the analogy with other Mediterranean passive margins lead us to favour the gravity-driven interpretation, with salt spreading and gliding on a tilted margin. The development of thick-skinned thrust faults along the inverted Algerian margin could have played a role in steepening the base salt.

The upper UU onlaps these precursor contractional folds and shows considerable thickening between diapiric salt structures (Figure 56b, Figure 57b), suggesting a higher rate of syn-depositional subsidence and diapir rise than along the Balearic ramp at the UU stage. The salt diapirs are sparse and squeezed, with crestal faulting ("SC5" in Figure 56b, Figure 57b) and strongly upturned flaps of UU to early PQ1 strata within ~300 m of the diapirs (e.g. "SW7" in Figure 57b). Generally, they do not penetrate strata younger than early PQ1, particularly in the western part of the study area (Figure 56b). They are interpreted as passive diapirs during UU deposition, which were then squeezed at the late UU-early PQ1 stage. The squeezing formed secondary wells that progressively disconnected the head of many diapirs from the salt source, inhibiting further rise. Similarly with the Balearic ramp, the squeezing is interpreted to be linked to a regional shortening episode. This event also generated large (up to 10 km) and widely spaced (3 to 8km) salt-cored anticlines (Figure 56b, 8b and 9a), overprinting the previously mentioned early UU short wavelength folds.

In the north-eastern part of the Algerian foredeep, this early PQ1 shortening resulted in the extrusion of salt sheets emplaced above the UU (Figure 58). Locally, minibasins were shunted into each other and salt was squeezed out into allochthonous extrusions. With continued shortening, some of the salt extrusions coalesced into a canopy, with local secondary diapirism as the new salt layer is loaded by sediments (Figure 58b, "SH3", "SH4").

Along the Algerian margin, south of the Algerian foredeep, this quaternary shortening is thick-skinned, with north-verging thrust ramps delineating uplifted perched (piggyback) basins (Figure 52; (Déverchère *et al.*, 2005; Yelles *et al.*, 2009; Leprêtre *et al.*, 2013; Leffondré *et al.*, 2021; Strzerzynski *et al.*, 2021). Salt structures adjacent to the margin are squeezed and the whole overburden is folded in response to regional shortening, whereas the pre-salt sequence still preserves extensional half-grabens (Soto *et al.*, 2019).

Following this early PQ1 contractional episode, the salt deformation decreases. To the south-eastern part of the study area, the early PQ1 is drape

folding slowly rising salt structures and thickening into wide minibasins. The aggradation rate of the PQ sequences soon overtakes the rate of diapir rise and buries them under a thick roof. Crestal faults extend up to the TOP PQ2, indicating some persisting salt movement, but the late PQ1 to PQ3 units are deposited sub-horizontally.

Locally, active salt diapirs are still rising today, uplifting their very thick (1km) roof 800 meters above regional ("SW8" in Figure 57b), and forming bathymetric highs on the seabed (Figure 53a). To the north-western part of Algerian foredeep, the salt sheets emplaced during the PQ1 shortening are still sourced at the autochthonous level and continue to inflate syn-depositionally with the PQ sequences aggradation (Figure 58a). Their inflation is interpreted to be load-driven, with expulsion of the salt beneath the thick and wide (>1.5 km) subsiding minibasins. The influence of a steady but mild regional shortening is not excluded, in response to the current slow-rate crustal shortening at the Africa-Eurasia plate boundary (Bougrine, Yelles-Chaouche and Calais, 2019). Locally, the presence of long sub-vertical faults and abrupt thickness variations within the PQ sequence (e.g. Figure 55a, along SF06 in the Transition zone) could potentially record a transpressional regime.

2.5.3 Outward shifting of the contractional deformation during the Plio-Quaternary

I have shown that the regional shortening due to the ongoing inversion at the Algerian margin has been recorded within the central Algerian Basin. Most of the shortening is accommodated by the salt and the deformation of its roof. The salt acts as a décollement within the central Algerian Basin, allowing northward propagation of the contractional deformation, from the Algerian margin to the Balearic margin. I distinguish two stages of contraction:

a) First, a short late Messinian episode (MSC Stage 3), synchronous with the UU deposition, that was localised along the Algerian foredeep. This episode is interpreted as gravity-driven, related to thrust faults that steepened the base-salt at the toe of the Algerian margin fold-and-thrust belt.

b) The second episode, longer and more widespread, occurred during the PQ1-PQ2 deposition. This regional shortening accommodated northward propagation of the Algerian deformation front, and its effects are diachronous across the basin. Along the Algerian foredeep, this shortening peaked during early PQ1. It resulted in high amplitude and widely spaced folds, with squeezing of pre-existing passive diapirs and extrusion of salt sheets. This contrasts with the Balearic ramp domain, where shortening peaked later, during latest PQ1. Precursor structures were squeezed with asymmetrical limbs tilted and uplifted. This second peak of salt deformation could be linked to the second phase of Atlas

inversion (Pliocene to lower Quaternary) and the related Tell shortening that could have been recorded through the whole Algerian Basin, with notably the initiation of the north-verging thrusts at the toe of the Algerian margin (Frizon de Lamotte *et al.*, 2000; Roure, Casero and Addoum, 2012; Strzerzynski *et al.*, 2021). The second episode is thick-skinned along the Algerian margin and could also reactivate more distal faults along the Balearic margin (see section 5.5). In between these contractional pulses, the diapirism was mostly passive, driven by sediment-loading.

The decreased intensity of the salt-related deformation in the Algerian foredeep compared to the Balearic ramp during the Plio-Quaternary could be related to the higher sedimentation rate in the Algerian foredeep (more than 1 km on average within ~5.3 Ma). The rate of sediment aggradation during PQ1 outpaces the rate of diapiric rise in the Algerian foredeep (the thickness of the PQ1 unit doubles from the Balearic ramp to the Algerian foredeep), resulting in burial of the diapirs beneath a strong overburden. The thicker, stronger overburden also results in propagation of the contractional stresses further out into the basin (on the Balearic ramp) along the salt décollement, where the strain is accommodated by folding of the thinner overburden and squeezing of pre-existing diapirs.

Salt décollement facilitated the sliding and folding of the overburden, hereby accommodating the stress applied by the ongoing shortening. Basinward propagation of the contractional stresses allowed a wide thin-skinned deformation with a focused folding out into the foreland, similarly with the Appalachian Plateau, the Franklin Mountains in north-western Canada, and the Jura of the Alps (Davis and Engelder, 1985). During the Plio-Quaternary, the thicker overburden of the Algerian foredeep, adjacent to the thrust front, can translate without deforming by sliding on the salt. The deformation is instead focused outward, to the Balearic side, where the overburden is weaker. Base-salt relief along the transition zone and the Balearic slope may be able to disrupt this gliding, resulting in a highly deformed overburden (Figure 55c, Figure 58). The poor imaging along the Transition zone do not allow use to confidently interpret the amplitude and the influence of the base salt relief there.

2.5.4 Lateral variability in the complexity of salt structures and magnitude of deformation

In the Algerian foredeep, I previously described an increased intensity of the salt-related deformation toward the north-east, beyond the Thenia fault that separates the Khair al Din bank thrust front from the Kabylia block (Figure 52, Figure 53a). Toward the south-west, most salt structures are inactive at present, buried under a thick sub-horizontal Plio-Quaternary succession, widely spaced between minibasins. Only a few active diapirs penetrate above the

early PQ1 unit at the front of the propagating thick-skinned thrust front (the Khair Al Din bank; Figure 52a, 3b). The across-strike width of the Algerian foredeep is less than 50 km. Toward the north-east, where the across-strike width increases up to 90 km, the salt structures become more complex and more closely spaced (Figure 52c). Diapirism is still active, recorded by recent growth strata within the PQ3 sequence. Wide salt sheets and salt canopies are observed on top of the UU (Figure 52c, Figure 58). Several factors could control this lateral variability in the intensity of the deformation. I consider the following: (i) an eastward increase in the rate of horizontal tectonic loading, due to segmentation of the margin across the strike-slip Thenia fault; (ii) the variability in salt distribution and precursor structures prior shortening; (iii) a differential thermal loading.

The Algerian margin is described as a transform-type (STEP) segmented margin, that displays contrasting structural domains of contraction and extension, with an important strike slip component (Govers and Wortel, 2005; Domzig *et al.*, 2006; Leprêtre *et al.*, 2013; Medaouri *et al.*, 2014; Hamai *et al.*, 2018). To the north-east, the convergence rate across the Algerian margin decreases from 3-4 to 1.5 mm/yr (Strzerzynski *et al.*, 2010; Bougrine, Yelles-Chaouche and Calais, 2019). However, even though the convergence rate is higher on the south-western segment of the margin, the displacement is mostly accommodated onshore within the Tell Atlas, while shortening along offshore reverse faults is minimal (Déverchère *et al.*, 2005; Domzig *et al.*, 2006; Yelles *et al.*, 2009; Arab *et al.*, 2016; Leffondré *et al.*, 2021). The thick-skinned thrust faults bordering the Khair al Din bank (Figure 53a) may accommodate most of the shortening and focus compressional deformation internally at the margin toe (Figure 50, Figure 52a, Figure 52b). Consequently, the displacement loading applied offshore to the salt and overburden may be lower and the deformation milder in the south-west. By contrast, even though the overall convergence rate is lower to the east of the Thenia fault, it concerns a much broader area and includes a component of strike slip (Domzig *et al.*, 2006; Yelles *et al.*, 2009; Leffondré *et al.*, 2021). Regional shortening is more widely distributed in the outer domain, resulting in a stronger tectonic loading accommodated by the salt and its overburden (Figure 52c).

Alternatively, this along-strike variations in salt deformation could be due to a different salt distribution prior to shortening. It is possible that precursor salt structures were more closely spaced to the east, where a wider basin width allowed the accumulation of a larger salt volume. This is still visible at present, where diapirs are more closely spaced to the east than to the west (Figure 52). The presence of precursor salt structures strongly influence the style of shortening in salt provinces (Letouzey *et al.*, 1995; Hudec and Jackson, 2007; Duffy *et al.*, 2018). To the west, where few, small scale precursor anticlines and diapirs are present, the shortening was accommodated through high amplitude and widely spaced buckling of the overburden. To the east, strain was localized on precursor structures, where

salt is thicker, resulting in highly squeezed diapirs and extrusion of salt sheets.

Lastly, thermal loading could potentially influence the variability in style of deformation along the margin. Offshore heat flow measurements showed a westwards increasing trend, from ~60 to > 150 mW m^{-2} (Jiménez-Munt *et al.*, 2003; Poort *et al.*, 2020). This could also have an influence on salt deformation through differential thermal loading, as recently argued by Bellucci et al., (2021a). However, the higher heat flow to the west should induce a higher buoyancy and greater mobility of the salt (Jackson and Hudec, 2017). Therefore, it cannot explain the lower intensity of deformation to the west.

2.5.5 The influence of the Emile-Baudot escarpment and the ocean-continent transition

The Balearic slope is divided in two by a WSW-ENE trending topographic high that may have influenced the salt deformation along the Balearic margin. I distinguish the "perched" basin along the EBE, where salt is thin or absent, from an overall basinward dipping ramp, with small amplitude salt structures (Figure 55a, Figure 55d). Camerlenghi et al. (2009) suggest that this ridge is formed by volcanic rocks intruded along re-activated Miocene normal faults. It would grow by local transtension/transpression along the south-western end of the EBE transform, between the Balearic promontory continental block and the Algerian Basin.

Abrupt termination of the Plio-Quaternary reflections above the crest of the ridge (Figure 55d, Figure 59), and migration of the adjacent PQ depocenters away from the high, suggest that the ridge has been rising since the pre-Messinian, and that it is actively rising at present. The steep seabed pinnacles support the hypothesis that the ridge is partly intruded by volcanic material, as do the steepness of the reflections dipping outward from the crest of the ridge (Figure 59). The interpreted Messinian units are onlapping and pinching out along this ridge, suggesting it was already forming a topographic high at the onset of the MSC (Figure 59).

There is evidence of thin-skinned extension along the Balearic slope expressed by salt-detached normal faults and rollovers of small amplitude (their vertical throw is < 15 m, with very small amplitude rotation of the reflector along the fault), suggesting a minor contribution of salt-detached gliding toward the basin (Figure 55, Figure 56a). Previous studies suggested that these faults could be linked to dewatering of gypsum into anhydrite (Wardell *et al.*, 2014), but recent overpressure models favoured hydrofracturing induced by over pressured fluids escapes (Dale *et al.*, 2021). I suggest that the faulting is mostly related to extension induced by gravitational instability on a gentle slope. The constant thickness of the UU and PQ1 units suggests that the onset of gliding was approximately coeval with the TOP PQ1 horizon. Because the
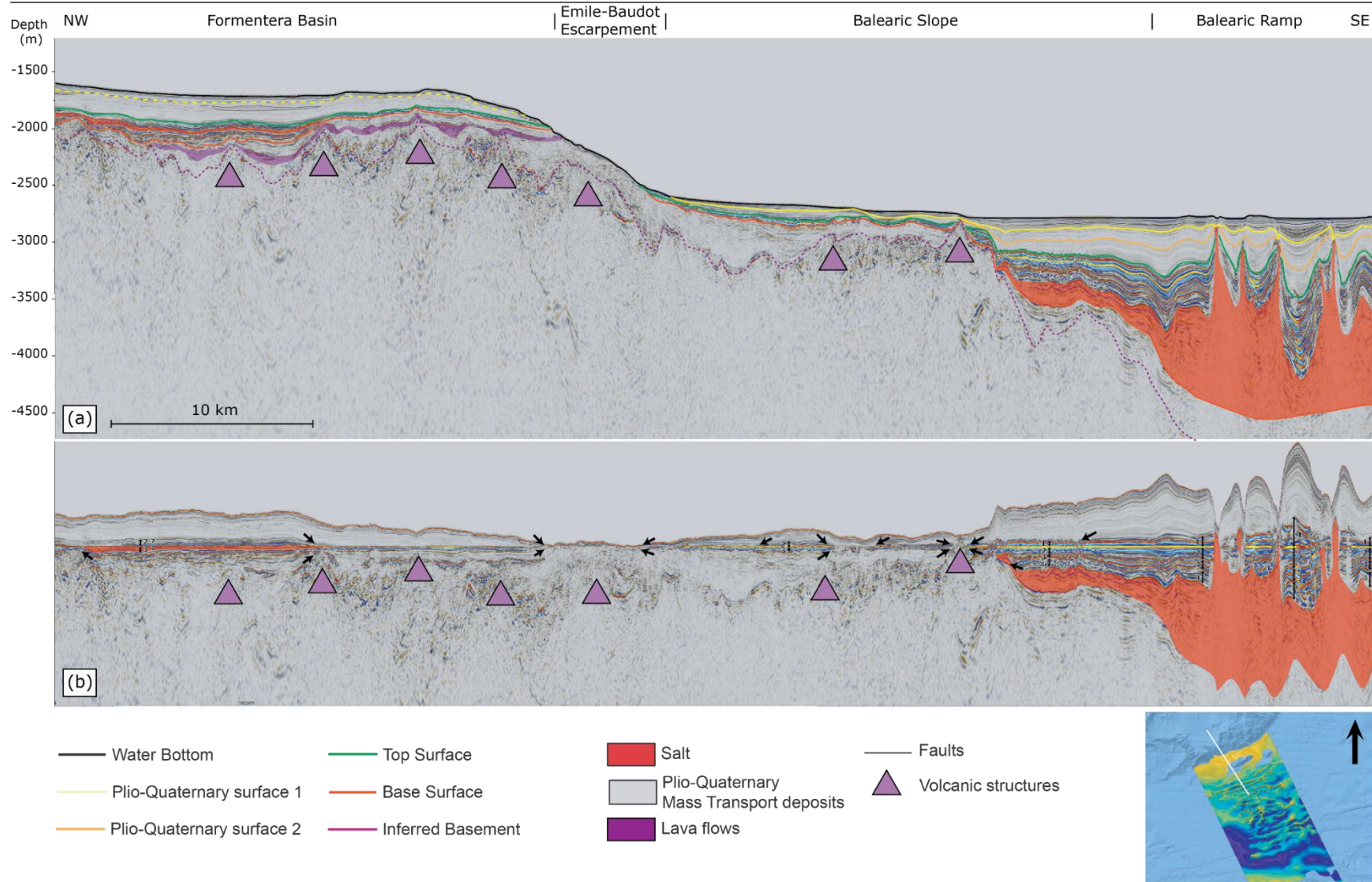
Figure 59 (a) Interpreted seismic profile SF07 showing the thinning and the pinching-out of the Messinian units along the basement highs and (b) flattened seismic profile along the strongest regional UU reflector. Black arrows point to the pinch-outs observed within the Messinian Evaporites. Location map represents the top salt depth from Figure 53b. Vertical exaggeration x6

salt is relatively thin along the Balearic slope, it is possible that frictional boundary forces prevented gliding until the base-salt was sufficiently steepened. This steepening of the Balearic slope can be explained either by subsidence in the deep basin (Dal Cin *et al.*, 2016) or by reactivation of pre-existing basement faults during the regional shortening. This instability could also be related to the presence of MTDs within PQ2 on the Balearic slope (Figure 55d), causing a destabilization event between TOP PQ1 and TOP PQ2.

The deposition of these MTDs and the onset of minor gravity gliding coincide with the general peak of salt tectonic activity previously described across the central Algerian deep basin (around TOP PQ1). I propose that the driving tectonic force that caused the contractional salt deformation within the Balearic ramp (the Top PQ1 shortening event) could have also re-activated the pre-existing Balearic faults. The reactivation of these faults could have steepened the base-salt and caused gravitational instability, triggering minor gravity gliding and mass transport processes. Local small depressions of the seabed suggest that extensional salt tectonics is still active today along the Balearic slope (SP1 in Figure 56).

As suggested by Camerlenghi et al. (2009), the ENE–WSW direction of the salt walls (parallel to the EBE) leads us to think that the salt tectonics is locally influenced by the synthetic strike slip fault that borders the ridge (Figure 53b, Figure 53c). However, I do not interpret this fault to represent the ocean–continent transition (OCT), as previously suggested, because the interpreted base-salt is dipping gently landward and exhibits a base-salt step down from 4500 to 5500 m at the transition zone (Figure 53c, Figure 55). I believe that if there is oceanic crust for this part of the Algerian Basin, it is restricted to the Algerian foredeep domain, where the maximum thickness of Plio-Quaternary sediments is recorded (Figure 52, Figure 54c). In that scenario, the Balearic ramp could constitute a thinned and stretched continental crust, or a transitional crustal domain. Our results suggest that there are two trends of lineaments in the pre-salt topography (Figure 53c): (i) the ENE-WSW trend parallel to the synthetic EBE strike–slip direction, and (iia) the NW-SE trend parallel to the antithetic EBE strike–slip direction or (iib) the synthetic DJFZ direction and the Thenia fault (Boudiaf, 1996; Acosta *et al.*, 2013). The imaging of the pre-salt and the sparsity of the data do not allow us to accurately identify the tectonic regime, but it is suspected to yield a strange strike-slip component, linked to the important strike-slip escarpment observed at the margins (the EBE, the DJFZ, the NAT). Further geophysical investigations and sampling of the crust could help understanding the nature of the basement here.

## 2.5.6 Messinian to current geological model of the central Algerian Basin

Based on the previous discussions, I suggest a new tectono-sedimentary model for the study area, in the central Algerian Basin (Figure 60):

1/ Salt movement begins shortly after deposition of the salt (MU), forming a series of gravity-driven passive salt diapirs throughout the basin (Figure 60). Syn-kinematic deposition of the UU causes differential sedimentary loading of the salt, driving salt spreading and passive diapirism within the central basin. In the Algerian foredeep, the deformation is also driven by the regional shortening at the front of the ongoing inversion of the North African margin, creating small magnitude folds and steepening the base salt-relief.

2/ During the deposition of PQ1 the regional shortening starts to increase and to affect the deformation. At early PQ1, diapirs continue to rise mostly passively on the Balearic ramp, but in the Algerian foredeep and in the Transition zone, shortening causes buckling of the overburden and squeezes precursor structures, with local expulsion and inflation of salt sheets at the base of the PQ1. The high aggradation rate of the PQ1 slowly drapes and buries the diapirs. At late PQ1, the shortening starts to affect the Balearic ramp, squeezing the precursor passive diapirs, arching the UU to PQ1 roof above active diapirs and salt-cored anticlines, and rotating the mini basins. Along the EBE, the TOP PQ1 shortening triggers the reactivation of pre-existing rifting faults in the basement, causing the rejuvenation of pre-existing topographic highs, steepening of the base-salt relief and destabilization of the sediments with the deposition of MTDs. The overall deformation creates topographic highs and lows where sediments preferentially accumulate, amplifying the formation of minibasins between salt structures.

3/ From TOP PQ1 the deformation seems to be focused predominantly along the Balearic ramp, with actively rising diapirs draped by PQ2 and PQ3. In the Algerian foredeep, the thick roof inhibits the rise of pre-existing salt structures. Deformation is interpreted to be mostly driven by sediment loading, with salt expulsion beneath subsiding minibasins. Locally, in the Algerian foredeep and along the EBE, some actively rising diapirs are uplifting their roof and the seabed, probably driven by ongoing, but milder, regional lateral shortening. Along the EBE, thick-skinned deformation causes minor basinward gliding along a steepened base-salt (post- PQ1 shortening event), inducing an extensional faulting of the UU to current overburden.
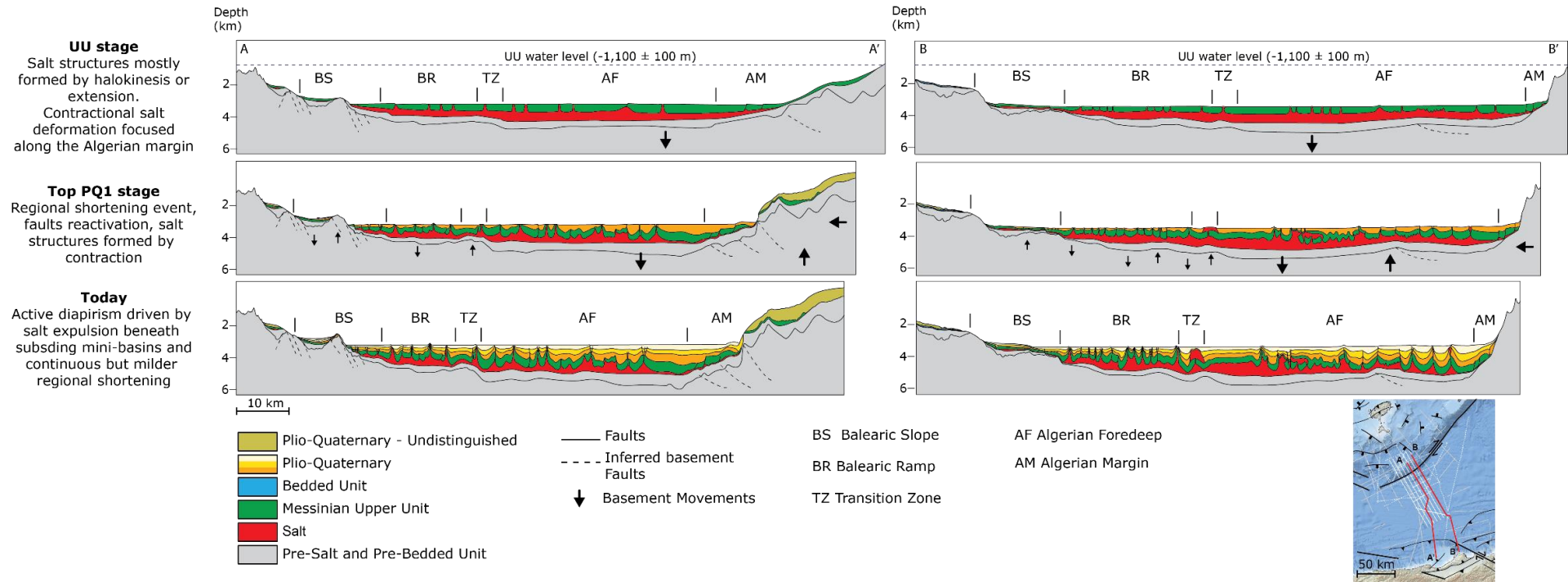
Figure 60 Schematic evolution of the basin showing the salt deformation from Messinian to current times along two NW-SE profiles across the central Algerian basin. The water level during the UU deposition is based on estimations from Heida et al. (2021)

2.6 Conclusion

I used reprocessed 2D seismic reflection data to examine the salt structures in the deep central Algerian Basin, a field analogue of early contractional salt deformation in an incipient orogenic Fold-and-thrust belts. Different structural domains have been recognized based on the thickness of the overburden, the thickness of the salt, and the types of salt structures. I have shown that the central Algerian Basin recorded contractional episodes, with salt-cored anticlines, squeezed diapirs and allochthonous salt sheets. I identified an early Messinian to Zanclean contractional deformation, synchronous with the deposition of the UU, that is more pronounced along the Algerian margin. It is followed by a later Plio-Quaternary deformation, around the TOP PQ1 regional seismic horizon. This later shortening is more pronounced on the Balearic slope because high aggradation rates inhibit further diapirism in the Algerian foredeep. This event could be related to the second phase of inversion of the Atlas system, at Pliocene to lower Quaternary. In the Algerian foredeep, the structural style of salt structures also varies from SW to NE, with an increase in salt deformation toward the NE marked by wide allochthonous salt sheets. I argue that this is controlled by the pre-shortening salt distribution and/or by an increasing tectonic contractional loading from SW to NE. In the south-western part the thick-skinned North African thrust fronts may accommodate most of shortening at the toe of the margin to the SW, while in the north-eastern part of the central Algerian basin, the oblique convergence is more pronounced offshore. I. show that the Balearic ramp is mainly landward dipping until a transition zone that is marked by a 500m base-salt step. I suggest that this transition could be the ocean-continent transition, with a wide transitional crust along the ramp. Finally, I show that locally along the Balearic slope, the system is currently extensional, driven by the seaward translation of salt and overburden along a steepening base-salt. A continuously rising basement high, parallel to the synthetic Emile-Baudot strike-slip direction, steepened the base salt along which salt could glide more readily, leading to locally extensional salt tectonics that is still active today.

Chapter 5

Conclusion and Perspectives

3.1 Summary

This thesis explores the geophysical imaging, the salt tectonics, and the fluid indicators of the MSG in the central Algerian basin.

In Chapter 3 I present a cost-effective method for reprocessed legacy 2-D airgun seismic reflection data. In an ever more challenging context for the acquisition of seismic data in the Mediterranean Sea, reprocessing to improve the quality of legacy data has become more important. I present several reprocessed datasets (SALTFLU, SBAL-DEEP, MS046) acquired in the Algerian basin by the National Institute of Oceanography and Applied Geophysics (OGS). I apply a 'broadband' reprocessing strategy adapted for short-offset, deep water airgun reflection seismic data and assess if the reprocessed images provide new geological insights on the Mediterranean sub-surface. The workflow relies on an integrated approach combining geophysics and geological interpretation to iteratively build the velocity model. In this way I aim to tackle some of the challenges linked to imaging complex geological structures containing high velocity contrasts with 2-D, short-offset seismic data. I first broaden the bandwidth of the data through multi-domain de-noising, deghosting and a source designature using an operator derived from the seabed reflection. I then perform iterative migration velocity analysis, Kirchhoff pre-stack time migration and multiple attenuation in the Radon domain to obtain time-migrated images. The initial velocity model is derived from the resulting time migration velocities, and geologically driven model updates are generated using a combination of travel-time tomography, seismic interpretation of the major salt horizons and velocity gradient flooding. The gradient flooding aims to reproduce the large scale first-order velocity variations, while the travel-time tomography aims to resolve the smaller second-order velocity variations. The results improve our deep geological knowledge of the under-explored Algerian basin down to the base salt and the pre-salt. Fluid indicators are imaged within the Plio-Quaternary of the Algerian basin, which I interpret as thermogenic or biogenic gas sourced from either the Messinian Upper Unit or from the pre-salt, migrating through a hydro-fractured salt. The reprocessed data image lateral and vertical seismic facies variation within the Messinian units that could shed new light on the tectono-stratigraphic processes acting during the Messinian Salinity Crisis. It also reveals numerous previously unresolved volcanic structures within the Formentera basin. Further improvements could be done by enhancing the S/N or using more accurate imaging algorithms, but this would require appropriate computing power.

Chapter 4 explores the Miocene to current salt deformation within the deep central Algerian back-arc basin using the result presented in Chapter 3. The Messinian salt of the Algerian basin is a unique analogue for studying the early stage of deformation of shortening structures in salt-bearing orogenic fold-and-thrust belts. The salt was deposited in an already inverted basin, after its extensive stage. Its inversion initiated in the Tortonian, with a N-NW shortening induced by the north-westward motion of the African plate. In this study, I use new 2D multichannel seismic data to identify, classify and map salt structures throughout the central Algerian Basin and re-assess its structural style. I interpret contractional salt tectonic structures, such as buckle folds, squeezed diapirs and related salt sheets as evidence of regional thick-skinned shortening episodes. I conclude that horizontal displacement loading has driven salt deformation within the basin since its deposition. I also show spatial variations in the structural style of the central Algerian Basin, both along- and down-dip. I demonstrate that the initial shortening-related salt deformation in the late Messinian was focussed along the Algerian margin and later shifted outward toward the Balearic margin in the Plio-Quaternary. The shifting of the deformation front is interpreted to be a result of the thickening and strengthening of the overburden. The second peak of deformation may have reactivated faults along the Emile-Baudot escarpment with thick-skinned deformation. I also observe a variation in the intensity of the salt deformation along the margin from SW to NE, which may be due to variable tectonic loading applied along the Algerian margin or the pre-shortening distribution of salt.

3.2 Synthesis

Can we develop a robust and cost-effective strategy to reprocess legacy seismic reflection data?

Chapter 3 presents a modern processing strategy for reprocessing short-offset legacy airgun multi-channel seismic data, improving the imaging of the MSG. Despite the many pitfalls of the legacy narrow azimuth data, broadband and amplitude preserving processing can successfully improve the quality of the imaging in time and/or depth. However, the benefit of the reprocessing is impeded by the acquisition parameters and our computing power. Putting aside the poor illumination of the complex MSG on legacy narrow azimuth 2D acquisitions, the towing depth and the length of the recording cable are the essential pitfalls. A shallow towing depth results in a low S/N ratio (particularly because of the low-frequency swell noise). Eliminating this noise while preserving the

lowest octaves of the primary signal is a difficult trade-off. Yet, the low-frequency signal is crucial for imaging the MSG and the pre-MSG because it is less subject to energy attenuation. The limited length of the cable decreases the velocity resolution because of the reduced moveout discrimination in the prestack gathers. In the western Mediterranean in particular, the strongly reflective UU generates internal peg-leg multiples that display medium to high velocity on CMP gathers. They appear difficult to discriminate through offset-based methods (e.g., Radon Domain demultiple) because their moveout difference with the underlying salt is low and requires long-offset records to appear. Furthermore, the mobile salt appears to yield internal reflectors that could be eliminated if the multiple elimination is done without caution. These internal reflectors should be carefully preserved, as they are essential indicators of the salt movement. These two pitfalls strongly affect the resolution and the veracity of the velocity models and lowers the benefit of pre-stack migration. The processing tools and the available computing power also play a crucial role. The processing flow that I had initially designed could not be optimally performed on the software used at the OGS. Only when I obtained REVEAL and new computing power, I could perform more tests to find the optimal processing parameters.

Is it worth investing time on reprocessing the legacy data? Does it provide new insights on fluid flow and on the salt tectonics of the MSG?

I would say that the value of reprocessing is easy to prove because the quality of the legacy images is relatively low, emphasizing the benefit of investing our resources for re-assessing the value of these "dormant" data. Even though the quality of legacy images can only be improved to a limited extent due to acquisition limitations, it provides brand new insights on: the salt tectonics of the central Algerian basin (Chapter 4), the seismic expression of the UU and the late (stage 3) stage of the MSC, the pore fluid circulations along the Balearic margins and in the Algerian foredeep, the geodynamics of the Formentera basin (Chapter 3).

In Chapter 4, I provide a whole new interpretation of the central Algerian basin salt-system using the new sections. Previous images were not imaging well the steep salt structures, with a limited bandwidth that wasn't highlighting the pre-salt events and the amplitude variations. Our understanding of salt tectonics is still limited because this is 2D data. Profiles rarely draw a perpendicular transect along the structures and many of them are poorly illuminated or out-of-plane. The direction of the MSG flow is mainly inferred based on the expression of the salt deformation on the seabed and the configuration of the basin's margins.

The new images also clearly revealed seismic fluid indicators within the Algerian basin. In particular, the Balearic margins display amplitude anomalies that suggest active fluid circulation. The origin and the nature of these fluids is still being studied, in collaboration with La Sorbonne ISTeP, who recorded anomalously low heat flow anomalies values along the EBE and positive HF in the proximal deep basin that could be related to the fluid indicators observed on the seismic images (Poort *et al.*, 2020). The new images show that the Formentera basin was already volcanic before the Messinian, and that volcanic activity persisted during the Plio-Quaternary. The influence of these volcanic episodes on fluid circulation along the Balearic margin is not yet clear, but we suspect that the two are tightly correlated. The high permeability fractured basaltic rocks sampled around the EBE, the thin sedimentary thickness, and the heat flow anomalies suggest a fluid circulation in the area of study. I think that the presence of mud volcanoes is unlikely, but it cannot be discarded considering the likeliness of overpressured zones beneath the MU and the presence of non-reflective diapirs. Due to the 2D dimension of the images, it is hard to assess clearly if they represent mud diapirs or out-of-plane reflections.

I also evidence lateral and vertical seismic facies variations in the seismic records of the MSC that were not described in the previous datasets (Chapter 3). The reflections of the UU are also characterized by oscillations between high (>4000 m/s) and medium to low velocities (2500-3000 m/s), with a globally downward increasing trend from 2500 to 3000 m/s. I suggest that the UU is predominantly made of clastics, with at least one regional bed of evaporites near its top (R4). I also suggest that the upward decrease in velocity is not only the result of decreasing compaction but also of an upward enrichment in terrigenous clastics, reflecting the freshening of the Mediterranean during stage 3. I observe 7 high amplitude reflectors that could be related to the precession cycles described on the onshore stage 3 records, this work is still in progress. The lateral amplitude variations in the last unit of the UU (between R4 and R5), with low amplitude seismic facies along the Balearic margin and in the Algerian foredeep, could translate to preferential erosion/deposition during the Zanclean flood.

What is the role of halokinesis in the structural and sedimentary development of a basin?

In Chapter 4, I identify and classify the salt structures within the central Algerian basin, and I study their distribution as a function of their distance from the margins, the deformation of the overburden, the pre-salt relief, and the ratio between the salt and the overburden thickness. I

observe 4 structural domains, with two important base-salt drops: the Balearic slope, the Balearic ramp, the transition zone, and the Algerian foredeep. I show that in the central Algerian basin, salt focused the strain applied by regional shortening. It acted as a décollement above which the overburden is highly folded and faulted above the deformed salt. The difference in salt tectonics distribution observed today can be explained by the outward migration of the salt deformation, away from the NAT thrust, in front of which the Plio-Quaternary sediments are preferentially accumulated in the foredeep.

In the new model, salt deformation starts early after its deposition, synchronously with the deposition of the UU, similarly with other margins of the western Mediterranean (Section 1.4.3). During that stage, passive diapirs and small amplitude salt-cored anticlines are formed driven by gravity gliding and spreading, with additional tectonic loading focused along the Algerian margin, at the foot of the NAT thrust front. During the Plio-Quaternary, the tectonic loading is enhanced by a north-westward regional shortening event applies a strong lateral loading on the MSG. I suggest that this shortening event could be related to the second orogenic episode of the Tell Atlas. The MU acts as a décollement and focus the strain applied to the basin. The whole overburden is folded above salt-cored anticlines, the pre-existing salt structures are squeezed, with megaflaps of UU-PQ1 on the flanks of the squeezed diapirs, and salt sheets of MU that start inflating above and within the UU. This event triggers thick-skinned thrusts along the NAT and increases the loading applied in the Algerian foredeep, where Plio-Quaternary sediments are preferentially accumulated until today. Thick-skinned tectonics is also observed on the conjugated Balearic margin. Pre-existing faults are reactivated in transpression/transtension, uplifting the Miocene to Plio-Quaternary roof. The important base salt drop between the Balearic slope and the Balearic ramp is amplified or generated at that moment. The steepened salt starts flowing preferentially by gravity gliding locally. The response of the EBE is hard to assess because of the poor seismic imaging of its structures. Due to the rapid deposition of the MSG, models suggest that the overpressure was already high before this shortening. I wonder how this additional stress was accommodated in the pre-salt, and if it did not trigger the overpressure-induced hydro fracturing of evaporites.

After this contractional episode, the central Algerian salt-system enters a quieter stage, with still rising active diapirs, probably driven dominantly by differential sedimentary loading applied by the thick overburden. However, in the Algerian basin, the rising rate of the diapirs could not compete with the accelerating sedimentation rate after the

shortening event, inhibited further inflation of salt structures. Consequently, salt deformation shifted outward toward the transition zone and the Balearic ramp. The base salt drop along the transition zone is puzzling if we consider the whole Algeria basin is oceanic. I believe it could mark the transition between two types of crusts, possibly between a transitional stretched continental crust (the Balearic ramp) and a purely oceanic crust (the Algerian foredeep).

3.3 Overall conclusion, discussion, and perspectives

Through a modern reprocessing strategy, this work resulted in the production of improved seismic images of the MSG within the central Algerian basin. This unlocked new understanding on the Messinian to recent tectono-stratigraphic evolution of the basin and pore fluid circulation within it. This work was performed to support safe drilling operations through salt giants and provide new knowledge on early deformation of salt giants. In this study, we show that the inversion of the southern margin of the Algerian basin has strongly impacted the structural and sedimentary development of the basin. Salt acted as a décollement and accommodated most of the shortening through thin-skinned deformation. Yet, I interpret geophysical evidence of faults rejuvenation and mass transport movements that I relate to thick-skinned deformation along the Balearic margin, suggesting a strong tectonic loading regionally. I believe it probably contributed to the fracturing of an already overpressured MSG, and I suspect it influenced the fluid circulation we observe along the EBE. Based on this work and on the studies from other researchers from the ETN SALTGIANT, it seems very likely to encounter overpressured zones within the MSG and the pre-MSG. Many seismic fluid indicators and anomalous heat flow measurements suggest the presence of active fluid circulation. It seems difficult to promote safe drilling operations without a drilling riser to the surface or blowout preventers.

The straightforward outlook of this work is to extend the reprocessing and the study of salt tectonics to other under-explored basins in Mediterranean. To do so, I suggest two broad perspectives based on my results and my experience during this thesis.

1 If we want to improve our knowledge of the offshore MSG, we need to implement an international FAIR (Findable, Accessible, Interoperable, Reusable) data system along with a vast

reprocessing campaign for the western and the central Mediterranean between the research institutes

Except for the explored oil and gas provinces (notably the Levant Basin and the Nile Delta in the eastern Mediterranean) and despite an overall good seismic coverage of the MSG, it is still surprisingly poorly imaged today. The main issue is that most legacy data were acquired using narrow azimuth 2D surveys that poorly illuminate the steep salt structures. But using modern methods and tools, we can nonetheless quickly improve the quality of the images of the MSG through a broadband and amplitude preserving strategy (Chapters 2). In this thesis I show that reprocessed images can bring new insights on the MSG and the related MSC, but also on the geodynamics of the Mediterranean Sea (Chapters 2 and 3). Yet very few legacy academic datasets have been optimally reprocessed so far. Even with these new images, there are many aspects about the geodynamics and the salt tectonics that I could not understand because I had access to a very restricted dataset.

I think that we need to find a compromise to collect Mediterranean seismic datasets to further extend the study of salt deformation at the Mediterranean scale. After this work, I wonder what the ways are to enhance the collaboration and the data sharing between at the national and European union scale. I believe there is also some room for collaboration with private actors, an aspect I have neglected because I was relying too much on the cooperation that was planned with ENI. I think these are the gaps to bridge to unlock further comprehension of salt deformation in the Mediterranean Sea.

During this work, I discovered that it was surprisingly difficult to collect the initial raw field data, and that the characteristics of the survey acquisition are often poorly documented. It was also difficult to enrich my dataset with other seismic data, even within my host institute. I have tried to expand the reprocessing work to other seismic datasets such as: the MS data stored at the OGS, the SPIRAL and the MARADJA datasets managed by Geo-Ocean, the B-74 stored at the CNR. However, I did not manage to obtain the authorization or the right contact to obtain or consult the data. To my knowledge, there is no existing public database that draws an exhaustive list of the offshore geoscience data acquired by and within the states of the European Union. There is no agreement within the European states, the private actors, and the public institutes to share the existing data. This highlights the need for a clear shared politic on FAIR data system, ideally making available offshore data at the national and the European Union scales. From my experience, the absence of a data life cycle results in:

- The monopolization of the seismic datasets by individuals, private actors or public institutes.

- The loss or the lack of access to seismic data.

This results in a decreased impact of the conducted studies and a reshuffling of the same studies. The Algerian basin is a good case example to illustrate this. In this work, I only use data acquired by the OGS on the Balearic margin because I simply didn't have access to other datasets. Most published studies in the region are also focused on one or two datasets either owned by the institute or provided by a private or public partner, covering only one of the basin's margins. Bellucci et al., (2021b) managed to centralize the interpretation of several seismic markers, but there is still no existing study that managed to simultaneously exploit all the datasets to unravel the geological settings of the underexplored Algerian basin.

I strongly believe that there is more to win by sharing the data than by keeping inside a sole institution. I hope to contribute to the scientific understanding of the region by sharing the results in open-access, and I hope that other studies will follow that approach.

2 Investigating the parameters explaining the different salt morphologies between the western and the central/eastern Mediterranean

I would have liked to investigate the factors explaining the different morphologies of the MSG between the western and the central/eastern Mediterranean (Section 1.4).

In the western Mediterranean, the MSG deformation in the contractional domains is typically characterized by high amplitude and high frequency intruding diapirism, up to the Plio-Quaternary and sometimes the water bottom. Paradoxically, contractional domains in the eastern Mediterranean display rare and low amplitude truncating diapirism. The strain is partly accommodated internally, and the MSG remains a coherent massive unit, with large salt-cored folds and faulting of the overburden. High frequency and high amplitude diapirism that deeply truncates the overburden, as observed in most of the western Mediterranean, is not observed. The mobile unit of the MSG seems less ductile than in the western Mediterranean.

The forces resisting active diapir rise are the weight and strength of the overburden and the viscosity of the salt (Jackson and Hudec, 2017). The roof thickness in the Gulf of Lions is relatively comparable to the Nile delta (Figure 61). The thickness ratio between the mobile salt and

overburden are contrasting though, the salt being much thicker in the east than in the west. During the Plio-Quaternary, relative sea-level variation did not exceed 200m, so I assume that the deep Mediterranean basins share a common lithology, hence a common strength. However, an important difference between west and east is the presence of the UU. It appears to be an anisotropic unit alternating between brittle clastics and ductile shales deposited during the very early Messinian stage of the salt deformation (Chapter 3 and 3). Anisotropic roof bends easily and forms an anticline when arched. One hypothesis could be that in the Levant, without the UU differential sediment loading, salt deformation remains accommodated internally by the thick salt. After the flooding, the aggrading PQ quickly reached its threshold thickness, inhibiting salt diapir rise. In the west, the UU quickly accumulated over the salt and generated differential sediment loading in addition to the gravity gliding. Because of its anisotropy, the roof easily and rapidly deforms before the flooding, and pre-existing salt structures form. During the Plio-Quaternary, the pre-existing structures are pressurized enough by differential and tectonic loading to arch, rotate aside, and break through their overburden. This early roof difference is surely one parameter to investigate, but I believe that the viscosity of the salt could be a more important controlling parameter to explain this different creeping behaviour.

The viscosity of salt increases with coarser grain size or as temperature falls (van Keken *et al.*, 1993). Studies also showed that the salt flow is highly governed by the presence of the intrasalt beds (section 1.4.1). At the scale of the whole salt unit the dragging against internal reflections may lower the overall viscosity of the unit, impeding the rise of salt diapirs. Alternatively, as suggested by Bellucci et al., (2021a) in the west Mediterranean, the distribution of salt morphologies could be correlated with the crustal segmentation and the differences in temperature between segments. The crustal nature difference and the contrasting heat flows between the west and the east (Figure 62) might influence the rheology of the MSG. The surface heat flows in the Neogenic crust of western Mediterranean (~70 to 150 mW/m2, except for the Gulf of Lions where heat flows go down to 90 mW/m2; Poort *et al.*, 2020) are two times higher than in the one recorded in the Mesozoic crust of the eastern Mediterranean (40 to 50 mW/m2 Jiménez-Munt et al., 2003 and references therein). The creeping behaviour of rock salt depends on its temperature: the viscosity of the rock decreases with temperature and the rock salt becomes less ductile (Carter *et al.*, 1993).
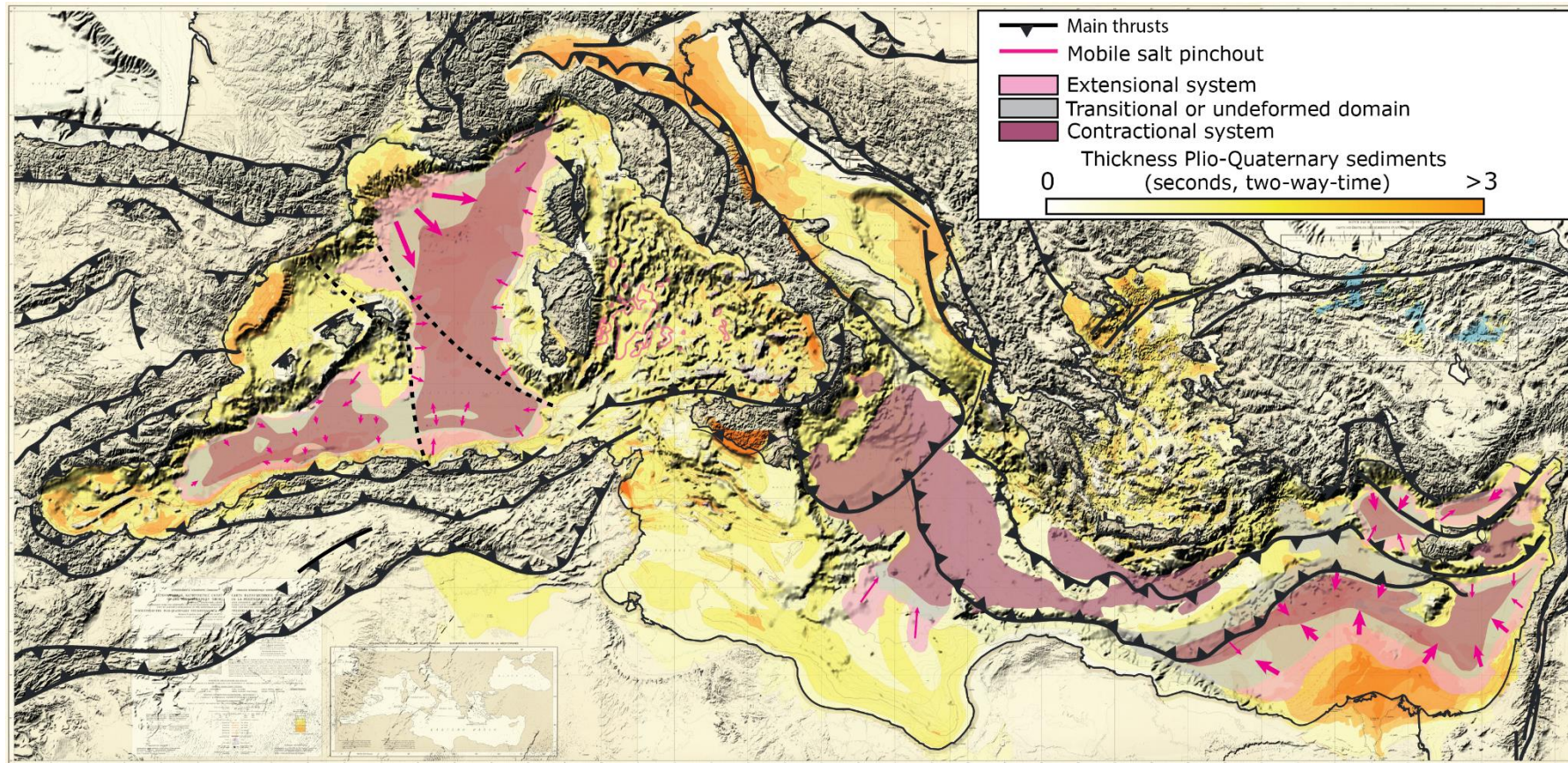
Figure 61 Structural segmentation of the mobile salt and interpreted direction of gravity-driven salt flow overlaid to the Plio-Quaternary thickness maps of the Mediterranean. The size of the arrows indicate a qualitative broad estimation of the amplitude of the flow. The background Plio-Quaternary thickness map is from IBO, (1981).
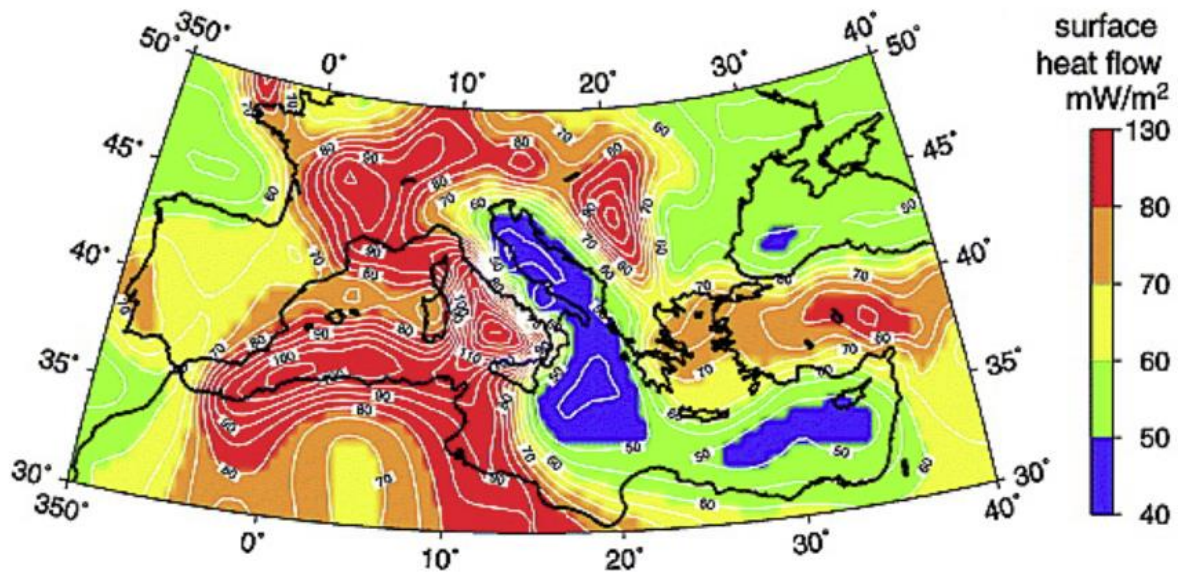
Figure 62 Surface heat flow of the Mediterranean region (mW/m²)(from Jiménez-Munt *et al.*, 2003 and references therein)

One hypothesis could be that the warmer salt in the west is more buoyant and less viscous, thereby facilitating vertical salt flow and diapirism.

Apart from this contrasting style between the west and the east I think there is a lot to understand about the distribution of salt gliding and salt spreading in the western Mediterranean, regarding the base salt relief. I think that the distribution of contractional salt structures is also strongly affected by the available space for salt to flow. Contrary to the Atlantic passive margins or the Gulf of Mexico, the salt flow is confined to an enclosed basin. As suggested by Allen et al. (2016), the extent of the contractional domain in the distal basins could be closely linked to the buttressing effect of the Mediterranean margins. In the Liguro-Provençal basin, for example, the seaward salt flow expulsed by the load of the Rhône cone could be buttressed by the Corso-Sardinia margin (Figure 61). I also wonder if the varying salt/overburden thickness ratio across the Mediterranean could play a role in delimiting the structural domains. The overburden thickness is a primary control on the fold wavelength in contractional domains (Letouzey *et al.*, 1995; Sherkati and Letouzey, 2004; Adam, Ge and Sanchez, 2012; Jackson and Hudec, 2017). The thicker the overburden during shortening, the longer the fold wavelength. A low thickness ratio between salt and overburden will also produce closely spaced tilt blocks dominated by basinward-dipping faults and relatively low salt rollers (Lin, 1992). This could be directly linked to the low aggradation rate on the steep margins, and could explain the

relatively narrow extensional domain of the steep margins with low aggradation rate (Balearic, Sardinia, Corsica).

I could not investigate these problems further with my limited dataset. A study of the distribution of salt structures within the whole Mediterranean is necessary. I think these parameters could also be further investigated analogue and numerical modelling.

Even though the geodynamic evolution of the Algerian basin is not well constrained, its young age and its narrowness (below 100 km at its shortest) implies it would be relatively easy to model in sandboxes, where salt is replaced by silicon. This could be done to try to assess in more detail the strike-slip component of the tectonic settings, an aspect I neglected because of the limited 2D dataset used in this study. Numerical modelling of salt deformation is also another option, but I think that it would require more reliable quantitative estimations of the lateral movement of the salt to constrain the models. The problem is that both would suffer from the lack of a borehole constraint because the salt and the pre-salt of the Algerian foredeep have never been drilled. The lithology and the timing of the tectonic shortening are not well constrained. The analysis of the seismic facies and the velocity models only provide an indirect indication of the lithology of these deposits. Only a well could allow to assess their nature. Should a borehole be drilled, it would be worth drilling until the crust to assess its nature (as early proposed by GOLD project; Rabineau *et al.*, 2015). The oceanic nature of the western Algerian basin is inferred from refraction velocity profiles and the gravity anomaly maps. However, as suggested in this work, there seems to be variations in the crust's nature within the basin, and its oceanic ridge is yet to be found. Hopefully, the seismic reflection and refraction profiles acquired during the METEOR cruises M 69 in 2006 (Grevemeyer, 2006) will also provide new images that could help us constraining the crustal segmentation of the western Algerian basin.

Reference list

Acosta, J. *et al.* (2001) 'Geodynamics of the Emile Baudot Escarpment and the Balearic Promontory, western Mediterranean', *Marine and Petroleum Geology*, 18(3), pp. 349–369. Available at: https://doi.org/10.1016/S0264-8172(01)00003-4.

Acosta, J. *et al.* (2004) 'Early Pleistocene volcanism in the Emile Baudot Seamount, Balearic Promontory (western Mediterranean Sea)', *Marine Geology*, 207(1–4), pp. 247–257.

Acosta, J. *et al.* (2013) 'The morpho-tectonic setting of the Southeast margin of Iberia and the adjacent oceanic Algero-Balearic Basin', *Marine and Petroleum Geology*, 45, pp. 17–41. Available at: https://doi.org/10.1016/j.marpetgeo.2013.04.005.

d'Acremont, E. *et al.* (2020) 'Polyphase Tectonic Evolution of Fore-Arc Basin Related to STEP Fault as Revealed by Seismic Reflection Data From the Alboran Sea (W-Mediterranean)', *Tectonics*, 39(3), p. e2019TC005885. Available at: https://doi.org/10.1029/2019TC005885.

Adam, J., Ge, Z. and Sanchez, M. (2012) 'Salt-structural styles and kinematic evolution of the Jequitinhonha deepwater fold belt, central Brazil passive margin', *Marine and Petroleum Geology*, 37(1), pp. 101–120. Available at: https://doi.org/10.1016/j.marpetgeo.2012.04.010.

Adler, A. (2019) *Neptune's laboratory: Fantasy, fear, and science at sea*. Harvard University Press.

Aksu, A.E. *et al.* (2014) 'The Pliocene-Quaternary tectonic evolution of the Cilicia and Adana Basins, eastern Mediterranean: Special reference to the development of the Kozan Fault zone', *Tectonophysics*, 622. Available at: https://doi.org/10.1016/j.tecto.2014.03.025.

Al-Balushi, A.N. *et al.* (2016) 'The impact of the Messinian salinity crisis on the petroleum system of the Eastern Mediterranean: a critical assessment using 2D petroleum system modelling', *Petroleum Geoscience*, 22(4), pp. 357–379. Available at: https://doi.org/10.1144/petgeo2016-054.

Alhammoud, B., Meijer, P.T. and Dijkstra, H.A. (2010) 'Sensitivity of Mediterranean thermohaline circulation to gateway depth: A model investigation', *Paleoceanography*, 25(2). Available at: https://doi.org/10.1029/2009PA001823.

Ali, E. *et al.* (2022) 'IPCC Sixth Assessment Report (AR6): Climate Change 2022-Impacts, Adaptation and Vulnerability: Cross-Chapter Paper 4:

Mediterranean Region', in *Climate Change 2022: Impacts, Adaptation, and Vulnerability. Contribution of Working Group II to the Sixth Assessment Report of the Intergovernmental Panel on Climate Change*. Cambridge University Press, p. 50. Available at: https://www.ipcc.ch/report/ar6/wg2/.

Allen, H., Jackson, C.A.-L. and Fraser, A.J. (2016) 'Gravity-driven deformation of a youthful saline giant: the interplay between gliding and spreading in the Messinian basins of the Eastern Mediterranean', *Petroleum Geoscience*, 22(4), pp. 340–356. Available at: https://doi.org/10.1144/petgeo2016-034.

Amadori, C. *et al.* (2018) 'Restored topography of the Po Plain-Northern Adriatic region during the Messinian base-level drop—Implications for the physiography and compartmentalization of the palaeo-Mediterranean basin', *Basin Research*, 30(6), pp. 1247–1263. Available at: https://doi.org/10.1111/bre.12302.

Amundsen, L. (1993) 'Wavenumber-based filtering of marine point-source data', *GEOPHYSICS*, 58(9), pp. 1335–1348. Available at: https://doi.org/10.1190/1.1443516.

Amundsen, L. and Zhou, H. (2013) 'Low-frequency seismic deghosting', *GEOPHYSICS*, 78(2), pp. WA15–WA20. Available at: https://doi.org/10.1190/geo2012-0276.1.

Andreetto, F., Aloisi, G., *et al.* (2021) 'Freshening of the Mediterranean Salt Giant: controversies and certainties around the terminal (Upper Gypsum and Lago-Mare) phases of the Messinian Salinity Crisis', *Earth-Science Reviews*, 216, p. 103577. Available at: https://doi.org/10.1016/j.earscirev.2021.103577.

Andreetto, F., Matsubara, K., *et al.* (2021) 'High Mediterranean water-level during the Lago-Mare phase of the Messinian Salinity Crisis: insights from the Sr isotope records of Spanish marginal basins (SE Spain)', *Palaeogeography, Palaeoclimatology, Palaeoecology*, 562, p. 110139. Available at: https://doi.org/10.1016/j.palaeo.2020.110139.

Andresen, K.J. (2012) 'Fluid flow features in hydrocarbon plumbing systems: What do they tell us about the basin evolution?', *Marine Geology*, 332–334, pp. 89–108. Available at: https://doi.org/10.1016/j.margeo.2012.07.006.

Arab, M. *et al.* (2016) 'Coupling stratigraphic and petroleum system modeling tools in complex tectonic domains: case study in the North Algerian Offshore', *Arabian Journal of Geosciences*, 9(4), p. 289. Available at: https://doi.org/10.1007/s12517-015-2296-3.

Araújo, F.V. *et al.* (1994) 'Inverse scattering series for multiple attenuation: An example with surface and internal multiples', in *SEG Technical Program Expanded Abstracts 1994*. Society of Exploration Geophysicists (SEG Technical Program Expanded Abstracts), pp. 1039–1041. Available at: https://doi.org/10.1190/1.1822691.

Auzende, J.M., Bonnin, J. and Olivet, J.L. (1973) 'The origin of the western Mediterranean basin', *Journal of the Geological Society*, 129(6), pp. 607–620. Available at: https://doi.org/10.1144/gsjgs.129.6.0607.

Bache, F. *et al.* (2009) 'Messinian erosional and salinity crises: View from the Provence Basin (Gulf of Lions, Western Mediterranean)', *Earth and Planetary Science Letters*, 286(1–2), pp. 139–157. Available at: https://doi.org/10.1016/j.epsl.2009.06.021.

Bache, F. *et al.* (2012) 'A two-step process for the reflooding of the Mediterranean after the Messinian Salinity Crisis', *Basin Research*, 24(2), pp. 125–153. Available at: https://doi.org/10.1111/j.1365-2117.2011.00521.x.

Badji, R. *et al.* (2015) 'Geophysical evidence for a transform margin offshore Western Algeria: a witness of a subduction-transform edge propagator?', *Geophysical Journal International*, 200(2), pp. 1029–1045. Available at: https://doi.org/10.1093/gji/ggu454.

Baldock, S. *et al.* (2013) 'Increasing the bandwidth of marine seismic data', *Petroleum Exploration Society of Australia New Resources, April/May*, pp. 55–57.

Barrier, E. *et al.* (2004) 'The Geodynamic Map of the Mediterranean'. Paris, France (Commission for the Geological Map of the World,).

Basak, R.L. *et al.* (2012) 'Removal of noises using Tau-P transformation - an indigenous tool for noise attenuation in shallow seismic data', in. Hyderabad: Society of Petroleum Geophysicists, p. 6.

Baysal, E., Kosloff, D.D. and Sherwood, J.W.C. (1983) 'Reverse time migration', *GEOPHYSICS*, 48(11), pp. 1514–1524. Available at: https://doi.org/10.1190/1.1441434.

Beccaluva, L. *et al.* (1977) 'Geochronology and magmatic character of the pliocene-pleistocene volcanism in Sardinia (Italy)', *Bulletin Volcanologique*, 40(3), pp. 153–168. Available at: https://doi.org/10.1007/BF02596997.

Bedenbender, J.W., Johnston, R.C. and Neitzel, E.B. (1970) 'Electroacoustic characteristics of marine seismic streamers',

GEOPHYSICS, 35(6), pp. 1054–1072. Available at: https://doi.org/10.1190/1.1440142.

Bellucci, M., Pellen, R., *et al.* (2021) 'A comprehensive and updated compilation of the seismic stratigraphy markers in the Western Mediterranean Sea'. SEANOE. Available at: https://doi.org/10.17882/80128.

Bellucci, M., Aslanian, D., *et al.* (2021) 'Salt morphologies and crustal segmentation relationship: New insights from the Western Mediterranean Sea', *Earth-Science Reviews*, 222, p. 103818. Available at: https://doi.org/10.1016/j.earscirev.2021.103818.

Ben-Avraham, Z. *et al.* (2006) 'Eastern Mediterranean basin systems', *Geological Society, London, Memoirs*, 32(1), pp. 263–276. Available at: https://doi.org/10.1144/GSL.MEM.2006.032.01.15.

Bernintsas, N., Sun, J. and Sicking, C. (1997) 'Prism Waves - an Explanation for Curved Seismic Horizons Below the Edge of Salt Bodies', ,. cp-131-00214: European Association of Geoscientists & Engineers,. Available at: https://www.earthdoc.org/content/papers/10.3997/2214-4609-pdb.131.GEN1997_E038.

Bertoni, C. and Cartwright, J. (2015) 'Messinian evaporites and fluid flow', *Marine and Petroleum Geology*, 66, pp. 165–176. Available at: https://doi.org/10.1016/j.marpetgeo.2015.02.003.

Bertoni, C., Cartwright, J. and Hermanrud, C. (2013) 'Evidence for large-scale methane venting due to rapid drawdown of sea level during the Messinian Salinity Crisis', *Geology*, 41(3), pp. 371–374. Available at: https://doi.org/10.1130/G33987.1.

Bertoni, C. and Cartwright, J.A. (2006) 'Controls on the basinwide architecture of late Miocene (Messinian) evaporites on the Levant margin (Eastern Mediterranean)', *Sedimentary Geology*, 188–189, pp. 93–114. Available at: https://doi.org/10.1016/j.sedgeo.2006.03.019.

Bickle, M. *et al.* (2011) 'Illuminating Earth's Past, Present and Future The Science Plan for the International Ocean Discovery Program 2013-2023'.

Bigot-Cormier, F. *et al.* (2004) 'Pliocene deformation of the north-Ligurian margin (France): consequences of a south-Alpine crustal thrust', *Bulletin de la Société Géologique de France*, 175(2), pp. 197–211. Available at: https://doi.org/10.2113/175.2.197.

Biju-Duval, B. (1978) 'Structure and evolution of the Mediterranean basins', *Initial Reports of the Deep Sea Drilling Project*. Edited by J. Letouzey et al., 42, p. 951.

Billi, A. *et al.* (2011) 'Recent tectonic reorganization of the Nubia-Eurasia convergent boundary heading for the closure of the western Mediterranean', *Bulletin de la Société Géologique de France*, 182(4), pp. 279–303. Available at: https://doi.org/10.2113/gssgfbull.182.4.279.

Blinova, V.N. *et al.* (2011) 'Active mud volcanism in the West Alboran Basin: Geochemical evidence of hydrocarbon seepage', *Marine and Petroleum Geology - MAR PETROL GEOL*, 28, pp. 1483–1504. Available at: https://doi.org/10.1016/j.marpetgeo.2011.06.001.

Blondel, C. *et al.* (2010) 'Dental mesowear analysis of the late Miocene Bovidae from Toros-Menalla (Chad) and early hominid habitats in Central Africa', *Palaeogeography, Palaeoclimatology, Palaeoecology*, 292(1), pp. 184–191. Available at: https://doi.org/10.1016/j.palaeo.2010.03.042.

Blondel, S. *et al.* (2022) 'Contractional salt deformation in a recently inverted basin: Miocene to current salt deformation within the central Algerian basin', *Basin Research*, 0, pp. 1–23. Available at: https://doi.org/10.1111/bre.12673.

Bonvalot, S. *et al.* (2012) 'World Gravity Map 1:50M'. Available at: https://doi.org/10.14682/2012GRAVISOST.

Booth-Rea, G. *et al.* (2007) 'Crustal types and Tertiary tectonic evolution of the Alborán sea, western Mediterranean', *Geochemistry, Geophysics, Geosystems*, 8(10). Available at: https://onlinelibrary.wiley.com/doi/abs/10.1029/2007GC001639 (Accessed: 5 January 2022).

Bornstein, R. (2018) *Eastern Mediterranean Regional Dynamics: Conflicts and Opportunities for Conflict Resolution Support*. 82.

Boudiaf, A. (1996) *Etude sismotectonique de la région d'Alger et de la Kabylie (Algérie) : utilisation des modèles numériques de terrains (MNT) et de la télédétection pour la reconnaissance des structures tectoniques actives : contribution à l'évaluation de l'aléa sismique*. PhD Thesis. Available at: http://www.theses.fr/1996MON20060.

Bougrine, A., Yelles-Chaouche, A.K. and Calais, E. (2019) 'Active deformation in Algeria from continuous GPS measurements', *Geophysical Journal International*, 217(1), pp. 572–588. Available at: https://doi.org/10.1093/gji/ggz035.

Bouyahiaoui, B. *et al.* (2015) 'Crustal structure of the eastern Algerian continental margin and adjacent deep basin: implications for late Cenozoic geodynamic evolution of the western Mediterranean', *Geophysical Journal International*, 201(3), pp. 1912–1938. Available at: https://doi.org/10.1093/gji/ggv102.

Bowman, S.A. (2012) 'A comprehensive review of the MSC facies and their origins in the offshore Sirt Basin, Libya', *Petroleum Geoscience*, 18(4), pp. 457–469. Available at: https://doi.org/10.1144/petgeo2011-070.

Breda, A. *et al.* (2009) 'Vertically stacked Gilbert-type deltas of Ventimiglia (NW Italy): The Pliocene record of an overfilled Messinian incised valley', *Sedimentary Geology*, 219(1), pp. 58–76. Available at: https://doi.org/10.1016/j.sedgeo.2009.04.010.

Bridge, C. *et al.* (2005) 'Salt tectonics in two convergent-margin basins of the Cyprus arc, Northeastern Mediterranean', *Marine Geology - MAR GEOLOGY*, 221, pp. 223–259. Available at: https://doi.org/10.1016/j.margeo.2005.03.008.

Bulian, F. *et al.* (2021) 'Messinian West Alboran Sea record in the proximity of Gibraltar: Early signs of Atlantic-Mediterranean gateway restriction', *Marine Geology*, 434, p. 106430. Available at: https://doi.org/10.1016/j.margeo.2021.106430.

Bulian, F. *et al.* (2022) 'Impact of the Mediterranean-Atlantic connectivity and the late Miocene carbon shift on deep-sea communities in the Western Alboran Basin', *Palaeogeography, Palaeoclimatology, Palaeoecology*, 589, p. 110841. Available at: https://doi.org/10.1016/j.palaeo.2022.110841.

Burliga, S., Koyi, H.A. and Chemia, Z. (2012) 'Analogue and numerical modelling of salt supply to a diapiric structure rising above an active basement fault', *Geological Society, London, Special Publications*, 363(1), pp. 395–408.

Burollet, P.F., Said, A. and Trouve, P. (1978) 'Slim holes drilled on the Algerian Shelf', *Initial Reports of the Deep Sea Drilling Project*. Edited by editor Usher J.L. and P. Supko, 42, p. 1181.

Busson, G. (1990) 'The Messinian of the Mediterranean... twenty years later', *Geologie de la France*, 3–4, pp. 3–58.

Camerlenghi, A. *et al.* (1995) 'Geophysical evidence of mud diapirism on the Mediterranean Ridge accretionary complex', *Marine Geophysical Researches*, 17(2), pp. 115–141. Available at: https://doi.org/10.1007/BF01203423.

Camerlenghi, A. *et al.* (2009) 'Morphogenesis of the SW Balearic continental slope and adjacent abyssal plain, Western Mediterranean Sea', *International Journal of Earth Sciences*, 98(4), pp. 735–750. Available at: https://doi.org/10.1007/s00531-008-0354-8.

Camerlenghi, A. *et al.* (2014) *Uncovering a Salt Giant: Umbrella proposal of the multi-phase drilling project (MDP*. IODP Proposal 857-MDP2, p. 2. Available at: https://docs.iodp.org/Proposal_Cover_Sheets/857-MDP2_Camerlenghi_cover.pdf.

Camerlenghi, A. *et al.* (2018) '2- Algero-Balearic basin', in *Seismic Atlas of the Messinian Salinity Crisis Markers in the Mediterranean Sea, Vol. 2*. Mem. Soc. géol. fr., n.s., 2018, t. 181, and Commission for the Geological Map of the World, pp. 14–17. Available at: https://ccgm.org/en/home/193-seismic-atlas-of-the-messinian-salinity-crisis-markers-in-the-mediterranean-sea-vol-2-9782917310373.html (Accessed: 6 December 2019).

Camerlenghi, A. *et al.* (2020) 'Seismic markers of the Messinian salinity crisis in the deep Ionian Basin', *Basin Research*, 32(4), pp. 716–738. Available at: https://doi.org/10.1111/bre.12392.

Camerlenghi, A. and Aloisi, V. (2019) 'Uncovering the Mediterranean Salt Giant (MEDSALT) - Scientific Networking as Incubator of Cross-disciplinary Research in Earth Sciences', *European Review*, pp. 1–22. Available at: https://doi.org/10.1017/S1062798719000255.

Camerlenghi, A. and Pini, G.A. (2009) 'Mud volcanoes, olistostromes and Argille scagliose in the Mediterranean region', *Sedimentology*, 56(1), pp. 319–365. Available at: https://doi.org/10.1111/j.1365-3091.2008.01016.x.

Capella, W. *et al.* (2018) 'Palaeogeographic evolution of the late Miocene Rifian Corridor (Morocco): Reconstructions from surface and subsurface data', *Earth-Science Reviews*, 180, pp. 37–59. Available at: https://doi.org/10.1016/j.earscirev.2018.02.017.

Capella, W. *et al.* (2020) 'Mantle resistance against Gibraltar slab dragging as a key cause of the Messinian Salinity Crisis', *Terra Nova*, 32(2), pp. 141–150. Available at: https://doi.org/10.1111/ter.12442.

Carminati, E. *et al.* (1998) 'The role of slab detachment processes in the opening of the western–central Mediterranean basins: some geological and geophysical evidence', *Earth and Planetary Science Letters*, 160(3), pp. 651–665. Available at: https://doi.org/10.1016/S0012-821X(98)00118-6.

Carminati, E., Lustrino, M. and Doglioni, C. (2012) 'Geodynamic evolution of the central and western Mediterranean: Tectonics vs. igneous petrology constraints', *Tectonophysics*, 579, pp. 173–192. Available at: https://doi.org/10.1016/j.tecto.2012.01.026.

Carter, N.L. *et al.* (1993) 'Rheology of rocksalt', *Journal of Structural Geology*, 15(9), pp. 1257–1271. Available at: https://doi.org/10.1016/0191-8141(93)90168-A.

Cartwright, J. *et al.* (2012) 'Strain partitioning in gravity-driven shortening of a thick, multilayered evaporite sequence'. Available at: https://doi.org/10.1144/SP363.21.

Cartwright, J. *et al.* (2018) 'Direct calibration of salt sheet kinematics during gravity-driven deformation', *Geology*, 46(7), pp. 623–626. Available at: https://doi.org/10.1130/G40219.1.

Cartwright, J.A. and Jackson, M.P.A. (2008) 'Initiation of gravitational collapse of an evaporite basin margin: The Messinian saline giant, Levant Basin, eastern Mediterranean', *GSA Bulletin*, 120(3–4), pp. 399–413. Available at: https://doi.org/10.1130/B26081X.1.

Caruso, A. *et al.* (2020) 'The late Messinian "Lago-Mare" event and the Zanclean Reflooding in the Mediterranean Sea: New insights from the Cuevas del Almanzora section (Vera Basin, South-Eastern Spain)', *Earth-Science Reviews*, 200, p. 102993. Available at: https://doi.org/10.1016/j.earscirev.2019.102993.

Catalano, R., Doglioni, C. and Merlini, S. (2001) 'On the Mesozoic Ionian Basin', *Geophysical Journal International*, 144(1), pp. 49–64. Available at: https://doi.org/10.1046/j.0956-540X.2000.01287.x.

Cavalca, M. and Lailly, P. (2005) 'Prismatic reflections for the delineation of salt bodies', in *SEG Technical Program Expanded Abstracts 2005*. Society of Exploration Geophysicists (SEG Technical Program Expanded Abstracts), pp. 2550–2553. Available at: https://doi.org/10.1190/1.2148243.

Charlou, J.L. *et al.* (2003) 'Evidence of methane venting and geochemistry of brines on mud volcanoes of the eastern Mediterranean Sea', *Deep-Sea Research Part I: Oceanographic Research Papers*, 50(8), pp. 941–958. Available at: https://doi.org/10.1016/S0967-0637(03)00093-1.

Chaumillon, E. *et al.* (1994) 'Réactivation tectonique et flexure de la marge continentale Ligure (Méditerranée Occidentale)', *Comptes Rendus de l'Académie des sciences Série 2-Mécanique-physique, Chimie, Sciences de l'univers, Sciences de la Terre*, 319, pp. 675–682.

Chertova, M.V. *et al.* (2014) 'Underpinning tectonic reconstructions of the western Mediterranean region with dynamic slab evolution from 3-D numerical modeling', *Journal of Geophysical Research: Solid Earth*, 119(7), pp. 5876–5902. Available at: https://doi.org/10.1002/2014JB011150.

Chopra, S. and Marfurt, K.J. (2007) *Seismic attributes for prospect identification and reservoir characterization*. SEG Books.

Chuan, S.C. *et al.* (2014) 'Step change enhancement of legacy 2D seismic data, an enabler for understanding basin architecture and identifying overlooked exploration potential', in, pp. 3406–3413.

CIESM, C. (2008) 'The Messinian Salinity Crisis from mega-deposits to microbiology–a consensus report', in *CIESM Workshop monographs*. Ciesm Monaco, pp. 1–168.

Civile, D. *et al.* (2021) 'Morphostructural Setting and Tectonic Evolution of the Central Part of the Sicilian Channel (Central Mediterranean)', *Lithosphere*, 2021(1), p. 7866771. Available at: https://doi.org/10.2113/2021/7866771.

Cobbold, P., Rossello, Eduard. and Vendeville, Brun. (1989) 'Some experiments on interacting sedimentation and deformation above salt horizons', *Bulletin de la Société Géologique de France*, (3), pp. 453–460.

Comas, M.C. *et al.* (1996) 'Site 975', *Proceedings of the Ocean Drilling Program, Part A: Initial Reports*. Edited by M.C. Comas et al., 161, p. 113.

Costa, A.M. *et al.* (2010) 'Geomechanics Applied to the Well Design Through Salt Layers In Brazil:A History of Success', in. OnePetro. Available at: https://onepetro.org/ARMAUSRMS/proceedings/ARMA10/All-ARMA10/ARMA-10-239/119468 (Accessed: 28 May 2022).

Costa, P.V.M. *et al.* (2015) 'Computer Modeling Applied in the Design of Underground Salt Caverns Opened by Solution Mining for Gas Storage', in. OnePetro. Available at: https://onepetro.org/ARMAUSRMS/proceedings/ARMA15/All-ARMA15/ARMA-2015-393/65837 (Accessed: 28 May 2022).

Costa, P.V.M. da *et al.* (2020) 'Parametric study and geomechanical design of Ultra-deep-water Offshore Salt Caverns for Carbon Capture and Storage in Brazil', *International Journal of Rock Mechanics and Mining Sciences*, 131, p. 104354. Available at: https://doi.org/10.1016/j.ijrmms.2020.104354.

Cozzi, A. *et al.* (2021) 'Chapter 14: Zohr Giant Gas Discovery—A Paradigm Shift in Nile Delta and East Mediterranean Exploration', pp. 405–431. Available at: https://doi.org/10.1306/13742365MGF.14.3881.

Cramer, W. *et al.* (2018) 'Climate change and interconnected risks to sustainable development in the Mediterranean', *Nature Climate Change*, 8(11), pp. 972–980. Available at: https://doi.org/10.1038/s41558-018-0299-2.

Cramer, W. *et al.* (2020) 'Climate and environmental change in the mediterranean basin–current situation and risks for the future', *First Mediterranean Assessment Report. MedECC (Mediterranean Experts on Climate and Environmental Change). Union for the Mediterranean, Plan Bleu, UNEP/MAP, Marseille, France* [Preprint].

Cumberpatch, Z.A. *et al.* (2021) 'Evolution of a mixed siliciclastic-carbonate deep-marine system on an unstable margin: The Cretaceous of the Eastern Greater Caucasus, Azerbaijan', *Basin Research*, 33(1), pp. 612–647. Available at: https://doi.org/10.1111/bre.12488.

Dal Cin, M. *et al.* (2016) 'Seismic imaging of Late Miocene (Messinian) evaporites from Western Mediterranean back-arc basins', *Petroleum Geoscience*, 22(4), pp. 297–308. Available at: https://doi.org/10.1144/petgeo2015-096.

Dale, M.S. *et al.* (2021) 'The Messinian Salinity Crisis as a trigger for high pore pressure development in the Western Mediterranean', *Basin Research*, n/a(n/a). Available at: https://doi.org/10.1111/bre.12554.

Dannowski, A. *et al.* (2020) 'Seismic evidence for failed rifting in the Ligurian Basin, Western Alpine domain', *Solid Earth*, 11(3), pp. 873–887. Available at: https://doi.org/10.5194/se-11-873-2020.

Davis, D.M. and Engelder, T. (1985) 'The role of salt in fold-and-thrust belts', *Tectonophysics*, 119(1), pp. 67–88. Available at: https://doi.org/10.1016/0040-1951(85)90033-2.

Davison, C.M. and Poole, G. (2015) 'Far-field Source Signature Reconstruction Using Direct Arrival Data', in. Madrid, Spain: European Association of Geoscientists &Engineers. Available at: https://doi.org/10.3997/2214-4609.201413326.

Davison, I., Anderson, L. and Nuttall, P. (2012) 'Salt deposition, loading and gravity drainage in the Campos and Santos salt basins', *Geological Society, London, Special Publications*, 363(1), pp. 159–174. Available at: https://doi.org/10.1144/SP363.8.

Day, A. *et al.* (2013) 'Wavefield-separation methods for dual-sensor towed-streamer data', *GEOPHYSICS*, 78(2), pp. WA55–WA70. Available at: https://doi.org/10.1190/geo2012-0302.1.

Del Ben, A. *et al.* (2018) '9- Western Sardinia', in *Seismic Atlas of the Messinian Salinity Crisis Markers in the Mediterranean Sea, Vol. 2 - CCGM - CGMW*. Mem. Soc. géol. fr., n.s., 2018, t. 181, and Commission for the Geological Map of the World. Available at: https://ccgm.org/en/home/193-seismic-atlas-of-the-messinian-salinity-crisis-markers-in-the-mediterranean-sea-vol-2-9782917310373.html (Accessed: 6 December 2019).

Del Ben, A., Barnaba, C. and Taboga, A. (2008) 'Strike-slip systems as the main tectonic features in the Plio-Quaternary kinematics of the Calabrian Arc', *Marine Geophysical Researches*, 29(1), pp. 1–12. Available at: https://doi.org/10.1007/s11001-007-9041-6.

Dellong, D. *et al.* (2018) 'Crustal Structure of the Ionian Basin and Eastern Sicily Margin: Results From a Wide-Angle Seismic Survey', *Journal of Geophysical Research: Solid Earth*, 123(3), pp. 2090–2114. Available at: https://doi.org/10.1002/2017JB015312.

Demercian, S., Szatmari, P. and Cobbold, P.R. (1993) 'Style and pattern of salt diapirs due to thin-skinned gravitational gliding, Campos and Santos basins, offshore Brazil', *Tectonophysics*, 228(3), pp. 393–433. Available at: https://doi.org/10.1016/0040-1951(93)90351-J.

DeMets, C., Iaffaldano, G. and Merkouriev, S. (2015) 'High-resolution Neogene and Quaternary estimates of Nubia-Eurasia-North America Plate motion', *Geophysical Journal International*, 203(1), pp. 416–427. Available at: https://doi.org/10.1093/gji/ggv277.

Denisov, M., Egorov, A. and Burtsev, A. (2018) 'A method for deghosting of data recorded with a streamer of arbitrary shape in rough sea conditions', *Geophysical Prospecting*. European Association of Geoscientists & Engineers. Available at: https://doi.org/10.1111/1365-2478.12694.

Desbrandes, R. (1994) 'Chapter 11 Relief Well Engineering to Control Blowouts', in W.H. Fertl†, R.E. Chapman, and R.F. Hotz (eds) *Developments in Petroleum Science*. Elsevier (Studies in Abnormal Pressures), pp. 319–341. Available at: https://doi.org/10.1016/S0376-7361(09)70235-3.

Déverchère, J. *et al.* (2005) 'Active thrust faulting offshore Boumerdes, Algeria, and its relations to the 2003 Mw 6.9 earthquake', *Geophysical*

Research Letters, 32(4). Available at: https://doi.org/10.1029/2004GL021646.

Dewey, J.F. *et al.* (1973) 'Plate Tectonics and the Evolution of the Alpine System', *GSA Bulletin*, 84(10), pp. 3137–3180. Available at: https://doi.org/10.1130/0016-7606(1973)84<3137:PTATEO>2.0.CO;2.

Diegel, F.A. *et al.* (1995) 'Cenozoic structural evolution and tectono-stratigraphic framework of the northern Gulf Coast continental margin'.

van Dijk, J.P. and Scheepers, P.J.J. (1995) 'Neotectonic rotations in the Calabrian Arc; implications for a Pliocene-Recent geodynamic scenario for the Central Mediterranean', *Earth-Science Reviews*, 39(3), pp. 207–246. Available at: https://doi.org/10.1016/0012-8252(95)00009-7.

Dimitrov, L.I. (2002) 'Mud volcanoes—the most important pathway for degassing deeply buried sediments', *Earth-Science Reviews*, 59(1), pp. 49–76. Available at: https://doi.org/10.1016/S0012-8252(02)00069-7.

Diviacco, P. *et al.* (2015) 'Data rescue to extend the value of vintage seismic data: The OGS-SNAP experience', *GeoResJ*, 6, pp. 44–52. Available at: https://doi.org/10.1016/j.grj.2015.01.006.

Dix, C.H. (1955) 'Seismic velocities from surface measurements', *GEOPHYSICS*, 20(1), pp. 68–86. Available at: https://doi.org/10.1190/1.1438126.

Domzig, A. *et al.* (2006) 'Searching for the Africa–Eurasia Miocene boundary offshore western Algeria (MARADJA'03 cruise)', *Comptes Rendus Geoscience*, 338(1), pp. 80–91. Available at: https://doi.org/10.1016/j.crte.2005.11.009.

Dondurur, D. (2018) *Acquisition and Processing of Marine Seismic Data*. Elsevier. Available at: https://doi.org/10.1016/B978-0-12-811490-2.00009-8.

Dooley, T.P. *et al.* (2017) 'The effects of base-salt relief on salt flow and suprasalt deformation patterns - Part 1: Flow across simple steps in the base of salt', *Interpretation*, 5(1), pp. SD1–SD23. Available at: https://doi.org/10.1190/INT-2016-0087.1.

Dooley, T.P., Jackson, M.P.A. and Hudec, M.R. (2009) 'Inflation and deflation of deeply buried salt stocks during lateral shortening', *Journal of Structural Geology*, 31(6), pp. 582–600. Available at: https://doi.org/10.1016/j.jsg.2009.03.013.

Driussi, O. *et al.* (2015) 'Messinian Salinity Crisis deposits widespread over the Balearic Promontory: Insights from new high-resolution seismic

data', *Marine and Petroleum Geology*, 66, pp. 41–54. Available at: https://doi.org/10.1016/j.marpetgeo.2014.09.008.

Driussi, O., Briais, A. and Maillard, A. (2015) 'Evidence for transform motion along the South Balearic margin and implications for the kinematics of opening of the Algerian basin', *Bulletin de la Société Géologique de France*, 186(4–5), pp. 353–370. Available at: https://doi.org/10.2113/gssgfbull.186.4-5.353.

Ducros, M. and Nader, F.H. (2020) 'Map-based uncertainty analysis for exploration using basin modeling and machine learning techniques applied to the Levant Basin petroleum systems, Eastern Mediterranean', *Marine and Petroleum Geology*, 120, p. 104560. Available at: https://doi.org/10.1016/j.marpetgeo.2020.104560.

Duffy, O.B. *et al.* (2018) 'Structural evolution of salt-influenced fold-and-thrust belts: A synthesis and new insights from basins containing isolated salt diapirs', *Journal of Structural Geology*, 114, pp. 206–221. Available at: https://doi.org/10.1016/j.jsg.2018.06.024.

Dusseault, M.B. *et al.* (2004a) 'Drilling Around Salt: Risks, Stresses, And Uncertainties', in. OnePetro. Available at: https://onepetro.org/ARMANARMS/proceedings/ARMA04/All-ARMA04/ARMA-04-647/117698 (Accessed: 16 September 2021).

Dusseault, M.B. *et al.* (2004b) 'Drilling Through Salt: Constitutive Behavior And Drilling Strategies', in, p. ARMA-04-608.

Edwards, E.J. *et al.* (2010) 'The Origins of C4 Grasslands: Integrating Evolutionary and Ecosystem Science', *Science*, 328(5978), pp. 587–591. Available at: https://doi.org/10.1126/science.1177216.

Eruteya, O.E. *et al.* (2015) 'Intra- to post-Messinian deep-water gas piping in the Levant Basin, SE Mediterranean', *Marine and Petroleum Geology*, 66, pp. 246–261. Available at: https://doi.org/10.1016/j.marpetgeo.2015.03.007.

Etheve, N. *et al.* (2016) 'Extensional vs contractional Cenozoic deformation in Ibiza (Balearic Promontory, Spain): Integration in the West Mediterranean back-arc setting', *Tectonophysics*, 682, pp. 35–55. Available at: https://doi.org/10.1016/j.tecto.2016.05.037.

EUROPEAN COMMISSION Research Executive Agency (2017) *Grant Agreement Number: 765256 - SALTGIANT - H2020-MSCA-ITN-2017*, p. 166.

Evans, S.L. and Jackson, C.A.-L. (2021) 'Intra-salt structure and strain partitioning in layered evaporites: implications for drilling through Messinian salt in the eastern Mediterranean', *Petroleum Geoscience*, 27(4), pp. petgeo2020-072. Available at: https://doi.org/10.1144/petgeo2020-072.

Evans, S.L., Jackson, C.A.-L. and Oppo, D. (2021) 'Taking the Pulse of Salt-Detached Gravity Gliding in the Eastern Mediterranean', *Tectonics*, 40(7), p. e2020TC006476. Available at: https://doi.org/10.1029/2020TC006476.

Faccenna, C. *et al.* (2001) 'History of subduction and back-arc extension in the Central Mediterranean', *Geophysical Journal International*, 145(3), pp. 809–820. Available at: https://doi.org/10.1046/j.0956-540x.2001.01435.x.

Faccenna, C. *et al.* (2004) 'Lateral slab deformation and the origin of the western Mediterranean arcs', *Tectonics*, 23(1). Available at: https://doi.org/10.1029/2002TC001488.

Faccenna, C. *et al.* (2014) 'Mantle dynamics in the Mediterranean: MEDITERRANEAN DYNAMIC', *Reviews of Geophysics*, 52(3), pp. 283–332. Available at: https://doi.org/10.1002/2013RG000444.

Farmer, P. *et al.* (1996) 'Exploring the subsalt', *Oilfield Review*, 8. Available at: https://www.osti.gov/etdeweb/biblio/420133 (Accessed: 16 September 2021).

Fauquette, S. *et al.* (2006) 'How much did climate force the Messinian salinity crisis? Quantified climatic conditions from pollen records in the Mediterranean region', *Palaeogeography, Palaeoclimatology, Palaeoecology*, 238(1), pp. 281–301. Available at: https://doi.org/10.1016/j.palaeo.2006.03.029.

Feng, Y., Steinberg, J. and Reshef, M. (2017) 'Intra-salt deformation: Implications for the evolution of the Messinian evaporites in the Levant Basin, eastern Mediterranean', *Marine and Petroleum Geology*, 88, pp. 251–267. Available at: https://doi.org/10.1016/j.marpetgeo.2017.08.027.

Feng, Y.E. *et al.* (2016) 'Lithology and characteristics of the Messinian evaporite sequence of the deep Levant Basin, eastern Mediterranean', *Marine Geology*, 376, pp. 118–131. Available at: https://doi.org/10.1016/j.margeo.2016.04.004.

Feng, Y.E. and Reshef, M. (2016) 'The Eastern Mediterranean Messinian salt-depth imaging and velocity analysis considerations', *Petroleum*

Geoscience, 22(4), pp. 333–339. Available at: https://doi.org/10.1144/petgeo2015-088.

Fernandez, N. *et al.* (2019) 'The competition for salt and kinematic interactions between minibasins during density-driven subsidence: observations from numerical models', *Petroleum Geoscience*, 26(1), pp. 3–15. Available at: https://doi.org/10.1144/petgeo2019-051.

Ferrer, O. *et al.* (2017) 'Modeling the interaction between presalt seamounts and gravitational failure in salt-bearing passive margins: The Messinian case in the northwestern Mediterranean Basin', *Interpretation*, 5(1), pp. SD99–SD117. Available at: https://doi.org/10.1190/INT-2016-0096.1.

Fiduk, J.C. and Rowan, M.G. (2012) 'Analysis of folding and deformation within layered evaporites in Blocks BM-S-8 & -9, Santos Basin, Brazil'. Available at: https://doi.org/10.1144/SP363.22.

Finetti, I. *et al.* (2005) 'Review of the main results of the pioneering MS seismic exploration programme in the deep water of the Mediterranean Sea (OGS, 1969–1980)', *CROP project, deep seismic exploration of the central mediterranean and Italy*, pp. 1–30.

Finetti, I. and Morelli, C. (1972) 'Wide scale digital seismic exploration of the Mediterranean Sea', *BOLLETTINO DI GEOFISICA TEORICA E APPLICATA*, 14(56), pp. 291–342.

Flecker, R. *et al.* (2015) 'Evolution of the Late Miocene Mediterranean–Atlantic gateways and their impact on regional and global environmental change', *Earth-Science Reviews*, 150, pp. 365–392. Available at: https://doi.org/10.1016/j.earscirev.2015.08.007.

Flecker, R. and Ellam, R. (2006) 'Identifying Late Miocene episodes of connection and isolation in the Mediterranean-Paratethyan realm using Sr isotopes', *Sedimentary Geology*, 188, pp. 189–203. Available at: https://doi.org/10.1016/j.sedgeo.2006.03.005.

Flinch, J. F. and Soto, J. I. (2017) 'Chapter 19 - Allochthonous Triassic and Salt Tectonic Processes in the Betic-Rif Orogenic Arc', in Juan I. Soto, Joan F. Flinch, and G. Tari (eds) *Permo-Triassic Salt Provinces of Europe, North Africa and the Atlantic Margins*. Elsevier, pp. 417–446. Available at: https://doi.org/10.1016/B978-0-12-809417-4.00020-3.

Fort, X., Brun, J.-P. and Chauvel, F. (2004) 'Salt tectonics on the Angolan margin, synsedimentary deformation processes', *AAPG Bulletin*, 88(11), pp. 1523–1544. Available at: https://doi.org/10.1306/06010403012.

Fortuin, A.R. and Krijgsman, W. (2003) 'The Messinian of the Nijar Basin (SE Spain): sedimentation, depositional environments and paleogeographic evolution', *Sedimentary Geology*, 160(1), pp. 213–242. Available at: https://doi.org/10.1016/S0037-0738(02)00377-9.

Fossen, H. (2016) *Structural Geology*. Cambridge University Press.

Frizon de Lamotte, D. *et al.* (2000) 'The two main steps of the Atlas building and geodynamics of the western Mediterranean', *Tectonics*, 19(4), pp. 740–761. Available at: https://doi.org/10.1029/2000TC900003.

Futterman, W.I. (1962) 'Dispersive body waves', *Journal of Geophysical Research (1896-1977)*, 67(13), pp. 5279–5291. Available at: https://doi.org/10.1029/JZ067i013p05279.

Gallais, F. *et al.* (2013) 'Propagation of a lithospheric tear fault (STEP) through the western boundary of the Calabrian accretionary wedge offshore eastern Sicily (Southern Italy)', *Tectonophysics*, 602, pp. 141–152. Available at: https://doi.org/10.1016/j.tecto.2012.12.026.

García, M. *et al.* (2011) 'The Catalan margin during the Messinian Salinity Crisis: Physiography, morphology and sedimentary record', *Marine Geology*, 284(1–4), pp. 158–174. Available at: https://doi.org/10.1016/j.margeo.2011.03.017.

Garcia-Castellanos, D. *et al.* (2009) 'Catastrophic flood of the Mediterranean after the Messinian salinity crisis', *Nature*, 462(7274), pp. 778–781. Available at: https://doi.org/10.1038/nature08555.

Garcia-Castellanos, D. *et al.* (2020) 'The Zanclean megaflood of the Mediterranean – Searching for independent evidence', *Earth-Science Reviews*, 201, p. 103061. Available at: https://doi.org/10.1016/j.earscirev.2019.103061.

Garcia-Castellanos, D. and Villaseñor, A. (2011) 'Messinian salinity crisis regulated by competing tectonics and erosion at the Gibraltar arc', *Nature*, 480(7377), pp. 359–363. Available at: https://doi.org/10.1038/nature10651.

Gaudin, M. *et al.* (2006) 'Massive sand beds attributed to deposition by dense water cascades in the Bourcart canyon head, Gulf of Lions (northwestern Mediterranean Sea)', *Marine Geology*, 234(1–4), pp. 111–128. Available at: https://doi.org/10.1016/j.margeo.2006.09.020.

Gaullier, V. *et al.* (2000) 'Salt tectonics in and around the Nile deep-sea fan: Insights from the PRISMED II cruise', *Geological Society Special*

Publication, 174, pp. 111–129. Available at: https://doi.org/10.1144/GSL.SP.1999.174.01.07.

Ge, H., Jackson, M.P.A. and Vendeville, B.C. (1997) 'Kinematics and dynamics of salt tectonics driven by progradation', *AAPG Bulletin*, 81(3), pp. 398–423.

Ge, Z. *et al.* (2019) 'Overprinting translational domains in passive margin salt basins: insights from analogue modelling', *Solid Earth*, 10(4), pp. 1283–1300. Available at: https://doi.org/10.5194/se-10-1283-2019.

Geletti, R. *et al.* (2014) 'The Messinian Salinity Crisis: New seismic evidence in the West-Sardinian Margin and Eastern Sardo-Provençal basin (West Mediterranean Sea)', *Marine Geology*, 351, pp. 76–90. Available at: https://doi.org/10.1016/j.margeo.2014.03.019.

Giles, K.A. and Rowan, M.G. (2012) 'Concepts in halokinetic-sequence deformation and stratigraphy', *Geological Society Special Publication*, 363(1), pp. 7–31. Available at: https://doi.org/10.1144/SP363.2.

Goldberg, D.S., Takahashi, T. and Slagle, A.L. (2008) 'Carbon dioxide sequestration in deep-sea basalt', *Proceedings of the National Academy of Sciences*, 105(29), pp. 9920–9925.

Gorini, C. *et al.* (2005) 'The Late Messinian salinity crisis and Late Miocene tectonism: Interaction and consequences on the physiography and post-rift evolution of the Gulf of Lions margin', *Marine and Petroleum Geology*, 22(6–7), pp. 695–712. Available at: https://doi.org/10.1016/j.marpetgeo.2005.03.012.

Gorini, C., Le Marrec, A. and Mauffret, A. (1993) 'Contribution to the structural and sedimentary history of the Gulf of Lions (western Mediterranean) from the ECORS profiles, industrial seismic profiles and well data', *Bulletin de la Société Géologique de France*, 164(3), pp. 353–363.

Gorini, C., Montadert, L. and Rabineau, M. (2015) 'New imaging of the salinity crisis: Dual Messinian lowstand megasequences recorded in the deep basin of both the eastern and western Mediterranean', *Marine and Petroleum Geology*, 66, pp. 278–294. Available at: https://doi.org/10.1016/j.marpetgeo.2015.01.009.

Goulart, M.B.R. *et al.* (2020) 'Technology readiness assessment of ultra-deep salt caverns for carbon capture and storage in Brazil', *International Journal of Greenhouse Gas Control*, 99, p. 103083. Available at: https://doi.org/10.1016/j.ijggc.2020.103083.

Govers, R. and Wortel, M.J.R. (2005) 'Lithosphere tearing at STEP faults: response to edges of subduction zones', *Earth and Planetary Science Letters*, 236(1), pp. 505–523. Available at: https://doi.org/10.1016/j.epsl.2005.03.022.

Graber, K.K. (2006) *Guidelines for site survey and safety*. ODP Tech. Note 32. Available at: http://www-odp.tamu.edu/ publications/tnotes/tn32/.

Gradmann, S. *et al.* (2005) 'Salt tectonics off northern Israel', *Marine and Petroleum Geology*, 22(5), pp. 597–611. Available at: https://doi.org/10.1016/j.marpetgeo.2005.02.001.

Graham, R. *et al.* (2019) 'Allochthonous Salt in the Fold and Thrust Belt of Haute Provence, S.W.Alps', 2019(1), pp. 1–5. Available at: https://doi.org/10.3997/2214-4609.201901289.

Granado, P. *et al.* (2018) 'Structural styles in fold-and-thrust belts involving early salt structures: The Northern Calcareous Alps (Austria)', *Geology*, 47(1), pp. 51–54. Available at: https://doi.org/10.1130/G45281.1.

Grevemeyer, I. (2006) 'Short Cruise Report RV METEOR: Cruise M69/2 Cartagena, Spain to Valletta, Malta August 31 to September 20, 2006'.

Grothe, A. *et al.* (2020) 'Paratethys pacing of the Messinian Salinity Crisis: Low salinity waters contributing to gypsum precipitation?', *Earth and Planetary Science Letters*, 532, p. 116029. Available at: https://doi.org/10.1016/j.epsl.2019.116029.

Gueguen, E., Doglioni, C. and Fernandez, M. (1998) 'On the post-25 Ma geodynamic evolution of the western Mediterranean', *Tectonophysics*, 298(1), pp. 259–269. Available at: https://doi.org/10.1016/S0040-1951(98)00189-9.

Guennoc, P. *et al.* (1998) 'Les marges ouest et nord de la Corse: nouvelle cartographie a 1/250 000', *Réunion des sciences de la terre* [Preprint].

Güneş, P., Aksu, A.E. and Hall, J. (2018) 'Structural framework and deformation history of the western Cyprus Arc', *Tectonophysics*, 744, pp. 438–457. Available at: https://doi.org/10.1016/j.tecto.2018.07.023.

Gutscher, M.-A. *et al.* (2016) 'Tectonic expression of an active slab tear from high-resolution seismic and bathymetric data offshore Sicily (Ionian Sea): SLAB TEAR OFFSHORE SICILY', *Tectonics*, 35(1), pp. 39–54. Available at: https://doi.org/10.1002/2015TC003898.

Gutscher, M.-A. *et al.* (2017) 'Active tectonics of the Calabrian subduction revealed by new multi-beam bathymetric data and high-resolution seismic

profiles in the Ionian Sea (Central Mediterranean)', *Earth and Planetary Science Letters*, 461, pp. 61–72. Available at: https://doi.org/10.1016/j.epsl.2016.12.020.

Gvirtzman, Z. *et al.* (2013) 'Intense salt deformation in the Levant Basin in the middle of the Messinian Salinity Crisis', *Earth and Planetary Science Letters*, 379, pp. 108–119. Available at: https://doi.org/10.1016/j.epsl.2013.07.018.

Gvirtzman, Z. *et al.* (2017) 'Intra-Messinian truncation surface in the Levant Basin explained by subaqueous dissolution', *Geology*, 45(10), pp. 915–918. Available at: https://doi.org/10.1130/G39113.1.

Haidar, S. *et al.* (2022) 'Back-Arc Dynamics Controlled by Slab Rollback and Tearing: A Reappraisal of Seafloor Spreading and Kinematic Evolution of the Eastern Algero-Balearic Basin (Western Mediterranean) in the Middle-Late Miocene', *Tectonics*, 41(2), p. e2021TC006877. Available at: https://doi.org/10.1029/2021TC006877.

Hale, D., Hill, N.R. and Stefani, J. (1992) 'Imaging salt with turning seismic waves', *GEOPHYSICS*, 57(11), pp. 1453–1462. Available at: https://doi.org/10.1190/1.1443213.

Hall, J. *et al.* (2005) 'Structural evolution of the Latakia Ridge and Cyprus Basin at the front of the Cyprus Arc, Eastern Mediterranean Sea', *Marine Geology*, 221(1), pp. 261–297. Available at: https://doi.org/10.1016/j.margeo.2005.03.007.

Hamai, L. *et al.* (2018) 'Towards subduction inception along the inverted North African margin of Algeria? Insights from thermo-mechanical models', *Earth and Planetary Science Letters*, 501, pp. 13–23. Available at: https://doi.org/10.1016/j.epsl.2018.08.028.

Handy, M.R. *et al.* (2010) 'Reconciling plate-tectonic reconstructions of Alpine Tethys with the geological–geophysical record of spreading and subduction in the Alps', *Earth-Science Reviews*, 102(3), pp. 121–158. Available at: https://doi.org/10.1016/j.earscirev.2010.06.002.

Haq, B. *et al.* (2020) 'Deep Mediterranean's Messinian evaporite giant: How much salt?', *Global and Planetary Change*, 184, p. 103052. Available at: https://doi.org/10.1016/j.gloplacha.2019.103052.

Hartley, A. and Evenstar, L. (2018) 'Fluvial architecture in actively deforming salt basins: Chinle Formation, Paradox Basin, Utah', *Basin Research*, 30(1), pp. 148–166. Available at: https://doi.org/10.1111/bre.12247.

Haugen, J.A., Arntsen, B. and Mispel, J. (2008) 'Modeling of "dirty salt"', in *SEG Technical Program Expanded Abstracts 2008*. Society of Exploration Geophysicists (SEG Technical Program Expanded Abstracts), pp. 2127–2131. Available at: https://doi.org/10.1190/1.3059308.

Hawie, N. *et al.* (2013) 'Tectono-stratigraphic evolution of the northern Levant Basin (offshore Lebanon)', *Marine and Petroleum Geology*, 48, pp. 392–410. Available at: https://doi.org/10.1016/j.marpetgeo.2013.08.004.

Hegna, S. and Parkes, G. (2011) 'The low frequency output of marine air-gun arrays', in *SEG Technical Program Expanded Abstracts 2011*. Society of Exploration Geophysicists (SEG Technical Program Expanded Abstracts), pp. 77–81. Available at: https://doi.org/10.1190/1.3628192.

Heida, H. *et al.* (2021) 'Flexural-isostatic reconstruction of the Western Mediterranean during the Messinian Salinity Crisis: Implications for water level and basin connectivity', *Basin Research* [Preprint]. Available at: https://doi.org/10.1111/bre.12610.

Herbert, T.D. *et al.* (2016) 'Late Miocene global cooling and the rise of modern ecosystems', *Nature Geoscience*, 9(11), pp. 843–847. Available at: https://doi.org/10.1038/ngeo2813.

van Hinsbergen, D.J.J. *et al.* (2005) 'Nappe stacking resulting from subduction of oceanic and continental lithosphere below Greece', *Geology*, 33(4), pp. 325–328. Available at: https://doi.org/10.1130/G20878.1.

Hirsch, F. *et al.* (1995) 'Palinspastic and Crustal Setting of the Eastern Mediterranean', *Journal of Petroleum Geology*, 18(2), pp. 149–170. Available at: https://doi.org/10.1111/j.1747-5457.1995.tb00895.x.

Holbourn, A.E. *et al.* (2018) 'Late Miocene climate cooling and intensification of southeast Asian winter monsoon', *Nature communications*, 9(1), pp. 1–13.

Hornbostel, S. (1991) 'Spatial prediction filtering in the t-x and f-x domains', *GEOPHYSICS*, 56(12), pp. 2019–2026. Available at: https://doi.org/10.1190/1.1443014.

House, K.Z. *et al.* (2006) 'Permanent carbon dioxide storage in deep-sea sediments', *Proceedings of the National Academy of Sciences*, 103(33), pp. 12291–12295.

Hsü, K.J. (1972) 'Origin of saline giants: A critical review after the discovery of the Mediterranean Evaporite', *Earth Science Reviews*, 8(4), pp. 371–396. Available at: https://doi.org/10.1016/0012-8252(72)90062-1.

Hsü, K.J. *et al.* (1977) 'History of the Mediterranean salinity crisis', *Nature*, 267(5610), pp. 399–403. Available at: https://doi.org/10.1038/267399a0.

Hsü, K.J. *et al.* (1978) 'Site 371; South Balearic Basin', *Initial Reports of the Deep Sea Drilling Project*. Edited by K.J. Hsu et al., 42, p. 29.

Hsü, K.J., Ryan, W.B.F. and Cita, M.B. (1973) 'Late Miocene Desiccation of the Mediterranean', *Nature*, 242(5395), pp. 240–244. Available at: https://doi.org/10.1038/242240a0.

Hubscher, C. *et al.* (2007) 'Evolution of a young salt giant: The example of the Messinian evaporites in the Levantine Basin', *Mechanical Behavior of Salt - Understanding of Thmc Processes in Salt*, pp. 175–182.

Hudec, M.R. and Jackson, M.P.A. (2004) 'Regional restoration across the Kwanza Basin, Angola: Salt tectonics triggered by repeated uplift of a metastable passive margin', *AAPG Bulletin*, 88(7), pp. 971–990. Available at: https://doi.org/10.1306/02050403061.

Hudec, M.R. and Jackson, M.P.A. (2007) 'Terra infirma: Understanding salt tectonics', *Earth-Science Reviews*, 82(1–2), pp. 1–28. Available at: https://doi.org/10.1016/j.earscirev.2007.01.001.

Hughes, M. and Davison, I. (1993) 'Geometry and growth kinematics of salt pillows in the southern North Sea', *Tectonophysics*, 228(3–4), pp. 239-241,245-254. Available at: https://doi.org/10.1016/0040-1951(93)90343-I.

Huguen, C. *et al.* (2004) 'Structural setting and tectonic control of mud volcanoes from the Central Mediterranean Ridge (Eastern Mediterranean)', *Marine Geology*, 209(1–4), pp. 245–263. Available at: https://doi.org/10.1016/j.margeo.2004.05.002.

Infante-Paez, L. and Marfurt, K.J. (2017) 'Seismic expression and geomorphology of igneous bodies: A Taranaki Basin, New Zealand, case study', *Interpretation*, 5(3), pp. SK121–SK140. Available at: https://doi.org/10.1190/INT-2016-0244.1.

Intergovernmental Oceanographic Commission (1981) 'International Bathymetric Chart of the Mediterranean (IBCM), 1:1,000,000'. St. Petersburg: UNESCO. Available at: https://www.ngdc.noaa.gov/mgg/ibcm/ibcmsedt.html (Accessed: 14 June 2022).

Işler, F.I. *et al.* (2005) 'Neogene development of the Antalya Basin, Eastern Mediterranean: An active forearc basin adjacent to an arc

junction', *Marine Geology*, 221(1), pp. 299–330. Available at: https://doi.org/10.1016/j.margeo.2005.03.006.

Ivanovic, R.F. *et al.* (2014) 'Modelling global-scale climate impacts of the late Miocene Messinian Salinity Crisis', *Climate of the Past*, 10(2), pp. 607–622. Available at: https://doi.org/10.5194/cp-10-607-2014.

Jackson, C., Jackson, M. and Hudec, M. (2015) 'Understanding the kinematics of salt-bearing passive margins: A critical test of competing hypotheses for the origin of the Albian Gap, Santos Basin, offshore Brazil', *Geological Society of America Bulletin*, 127, pp. 1730–1751. Available at: https://doi.org/10.1130/B31290.1.

Jackson, C. and Talbot, C.J. (1986) 'External shapes, strain rates, and dynamics of salt structures', *GSA Bulletin*, 97(3), pp. 305–323. Available at: https://doi.org/10.1130/0016-7606(1986)97<305:ESSRAD>2.0.CO;2.

Jackson, J. and McKenzie, D. (1988) 'The relationship between plate motions and seismic moment tensors, and the rates of active deformation in the Mediterranean and Middle East', *Geophysical Journal*, 93(1), pp. 45–73. Available at: https://doi.org/10.1111/j.1365-246X.1988.tb01387.x.

Jackson, M.P.A. and Hudec, M.R. (2017) *Salt Tectonics: Principles and Practice*. Cambridge University Press.

Jackson, M.P.A. and Vendeville, B.C. (1994) 'Regional extension as a geologic trigger for diapirism', *GSA Bulletin*, 106(1), pp. 57–73. Available at: https://doi.org/10.1130/0016-7606(1994)106<0057:REAAGT>2.3.CO;2.

Jackson, M.P.A., Vendeville, B.C. and Schultz-Ela, D.D. (1994) 'Structural Dynamics of Salt Systems', *Annual Review of Earth and Planetary Sciences*, 22(1), pp. 93–117. Available at: https://doi.org/10.1146/annurev.ea.22.050194.000521.

Jakubowicz, H. (1998) 'Wave Equation Prediction and Removal of Interbed Multiples', in. European Association of Geoscientists & Engineers, p. cp. Available at: https://doi.org/10.3997/2214-4609.201408173.

Jiménez-Munt, I. *et al.* (2003) 'Active deformation in the Mediterranean from Gibraltar to Anatolia inferred from numerical modeling and geodetic and seismological data', *Journal of Geophysical Research: Solid Earth*, 108(B1), p. ETG 2-1-ETG 2-24. Available at: https://doi.org/10.1029/2001JB001544.

Jolivet, L. *et al.* (2006) 'Lithospheric-scale geodynamic context of the Messinian salinity crisis', *Sedimentary Geology*, 188–189, pp. 9–33. Available at: https://doi.org/10.1016/j.sedgeo.2006.02.004.

Jolivet, L. and Faccenna, C. (2000) 'Mediterranean extension and the Africa-Eurasia collision', *Tectonics*, 19(6), pp. 1095–1106. Available at: https://doi.org/10.1029/2000TC900018.

Jones, I. (2015) 'Estimating subsurface parameter fields for seismic migration : velocity model building', in. Available at: https://doi.org/10.1190/1.9781560803027.

Jones, I.F. *et al.* (2007) 'Application of anisotropic 3D reverse time migration to complex North Sea imaging', in *SEG Technical Program Expanded Abstracts 2007*. Society of Exploration Geophysicists (SEG Technical Program Expanded Abstracts), pp. 2140–2144. Available at: https://doi.org/10.1190/1.2792911.

Jones, I.F. (2008) 'A modeling study of preprocessing considerations for reverse-time migration', *GEOPHYSICS*, 73(6), pp. T99–T106. Available at: https://doi.org/10.1190/1.2981183.

Jones, I.F. and Davison, I. (2014) 'Seismic imaging in and around salt bodies', *Interpretation*, 2(4), pp. SL1–SL20. Available at: https://doi.org/10.1190/INT-2014-0033.1.

Jovanovich, D.B., Sumner, R.D. and Akins-Easterlin, S.L. (1983) 'Ghosting and marine signature deconvolution: A prerequisite for detailed seismic interpretation', *GEOPHYSICS*, 48(11), pp. 1468–1485. Available at: https://doi.org/10.1190/1.1441431.

Kahle, H.-G. and Mueller, S. (1998) 'Structure and dynamics of the Eurasian-African/Arabian plate boundary system: Objectives, tasks and resources of the WEGENER group', *Journal of Geodynamics*, 25(3), pp. 303–325. Available at: https://doi.org/10.1016/S0264-3707(97)00033-1.

Karakitsios, V. *et al.* (2017) 'A record of the Messinian salinity crisis in the eastern Ionian tectonically active domain (Greece, eastern Mediterranean)', *Basin Research*, 29(2), pp. 203–233. Available at: https://doi.org/10.1111/bre.12173.

Kartveit, K.H., Ulsund, H.B. and Johansen, S.E. (2019) 'Evidence of sea level drawdown at the end of the Messinian salinity crisis and seismic investigation of the Nahr Menashe unit in the northern Levant Basin, offshore Lebanon', *Basin Research*, 31(5), pp. 827–840. Available at: https://doi.org/10.1111/bre.12347.

Kastens, K.A. and Mascle, J. (1990) 'The geological evolution of the Tyrrhenian Sea; an introduction to the scientific results of ODP Leg 107', *Proceedings of the Ocean Drilling Program, Scientific Results*. Edited by K.A. Kastens et al., 107, p. 3. Available at: https://doi.org/10.2973/odp.proc.sr.107.187.1990.

van Keken, P.E. *et al.* (1993) 'The effective viscosity of rocksalt: implementation of steady-state creep laws in numerical models of salt diapirism', *Tectonophysics*, 225(4), pp. 457–476. Available at: https://doi.org/10.1016/0040-1951(93)90310-G.

Kelemen, P.B. and Matter, J. (2008) 'In situ carbonation of peridotite for CO2 storage', *Proceedings of the National Academy of Sciences*, 105(45), pp. 17295–17300.

Kherroubi, A. *et al.* (2009) 'Recent and active deformation pattern off the easternmost Algerian margin, Western Mediterranean Sea: New evidence for contractional tectonic reactivation', *Marine Geology*, 261(1), pp. 17–32. Available at: https://doi.org/10.1016/j.margeo.2008.05.016.

Kirkham, C. *et al.* (2019) '3D kinematics of a thick salt layer during gravity-driven deformation', *Marine and Petroleum Geology*, 110, pp. 434–449. Available at: https://doi.org/10.1016/j.marpetgeo.2019.07.036.

Kirschbaum, M.A. *et al.* (2010) *Assessment of Undiscovered Oil and Gas Resources of the Nile Delta Basin Province, Eastern Mediterranean*. Report 2010–3027. Available at: https://doi.org/10.3133/fs20103027.

Kontakiotis, G. *et al.* (2022) 'Hypersalinity accompanies tectonic restriction in the eastern Mediterranean prior to the Messinian Salinity Crisis', *Palaeogeography, Palaeoclimatology, Palaeoecology*, 592. Available at: https://doi.org/10.1016/j.palaeo.2022.110903.

Kopf, A. and Behrmann, J.H. (2000) 'Extrusion dynamics of mud volcanoes on the Mediterranean Ridge accretionary complex', *Geological Society Special Publication*, 174, pp. 169–204. Available at: https://doi.org/10.1144/GSL.SP.1999.174.01.10.

Kopf, A., Mascle, J. and Klaeschen, D. (2003) 'The Mediterranean Ridge: A mass balance across the fastest growing accretionary complex on Earth', *Journal of Geophysical Research: Solid Earth*, 108(B8). Available at: https://doi.org/10.1029/2001JB000473.

Kostianoy, A.G. and Carpenter, A. (2018) 'Oil and Gas Exploration and Production in the Mediterranean Sea', in A. Carpenter and A.G. Kostianoy (eds) *Oil Pollution in the Mediterranean Sea: Part I: The International Context*. Cham: Springer International Publishing (The Handbook of

Environmental Chemistry), pp. 53–77. Available at: https://doi.org/10.1007/698_2018_373.

Kouwenhoven, T., Hilgen, F. and van der Zwaan, G. (2003) 'Late Tortonian-early Messinian stepwise disruption of the Mediterranean-Atlantic connections: constraints from benthic foraminiferal and geochemical data', *Palaeogeography Palaeoclimatology Palaeoecology*, 198(3–4), pp. 303–319. Available at: https://doi.org/10.1016/S0031-0182(03)00472-3.

Krijgsman, W. *et al.* (1997) 'The Monte del Casino section (Northern Apennines, Italy): a potential Tortonian/Messinian boundary stratotype?', *Palaeogeography, Palaeoclimatology, Palaeoecology*, 133(1), pp. 27–47. Available at: https://doi.org/10.1016/S0031-0182(97)00039-4.

Krijgsman, W. *et al.* (1999) 'Chronology, causes and progression of the Messinian salinity crisis', *Nature*, 400(6745), pp. 652–655. Available at: https://doi.org/10.1038/23231.

Krijgsman, W. *et al.* (2006) 'Tectonic control for evaporite formation in the Eastern Betics (Tortonian; Spain)', *Sedimentary Geology*, 188–189, pp. 155–170. Available at: https://doi.org/10.1016/j.sedgeo.2006.03.003.

Krijgsman, W. *et al.* (2010) 'Rise and fall of the Paratethys Sea during the Messinian Salinity Crisis', *Earth and Planetary Science Letters*, 290(1–2), pp. 183–191. Available at: https://doi.org/10.1016/j.epsl.2009.12.020.

ten Kroode, F. *et al.* (2013) 'Broadband seismic data — The importance of low frequencies', *GEOPHYSICS*, 78(2), pp. WA3–WA14. Available at: https://doi.org/10.1190/geo2012-0294.1.

Kukla, P.A., Strozyk, F. and Mohriak, W.U. (2018) 'South Atlantic salt basins – Witnesses of complex passive margin evolution', *Gondwana Research*, 53, pp. 41–57. Available at: https://doi.org/10.1016/j.gr.2017.03.012.

Lanaja, J.M. (1987) *Contribución de la exploración petrolífera al conocimiento de la geología de España*. Instituto Geológico y Minero de España.

Leffondré, P. *et al.* (2021) 'Ongoing Inversion of a Passive Margin: Spatial Variability of Strain Markers Along the Algerian Margin and Basin (Mediterranean Sea) and Seismotectonic Implications', *Frontiers in Earth Science*, 9, p. 365. Available at: https://doi.org/10.3389/feart.2021.674584.

Leila, M. *et al.* (2022) 'Controls of facies distribution on reservoir quality in the Messinian incised-valley fill Abu Madi Formation in Salma delta gas field, northeastern onshore Nile Delta, Egypt', *Journal of Natural Gas Science and Engineering*, 97, p. 104360. Available at: https://doi.org/10.1016/j.jngse.2021.104360.

Leprêtre, A. (2012a) 'Constraints by penetrating seismic imaging on the evolution of a Cenozoic margin reactivated in compression (Algerian margin, sector of Tipaza)'.

Leprêtre, A. (2012b) *Contraintes par imagerie sismique pénétrante sur l'évolution d'une marge Cénozoïque réactivée en compression (cas de la marge algérienne, secteur de Tipaza), Constraints by penetrating seismic imaging on the evolution of a Cenozoic margin reactivated in compression (Algerian margin, sector of Tipaza)*. PhD Thesis. Université de Bretagne occidentale. Available at: https://archimer.ifremer.fr/doc/00498/60955/ (Accessed: 19 October 2020).

Leprêtre, A. *et al.* (2013) 'Multiphased tectonic evolution of the Central Algerian margin from combined wide-angle and reflection seismic data off Tipaza, Algeria', *Journal of Geophysical Research: Solid Earth*, 118(8), pp. 3899–3916. Available at: https://doi.org/10.1002/jgrb.50318.

Leroux, E *et al.* (2015) 'Post-rift evolution of the Gulf of Lion margin tested by stratigraphic modelling', *Bulletin De La Societe Geologique De France*, 186(4–5), pp. 291–308. Available at: https://doi.org/10.2113/gssgfbull.186.4-5.291.

Leroux, Estelle *et al.* (2015) 'Sedimentary markers in the Provençal Basin (western Mediterranean): a window into deep geodynamic processes', *Terra Nova*, 27(2), pp. 122–129. Available at: https://doi.org/10.1111/ter.12139.

Leroux, E. *et al.* (2017) 'High-resolution evolution of terrigenous sediment yields in the Provence Basin during the last 6 Ma: relation with climate and tectonics', *Basin Research*, 29(3), pp. 305–339. Available at: https://doi.org/10.1111/bre.12178.

Leroux, E. (2019) *ATLAS of the stratigraphic markers in the Western Mediterranean with focus on the Messinian, Pliocene and Pleistocene of the Gulf of Lion*. Commission for the Geological Map of the World.

Letouzey, J. *et al.* (1995) 'Evolution of Salt-Related Structures in Compressional Settings', in M.P.A. Jackson, D.G. Roberts, and S. Snelson (eds) *Salt Tectonics: A Global Perspective*. American Association of Petroleum Geologists. Available at: https://doi.org/10.1306/M65604C3.

Leveille, J., Larner, K. and Higginbotham, J. (2005) 'A problem workshop', *The Leading Edge*, 24(11), pp. 1126–1132. Available at: https://doi.org/10.1190/1.2135107.

Leveille, J.P. *et al.* (2011) 'Subsalt imaging for exploration, production, and development: A review', *GEOPHYSICS*, 76(5), pp. WB3–WB20. Available at: https://doi.org/10.1190/geo2011-0156.1.

Li, C. *et al.* (2021) 'Effects of Salt Thickness on the Structural Deformation of Foreland Fold-and-Thrust Belt in the Kuqa Depression, Tarim Basin: Insights From Discrete Element Models', *Frontiers in Earth Science*, 9. Available   at: https://www.frontiersin.org/article/10.3389/feart.2021.655173 (Accessed: 17 March 2022).

Lille, H. *et al.* (2017) 'Reviving Old Seismic Data Using Latest Broadband Processing Technology - A Case Study from West Of Shetland', in. Available at: https://doi.org/10.3997/2214-4609.201700814.

Lin, S.-T. (1992) *Experimental study of syndepositional and postdepositional gravity spreading of a brittle overburden and viscous substratum*. University of Texas at Austin.

Litak, R.K. *et al.* (1997) 'Mesozoic-Cenozoic evolution of the intraplate Euphrates fault system, Syria: implications for regional tectonics', *Journal of the Geological Society*, 154(4), pp. 653–666. Available at: https://doi.org/10.1144/gsjgs.154.4.0653.

Liu, X. and Goulty, N.R. (1999) 'Comparison of 2D filters for suppressing noise in common shot gathers', *First Break*. European Association of Geoscientists & Engineers. Available at: https://doi.org/10.1046/j.1365-2397.1999.00702.x.

Lofi, J. *et al.* (2003) 'Plio–Quaternary prograding clinoform wedges of the western Gulf of Lion continental margin (NW Mediterranean) after the Messinian Salinity Crisis', *Marine Geology*, 198(3–4), pp. 289–317. Available at: https://doi.org/10.1016/S0025-3227(03)00120-8.

Lofi, J. *et al.* (2005) 'Erosional processes and paleo-environmental changes in the Western Gulf of Lions (SW France) during the Messinian Salinity Crisis', *Marine Geology*, 217(1–2), pp. 1–30. Available at: https://doi.org/10.1016/j.margeo.2005.02.014.

Lofi, J. *et al.* (2011) *Seismic Atlas of the Messinian Salinity Crisis markers in the Mediterranean and Black Seas*, *Mémoire de la Société Géologique n.s.* Société Géologique de France, p. 1. Available at: https://hal-brgm.archives-ouvertes.fr/hal-00593502 (Accessed: 9 February 2021).

Lofi, J. *et al.* (2017) 'The "DREAM" IODP project to drill the Mediterranean Salt Giant on the Balearic Promontory', p. 13670.

Lofi, J. (2018) *Seismic atlas of the Messinian salinity crisis markers in the Mediterranean Sea*. Mem. Soc. géol. fr., n.s., 2018, t. 181, and Commission for the Geological Map of the World.

Loncke, L. *et al.* (2006) 'The Nile deep-sea fan: An example of interacting sedimentation, salt tectonics, and inherited subsalt paleotopographic features', *Marine and Petroleum Geology*, 23(3), pp. 297–315. Available at: https://doi.org/10.1016/j.marpetgeo.2006.01.001.

Loncke, L. and Mascle, J. (2004) 'Mud volcanoes, gas chimneys, pockmarks and mounds in the Nile deep-sea fan (Eastern Mediterranean): Geophysical evidences', *Marine and Petroleum Geology*, 21(6), pp. 669–689. Available at: https://doi.org/10.1016/j.marpetgeo.2004.02.004.

Lugli, S. *et al.* (2015) 'The deep record of the Messinian salinity crisis: Evidence of a non-desiccated Mediterranean Sea', *Palaeogeography, Palaeoclimatology, Palaeoecology*, 433, pp. 201–218. Available at: https://doi.org/10.1016/j.palaeo.2015.05.017.

Lundin, E.R. (1992) 'Thin-skinned extensional tectonics on a salt detachment, northern Kwanza Basin, Angola', *Marine and Petroleum Geology*, 9(4), pp. 405–411. Available at: https://doi.org/10.1016/0264-8172(92)90051-F.

Luo, G. *et al.* (2015) 'The role of pore fluid overpressure in the substrates of advancing salt sheets, ice glaciers, and critical-state wedges', *Journal of Geophysical Research: Solid Earth*, 120(1), pp. 87–105. Available at: https://doi.org/10.1002/2014JB011326.

Lustrino, M., Melluso, L. and Morra, V. (2000) 'The role of lower continental crust and lithospheric mantle in the genesis of Plio–Pleistocene volcanic rocks from Sardinia (Italy)', *Earth and Planetary Science Letters*, 180(3), pp. 259–270. Available at: https://doi.org/10.1016/S0012-821X(00)00185-0.

Machel, H.G. and Foght, J. (2000) 'Products and Depth Limits of Microbial Activity in Petroliferous Subsurface Settings', in R.E. Riding and S.M. Awramik (eds) *Microbial Sediments*. Berlin, Heidelberg: Springer, pp. 105–120. Available at: https://doi.org/10.1007/978-3-662-04036-2_13.

Madof, A.S., Bertoni, C. and Lofi, J. (2019) 'Discovery of vast fluvial deposits provides evidence for drawdown during the late Miocene Messinian salinity crisis', *Geology*, 47(2), pp. 171–174. Available at: https://doi.org/10.1130/G45873.1.

Maesano, F.E., Tiberti, M.M. and Basili, R. (2017) 'The Calabrian Arc: three-dimensional modelling of the subduction interface', *Scientific Reports*, 7(1), p. 8887. Available at: https://doi.org/10.1038/s41598-017-09074-8.

Maesano, F.E., Tiberti, M.M. and Basili, R. (2020) 'Deformation and Fault Propagation at the Lateral Termination of a Subduction Zone: The Alfeo Fault System in the Calabrian Arc, Southern Italy', *Frontiers in Earth Science*, 8. Available at: https://www.frontiersin.org/article/10.3389/feart.2020.00107.

Mahgoub, M.A.G. *et al.* (2017) 'Cost-effective Seismic Data Reprocessing for Sub-salt Imaging Enhancement.' Available at: https://doi.org/10.3997/2214-4609.201702344.

Maillard, A. *et al.* (2003) 'Influence of differential compaction above basement steps on salt tectonics in the Ligurian-Provençal Basin, northwest Mediterranean', *Marine and Petroleum Geology*, 20(1), pp. 13–27. Available at: https://doi.org/10.1016/S0264-8172(03)00022-9.

Maillard, A. *et al.* (2011) 'Deformed Messinian markers in the Cyprus Arc: tectonic and/or Messinian Salinity Crisis indicators?: Deformed Messinian markers in the Cyprus Arc', *Basin Research*, 23(2), pp. 146–170. Available at: https://doi.org/10.1111/j.1365-2117.2010.00464.x.

Mancilla, F. de L. *et al.* (2018) 'A STEP fault in Central Betics, associated with lateral lithospheric tearing at the northern edge of the Gibraltar arc subduction system', *Earth and Planetary Science Letters*, 486, pp. 32–40. Available at: https://doi.org/10.1016/j.epsl.2018.01.008.

Manzi, V. *et al.* (2005) 'Deep-water clastic evaporites deposition in the Messinian Adriatic foredeep (northern Apennines, Italy): did the Mediterranean ever dry out?', *Sedimentology*, 52(4), pp. 875–902. Available at: https://doi.org/10.1111/j.1365-3091.2005.00722.x.

Manzi, V. *et al.* (2007) 'The deep-water counterpart of the Messinian lower evaporites in the Apennine foredeep: The fanantello section (Northern Apennines, Italy)', *Palaeogeography Palaeoclimatology Palaeoecology*, 251(3–4), pp. 470–499. Available at: https://doi.org/10.1016/j.palaeo.2007.04.012.

Manzi, V. *et al.* (2013) 'Age refinement of the Messinian salinity crisis onset in the Mediterranean', *Terra Nova*, 25(4), pp. 315–322. Available at: https://doi.org/10.1111/ter.12038.

Manzi, V. *et al.* (2018) 'The onset of the Messinian salinity crisis in the deep Eastern Mediterranean basin', *Terra Nova* [Preprint]. Available at: https://doi.org/10.1111/ter.12325.

Manzi, Vinicio *et al.* (2021) 'Large-scale mass-transport deposits recording the collapse of an evaporitic platform during the Messinian salinity crisis (Caltanissetta basin, Sicily)', *Sedimentary Geology*, 424, p. 106003. Available at: https://doi.org/10.1016/j.sedgeo.2021.106003.

Manzi, V. *et al.* (2021) 'Synchronous onset of the Messinian salinity crisis and diachronous evaporite deposition: New evidences from the deep Eastern Mediterranean basin', *Palaeogeography, Palaeoclimatology, Palaeoecology*, 584, p. 110685. Available at: https://doi.org/10.1016/j.palaeo.2021.110685.

Marsaglia, K.M. (1999) 'Petrography and mineralogy of the uppermost Messinian section and the Pliocene/Miocene boundary at Site 975, western Mediterranean Sea', *Proceedings of the Ocean Drilling Program, Scientific Results*. Edited by J.S. Tribble et al., 161, p. 3.

Martin, J., Braga, J. and Betzler, C. (2001) 'The Messinian Guadalhorce corridor: the last northern, Atlantic-Mediterranean gateway', *Terra Nova*, 13(6), pp. 418–424. Available at: https://doi.org/10.1046/j.1365-3121.2001.00376.x.

Martínez-Rius, B. (2020) 'For the Benefit of All Men: Oceanography and Franco-American Scientific Diplomacy in the Cold War, 1958–1970**', *Berichte zur Wissenschaftsgeschichte*, 43(4), pp. 581–605. Available at: https://doi.org/10.1002/bewi.202000015.

Martínez-Rius, B. (2022) *Making the seafloor. French geologists, marine resources and new deep territories (1945-1975)*. PhD thesis. Sorbonne Université.

Martínez-Rius, B. and Herran, N. (2022) 'The underwater exploration of the Mediterranean, from the surface to the deep sea', *Encyclopédie d'histoire numérique de l'Europe* [Preprint]. Available at: https://ehne.fr/en/node/21781 (Accessed: 28 May 2022).

Marton, L., Tari, G. and Lehmann, C. (2000) 'Evolution of the Angolan passive margin, West Africa, with emphasis on post-salt structural styles', in *Washington DC American Geophysical Union Geophysical Monograph Series*, pp. 129–149. Available at: https://doi.org/10.1029/GM115p0129.

Marzocchi, A. *et al.* (2016) 'Mediterranean outflow pump: An alternative mechanism for the Lago-mare and the end of the Messinian Salinity

Crisis', *Geology*, 44(7), pp. 523–526. Available at: https://doi.org/10.1130/G37646.1.

Mascle, G. and Mascle, J. (2019) 'The Messinian salinity legacy: 50 years later', *Mediterranean Geoscience Reviews*, 1(1), pp. 5–15. Available at: https://doi.org/10.1007/s42990-019-0002-5.

Masoomzadeh, H., Woodburn, N. and Hardwick, A. (2013) 'Broadband processing of linear streamer data', in *SEG Technical Program Expanded Abstracts 2013*. Society of Exploration Geophysicists, pp. 4635–4639. Available at: https://doi.org/10.1190/segam2013-0872.1.

Mauffret, A. *et al.* (1995) 'Tectonics and deep structure of the north-western Mediterranean Basin', *Marine and Petroleum Geology*, 12(6), pp. 645–666. Available at: https://doi.org/10.1016/0264-8172(95)98090-R.

Mauffret, A. *et al.* (2004) 'E–W opening of the Algerian Basin (Western Mediterranean)', *Terra Nova*, 16, pp. 257–264. Available at: https://doi.org/10.1111/j.1365-3121.2004.00559.x.

Maunde, A. *et al.* (2017) 'Approaches for Suppressing Seismic Bubble Pulse Reverberations', *International Research Journal of Geology and Mining*, 7(2276–6618), pp. 1–8.

Mavko, G., Mukerji, T. and Dvorkin, J. (2009) *The Rock Physics Handbook: Tools for Seismic Analysis of Porous Media*. 2nd edn. Cambridge: Cambridge University Press. Available at: https://doi.org/10.1017/CBO9780511626753.

Medaouri, M. *et al.* (2012) 'Structural styles and Neogene petroleum system around the Yusuf-Habibas Ridge (Alboran Basin, Mediterranean Sea)', *The Leading Edge*, 31(7), pp. 776–785. Available at: https://doi.org/10.1190/tle31070776.1.

Medaouri, M. *et al.* (2014) 'The transition from Alboran to Algerian basins (Western Mediterranean Sea): Chronostratigraphy, deep crustal structure and tectonic evolution at the rear of a narrow slab rollback system', *JGeo*, 77, pp. 186–205. Available at: https://doi.org/10.1016/j.jog.2014.01.003.

Medialdea, T. *et al.* (2012) 'Seismic architecture of mud volcano systems in the Ceuta Contourite Depositional System (Western Alboran Sea)', *Geo-Temas*, 13, pp. 629–632.

Meilijson, A. *et al.* (2018) 'Deep-basin evidence resolves a 50-year-old debate and demonstrates synchronous onset of Messinian evaporite deposition in a non-desiccated Mediterranean', *Geology*, 46(3), pp. 243–246. Available at: https://doi.org/10.1130/G39868.1.

Meilijson, A. *et al.* (2019) 'Chronology with a pinch of salt: Integrated stratigraphy of Messinian evaporites in the deep Eastern Mediterranean reveals long-lasting halite deposition during Atlantic connectivity', *Earth-Science Reviews*, 194, pp. 374–398. Available at: https://doi.org/10.1016/j.earscirev.2019.05.011.

Meyer, B., Saltus, R. and Chulliat, A. (2017) 'EMAG2v3: Earth Magnetic Anomaly Grid (2-arc-minute resolution). Version 3', *National Centers for Environmental Information* [Preprint]. Available at: https://doi.org/10.7289/V5H70CVX.

Mianaekere, V. and Adam, J. (2020) '"Halo-kinematic" sequence stratigraphic analysis adjacent to salt diapirs in the deepwater contractional province, Liguro-Provençal Basin, Western Mediterranean Sea', *Marine and Petroleum Geology*, 115, p. 104258. Available at: https://doi.org/10.1016/j.marpetgeo.2020.104258.

Micallef, A. *et al.* (2018) 'Evidence of the Zanclean megaflood in the eastern Mediterranean Basin', *Scientific Reports*, 8(1), p. 1078. Available at: https://doi.org/10.1038/s41598-018-19446-3.

Migeon, S. *et al.* (2006) 'The Var turbidite system (Ligurian Sea, northwestern Mediterranean)—morphology, sediment supply, construction of turbidite levee and sediment waves: implications for hydrocarbon reservoirs', *Geo-Marine Letters*, 26(6), p. 361. Available at: https://doi.org/10.1007/s00367-006-0047-x.

Mocnik, A. *et al.* (2014) 'The Messinian Salinity Crisis in the West-Mediterranean Basins: comparison between two rifted margins', in. Bologna, pp. 156–163.

Montadert, L. *et al.* (1970) 'De l'âge tertiaire de la série salifère responsable des structures diapiriques en Méditerranée Occidentale (Nord-Est des Baléares)', *CRAS*, 271, pp. 812–815.

Nader, F.H. *et al.* (2018) 'Key geological characteristics of the Saida-Tyr Platform along the eastern margin of the Levant Basin, offshore Lebanon: implications for hydrocarbon exploration', *Oil & Gas Science and Technology – Revue d'IFP Energies nouvelles*, 73, p. 50. Available at: https://doi.org/10.2516/ogst/2018045.

Najafi, M. and Lajmorak, S. (2020) 'Contractional salt-tectonic system in the south Dezful embayment, Zagros', *Journal of Structural Geology*, 141, p. 104204. Available at: https://doi.org/10.1016/j.jsg.2020.104204.

Nasir, N.E. and Dabbousi, O.B. (1978) 'Fluid dynamics model for salt-dome evolution', *Tectonophysics*, 47(1), pp. 85–107. Available at: https://doi.org/10.1016/0040-1951(78)90153-1.

Negredo, A.M. *et al.* (2020) 'Geodynamic Modeling of Edge-Delamination Driven by Subduction-Transform Edge Propagator Faults: The Westernmost Mediterranean Margin (Central Betic Orogen) Case Study', *Frontiers in Earth Science*, 8. Available at: https://www.frontiersin.org/article/10.3389/feart.2020.533392 (Accessed: 11 June 2022).

Netzeband, G.L., Hübscher, C.P. and Gajewski, D. (2006) 'The structural evolution of the Messinian evaporites in the Levantine Basin', *Marine Geology*, 230(3–4), pp. 249–273. Available at: https://doi.org/10.1016/j.margeo.2006.05.004.

Ng, Z.L. *et al.* (2021) 'Latest Miocene restriction of the Mediterranean Outflow Water: a perspective from the Gulf of Cádiz', *Geo-Marine Letters*, 41(2), p. 23. Available at: https://doi.org/10.1007/s00367-021-00693-9.

Obone-Zue-Obame, E.M. *et al.* (2011) 'The sedimentary markers of the Messinian salinity crisis and their relation with salt tectonics on the Provençal margin (western Mediterranean): results from the "MAURESC" cruise', *Bulletin de la Société Géologique de France*, 182(2), pp. 181–196. Available at: https://doi.org/10.2113/gssgfbull.182.2.181.

Ochoa, D. *et al.* (2015) 'Synchronous onset of the Messinian evaporite precipitation: First Mediterranean offshore evidence', *Earth and Planetary Science Letters*, 427, pp. 112–124. Available at: https://doi.org/10.1016/j.epsl.2015.06.059.

Ode, H. (1968) 'Review of Mechanical Properties of Salt Relating to Salt-Dome Genesis', 153, pp. 53–78.

O'Driscoll, R. *et al.* (2013) 'Broad-bandwidth data processing of conventional marine streamer data: An offshore West Africa field case study', in *SEG Technical Program Expanded Abstracts 2013*. Society of Exploration Geophysicists, pp. 4231–4235.

Olivet, J.-L. (1996) 'La cinématique de la plaque ibérique', *Bulletin des centres de recherches exploration-production Elf-Aquitaine*, 20(1), pp. 131–195.

Oppo, D. *et al.* (2021) 'Leaky salt: Pipe trails record the history of cross-evaporite fluid escape in the northern Levant Basin, Eastern Mediterranean', *Basin Research*, 33(3), pp. 1798–1819. Available at: https://doi.org/10.1111/bre.12536.

Oren, A. (2014) 'Halophilic archaea on Earth and in space: growth and survival under extreme conditions', *Philosophical Transactions. Series A, Mathematical, Physical, and Engineering Sciences*, 372(2030), p. 20140194. Available at: https://doi.org/10.1098/rsta.2014.0194.

Orszag-Sperber, F., Rouchy, J.-M. and Blanc-Valleron, M.-M. (2000) 'La transition Messinien–Pliocène en Méditerranée orientale (Chypre) : la période du Lago-Mare et sa signification', *Comptes Rendus de l'Académie des Sciences - Series IIA - Earth and Planetary Science*, 331(7), pp. 483–490. Available at: https://doi.org/10.1016/S1251-8050(00)01433-6.

Özbakır, A.D., Govers, R. and Fichtner, A. (2020) 'The Kefalonia Transform Fault: A STEP fault in the making', *Tectonophysics*, 787, p. 228471. Available at: https://doi.org/10.1016/j.tecto.2020.228471.

Peel, F.J., Travis, C.J. and Hossack, J.R. (1995) 'Genetic structural provinces and salt tectonics of the Cenozoic offshore US Gulf of Mexico: A preliminary analysis'.

Pellen, R. *et al.* (2019) 'The Messinian Ebro River incision', *Global and Planetary Change*, 181, p. 102988. Available at: https://doi.org/10.1016/j.gloplacha.2019.102988.

Perez-Asensio, J. *et al.* (2013) 'Glacioeustatic control on the origin and cessation of the Messinian salinity crisis', *Global and Planetary Change*, 111, pp. 1–8. Available at: https://doi.org/10.1016/j.gloplacha.2013.08.008.

Piante, C., Ody, D. and Roberts, C. (2015) 'Blue growth in the Mediterranean Sea: the challenge of good environmental status', *MedTrends Project. WWF-France*, p. 192.

Pichel, L.M. *et al.* (2019) 'The influence of base-salt relief, rift topography and regional events on salt tectonics offshore Morocco', *Marine and Petroleum Geology*, 103, pp. 87–113. Available at: https://doi.org/10.1016/j.marpetgeo.2019.02.007.

Pichel, L.M., Finch, E. and Gawthorpe, R.L. (2019) 'The Impact of Pre-Salt Rift Topography on Salt Tectonics: A Discrete-Element Modeling Approach', *Tectonics*, 38(4), pp. 1466–1488. Available at: https://doi.org/10.1029/2018TC005174.

Pichel, L.M. and Jackson, C.A.-L. (2020) 'Four-dimensional Variability of Composite Halokinetic Sequences', *Basin Research*, 32(6), pp. 1277–1299. Available at: https://doi.org/10.1111/bre.12428.

Pinardi, N. and Masetti, E. (2000) 'Variability of the large scale general circulation of the Mediterranean Sea from observations and modelling: a review', *Palaeogeography, Palaeoclimatology, Palaeoecology*, 158(3), pp. 153–173. Available at: https://doi.org/10.1016/S0031-0182(00)00048-1.

Pinkston, F.W.M. and Flemings, P.B. (2019) 'Overpressure at the Macondo Well and its impact on the Deepwater Horizon blowout', *Scientific Reports*, 9, p. 7047. Available at: https://doi.org/10.1038/s41598-019-42496-0.

Polonia, A. *et al.* (2011) 'The Calabrian Arc subduction complex in the Ionian Sea: Regional architecture, active deformation, and seismic hazard', *Tectonics*, 30(5). Available at: https://doi.org/10.1029/2010TC002821.

Polonia, A. *et al.* (2016) 'The Ionian and Alfeo–Etna fault zones: New segments of an evolving plate boundary in the central Mediterranean Sea?', *Tectonophysics*, 675, pp. 69–90. Available at: https://doi.org/10.1016/j.tecto.2016.03.016.

Poort, J. *et al.* (2020) 'Heat flow in the Western Mediterranean: Thermal anomalies on the margins, the seafloor and the transfer zones', *Marine Geology*, 419, p. 106064. Available at: https://doi.org/10.1016/j.margeo.2019.106064.

Pound, M.J. *et al.* (2012) 'Global vegetation dynamics and latitudinal temperature gradients during the Mid to Late Miocene (15.97–5.33Ma)', *Earth-Science Reviews*, 112(1), pp. 1–22. Available at: https://doi.org/10.1016/j.earscirev.2012.02.005.

Praeg, D. *et al.* (2009) 'Tectonically-driven mud volcanism since the late Pliocene on the Calabrian accretionary prism, central Mediterranean Sea', *Marine and Petroleum Geology*, 26(9), pp. 1849–1865. Available at: https://doi.org/10.1016/j.marpetgeo.2009.03.008.

Quirk, D. *et al.* (2012) 'Salt tectonics on passive margins: Examples from Santos, Campos and Kwanza Basins', *Geological Society of London Special Publications*, 363, pp. 207–244. Available at: https://doi.org/10.1144/SP363.10.

Raad, F. *et al.* (2021) 'The Messinian Salinity Crisis deposits in the Balearic Promontory: An undeformed analog of the MSC Sicilian basins??', *Marine and Petroleum Geology*, 124, p. 104777. Available at: https://doi.org/10.1016/j.marpetgeo.2020.104777.

Rabineau, M. *et al.* (2015) 'Probing connections between deep earth and surface processes in a land-locked ocean basin transformed into a giant saline basin: The Mediterranean GOLD project#', *Marine and Petroleum*

Geology, 66, pp. 6–17. Available at: https://doi.org/10.1016/j.marpetgeo.2015.03.018.

Radeff, G. *et al.* (2017) 'Sedimentary evidence for late Messinian uplift of the SE margin of the Central Anatolian Plateau: Adana Basin, southern Turkey', *Basin Research*, 29, pp. 488–514. Available at: https://doi.org/10.1111/bre.12159.

Raith, A.F. *et al.* (2016) 'Evolution of rheologically heterogeneous salt structures: a case study from the NE Netherlands', *Solid Earth*, 7(1), pp. 67–82. Available at: https://doi.org/10.5194/se-7-67-2016.

Raj, A. *et al.* (2016) 'Data Dependent Adaptive Deghosting -Application to Vintage Data', in. European Association of Geoscientists & Engineers, pp. 1–5. Available at: https://doi.org/10.3997/2214-4609.201601217.

Recanati, A. *et al.* (2019) 'A Tortonian onset for the Algerian margin inversion: Evidence from low-temperature thermochronology', *Terra Nova*, 31(1), pp. 39–48. Available at: https://doi.org/10.1111/ter.12367.

Regone, C.J. (2006) 'A modeling approach to wide-azimuth design for subsalt imaging', *The Leading Edge*, 25(12), pp. 1467–1475. Available at: https://doi.org/10.1190/1.2405331.

Rehault, J.-P., Boillot, G. and Mauffret, A. (1984) 'The Western Mediterranean Basin geological evolution', *Marine Geology*, 55(3), pp. 447–477. Available at: https://doi.org/10.1016/0025-3227(84)90081-1.

Reiche, S., Hübscher, C. and Beitz, M. (2014) 'Fault-controlled evaporite deformation in the Levant Basin, Eastern Mediterranean', *Marine Geology*, 354, pp. 53–68. Available at: https://doi.org/10.1016/j.margeo.2014.05.002.

dos Reis, A.T., Gorini, C. and Mauffret, A. (2005) 'Implications of salt–sediment interactions on the architecture of the Gulf of Lions deep-water sedimentary systems—western Mediterranean Sea', *Marine and Petroleum Geology*, 22(6–7), pp. 713–746. Available at: https://doi.org/10.1016/j.marpetgeo.2005.03.006.

Reston, T.J. *et al.* (2002) 'Frontal accretion along the western Mediterranean Ridge: the effect of Messinian evaporites on wedge mechanics and structural style', *Marine Geology*, 186(1), pp. 59–82. Available at: https://doi.org/10.1016/S0025-3227(02)00173-1.

Revil, A. (1999) 'Fluid overpressures in western Mediterranean sediments, sites 974-979', *Proceedings of the Ocean Drilling Program, Scientific Results*. Edited by P.A. Pezard et al., 161, p. 117.

Robertson, A. (1996) 'Mud volcanism on the Mediterranean Ridge: Initial results of Ocean Drilling Program Leg 160', *Geology*, 24(3), pp. 239–242. Available at: https://doi.org/10.1130/0091-7613(1996)024<0239:MVOTMR>2.3.CO;2.

Robertson, A.H.F. and Grasso, M. (1995) 'Overview of the Late Tertiary–Recent tectonic and palaeo-environmental development of the Mediterranean region', *Terra Nova*, 7(2), pp. 114–127. Available at: https://doi.org/10.1111/j.1365-3121.1995.tb00680.x.

Roether, W. and Well, R. (2001) 'Oxygen consumption in the Eastern Mediterranean', *Deep Sea Research Part I: Oceanographic Research Papers*, 48(6), pp. 1535–1551. Available at: https://doi.org/10.1016/S0967-0637(00)00102-3.

Rollet, N. *et al.* (2002) 'Back arc extension, tectonic inheritance, and volcanism in the Ligurian Sea, Western Mediterranean', *Tectonics*, 21(3), pp. 6-1-6–23. Available at: https://doi.org/10.1029/2001TC900027.

Rosenbaum, G. *et al.* (2008) 'Kinematics of slab tear faults during subduction segmentation and implications for Italian magmatism', *Tectonics*, 27(2). Available at: https://doi.org/10.1029/2007TC002143.

Rosenbaum, G., Lister, G. and Duboz, C. (2002) 'Reconstruction of the tectonic evolution of the Western Mediterranean since the Oligocene', *Journal of the Virtual Explorer*, 8, pp. 107–130. Available at: https://doi.org/10.3809/jvirtex.2002.00053.

Roure, F., Casero, P. and Addoum, B. (2012) 'Alpine inversion of the North African margin and delamination of its continental lithosphere', *Tectonics*, 31(3). Available at: https://doi.org/10.1029/2011TC002989.

Roveri, M., Manzi, V., *et al.* (2014) 'Dense shelf water cascading and Messinian Canyons: A new scenario for the Mediterranean salinity crisis', *American Journal of Science*, 314(3), pp. 751–784. Available at: https://doi.org/10.2475/05.2014.03.

Roveri, M., Lugli, S., *et al.* (2014) 'High-resolution strontium isotope stratigraphy of the Messinian deep Mediterranean basins: Implications for marginal to central basins correlation', *Marine Geology*, 349, pp. 113–125. Available at: https://doi.org/10.1016/j.margeo.2014.01.002.

Roveri, M., Flecker, R., *et al.* (2014) 'The Messinian Salinity Crisis: Past and future of a great challenge for marine sciences', *Marine Geology*, 352, pp. 25–58. Available at: https://doi.org/10.1016/j.margeo.2014.02.002.

Roveri, M. *et al.* (2016) 'The Messinian salinity crisis: open problems and possible implications for Mediterranean petroleum systems', *Petroleum Geoscience*, 22(4), pp. 283–290. Available at: https://doi.org/10.1144/petgeo2015-089.

Roveri, M. *et al.* (2019) 'The synthetic seismic expression of the Messinian salinity crisis from onshore records: Implications for shallow- to deep-water correlations', *Basin Research*, pp. 1121–1152. Available at: https://doi.org/10.1111/bre.12361.

Rowan, M. *et al.* (2016) 'Megaflaps adjacent to salt diapirs', *AAPG Bulletin*, 100(11), pp. 1723–1747. Available at: https://doi.org/10.1306/05241616009.

Rowan, M.G. (2014) 'Passive-margin salt basins: hyperextension, evaporite deposition, and salt tectonics', *Basin Research*, 26(1), pp. 154–182. Available at: https://doi.org/10.1111/bre.12043.

Rowan, M.G. *et al.* (2019) 'Deformation of intrasalt competent layers in different modes of salt tectonics', *Solid Earth*, 10(3), pp. 987–1013. Available at: https://doi.org/10.5194/se-10-987-2019.

Rowan, M.G. and Giles, K.A. (2021) 'Passive versus active salt diapirism', *AAPG Bulletin*, 105(1), pp. 53–63. Available at: https://doi.org/10.1306/05212020001.

Rowan, M.G., Peel, F.J. and Vendeville, B.C. (2004) 'Gravity-driven Fold Belts on Passive Margins', in K.R. McClay (ed.) *Thrust Tectonics and Hydrocarbon Systems*. American Association of Petroleum Geologists (AAPG MEMOIR), pp. 159–184. Available at: https://doi.org/10.1306/M82813C9 (Accessed: 5 January 2022).

Ryan, W.B.F. (2009) 'Decoding the Mediterranean salinity crisis', *Sedimentology*, 56(1), pp. 95–136. Available at: https://doi.org/10.1111/j.1365-3091.2008.01031.x.

Ryan, W.B.F. *et al.* (2009) 'Global Multi-Resolution Topography synthesis', *Geochemistry, Geophysics, Geosystems*, 10(3). Available at: https://doi.org/10.1029/2008GC002332.

Ryan, W.B.F. and Cita, M.B. (1978) 'The nature and distribution of Messinian erosional surfaces - Indicators of a several-kilometer-deep Mediterranean in the Miocene', *Marine Geology*, 27(3–4), pp. 193–230. Available at: https://doi.org/10.1016/0025-3227(78)90032-4.

Ryan, W.B.F., Hsu, K.J., and et al. (1973) *Initial Reports of the Deep Sea Drilling Project, 13*. U.S. Government Printing Office (Initial Reports of the

Deep Sea Drilling Project). Available at: http://deepseadrilling.org/13/dsdp_toc.htm (Accessed: 11 December 2015).

Sacchi, M.D. and Porsani, M. (1999) 'Fast high resolution parabolic Radon transform', in *SEG Technical Program Expanded Abstracts 1999*. Society of Exploration Geophysicists (SEG Technical Program Expanded Abstracts), pp. 1477–1480. Available at: https://doi.org/10.1190/1.1820798.

Sadhu, P. *et al.* (2008) 'Value Addition from Reprocessing of Seismic Data: An Analysis of Some of the Case Histories', in. Hyperabad: Society of Petroleum Geophysicists, p. 7.

Sage, F. *et al.* (2005) 'Seismic evidence for Messinian detrital deposits at the western Sardinia margin, northwestern Mediterranean', *Marine and Petroleum Geology*, 22(6–7), pp. 757–773. Available at: https://doi.org/10.1016/j.marpetgeo.2005.03.007.

Sams, M.S. *et al.* (1997) 'The measurement of velocity dispersion and frequency-dependent intrinsic attenuation in sedimentary rocks', *GEOPHYSICS*, 62(5), pp. 1456–1464. Available at: https://doi.org/10.1190/1.1444249.

Sans, M. and Vergés, J. (1995) 'Fold Development Related to Contractional Salt Tectonics: Southeastern Pyrenean Thrust Front, Spain', in M.P.A. Jackson, D.G. Roberts, and S. Snelson (eds) *Salt Tectonics: A Global Perspective*. American Association of Petroleum Geologists (AAPG Memoir), pp. 369–378. Available at: https://doi.org/10.1306/M65604C18.

Sargent, C., Hobbs, R.W. and Gröcke, D.R. (2011) 'Improving the interpretability of air-gun seismic reflection data using deterministic filters: A case history from offshore Cape Leeuwin, southwest Australia', *GEOPHYSICS*, 76(3), pp. B113–B125. Available at: https://doi.org/10.1190/1.3554396.

Sarkarinejad, K., Sarshar, M.A. and Adineh, S. (2018) 'Structural, micro-structural and kinematic analyses of channel flow in the Karmostaj salt diapir in the Zagros foreland folded belt, Fars province, Iran', *Journal of Structural Geology*, 107, pp. 109–131. Available at: https://doi.org/10.1016/j.jsg.2017.12.005.

Sartori, R. (1990) 'The main results of ODP Leg 107 in the frame of Neogene to Recent geology of Perityrrhenian areas', *Proceedings of the Ocean Drilling Program, Scientific Results*. Edited by K.A. Kastens et al., 107, p. 715.

Sautkin, A. *et al.* (2003) 'Mud volcanoes in the Alboran Sea: evidence from micropaleontological and geophysical data', *Marine Geology*, 195(1), pp. 237–261. Available at: https://doi.org/10.1016/S0025-3227(02)00691-6.

Schenk, C.J. *et al.* (2010) *Assessment of Undiscovered Oil and Gas Reserves in the Levant Basin Province, Eastern Mediterranean*. 2010–3014. Denver, p. 4. Available at: https://pubs.usgs.gov/fs/2010/3014/.

Schettino, A. and Turco, E. (2006) 'Plate kinematics of the Western Mediterranean region during the Oligocene and Early Miocene', *Geophysical Journal International*, 166(3), pp. 1398–1423. Available at: https://doi.org/10.1111/j.1365-246X.2006.02997.x.

Schlitzer, R. *et al.* (1991) 'Chlorofluoromethane and oxygen in the Eastern Mediterranean', *Deep Sea Research Part A. Oceanographic Research Papers*, 38(12), pp. 1531–1551. Available at: https://doi.org/10.1016/0198-0149(91)90088-W.

Schmid, S.M. *et al.* (2008) 'The Alpine-Carpathian-Dinaridic orogenic system: correlation and evolution of tectonic units', *Swiss Journal of Geosciences*, 101(1), pp. 139–183. Available at: https://doi.org/10.1007/s00015-008-1247-3.

Schneck, R., Micheels, A. and Mosbrugger, V. (2010) 'Climate modelling sensitivity experiments for the Messinian Salinity Crisis', *Palaeogeography, Palaeoclimatology, Palaeoecology*, 286(3), pp. 149–163. Available at: https://doi.org/10.1016/j.palaeo.2009.12.011.

Scholtz, P., Masoomzadeh, H. and Camp, R. (2015) 'Directional designature without near-field hydrophone recordings', in *SEG Technical Program Expanded Abstracts 2015*. New Orleans, Louisiana: Society of Exploration Geophysicists, pp. 4423–4427. Available at: https://doi.org/10.1190/segam2015-5843268.1.

Schonewille, M., Vigner, A. and Ryder, A. (2008) 'Swell-noise Attenuation Using an Iterative FX Prediction Filtering Approach', in.

Schreiber, E., Fox, P.J. and Peterson, J.J. (1973) 'Compressional Wave Velocities in Selected Samples of Gabbro, Schist, Limestone, Anhydrite, Gypsum and Halite', in.

Schultz, P.S. (1985) 'Seismic data processing: Current industry practice and new directions', *GEOPHYSICS*, 50(12), pp. 2452–2457. Available at: https://doi.org/10.1190/1.1441876.

Seidenkrantz, M.-S. *et al.* (2000) 'Benthic foraminifera as indicators of changing Mediterranean–Atlantic water exchange in the late Miocene', *Marine Geology*, 163(1), pp. 387–407. Available at: https://doi.org/10.1016/S0025-3227(99)00116-4.

Selli, R. (1960) 'Il Messiniano Mayer-Eymar 1867: proposta di un neostratotipo', *Giornale di geologia.*, 28.

Sellier, N.C. *et al.* (2013) 'Post-Messinian evolution of the Florence Ridge area (Western Cyprus Arc), Part I: Morphostructural analysis', *Tectonophysics*, 591, pp. 131–142. Available at: https://doi.org/10.1016/j.tecto.2012.04.001.

Serpelloni, E. *et al.* (2007) 'Kinematics of the Western Africa-Eurasia Plate Boundary From Focal Mechanisms and GPS Data', *Geophysical Journal International*, 25. Available at: https://doi.org/10.1111/j.1365-246X.2007.03367.x.

Sheriff, R.E. and Geldart, L.P. (1995) *Exploration Seismology*. 2nd edn. Cambridge: Cambridge University Press. Available at: https://doi.org/10.1017/CBO9781139168359.

Sherkati, S. and Letouzey, J. (2004) 'Variation of structural style and basin evolution in the central Zagros (Izeh zone and Dezful Embayment), Iran', *Marine and Petroleum Geology*, 21(5), pp. 535–554. Available at: https://doi.org/10.1016/j.marpetgeo.2004.01.007.

Shin, S.Y. and Kim, T. (2021) 'Eastern Mediterranean Gas Discoveries: Local and Global Impact', *Middle East Policy*, 28(1), pp. 135–146. Available at: https://doi.org/10.1111/mepo.12546.

Sierro, F. *et al.* (2003) 'Orbitally-controlled oscillations in planktic communities and cyclic changes in western Mediterranean hydrography during the Messinian', *Palaeogeography Palaeoclimatology Palaeoecology*, 190, pp. 289–316. Available at: https://doi.org/10.1016/S0031-0182(02)00611-9.

Smith, A.G. (1971) 'Alpine Deformation and the Oceanic Areas of the Tethys, Mediterranean, and Atlantic', *GSA Bulletin*, 82(8), pp. 2039–2070. Available at: https://doi.org/10.1130/0016-7606(1971)82[2039:ADATOA]2.0.CO;2.

Somoza, L. *et al.* (2012) 'Structure of mud volcano systems and pockmarks in the region of the Ceuta Contourite Depositional System (Western Alborán Sea)', *Marine Geology*, 332–334, pp. 4–26. Available at: https://doi.org/10.1016/j.margeo.2012.06.002.

Soto, J.I. *et al.* (2019) 'The Messinian Salt Layer Squeezed by Active Plate Convergence in the Western Mediterranean Margins', in. Available at: https://www.searchanddiscovery.com/abstracts/html/2019/ace2019/abstracts/1595.html (Accessed: 5 July 2021).

Soulet, Q. *et al.* (2016) 'Erosional versus aggradational canyons along a tectonically-active margin: The northeastern Ligurian margin (western Mediterranean Sea)', *Marine Geology*, 382, pp. 17–36. Available at: https://doi.org/10.1016/j.margeo.2016.09.015.

Spakman, W. and Wortel, R. (2004) 'A Tomographic View on Western Mediterranean Geodynamics', in W. Cavazza et al. (eds) *The TRANSMED Atlas. The Mediterranean Region from Crust to Mantle: Geological and Geophysical Framework of the Mediterranean and the Surrounding Areas*. Berlin, Heidelberg: Springer, pp. 31–52. Available at: https://doi.org/10.1007/978-3-642-18919-7_2.

Speranza, F. *et al.* (2012) 'The Ionian Sea: The oldest in situ ocean fragment of the world?', *Journal of Geophysical Research: Solid Earth*, 117(B12). Available at: https://doi.org/10.1029/2012JB009475.

Spitz, S. (1991) 'Seismic trace interpolation in the F-X domain', *GEOPHYSICS*, 56(6), pp. 785–794. Available at: https://doi.org/10.1190/1.1443096.

Stich, D. *et al.* (2006) 'Kinematics of the Iberia–Maghreb plate contact from seismic moment tensors and GPS observations', *Tectonophysics*, 426(3), pp. 295–317. Available at: https://doi.org/10.1016/j.tecto.2006.08.004.

Stoica, M. *et al.* (2016) 'Paratethyan ostracods in the Spanish Lago-Mare: More evidence for interbasinal exchange at high Mediterranean sea level', *Palaeogeography Palaeoclimatology Palaeoecology*, 441, pp. 854–870. Available at: https://doi.org/10.1016/j.palaeo.2015.10.034.

Struglia, M.V., Mariotti, A. and Filograsso, A. (2004) 'River Discharge into the Mediterranean Sea', *Journal of Climate*, 17(24), pp. 4740–4751.

Strzerzynski, P. *et al.* (2010) 'Tectonic inheritance and Pliocene-Pleistocene inversion of the Algerian margin around Algiers: Insights from multibeam and seismic reflection data', *Tectonics*, 29(2). Available at: https://doi.org/10.1029/2009TC002547.

Strzerzynski, P. *et al.* (2021) 'Tectonic Inversion and Geomorphic Evolution of the Algerian Margin Since Messinian Times: Insights From New Onshore/Offshore Analog Modeling Experiments', *Tectonics*, 40(2), p. e2020TC006369. Available at: https://doi.org/10.1029/2020TC006369.

Taner, M.T. and Koehler, F. (1981) 'Surface consistent corrections', *GEOPHYSICS*, 46(1), pp. 17–22. Available at: https://doi.org/10.1190/1.1441133.

Tibor, G. *et al.* (1992) 'Late Tertiary subsidence history of the southern Levant Margin, eastern Mediterranean Sea, and its implications to the understanding of the Messinian Event', *Journal of Geophysical Research: Solid Earth*, 97(B12), pp. 17593–17614. Available at: https://doi.org/10.1029/92JB00978.

Topper, R.P.M. and Meijer, P.T. (2015) 'Changes in Mediterranean circulation and water characteristics due to restriction of the Atlantic connection: a high-resolution ocean model', *Climate of the Past*, 11(2), pp. 233–251.

Trabant, P.K. (1984) 'Multifold Acquisition and Digital Processing', in P.K. Trabant (ed.) *Applied High-Resolution Geophysical Methods: Offshore Geoengineering Hazards*. Dordrecht: Springer Netherlands, pp. 131–165. Available at: https://doi.org/10.1007/978-94-009-6493-8_9.

Trájer, A.J., Sebestyén, V. and Padisák, J. (2021) 'The impacts of the Messinian Salinity Crisis on the biogeography of three Mediterranean sandfly (Diptera: Psychodidae) species', *Geobios*, 65, pp. 51–66. Available at: https://doi.org/10.1016/j.geobios.2021.02.003.

Trudgill, B.D. (2011) 'Evolution of salt structures in the northern Paradox Basin: controls on evaporite deposition, salt wall growth and supra-salt stratigraphic architecture', *Basin Research*, 23(2), pp. 208–238. Available at: https://doi.org/10.1111/j.1365-2117.2010.00478.x.

Tsvankin, I. and Thomsen, L. (1994) 'Nonhyperbolic reflection moveout in anisotropic media', *GEOPHYSICS*, 59(8), pp. 1290–1304. Available at: https://doi.org/10.1190/1.1443686.

Tyagi, C. *et al.* (2016) 'Efficient Broadband Reprocessing of a Conventional Towed-Streamer Dataset - A Case Study from the North Sea', in. European Association of Geoscientists & Engineers, pp. 1–5. Available at: https://doi.org/10.3997/2214-4609.201601564.

Tzanova, A., Herbert, T.D. and Peterson, L. (2015) 'Cooling Mediterranean Sea surface temperatures during the Late Miocene provide a climate context for evolutionary transitions in Africa and Eurasia', *Earth and Planetary Science Letters*, 419, pp. 71–80. Available at: https://doi.org/10.1016/j.epsl.2015.03.016.

Tzevahirtzian, A. *et al.* (2022) 'Onset of the Messinian Salinity Crisis: Sedimentological, petrographic and geochemical characterization of the

pre-salt sediments from a new core (Caltanissetta Basin, Sicily)', *Marine and Petroleum Geology*, 141, p. 105686. Available at: https://doi.org/10.1016/j.marpetgeo.2022.105686.

United Nations Environment Programme/Mediterranean Action Plan and Plan Bleu (2020) *State of the Environment and Development in the Mediterranean*. Marseille: United Nations Environment Programme, p. 341. Available at: https://planbleu.org/wp-content/uploads/2021/04/SoED_full-report.pdf.

Uranga, R.M. *et al.* (2022) 'Salt tectonics of the offshore Tarfaya Basin, Moroccan Atlantic margin', *Marine and Petroleum Geology*, 138, p. 105521. Available at: https://doi.org/10.1016/j.marpetgeo.2021.105521.

Urgeles, R. *et al.* (2011) 'New constraints on the Messinian sealevel drawdown from 3D seismic data of the Ebro Margin, western Mediterranean', *Basin Research*, 23(2), pp. 123–145. Available at: https://doi.org/10.1111/j.1365-2117.2010.00477.x.

Urgeles, R. *et al.* (2013) 'Salt Deformation and Sub-salt Fluid Circulation in the Algero-Balearic Abyssal Plain', in. Barcelona. Available at: http://www.searchanddiscovery.com/abstracts/html/2013/90161er/abstracts/urgele.htm (Accessed: 26 March 2021).

Van Hinsbergen, D.J.J., Vissers, R.L.M. and Spakman, W. (2014) 'Origin and consequences of western Mediterranean subduction, rollback, and slab segmentation', *Tectonics*, 33(4), pp. 393–419. Available at: https://doi.org/10.1002/2013TC003349.

Vardy, M.E. and Henstock, T.J. (2010) 'A frequency-approximated approach to Kirchhoff migration', *GEOPHYSICS*, 75(6), pp. S211–S218. Available at: https://doi.org/10.1190/1.3491196.

Vasiliev, I. *et al.* (2017) 'How dry was the Mediterranean during the Messinian salinity crisis?', *Palaeogeography, Palaeoclimatology, Palaeoecology*, 471, pp. 120–133. Available at: https://doi.org/10.1016/j.palaeo.2017.01.032.

Vendeville, B.C. (2005) 'Salt tectonics driven by sediment progradation: Part I—Mechanics and kinematics', *AAPG Bulletin*, 89(8), pp. 1071–1079. Available at: https://doi.org/10.1306/03310503063.

Venus, J.H., Mountney, N.P. and McCaffrey, W.D. (2015) 'Syn-sedimentary salt diapirism as a control on fluvial-system evolution: an example from the proximal Permian Cutler Group, SE Utah, USA', *Basin Research*, 27(2), pp. 152–182. Available at: https://doi.org/10.1111/bre.12066.

Vergés, J. *et al.* (2017) 'Chapter 26 - Salt Tectonics in the Atlas Mountains of Morocco', in J.I. Soto, J.F. Flinch, and G. Tari (eds) *Permo-Triassic Salt Provinces of Europe, North Africa and the Atlantic Margins*. Elsevier, pp. 563–579. Available at: https://doi.org/10.1016/B978-0-12-809417-4.00027-6.

Vergés, J. and Fernàndez, M. (2012) 'Tethys–Atlantic interaction along the Iberia–Africa plate boundary: The Betic–Rif orogenic system', *Tectonophysics*, 579, pp. 144–172. Available at: https://doi.org/10.1016/j.tecto.2012.08.032.

Vergés, J. and Sàbat, F. (1999) 'Constraints on the Neogene Mediterranean kinematic evolution along a 1000 km transect from Iberia to Africa', *Geological Society, London, Special Publications*, 156(1), p. 63. Available at: https://doi.org/10.1144/GSL.SP.1999.156.01.05.

Verschuur, D.J. (2013) *Seismic multiple removal techniques: past, present and future*. Rev. ed. Houten: EAGE Publ (Education tour series, 1).

Verschuur, D.J. and Berkhout, A.J. (1996) 'Removal of interbed multiples', in. European Association of Geoscientists & Engineers, p. cp. Available at: https://doi.org/10.3997/2214-4609.201409164.

Vidal, L. *et al.* (2002) 'Late miocene stable isotope stratigraphy of SE Atlantic ODP Site 1085: Relation to Messinian events', *Marine Geology*, 180(1–4), pp. 71–85. Available at: https://doi.org/10.1016/S0025-3227(01)00206-7.

Vidal, N., Alvarez-Marrón, J. and Klaeschen, D. (2000) 'The structure of the Africa-Anatolia plate boundary in the eastern Mediterranean', *Tectonics*, 19(4), pp. 723–739.

Virieux, J. and Operto, S. (2009) 'An overview of full-waveform inversion in exploration geophysics', *GEOPHYSICS*, 74(6), pp. WCC1–WCC26. Available at: https://doi.org/10.1190/1.3238367.

Wagner, B.H. and Jackson, M.P.A. (2011) 'Viscous flow during salt welding', *Tectonophysics*, 510(3), pp. 309–326. Available at: https://doi.org/10.1016/j.tecto.2011.07.012.

Wang, B., Wu, R.-S. and Chen, X. (2017) 'Deghosting based on the transmission matrix method', *Journal of Geophysics and Engineering*, 14(6), pp. 1572–1581. Available at: https://doi.org/10.1088/1742-2140/aa82da.

Wang, Y. (2006) 'Inverse Q -filter for seismic resolution enhancement', *GEOPHYSICS*, 71(3), pp. V51–V60. Available at: https://doi.org/10.1190/1.2192912.

Wardell, N. *et al.* (2014) 'Seismic evidence for Messinian salt deformation and fluid circulation on the South Balearic margin (Western Mediterranean)', in, p. 11078. Available at: http://adsabs.harvard.edu/abs/2014EGUGA..1611078W (Accessed: 23 April 2020).

Warren, J.K. (2016) *Evaporites: a geological compendium*. Second edition. Cham Heidelberg New York: Springer.

Watson, L.M., Werpers, J. and Dunham, E.M. (2019) 'What controls the initial peak of an air-gun source signature?', *GEOPHYSICS*, 84(2), pp. P27–P45. Available at: https://doi.org/10.1190/geo2018-0298.1.

Weijermars, R. (1988) 'Neogene tectonics in the Western Mediterranean may have caused the Messinian salinity crisis and an associated glacial event', *Tectonophysics*, 148(3), pp. 211–219. Available at: https://doi.org/10.1016/0040-1951(88)90129-1.

Weijermars, R. and Jackson, M.P.A. (2014) 'Predicting the depth of viscous stress peaks in moving salt sheets: Conceptual framework and implications for drilling', *AAPG Bulletin*, 98(5), pp. 911–945. Available at: https://doi.org/10.1306/09121313044.

Weijermars, R., Jackson, M.P.A. and Vendeville, B. (1993) 'Rheological and tectonic modeling of salt provinces', *Tectonophysics*, 217(1), pp. 143–174. Available at: https://doi.org/10.1016/0040-1951(93)90208-2.

Westbrook, G.K. and Reston, T.J. (2002) 'The accretionary complex of the Mediterranean Ridge: tectonics, fluid flow and the formation of brine lakes – an introduction to the special issue of Marine Geology', *Marine Geology*, 186(1), pp. 1–8. Available at: https://doi.org/10.1016/S0025-3227(02)00169-X.

Willett, S.D., Schlunegger, F. and Picotti, V. (2006) 'Messinian climate change and erosional destruction of the central European Alps', *Geology*, 34(8), pp. 613–616. Available at: https://doi.org/10.1130/G22280.1.

Willis, A. *et al.* (2018) 'How Broadband Processing Can Improve Multiple Attenuation Processes for Conventional Flat Streamer Data', in.

Woidt, W.-D. (1978) 'Finite element calculations applied to salt dome analysis', *Tectonophysics*, 50(2), pp. 369–386. Available at: https://doi.org/10.1016/0040-1951(78)90143-9.

Woodside, J.M. (2000) 'General Tectonic Framework of the Eastern Mediterranean', in. European Association of Geoscientists & Engineers, p. cp. Available at: https://doi.org/10.3997/2214-4609.201406009.

Wortel, R., Govers, R. and Spakman, W. (2009) 'Continental Collision and the STEP-wise Evolution of Convergent Plate Boundaries: From Structure to Dynamics', in S. Lallemand and F. Funiciello (eds) *Subduction Zone Geodynamics*. Berlin, Heidelberg: Springer (Frontiers in Earth Sciences), pp. 47–59. Available at: https://doi.org/10.1007/978-3-540-87974-9_3.

Würtz, M. (2010) *Mediterranean pelagic habitat : oceanographic and biological processes, an overview*. IUCN. Available at: https://portals.iucn.org/library/node/9533 (Accessed: 16 September 2021).

Yelles, A. *et al.* (2009) 'Plio-Quaternary reactivation of the Neogene margin off NW Algiers, Algeria: The Khayr al Din bank', *Tectonophysics*, 475(1), pp. 98–116. Available at: https://doi.org/10.1016/j.tecto.2008.11.030.

Yilmaz, Ö. (2001) *Seismic Data Analysis*. Society of Exploration Geophysicists (Investigations in Geophysics). Available at: https://doi.org/10.1190/1.9781560801580.

Yilmaz, O. and Baysal, E. (2015) 'An Effective Ghost Removal Method for Marine Broadband Seismic Data Processing', in. Madrid, Spain. Available at: https://doi.org/10.3997/2214-4609.201413195.

Yohann, P. *et al.* (2016) 'Halokinetic sequences in carbonate systems: An example from the Middle Albian Bakio Breccias Formation (Basque Country, Spain)', *Sedimentary Geology*, 334, pp. 34–52. Available at: https://doi.org/10.1016/j.sedgeo.2016.01.013.

Zhang, D. *et al.* (2020) 'Experimental Investigation of Gas Transfer Properties and Stress Coupling Effects of Salt Rocks', *Rock Mechanics and Rock Engineering*, 53(9), pp. 4015–4029. Available at: https://doi.org/10.1007/s00603-020-02151-x.

Zhang, G. *et al.* (2019) 'Giant discoveries of oil and gas fields in global deepwaters in the past 40 years and the prospect of exploration', *Journal of Natural Gas Geoscience*, 4(1), pp. 1–28. Available at: https://doi.org/10.1016/j.jnggs.2019.03.002.

Ziolkowski, A. (1970) 'A Method for Calculating the Output Pressure Waveform from an Air Gun', *Geophysical Journal International*, 21(2), pp. 137–161. Available at: https://doi.org/10.1111/j.1365-246X.1970.tb01773.x.

Zucker, E. *et al.* (2019) 'Salt tectonics in the Eastern Mediterranean Sea: Where a giant delta meets a salt giant', *Geology*, 48(2), pp. 134–138. Available at: https://doi.org/10.1130/G47031.1.